

WESTERN SYDNEY UNIVERSITY



Automating the synthesis of platinum(II) complexes and modifying the pharmacokinetics of platinum(IV) complexes

Brondwyn McGhie

Supervisor: Professor Janice R. Aldrich-Wright

Co-Supervisor: Doctor Ming Wu

School of Science and Health

Western Sydney University

A Thesis presented to

The Western Sydney University

In fulfilment of the requirements

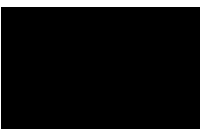
For the Degree of

Master of Philosophy

© Brondwyn McGhie, 2018

Statement of Authentication

This thesis is submitted in fulfilment of the requirements of the Master of Philosophy (Science) course at Western Sydney University (WSU), School of Science. The work presented in this thesis is, to the best of my knowledge and belief, original except as acknowledged in the text. I hereby declare that I have not submitted this material, either in full or in part, for a degree at this or any other institution.

	30/11/2018
-----	-----
Signed	Date

Acknowledgements

Firstly, I would like to thank my supervisor Professor Janice Aldrich-Wright for her wisdom, guidance and support she has provided throughout my candidature. Without Janice's guidance my career would have taken a very different path, and I am thankful to her for convincing me to take on the challenge of postgraduate research and for giving me the support and knowledge to find my feet. Janice, you have been everything a supervisor should be and more, your passion and commitment has inspired me, and your work ethic driven me to achieve more.

Secondly, I would like to thank Dr Christopher Gordan and my co-supervisor Dr Ming Wu, who have worked closely with our lab and offered knowledge and guidance. You have also shown the value in collaboration and an outsider's perspective, thank you.

Thirdly I would like to thank other groups within the university who have helped with different aspects of my project. I would like to thank the Nanoscale Organisation and Dynamics Group, in particular Scott Willis, for allowing me access to the NMR equipment, as well as education and guidance in its use. I would also like to thank the School of Medicine for their similar help and access to the Mass spectrometry Facility especially Meena Mikhael and David Harmen for their guidance in the use of the equipment.

During my candidature I was also fortunate enough to collaborate with groups outside the university. I would like to thank our collaborators at the Cavalry Mater Facility in Newcastle who undertook the biological studies of my complexes. I would also like to thank Department of Physics and Astronomy of Aarhus University and Nyk Jones for teaching me how to use their synchrotron, as well as giving me the opportunity to see their beautiful country.

Next, I would like to thank my peers in the office for providing a fun, easy-going, supportive environment throughout my candidature. Although frustrating at times, the office antics kept my mood light and provided entertainment when lab work was repetitive and monotonous. You each contributed in your own way to this fun and supportive environment and for that I thank you.

I would also like to thank my friends and family for their role in supporting my studies. For the late-night phone calls, tedious editing, study breaks, and their continued belief in my ability to succeed. I appreciate you making sure that I looked after myself and didn't lose myself in my studies. To my family in particular, thank you for shaping me into the person I am today and for being proud of all my achievements.

Lastly, I would like to thank my wonderful partner Dr Ben Pages for his love and commitment as well as the guidance he provided as a fellow researcher. When I was feeling unmotivated or unsure of myself you picked me up and pushed me to do better; although there were many grumbles of discontentment at the time, I do really appreciate it and know that I would not be where I am now without you.

Abstract

Cancer is one of the most common diseases worldwide and one of the leading causes of death globally each year. Current mortality rates are high despite the many treatment options, leading many researchers to investigate new more effective cancer treatments. Currently the majority of patients receive chemotherapy as a part of their treatment and the most common drugs are platinum based cisplatin, oxaliplatin and carboplatin. These drugs covalently bind to DNA subsequently causing apoptosis. Although effective at killing cancerous cells these drugs are non-specific and also destroy non target cells. Their non-specificity results in a variety of negative side effects, many of them so severe that patients terminate treatment early or move to a lower than optimal dosage. Resistance is another area of concern for these drugs, with both intrinsic and acquired resistance resulting in poor prognosis for patients.

New complexes proposed for anticancer treatments hope to mitigate these issues by utilising different mechanisms of action. Polyaromatic platinum complexes are an example of a class of promising new complexes that have a different mechanism of action than the traditional platinum drugs. These complexes have the general formula $[\text{Pt}(\text{P}_L)(\text{A}_L)]^{2+}$ incorporating polyaromatic ligands (P_L) with a coordinated ancillary ligand (A_L), they have achieved GI_{50} results up to 1000 times better than cisplatin. These polyaromatic complexes can be oxidised to platinum(IV) which may allow oral administration, improved extracellular stability and fine tuning of the pharmacokinetics through modification of the axial ligands.

In this work the method for the synthesis of a series of novel platinum(IV) polyaromatic complexes was developed and these complexes were characterised using ESIMS, UV spectroscopy, CD spectroscopy, SRCD spectroscopy, microanalysis, NMR and HPLC. These complexes were synthesised via the coordination of halides Cl, Br and I in the axial positions producing the di-halogenated platinum(IV) complexes desired. The effectiveness of substitution in the axial position by various ligands was assessed, as well as the cytotoxicity of the resulting compounds in cell lines. It was revealed that these compounds allow the development of new synthetic methods which were previously closed to these complexes, allowing the

synthesis of targeted complexes that have the potential to improve prognosis. The developed method is much less time consuming than the current oxidation methods, reducing time spent on synthesising intermediates which will maximise outcomes for further synthesis. The GI₅₀'s revealed that these complexes are of comparable cytotoxicity to the platinum(II) complexes and are more cytotoxic than dihydroxido platinum(IV) complexes of the same type.

Further development of these complexes was achieved through the linkage of targeting and cytotoxic ligands. These ligands were provided by collaborators and will undergo biological testing in their respective laboratories. DCF, a cytotoxic ligand, was bound in both axial positions through an ethylene diamine linker. The synthesis was confirmed by NMR, providing proof of concept for the attachment of such ligands, further diversifying the skillset of the research group. The PSMA targeting ligand DCL was bound using a succinate linker to one of the axial ligands. This synthesis provided proof of concept for the synthesis of asymmetric compounds with large targeting ligands; whose pharmacokinetics can be further adjusted through derivatisation of the remaining axial ligand. The synthesis of more novel asymmetric complexes was developed, platinum compounds with both a hydroxido and acetato ligand. The asymmetric design of these compounds will allow further asymmetric derivatisation of the Pt(IV) which may be advantageous in the design and synthesis of multi action drugs.

The use of flow chemistry to streamline the synthesis of these compounds was also trailed. Although the resulting protocol was successful, being the first reported use of flow chemistry for the synthesis of an inorganic complex; yields were not improved to the ~90% typically achieved in batch chemistry. As such this method of synthesis was not pursued in the synthesis of platinum(II) starting materials in our research group; instead working as a proof of concept in the use of flow chemistry in the synthesis of such complexes.

Table of Contents

Statement of Authentication	ii
Acknowledgements	iii
Abstract	v
List of Tables	4
List of Figures	5
Publications	10
Abbreviations	11
Chapter 1 Introduction	14
1.1 Cancer	14
1.2 Cancer treatments	14
1.2.1 Cisplatin	15
1.2.2 Carboplatin and oxaliplatin.....	16
1.3 Unconventional Pt drugs	17
1.3.1 Polyaromatic platinum(II) complexes	18
1.3.2 Platinum(IV) complexes	19
1.3.3 Advantages of platinum(IV) complexes with targeting Vectors.	20
1.3.4 Advantages of Pt(IV) complexes with bio-active ligands.....	22
1.3.5 Advantages of asymmetric Pt(IV) complexes.	24
1.4 New synthetic procedures: continuous flow chemistry	27
1.5 Project Aims	29
Chapter 2 Materials and Methodology	32
2.1 Materials	32
2.2 Instrumentation.....	32
2.3 Synthesis	34
2.3.1 Synthesis of $[\text{Pt}(1S,2S\text{-diaminocyclohexane})\text{Cl}_2]^{2+}$	34
2.3.2 Synthesis of $[\text{Pt}(1,10\text{phenanthroline})(1S,2S\text{-diaminocyclohexane})]^{2+}$ (Batch).....	35
2.3.3 Synthesis of $[\text{Pt}(1,10\text{-phenanthroline})(1S,2S\text{-diaminocyclohexane})]^{2+}$ (Flow)	35
2.3.4 Synthesis of Pt(II) complexes of the type $[\text{Pt}(\text{PL})(\text{AL})]^{2+}$	36
2.3.5 Synthesis of complexes of the type $[\text{Pt}(\text{PL})(\text{AL})\text{X}_2]^{2+}$	39
2.3.6 Synthesis of Pt(IV) complexes of the type $[\text{Pt}(\text{PL})(\text{AL})(\text{OH})_2]^{2+}$	42
2.3.7 Synthesis of Pt(IV) complexes of the type $[\text{Pt}(\text{PL})(\text{AL})(\text{OH})(\text{C}_2\text{H}_3\text{O}_2)]^{2+}$	44
2.3.8 Synthesis of 2-aminoethylclufenacamide (enDCF)	46
2.3.9 Synthesis of $[\text{Pt}(1,10\text{-phenanthroline})(1S,2S\text{-diaminocyclohexane})$ $(\text{DMSO})_2]^{2+}$	46

2.3.10	Synthesis of [Pt(1,10-phenanthroline)(1 <i>S</i> ,2 <i>S</i> -diaminocyclohexane) (2-aminoethylidiclofenacamide) ₂] ²⁺	47
2.3.11	Synthesis of Pt(IV) complexes of the type [Pt(P _L)(A _L)(OH)(succinimide)] ²⁺ ...	48
2.3.12	Synthesis of [Pt(1,10-phenanthroline)(1 <i>S</i> ,2 <i>S</i> -diaminocyclohexane) (OH)(succinatePFP)] ²⁺	49
2.3.13	Synthesis of [Pt(1,10-phenanthroline)(1 <i>S</i> ,2 <i>S</i> -diaminocyclohexane) (OH)(PSMA)] ²⁺	49
2.4	Cytotoxicity methodology.....	50
Chapter 3 Results and Discussion		52
3.1	Synthesis	52
3.1.1	Synthesis of [Pt(1,10-phenanthroline)(1 <i>S</i> ,2 <i>S</i> -diaminocyclohexane)] ²⁺	52
3.1.2	Synthesis of [Pt(1,10-phenanthroline)(1 <i>S</i> ,2 <i>S</i> -diaminocyclohexane)] ²⁺ , [Pt(1,10-phenanthroline)(1 <i>R</i> ,2 <i>R</i> -diaminocyclohexane)] ²⁺ , [Pt(5 methyl-1,10-phenanthroline)(1 <i>S</i> ,2 <i>S</i> -diaminocyclohexane)] ²⁺ , [Pt(5-methyl-1,10-phenanthroline)(1 <i>R</i> ,2 <i>R</i> -diaminocyclohexane)] ²⁺ [Pt(5,6 dimethyl-1,10-phenanthroline)(1 <i>S</i> ,2 <i>S</i> -diaminocyclohexane)] ²⁺ , [Pt(5,6 dimethyl-1,10-phenanthroline)(1 <i>R</i> ,2 <i>R</i> -diaminocyclohexane)] ²⁺	59
3.1.3	The Synthesis of [Pt(1,10-phenanthroline)(1 <i>S</i> ,2 <i>S</i> -diaminocyclohexane)X ₂] ²⁺	60
3.1.4	Synthesis of [Pt(5,6-dimethylphenanthroline)(1 <i>S</i> ,2 <i>S</i> -diaminocyclohexane)X ₂] ²⁺ and [Pt(5-methylphenanthroline)(1 <i>S</i> ,2 <i>S</i> -diaminocyclohexane)X ₂] ²⁺	64
3.1.5	Synthesis of Pt(IV) complexes of the type [Pt(P _L)(A _L)(OH) ₂] ²⁺	65
3.1.6	Synthesis of Pt(IV) complexes of the type [Pt(P _L)(A _L)(OH)(C ₂ H ₃ O ₂)] ²⁺	66
3.1.7	Synthesis of 2-aminoethylidiclofenacamide.....	68
3.1.8	Synthesis of [Pt(1,10-phenanthroline)(1 <i>S</i> ,2 <i>S</i> -diaminocyclohexane) (DMSO) ₂] ²⁺	68
3.1.9	Synthesis of [Pt(1,10-phenanthroline)(1 <i>S</i> ,2 <i>S</i> -diaminocyclohexane)(2-aminoethylidiclofenacamide) ₂] ²⁺	70
3.1.10	Synthesis of of Pt(IV) complexes of the type [Pt(P _L)(A _L)(OH)(succinimide)] ²⁺	71
3.1.11	Synthesis of [Pt(1,10-phenanthroline)(1 <i>S</i> ,2 <i>S</i> -diaminocyclohexane) (OH)(succinatePFP)] ²⁺	72
3.1.12	Synthesis of [Pt(1,10-phenanthroline)(1 <i>S</i> ,2 <i>S</i> -diaminocyclohexane) (OH)(DCL)] ²⁺	72
3.2	Characterisation.....	74
3.2.1	The characterisation of Pt(II) complexes of the type [Pt(P _L)(A _L)] ²⁺	75
3.2.2	The characterisation of complexes of the type [Pt(P _L)(A _L) X ₂] ²⁺	78
3.2.3	The characterisation of Pt(IV) complexes of the type [Pt(P _L)(A _L)(OH)(C ₂ H ₃ O ₂)] ²⁺	102
3.2.4	The characterisation 2-aminoethylidiclofenacamide	105

3.2.5	The characterisation of [Pt(1,10-phenanthroline)(1 <i>S</i> ,2 <i>S</i> -diaminocyclohexane) (DMSO) ₂] ²⁺	108
3.2.6	The characterisation of [Pt(1,10-phenanthroline)(1 <i>S</i> ,2 <i>S</i> -diaminocyclohexane)(2-Aminoethylchlorfenacamide) ₂] ²⁺	110
3.2.7	The characterisation of Pt(IV) complexes of the type [Pt(P _L)(A _L)(OH)(succinimide)] ²⁺	112
3.2.8	The characterisation of [Pt(1,10-phenanthroline)(1 <i>S</i> ,2 <i>S</i> -diaminocyclohexane) (OH)(succinatePFP)] ²⁺	114
3.2.9	The characterisation of [Pt(1,10-phenanthroline)(1 <i>S</i> ,2 <i>S</i> -diaminocyclohexane)(OH)(PSMA)] ²⁺	116
3.3	Summary of characterisation: ¹⁹⁵ Pt(IV) NMR trends	120
3.5	Cytotoxicity	123
3.5.1	Cytotoxicity of [Pt(P _L)(A _L)(X) ₂] ²⁺ type complexes	123
Chapter 4 Conclusions		126
References		131

List of Tables

Table 1.3.1.1: Cytotoxicity of complexes of the type $[\text{Pt}(\text{P}_L)(\text{A}_L)]^{2+}$ and $[\text{Pt}(\text{P}_L)(\text{A}_L)(\text{OH})_2]^{2+}$ compared to cisplatin, oxaliplatin and carboplatin.....	19
Table 2.3.4.1 Summary of NMR data of Pt(II) complexes of the type $[\text{Pt}(\text{P}_L)(\text{A}_L)]^{2+}$ complexes, showing chemical shift (ppm) with integration, multiplicity and coupling constants. Experiments were performed in D_2O , so amine resonances were not observed due to proton exchange.	38
Table 2.3.5.1: Summary of NMR data of complexes of the type $[\text{Pt}(\text{A}_L)(\text{P}_L)\text{X}_2]^{2+}$, showing chemical shift (ppm) with integration, multiplicity and coupling constants. Experiments were performed in D_2O , so amine resonances were not observed due to proton exchange.	40
Table 2.3.5.2: Summary of the characterisation data of complexes of the type $[\text{Pt}(\text{P}_L)(\text{A}_L)(\text{X})_2]^{2+}$	41
Table 2.3.5.3: Summary of cytotoxicity results in GI_{50} = Concentration (μM) that inhibits cell growth by 50%	41
Table 2.3.6.1. Summary of NMR data of dihydroxido complexes, showing chemical shift (ppm) with integration, multiplicity and coupling constants. Experiments were performed in D_2O , so amine resonances were not observed due to proton exchange.	43
Table 2.3.7.1. Summary of NMR data of Asymmetric $(\text{OH})(\text{OAc})$ complexes, showing chemical shift (ppm) with integration, multiplicity and coupling constants. Experiments were performed in D_2O , so amine resonances were not observed due to proton exchange.	45
Table 2.3.7.1. Summary of NMR data of $[\text{Pt}(\text{P}_L)(\text{A}_L)(\text{OH})(\text{Succ})]$ complexes, showing chemical shift (ppm), integration, multiplicity and coupling constants. Experiments were performed in D_2O , so amine resonances were not observed.	48

List of Figures

Figure 1.2.1: The chemical structure of the platinum(II) compound Cisplatin.	15
Figure 1.2.2: The chemical structures of the platinum(II) (Pt(II)) compounds carboplatin and oxaliplatin.....	17
Figure 3.3.3: Intra- and extracellular reduction of Pt(IV), resulting in the loss of the axial ligands, producing a Pt(II) compound, showing potential mechanisms of action. ^{41, 45} (X= axial ligand).....	20
Figure 3.3.4: Enhanced permeability and retention (EPR) effect: A) Small drug size results in the diffusion of the unconjugated drug into both the healthy and tumour tissue. B) Larger drug size results in the diffusion of the conjugated drug into tumour tissue only.	21
Figure 1.3.4.1: Examples of DCL complexes; complex 1: <i>cis</i> -[PtCl ₂ (DCF) ₂ (NH)], complex 2: <i>cis</i> -[Pt(DCF) ₂ (NH ₃) ₂] and complex 3: [Pt(1,10-phenanthroline)(1 <i>S</i> ,2 <i>S</i> -diaminocyclohexane)(2-Aminoethylidiclofenacamide) ₂] ²⁺	24
Figure 1.3.5.1: An example of an asymmetric dineclear anticancer agent made up of 56MESS, cisplatin, PhB and DCA. ⁹²	27
Figure 1.4.1: Reaction scheme for the batch chemistry method (top) and the flow chemistry method (bottom).....	28
Figure 3.1.1.1: Set up for flow chemistry synthesis of [Pt(P _L)(A _L) ₂] ²⁺	53
Figure 3.1.1.2: Standard HPLC curve for PhenSS from gradient elution of acetonitrile.	54
Figure 3.1.1.3: Concentration of fractions collected off the column containing [Pt(dach)Cl ₂] and 1,10-Phenanthroline (1:1.1 mole ratio) every 15 minutes for three hours at a flow rate of 0.25 mL/min at 80 °C.	55
Figure: 3.1.1.4: Average percentage yield of PhenSS calculated based on HPLC trace, synthesised at 80, 100 and 120 °C, with a flow rate of 0.25 mL/min with a [Pt(DACH)Cl ₂] to 1,10-phenanthroline more ratio of 1:1.1.....	56
Figure: 3.1.1.5: Average percentage yield of PhenSS calculated based on isolated pure complex, synthesised at 80, 100 and 120 °C, with a flow rate of 0.25 mL/min and a [Pt(dach)Cl ₂] to phen ratio of 1:1.1.....	57
Figure 3.1.4.2: Reaction scheme for the formation of [Pt(1,10phenanthroline)(1 <i>S</i> ,2 <i>S</i> -diaminocyclohexane)Cl ₂] ²⁺ using NCS.....	62
Figure 3.1.4.3: Structure of PHENSSX ₂ and PhenSSX(succinimide), showing the distortion of the DACH region.	63
Figure 3.1.10.1: Reaction scheme for the synthesis of PHENSS(enDCF).....	71

Figure 3.1.13.1: Reaction scheme for the synthesis of PHENSS(OH)(DCL).....	73
Figure 3.2.1.1: The ^1H - ^{195}Pt HMQC spectrum of PHENSS in D_2O , performed on a Bruker Avance 400 MHz NMR spectrometer.	76
Figure 3.2.1.2: The ^1H NMR spectra of PHENSS in D_2O , showing proton assignment; performed on a Bruker Avance 400 MHz NMR spectrometer.	77
Figure 3.3.2.1: The ^1H - ^{195}Pt HMQC spectrum of PHENSSCl ₂ in D_2O , displaying the correlations between the platinum centre and the protons from each ligand; performed on a Bruker Avance 400 MHz NMR spectrometer.	79
Figure 3.3.2.2: The ^1H NMR spectra of PHENSSCl ₂ in D_2O , showing proton assignment; performed on a Bruker Avance 400 MHz NMR spectrometer.	80
Figure 3.3.2.3: The ^1H NMR spectra of 56MESSCl ₂ in D_2O , showing proton assignment; performed on a Bruker Avance 400 MHz NMR spectrometer.	81
Figure 3.3.2.4: The ^1H - ^{195}Pt HMQC spectrum of 56MESSCl ₂ in D_2O , displaying the correlations between the platinum centre and the protons from each ligand; performed on a Bruker Avance 400 MHz NMR spectrometer.	81
Figure 3.3.2.5: The ^1H NMR spectra of 5MESSCl ₂ in D_2O , showing proton assignment; performed on a Bruker Avance 400 MHz NMR spectrometer.	82
Figure 3.3.2.6: The ^1H - ^{195}Pt HMQC spectrum of 5MESSCl ₂ in D_2O , displaying the correlations between the platinum centre and the protons from each ligand; performed on a Bruker Avance 400 MHz NMR spectrometer.	83
Figure 3.3.2.7: Titration of a stock solution of PHENSSCl ₂ into a known concentration of H_2O and the resulting extinction coefficient calculated based on the two main peaks at 278 (red) and 208 nm (blue).....	84
Figure 3.3.2.8: UV spectra of PHENSSCl ₂ (green), PHENSSBr ₂ (purple)and, PHENSSI ₂ (blue); at room temperature in the 200–350 nm range, using a 10 mm quartz cell, corrected for solvent baseline.	84
Figure 3.3.2.9: Titration of a stock solution of 56MESSCl ₂ into a known concentration of H_2O and the resulting extinction coefficient calculated based on the two main peaks at 289 (red) and 211 nm (blue).....	85
Figure 3.3.2.10: UV spectra of 56MESSCl ₂ (green), 56MESSBr ₂ (purple)and, 56MESSI ₂ (blue); at room temperature in the 200–350 nm range, using a 10 mm quartz cell, corrected for solvent baseline.	86

Figure 3.3.2.11: Titration of a stock solution of 5MESSCL ₂ into a known concentration of H ₂ O and the resulting extinction coefficient calculated based on the two main peaks at 283 (red) and 210 nm (blue).....	87
Figure 3.3.2.12: UV spectra of 5MESSCL ₂ (green), 5MESSBr ₂ (purple) and, 5MESSI ₂ (blue); at room temperature in the 200–350 nm range, using a 10 mm quartz cell, corrected for solvent baseline.	88
Figure 3.3.2.13: UV spectra of PHENSSCL ₂ (green), 5MESSCL ₂ (purple) and, 56MESSCL ₂ (blue); at room temperature in the 200–350 nm range, using a 10 mm quartz cell, corrected for solvent baseline.	89
Figure 3.3.2.14: UV spectra of PHENSSBr ₂ (green), 5MESSBr ₂ (purple) and, 56MESSBr ₂ (blue); at room temperature in the 200–350 nm range, using a 10 mm quartz cell, corrected for solvent baseline.	90
Figure 3.3.2.15: UV spectra of PHENSSI ₂ (green), 5MESSI ₂ (purple) and, 56MESSI ₂ (blue); at room temperature in the 200–350 nm range, using a 10 mm quartz cell, corrected for solvent baseline.	91
Figure 3.2.2.17: CD spectra of 56MESSCL ₂ (green), 56MESSBr ₂ (purple) and, 56MESSI ₂ (blue); at room temperature in the 200–350 nm range, using a 10 mm quartz cell, corrected for solvent baseline.	93
Figure 3.2.2.18: CD spectra of 5MESSCL ₂ (green), 5MESSBr ₂ (purple) and, 5MESSI ₂ (blue); at room temperature in the 200–350 nm range, using a 10 mm quartz cell, corrected for solvent baseline.	94
Figure 3.2.2.20: SRCD spectra of PHENSSBr ₂ showing the raw data (black) and the 11 point smoothed data (red).....	95
Figure 3.2.2.21: SRCD spectra of PHENSSCl ₂ (black), PHENSSBr ₂ (red) and, PHENSSI ₂ (blue); at room temperature in the 170-400 nm range, using a 0.1 mm cell, corrected for solvent baseline.....	96
Figure 3.2.2.22: SRCD spectra of 5MESSCl ₂ (black), 5MESSBr ₂ (red) and, 5MESSI ₂ (blue); at room temperature in the 170-400 nm range, using a 0.1 mm cell, corrected for solvent baseline.....	97
Figure 3.2.2.23: SRCD spectra of 56MESSCl ₂ (black), 56MESSBr ₂ (red) and, 56MESSI ₂ (blue); at room temperature in the 170-400 nm range, using a 0.1 mm cell, corrected for solvent baseline.....	98
Figure 3.2.2.26: SRCD spectra of PHENSSI ₂ (black), 5MESSI ₂ (red) and, 56MESSI ₂ (blue); at room temperature in the 170-400 nm range, using a 0.1 mm cell, corrected for solvent baseline.	102
Figure 3.2.3.1: The ¹ H- ¹⁹⁵ Pt HMQC spectrum of PHENSS(OH)(OAc) in D ₂ O, displaying the correlations between the platinum centre and the protons from each ligand; performed on a Bruker Avance 400 MHz NMR spectrometer.	103
Figure 3.3.3.2: The ¹ H NMR spectra of PHENSS(OH)(OAc) in D ₂ O, showing proton assignment and Pt(II) impurity; performed on a Bruker	

Avance 400 MHz NMR spectrometer. * indicates stereocenter (SS).....	105
Figure 3.3.4.1: The ^1H NMR spectra of en-DCF in DMSO showing proton assignment; performed on a Bruker Avance 400 MHz NMR spectrometer.....	107
Figure 3.3.4.2: The ^1H NMR spectra of en-DCF in DMSO (blue) in comparison to the ^1H NMR spectra of DCF in DMSO (red) ; performed on a Bruker Avance 400 MHz NMR spectrometer.....	107
Figure 3.3.5.1: The ^1H NMR spectra of PHENSSDMSO ₂ in <i>d</i> -DMSO, showing proton assignment; performed on a Bruker Avance 400 MHz NMR spectrometer.....	109
Figure 3.3.6.1: ^1H NMR spectra of PHENSSenDCF ₂ in MeOD, showing proton assignment; performed on a Bruker Avance 400 MHz NMR spectrometer.....	111
Figure 3.2.7.1: The ^1H - ^{195}Pt HMQC spectrum of PHENSS(OH)(Succ) in D ₂ O, displaying the correlations between the platinum centre and the protons from each ligand; performed on a Bruker Avance 400 MHz NMR spectrometer.	112
Figure 3.2.7.2: ^1H NMR spectra of PHENSSenDCF ₂ in MeOD, showing proton assignment; performed on a Bruker Avance 400 MHz NMR spectrometer.....	114
Figure 3.2.8.1: The ^1H - ^{195}Pt HMQC spectrum of PHENSS(OH)(SuccPFP) in D ₂ O, performed on a Bruker Avance 400 MHz NMR spectrometer.....	115
Figure 3.2.8.1: The ^1H spectrum of PHENSS(OH)(SuccPFP) in D ₂ O, performed on a Bruker Avance 400 MHz NMR spectrometer.	115
Figure 3.3.9.1: The ^1H - ^{195}Pt HMQC spectrum of PHENSS(OH)(PSMA) in D ₂ O, displaying the correlations between the platinum centre and the protons from each ligand; performed on a Bruker Avance 400 MHz NMR spectrometer.	116
Figure 3.3.9.2: ^1H NMR spectra of DCF in D ₂ O, showing proton assignment; performed on a Bruker Avance 400 MHz NMR spectrometer.....	117
Figure 3.3.9.3: ^1H NMR spectra of PHENSS(OH)(PSMA) in D ₂ O, showing proton assignment; performed on a Bruker Avance 400 MHz NMR spectrometer.....	119
Figure 3.3.9.4: The aliphatic region of the ^1H NMR spectra of PHENSS(OH)(PSMA) in D ₂ O (blue) in comparison to the ^1H NMR spectra of PHENSS in D ₂ O (red) and DCL in D ₂ O (green); performed on a Bruker Avance 400 MHz NMR spectrometer.....	120
Figure 3.5.1.1: Cytotoxicity of 56MESS, 56MESS(OH) ₂ , cisplatin carboplatin and oxaliplatin over multiple cell lines: HT29 colon, U87 glioblastoma, MCF-7 breast, A2780 ovarian, H460 lung, A431 skin, Du145	

prostate, BE2-C neuroblastoma, SJ-G2 glioblastoma, and MIA
pancreas. 124

Figure 3.5.1.2: IC₅₀ values of 56MESSCl₂, 56MESSBr₂, 56MESSI₂, 56MESS, and
56MESSOH₂ in multiple cell lines: HT29 colon, U87 glioblastoma,
MCF-7 breast, A2780 ovarian, H460 lung, A431 skin, Du145
prostate, BE2-C neuroblastoma, SJ-G2 glioblastoma, MIA
pancreas, MCF10A breast (normal), and SMA glioblastoma
(murine)..... 126

Publications

Publications produced during candidature:

1. Brondwyn McGhie, N-Halogen Succinimides: Alternative Oxidants of Platinum Anticancer Agents, Australian Journal of Chemistry 2018, 397-398. DOI: 10.1071/CH18068 (solo author paper, impact factor: 1.059, 0 citations)
2. Krishant M.Deo, Dale L.Ang, Brondwyn McGhie, Adeline Rajamanickam, Ankita Dhiman, Aleen Khoury, Jason Holland, Aleksandra Bjelosevic, Benjamin Pages, Christopher Gordon, Janice R. Aldrich-Wright, Platinum coordination compounds with potent anticancer activity, 2018, 148-163. DOI: 10.1016/j.ccr.2017.11.014 (Impact factor: 14.499, 2 citations)

Abbreviations

44BPYRR	[Pt(4,4'-Dimethyl-2,2'-dipyridyl)(1 <i>R</i> ,2 <i>R</i> -diaminocyclohexane)] ²⁺
44BPYRR(OH)(OAc)	[Pt(4,4'-Dimethyl-2,2'-dipyridyl)(1 <i>R</i> ,2 <i>R</i> -diaminocyclohexane)(OH)(C ₂ H ₃ O ₂)] ²⁺
44BPYRR(OH) ₂	[Pt(4,4'-Dimethyl-2,2'-dipyridyl)(1 <i>R</i> ,2 <i>R</i> -diaminocyclohexane)(OH) ₂] ²⁺
44BPYSS	Pt(4,4'-Dimethyl-2,2'-dipyridyl)(1 <i>S</i> ,2 <i>S</i> -diaminocyclohexane)] ²⁺
44BPYSS(OH)(OAc)	[Pt(4,4'-Dimethyl-2,2'-dipyridyl)(1 <i>S</i> ,2 <i>S</i> -diaminocyclohexane)(OH)(C ₂ H ₃ O ₂)] ²⁺
44BPYSS(OH) ₂	Pt(4,4'-Dimethyl-2,2'-dipyridyl)(1 <i>S</i> ,2 <i>S</i> -diaminocyclohexane)(OH) ₂] ²⁺
4MERR	[Pt(4-methyl-1,10-phenanthroline)(1 <i>R</i> ,2 <i>R</i> -diaminocyclohexane)] ²⁺
4MERR(OH)(OAc)	[Pt(4-methyl-1,10-phenanthroline)(1 <i>R</i> ,2 <i>R</i> -diaminocyclohexane)(OH)(C ₂ H ₃ O ₂)] ²⁺
4MERR(OH) ₂	[Pt(4-methyl-1,10-phenanthroline)(1 <i>R</i> ,2 <i>R</i> -diaminocyclohexane)(OH) ₂] ²⁺
4MESS	[Pt(4-methyl-1,10-phenanthroline)(1 <i>S</i> ,2 <i>S</i> -diaminocyclohexane)] ²⁺
4MESS(OH)(OAc)	[Pt(4-methyl-1,10-phenanthroline)(1 <i>S</i> ,2 <i>S</i> -diaminocyclohexane)(OH)(C ₂ H ₃ O ₂)] ²⁺
4MESS(OH) ₂	[Pt(4-methyl-1,10-phenanthroline)(1 <i>S</i> ,2 <i>S</i> -diaminocyclohexane)(OH) ₂] ²⁺
56MERR	[Pt(5,6-dimethyl-1,10-phenanthroline)(1 <i>R</i> ,2 <i>R</i> -diaminocyclohexane)] ²⁺
56MERR(OH)(OAc)	[Pt(5,6-dimethyl-1,10-phenanthroline)(1 <i>R</i> ,2 <i>R</i> -diaminocyclohexane)(OH)(C ₂ H ₃ O ₂)] ²⁺
56MERR(OH) ₂	[Pt(5,6-dimethyl-1,10-phenanthroline)(1 <i>R</i> ,2 <i>R</i> -diaminocyclohexane)(OH) ₂] ²⁺
56MESS	[(5,6-dimethyl-1,10-phenanthroline)(1 <i>S</i> ,2 <i>S</i> -diaminocyclohexane)platinum(II)]
56MESS(OH)(OAc)	[Pt(5,6-dimethyl-1,10-phenanthroline)(1 <i>S</i> ,2 <i>S</i> -diaminocyclohexane)(OH)(C ₂ H ₃ O ₂)] ²⁺
56MESS(OH) ₂	Pt(5,6-dimethyl-1,10-phenanthroline)(1 <i>S</i> ,2 <i>S</i> -diaminocyclohexane)(OH) ₂] ²⁺
56MESSBr ₂	[Pt(5,6 dimethyl-1,10-phenanthroline)(1 <i>S</i> ,2 <i>S</i> -diaminocyclohexane)Br ₂] ²⁺
56MESSCl ₂	[Pt(5,6 dimethyl-1,10-phenanthroline)(1 <i>S</i> ,2 <i>S</i> -diaminocyclohexane)Cl ₂] ²⁺
56MESSI ₂	[Pt(5,6 dimethylphenanthroline)(1 <i>S</i> ,2 <i>S</i> -diaminocyclohexane)I ₂] ²⁺
5MERR	[Pt(5-methyl-1,10-phenanthroline)(1 <i>R</i> ,2 <i>R</i> -diaminocyclohexane)] ²⁺
5MERR(OH)(OAc)	[Pt(5-methyl-1,10-phenanthroline)(1 <i>R</i> ,2 <i>R</i> -diaminocyclohexane)(OH)(C ₂ H ₃ O ₂)] ²⁺
5MERR(OH) ₂	[Pt(5-methyl-1,10-phenanthroline)(1 <i>R</i> ,2 <i>R</i> -diaminocyclohexane)(OH) ₂] ²⁺
5MESS	[Pt(5-methyl-1,10-phenanthroline)(1 <i>S</i> ,2 <i>S</i> -diaminocyclohexane)] ²⁺
5MESS(OH)(OAc)	[Pt(5-methyl-1,10-phenanthroline)(1 <i>S</i> ,2 <i>S</i> -diaminocyclohexane)(OH)(C ₂ H ₃ O ₂)] ²⁺
5MESS(OH) ₂	[Pt(5-methyl-1,10-phenanthroline)(1 <i>S</i> ,2 <i>S</i> -diaminocyclohexane)(OH) ₂] ²⁺
5MESSBr ₂	[Pt(5 methyl-1,10-phenanthroline)(1 <i>S</i> ,2 <i>S</i> -diaminocyclohexane)Br ₂] ²⁺
5MESSCl ₂	[Pt(5 methyl-1,10-lphenanthroline)(1 <i>S</i> ,2 <i>S</i> -diaminocyclohexane)Cl ₂] ²⁺
5MESSI ₂	[Pt(5 methyl-1,10-phenanthroline)(1 <i>S</i> ,2 <i>S</i> -diaminocyclohexane)I ₂] ²⁺
A _L	Ancillary ligand
bpy	2,2-bipyridine
Carboplatin	Diammine[1,1-cyclobutanedicarboxylato(2-)]-O,O'-platinum(II)
CD	Circular dichroism
Cisplatin	Cis-diamminedichloroplatinum
d	Doublet
DCA	dichloroacetate
DCF	2-[2,6-dichlorophenylamino]phenyl acetate
DCFen	2-Aminoethyldiclofenacamide

DCL	N-[N-[(S)-1,3-dicarboxypropyl]carbamoyl]-(S)-lysine
DCM	Dichloromethane
dd	Doublet of doublets
DMSO	Dimethylsulfoxide
DNA	Deoxyribonucleic acid
EA	Elemental analysis
en	1,2 ethylenediamine
EPR	Enhanced permeability and the retention
ESIMS	Electrospray ionisation mass spectrometry
ϵ	Extinction coefficient
EtOH	Ethanol
Equiv	Equivalents
FR -	Folate receptor
HPLC	High-performance liquid chromatography
GI ₅₀	Half maximal inhibitory concentration
m	Multiplet
MeOH	Methanol
NASID	Nonsteroidal anti-inflammatory
NBS	N-bromosucinimide
NCS	N-chlorosucinimide
NIS	N-iodosucinimide
NMR	Nuclear magnetic resonance
OAc	Acetate
Oxaliplatin	(1 <i>R</i> ,2 <i>R</i>)-cyclohexane-1,2-diamine](ethanedioato-O,O')platinum(II)
PFP -	pentafluorophenol
PhB	phenylbutyrate
phen	1,10-phenanthroline
PHENRR	[Pt(1,10-phenanthroline)(1 <i>R</i> ,2 <i>R</i> -diaminocyclohexane)] ²⁺
PHENRR(OH)(OAc)	[Pt(1,10-phenanthroline)(1 <i>R</i> ,2 <i>R</i> -diaminocyclohexane)(OH)(C ₂ H ₃ O ₂)] ²⁺
PHENRR(OH) ₂	[Pt(1,10-phenanthroline)(1 <i>R</i> ,2 <i>R</i> -diaminocyclohexane)(OH) ₂] ²⁺
PHENSS	[Pt(1,10-phenanthroline)(<i>SS</i> -dach)] ²⁺
PHENSS(DMSO) ₂	[Pt(1,10-phenanthroline)(1 <i>S</i> ,2 <i>S</i> -diaminocyclohexane)(DMSO) ₂] ²⁺
PHENSS(OH)(OAc)	[Pt(1,10-phenanthroline)(1 <i>S</i> ,2 <i>S</i> -diaminocyclohexane)(OH)(C ₂ H ₃ O ₂)] ²⁺
PHENSS(OH) ₂	[Pt(1,10-phenanthroline)(1 <i>S</i> ,2 <i>S</i> -diaminocyclohexane)(OH) ₂] ²⁺
PHENSSBr ₂	[Pt(1,10-phenanthroline)(1 <i>S</i> ,2 <i>S</i> -diaminocyclohexane)Br ₂] ²⁺
PHENSSCl ₂	[Pt(1,10-phenanthroline)(1 <i>S</i> ,2 <i>S</i> -diaminocyclohexane)Cl ₂] ²⁺
PHENSSI ₂	[Pt(1,10-phenanthroline)(1 <i>S</i> ,2 <i>S</i> -diaminocyclohexane)I ₂] ²⁺
P _L	Polyaromatic ligands
PPC	Polyaromatic platinum complex
PSMA	Prostate-specific membrane antigen
Pt	Platinum
Pt(II)	Platinum(II)

Pt(IV)	Platinum(IV)
Pt(0)	Platinum (0)
RR-dach -	1 <i>R</i> ,2 <i>R</i> -diaminocyclohexane
s	Singlet
Satraplatin-	IS(acetatoO)amminedichlorido(cyclohexylamine)platinum(IV)
SS-dach	1 <i>S</i> ,2 <i>S</i> -diaminocyclohexane
SRCD	Synchrotron radiation circular dichroism
UV	Ultra violet
WSU	Western Sydney University

Chapter 1 Introduction

1.1 Cancer

Cancer is one of the leading causes of death worldwide with approximately 8 million deaths occurring each year.¹ In Australia approximately 470 per 100,000 people are predicted to be diagnosed with cancer in 2017 with a mortality rate of 161 per 100,000 people.² This takes a large toll on the quality of Australian lives and hospitals, with just under 40% of deaths being attributed to cancer.²⁻⁴ Cancer is characterised by the rapid uncontrolled proliferation of abnormal cells which can metastasise to different sites in the body. These growths result in obstruction of normal tissue function, eventually causing death.⁵ These abnormal cells are the result of mutation of deoxyribonucleic acid (DNA), occurring due to mutagens or during normal cell division. There are many different types of cancers; some are more easily prevented or cured when diagnosed early such as skin cancer, while others have high mortality rates.⁴ For example, brain cancer patients only have a 22% chance of surviving the first five years after diagnosis.^{6, 7}

1.2 Cancer treatments

Although changes in lifestyle and diet can reduce the occurrence of some cancers, over 70% cannot be prevented and thus treatment is needed.¹ There are currently several treatment options for most types of cancer; however, many of them have severe side effects and low success rates. For example brain cancer is treated with a combination of surgery, radiotherapy, chemotherapy or steroid therapy, and yet the low survival rates persist.⁷ Chemotherapy is the most common form of cancer therapy with just over 60% of patients receiving it as their primary form of treatment.^{4, 8} Of these patients, many are treated with platinum based drugs such as cisplatin or oxaliplatin in combination with other organic anticancer agents or physical techniques such as radiotherapy or surgery.^{4, 9} Most “traditional” platinum anticancer drugs have the basic formula *cis*-[PtX₂(NHR₂)₂], in which R = organic ligand and X = leaving group. The main

challenge of these treatments is low specificity for cancer cells, which results in lower than optimal dosage to mitigate negative side effects. The risk of resistance to the treatment developing is heightened when a suboptimal dosage is used.⁴ There are many researchers focusing on developing improved strategies for cancer to solve these problems.

1.2.1 Cisplatin

Cis-diamminedichloroplatinum(II) (cisplatin) was first identified by Barnett Rosenberg in 1965 as the compound that prevented cell division of *Escherichia coli*.¹⁰ He hypothesized that cisplatin and other platinum complexes would also be able to prevent the division of cancerous cells thus resulting in the death of the tumours. In 1978 it gained FDA approval and it is now one of the most widely used anticancer drugs.^{4, 11} Cisplatin is composed of a square planar platinum(II) coordinated to two chloride ligands and two ammine ligands (Figure 1.2.1). Its mechanism of action requires that the chloride ligands leave, allowing the platinum to bind covalently to DNA;¹² however, it has many other intracellular targets such as RNA, thiols, cytoskeletal microfilaments and phospholipids.^{13, 14} When cisplatin binds, it alters the shape of the DNA by unwinding, bending or forming crosslinks within the strand; these changes prevent transcription and trigger apoptosis.¹¹ Cisplatin can be absorbed by cells though both active and passive pathways.¹⁵ This interaction occurs in both cancerous and normal cells, although uptake of cisplatin is greater in rapidly dividing cells.⁴ This includes cancerous cells as well as epithelial and hair cells, resulting in deterioration of the skin and hair loss.¹⁶

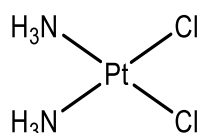


Figure 1.2.1: The chemical structure of the platinum(II) compound Cisplatin.

Cisplatin is highly effective against some forms of cancer; for example, the cure rate for testicular cancer is 95%. Cisplatin is also very effective against

lung, ovarian head and neck cancer.⁴ Despite this success, there are many disadvantages to the use of cisplatin as an anticancer drug. Cisplatin is susceptible to acquired resistance by cancer cells, in most cases only one treatment schedule can be completed before resistance occurs; thus, if a follow up treatment is required a different drug must be used.¹⁷ There are several mechanism by which resistance can occur, including upregulation of cisplatin binding proteins and peptides which deactivate cisplatin, reduced retention time within the cell, and upregulation of the natural repair mechanisms for DNA.^{18, 19} There are also several cancers that are inherently resistant to cisplatin treatments.^{17, 18, 20} The high toxicity of cisplatin is dose limiting, reducing the likelihood of curing the disease. Cisplatin is administered intravenously, which is complicated by its low solubility in aqueous solution and inflammation at the injection site.²¹ There are many side effects, including nausea and low white blood cell counts, which leaves the patient susceptible to disease.^{4, 22} Cisplatin is also toxic to the kidneys and can cause hearing loss.²³ Researchers aspire to create more potent platinum complexes with increased cytotoxicity that target cancer cells more effectively and will result in a better prognosis.

1.2.2 Carboplatin and oxaliplatin

Diammine[1,1-cyclobutanedicarboxylato(2-)]-O,O'-platinum(II) (carboplatin) (Figure 1.2.2) gained FDA approval following a collaboration between Johnson Matthey and the Institute of Cancer Research in London, when it was tested to see if a more stable leaving group would reduce the toxicity of the drug without reducing its anticancer activity.⁴ They were successful, with nephrotoxicity and neurotoxicity of carboplatin greatly reduced compared with cisplatin; this allowed it to be administered at two hundred times the dose of cisplatin (2000 mg/dose).²⁴ However, carboplatin has similar side effects to cisplatin, with greater than 30% of patients experiencing hair loss, taste changes, nausea and vomiting, weakness and blood test abnormalities (low magnesium).²⁵ Despite a higher administrative dose of carboplatin, the rate of DNA adduct formation is approximately ten times slower, resulting in treatment success rates that are essentially the same as

that of cisplatin.^{26, 27} Like cisplatin, carboplatin is susceptible to acquired resistance by cancer cells and is also cross-resistant, because it works *via* the same mechanism of action as cisplatin and induces what can be considered the same type of DNA crosslinks.^{4, 20, 25, 26}

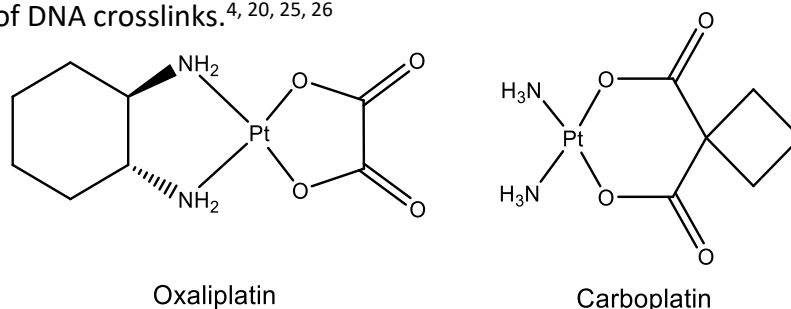


Figure 1.2.2: The chemical structures of the platinum(II) (Pt(II)) compounds carboplatin and oxaliplatin.

[(1*R*,2*R*)-cyclohexane-1,2-diamine](ethanedioato-*O*,*O'*)platinum(II) (Oxaliplatin) (Figure 1.2.2) was discovered in 1979 and approved internationally in 2009.⁴ It was used predominantly as a treatment for colorectal cancer.⁴ Oxaliplatin has similar anticancer activity to cisplatin, although it works *via* a slightly different mechanism; this limits the chance of cross resistance to cisplatin and carboplatin.^{20, 24} Oxaliplatin has many of the same side effects as cisplatin, and can also cause temporary nerve damage and loss of breath, but it is still widely used due to its lack of cross resistance and effectiveness against bowel and colorectal cancer, for which cisplatin has limited effectiveness.²⁸

1.3 Unconventional Pt drugs

By developing treatments with a different mechanism of action to cisplatin and its analogues we are potentially able to overcome both intrinsic and acquired resistance.²⁹ In fact, it has been suggested that the only way to improve the oncology of cancer treatments is to develop compounds whose structure and mechanism of action are significantly different to that of cisplatin.²⁹⁻³¹ These compounds are often referred to as non-classical or unconventional metal complexes and do not follow the same design “rules” as classical anticancer compounds. For example, it had been proposed that potential anticancer compounds should have no charge, and yet many non-classical metal complexes with proven anticancer activity are charged.^{18, 32, 33}

1.3.1 Polyaromatic platinum(II) complexes

One form of unconventional platinum complexes with a different mechanism of action to cisplatin are polyaromatic platinum complexes (PPCs) which have the general formula $[\text{Pt}(\text{P}_L)(\text{A}_L)]^{2+}$. The design of these complexes incorporates polyaromatic ligands (P_L) with a coordinated ancillary ligand (A_L) (Figure 1.3.1). Unlike cisplatin, this type of complex is substitutionally inert, thus it cannot covalently bind to DNA. Although no longer thought to be the mechanism of action they do bind to DNA through non-covalent intercalation where the P_L inserts between the base pairs of DNA.³⁴ This interaction does not form adducts with DNA although the interactions can both stretch or bend the helix (Figure 1.3.1). Intercalation is stabilised by hydrogen bonding and electrostatic interactions between the negative charge on the DNA phosphate backbone and the net positive charge of the PPC.³⁵ Although it was hypothesised that intercalation was responsible for the cytotoxicity of PPCs, it was subsequently demonstrated that enantiomeric pairs have bound to DNA with similar affinity despite large differences in cytotoxicity.³⁵ The mechanism of cytotoxicity is now proposed to be a result of interactions with other cellular mechanisms.^{34, 36} Complexes of this type have been reported to be significantly more potent than cisplatin in all cancer cell lines tested,³⁴ indicating the potential of these unconventional platinum complexes as a viable cancer treatment option.³² In particular, the complex [(5,6-dimethyl-1,10-phenanthroline)(1*S*,2*S*-diaminocyclohexane)platinum(II)] dichloride (56MESS, Figure 1.3.2) is over 100 times more cytotoxic than cisplatin to several cancer cells (Table 1.3.1.1). Improved cytotoxicity reduces the dosage required, treatment time and the reduces the chance of acquired resistance.³⁷ Despite encouraging *in vitro* activity, *in vivo* studies demonstrated low specificity and high toxicity in non-target organs similarly to cisplatin.³⁸ Subsequent studies are developing new methods to increase specificity and reduce toxicity.

Table 1.3.1.1: Cytotoxicity of complexes of the type $[\text{Pt}(\text{P}_L)(\text{A}_L)]^{2+}$ and $[\text{Pt}(\text{P}_L)(\text{A}_L)(\text{OH})_2]^{2+}$ compared to cisplatin, oxaliplatin and carboplatin.

Complex	MCF-7 <i>Breast</i> <i>n=3-4</i>	A2780 <i>Ovarian</i> <i>n=3-4</i>	H460 <i>Lung</i> <i>n=3-4</i>	A431 <i>Skin</i> <i>n=3-4</i>	Du145 <i>Prostate</i> <i>n=3-4</i>	MIA <i>Pancreas</i> <i>n=3-4</i>	ADDP <i>Ovarian</i> <i>n=3-4</i>
PHENSSDACH	0.53 ± 0.15	0.27 ± 0.029	0.48 ± 0.15	0.87 ± 0.28	0.081 ± 0.050	0.80 ± 0.65	0.24 ± 0.038
56MESSDACH	0.050 ± 0.020	0.030 ± 0.004	0.037 ± 0.009	0.051 ± 0.021	0.007 ± 0.002	0.015 ± 0.002	0.032 ± 0.007
56MESSDACH(OH) ₂	0.14 ± 0.000	0.063 ± 0.016	0.053 ± 0.010	0.10 ± 0.015	0.009 ± 0.003	0.027 ± 0.002	0.075 ± 0.019
cisplatin	6.5 ± 0.8	1.0 ± 0.1	0.9 ± 0.2	2.4 ± 0.3	1.2 ± 0.1	7.5 ± 1.3	1.2 ± 0.1
oxaliplatin	0.5 ± 0.1	0.16 ± 0.0	1.6 ± 0.1	4.1 ± 0.5	2.9 ± 0.4	0.9 ± 0.2	1.4 ± 0.1
carboplatin	>50	9.2 ± 2.9	14 ± 1.0	24.3 ± 2.2	14.7 ± 1.2	>50	14.3 ± 0.7

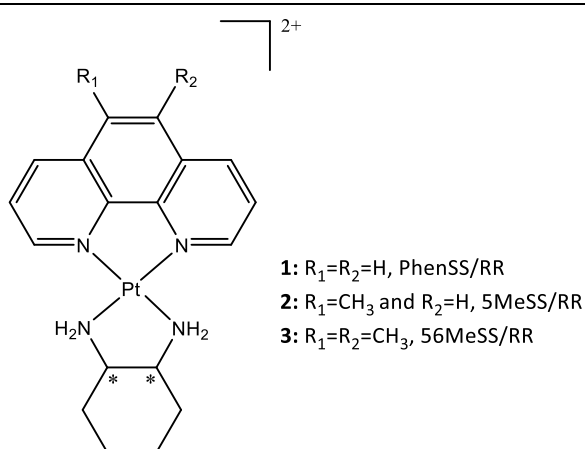


Figure 1.3.2 General structure of polyaromatic platinum(II) complexes.

*indicates a stereocentre, either *S* or *R*.

1.3.2 Platinum(IV) complexes

The oxidization of PPCs from Pt(II) to Pt(IV) enables two additional ligands to be bound to Pt, thus offering new design features to be explored.³⁹ Many different ligands have been assessed, several of which show increased targeting of cancer cells and comparable activity to cisplatin.^{34, 40, 41} Platinum(IV) complexes are hypothesised to act as prodrugs, i.e. they are inert *in vivo* until they are absorbed by the target cells and are reduced to the active platinum(II) form (Figure 1.3.3).⁴² The *in vitro* intercellular inertness is thought to minimise unwanted interactions with nucleophiles in the human blood serum; thus reducing side effects, increasing cellular dosage and, enhancing bioavailability.⁴³ This mechanism has been proven by the completion of phase three clinical trials by satraplatin; however, it was not approved for

chemotherapy worldwide due to not significantly improving the patients survival compared to drugs currently in the clinic.⁴⁴ The cytotoxicity of the Pt(II) complex correlates with that of the Pt(IV), i.e. the Pt(IV) complex should reduce to Pt(II) *in vitro* and produce the same cytotoxic effect.³⁹ There have been several different lines of inquiry as to which ligands would produce maximal efficacy. These include ligands that: change the overall lipophilicity or charge of the PC, increase the size of the complex to utilize the enhanced permeability and the retention (EPR) effect, have anticancer activity of their own or contain known targeting groups.^{34, 40, 41}

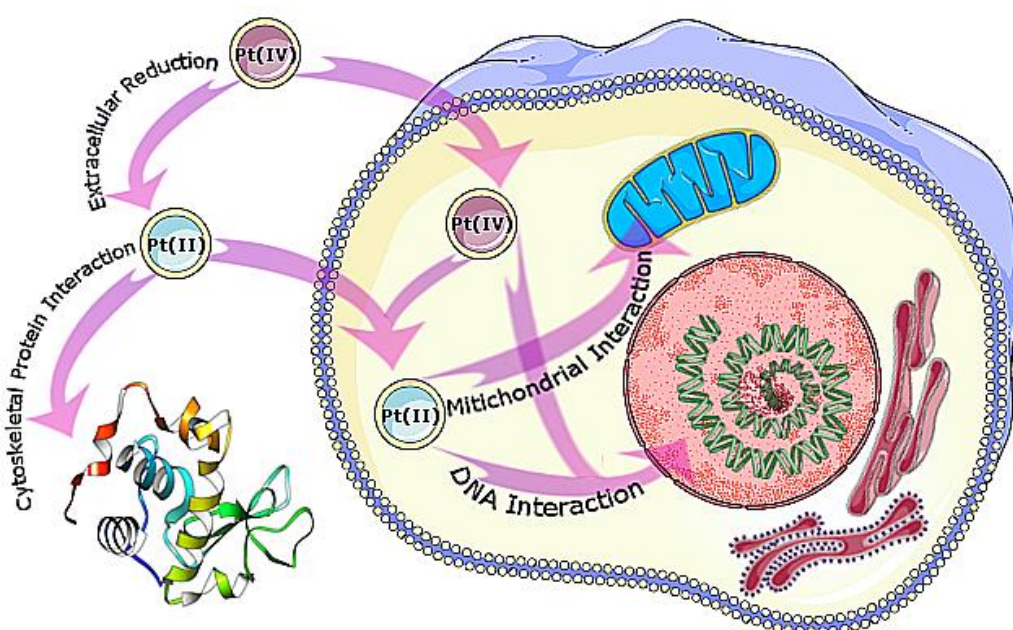


Figure 3.3.3: Intra- and extracellular reduction of Pt(IV), resulting in the loss of the axial ligands, producing a Pt(II) compound, showing potential mechanisms of action.^{41, 45} (X= axial ligand)

1.3.3 Advantages of platinum(IV) complexes with targeting Vectors.

Platinum(IV) prodrugs have the potential to deliver drugs specifically to tumour cells, which should limit unwanted side-effects and reduce the quantity of drug required for effective treatment.⁴³ Targeting may be accomplished through either active or passive methods.⁴⁶⁻⁴⁸ Passive targeting makes use of the disorganised vasculature and poor lymphatic drainage of cancer tissue.⁴⁷⁻

^{51,46, 52, 53} Macromolecules that range in size from 100 – 1200 nm are able to passively cross the cancer endothelium *via* the fenestrations, while normal cells have pore sizes smaller than 2 nm.⁴⁹ Additionally, removal of these molecules from cancer cells is impeded by poor lymphatic drainage. This phenomenon is termed the enhanced permeability and retention (EPR) effect (Figure 3.3.4).⁵⁴

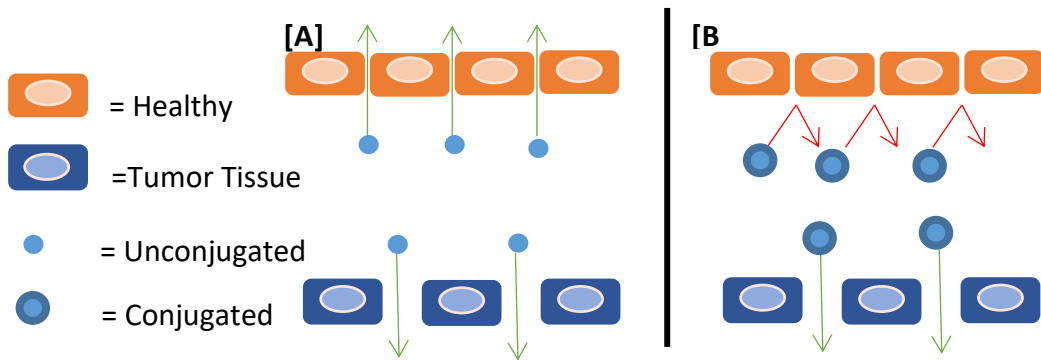


Figure 3.3.4: Enhanced permeability and retention (EPR) effect: A) Small drug size results in the diffusion of the unconjugated drug into both the healthy and tumour tissue. B) Larger drug size results in the diffusion of the conjugated drug into tumour tissue only.

Active targeting requires specific interactions between the prodrug and cancer cell; for example, receptors that are over-expressed on the surface of cancer cells have potential as cellular targets.^{46, 48, 50, 55} Active targeting then requires that the prodrug contains a targeting vector for that specific cellular receptor.^{46, 48, 50} However, the receptor must be overexpressed relative to normal cells,⁵⁶ should be recycled frequently,⁵⁷ and it must be in an accessible location such as the surface of cells.⁵⁸ Based on these principles, several prospective targets have been identified, including: folate receptor (FR); glucose transporter 1; prostate-specific membrane antigen (PSMA); and epidermal growth factor receptor.⁵⁸⁻⁶¹ Folic acid for example is an excellent candidate for a targeting ligand due to the overexpression of FR, the ease at which it may be derivatised, its high specificity and affinity, resistance to denaturing and low immunogenicity.^{58, 62-66} FRs are also largely absent from healthy tissue, reducing the likelihood of unwanted side effects while being

present in several different cancer types.^{58, 65-67} PSMA is also a good target for cancer treatment, as it is a trans-membrane protein overexpressed by essentially all prostate cancer cells. The expression of PSMA is increased in fast growing, poorly differentiated, intrinsically resistant, and metastatic cancers. PSMA is also expressed in gliomas (most common primary brain tumours) and several other solid tumours including those found in the pancreas, kidney and lung. There is also evidence that PSMA is overexpressed in the vascular endothelium, and targeting this structure may “starve” the cancer and consequently kill it.⁶⁸ Although some normal tissue (apart from in prostate cells) express PSMA, it is in relatively small amounts in cells not accessible through the vasculature, or are within the kidneys where they are potentially protected by the glomerulus (which would stop larger molecules passing). Treatments targeted to PSMA are hypothesised to: selectively target prostate cancers or vessels perfusing to cancer cells, accumulate significantly, reducing the risk of acquired resistance, and spare non target tissue in which PSMA is not expressed. A Lu-PSMA complex was recently awarded best image of the year by Society of Nuclear Medicine and Molecular Imaging, for a demonstration of exceptional responsiveness in patients with metastatic prostate cancer. This Phase II clinical trial drug demonstrated the viability of PSMA targeted therapies.⁶⁹ *N*-[*N*-[(*S*)-1,3-dicarboxypropyl]carbonyl]-(*S*)-lysine (DCL) is a part of a series of PSMA targeting ligands consisting of a urea base with attached amino acids, in this case lysine and glutamic acid.⁷⁰ DCL has been proven as a selective targeting agent as both a radio-imaging tool and as a delivery ligand for a non-platinum anticancer agent.⁷⁰⁻⁷² Binding DCL to Pt drugs is hypothesised to result in the active intake of the Pt-DCL complex in cells over expressing PSMA. The carboxylic acid groups make crossing lipophilic cell membranes of healthy tissue difficult, thus targeting cancer cells and reducing the risk of side effects.⁶⁸ DCL is therefore an excellent candidate to bind to Pt(IV) prodrugs to increase the specificity of their cytotoxic action.

1.3.4 Advantages of Pt(IV) complexes with bio-active ligands.

Pt(IV) derivatives of active Pt(II) complexes with bio-active ligands present a new method to further refine and enhance the suitability of Pt drugs as anticancer agent. As discussed above Pt(IV) analogues are considered pro-drugs as they are activated by reduction within cells. The hypothesis behind the use of bio-active ligands is that upon reduction of the Pt prodrug the axial ligands are released within cells and these ligands can be utilised to further enhance the cytotoxicity of the drug. The literature has many examples of ligands that are known antiproliferative agents, enzyme inhibitors/enhancers, cytotoxic agents or exhibit biological activity that works alongside Pt drugs or that help to overcome resistance to Pt drugs.⁷³⁻⁷⁸ Because these bioactive ligands have the potential to affect a variety of cellular mechanisms, their cytotoxic activity cannot be attributed to just one pathway; hence it would be more accurate to call them multi-action rather than dual action drugs.⁷⁷

Nonsteroidal anti-inflammatory drugs (NSAIDs) have been shown to inhibit the cyclooxygenase enzyme system which consequently leads to reduced tumour growth and angiogenesis.⁷⁹⁻⁸⁴ The anticancer effect of these compounds is achieved only at high concentrations and thus they have limited pharmacological activity.⁸⁴ However, these compounds attached to a Pt(IV) prodrug may achieve a high intracellular concentration without a high dosage. This hypothesis has been confirmed in the literature; a study in which NSAIDs were bound to cisplatin and its derivatives found that NSAID cellular concentration was high enough to change the reaction of the cell to the Pt(II) drug, promoting apoptosis.^{85, 86} An example of one such NSAID is 2-[2,6-dichlorophenylamino]phenyl acetate (DCF) which has proven anticancer activity and has also been bound to cisplatin by Brabec *et al.*⁸⁷ Their study demonstrates that cisplatin bound DCF is cytotoxic against cancer cell lines, and is more potent than cisplatin alone against cisplatin resistant cell lines. The DCF was bound to cisplatin in place of the chloride ions, forming a square planar Pt(II) complex (Figure 1.3.4.1). The DCF ligands are still cleaved intracellularly as per the normal cisplatin mechanism, allowing the cisplatin to bind to the DNA while the DCF affects multiple cellular pathways. Unlike most NSAIDs, DCF is not cyclooxygenase enzyme dependant; it instead works through mitochondrial

interaction, inhibiting glycolysis and lactate transport. DCF also modulates the phases of the cell cycle, enabling damaged cells to traverse the S phase. Thus DCF is a good candidate for further experimentation with different Pt anticancer agents and potentially new linkers.

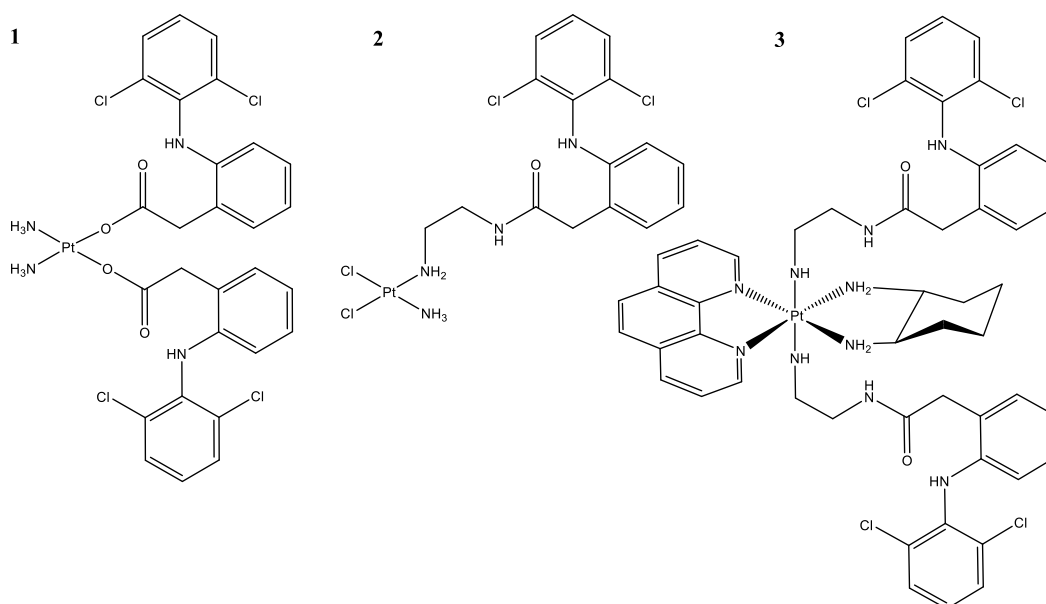


Figure 1.3.4.1: Examples of DCL complexes; complex **1**: *cis*-[PtCl₂(DCF)₂(NH₃)], complex **2**: *cis*-[Pt(DCF)₂(NH₃)₂] and complex **3**: [Pt(1,10-phenanthroline)(1S,2S-diaminocyclohexane)(2-Aminoethyldiclofenacamide)₂]²⁺.

1.3.5 Advantages of asymmetric Pt(IV) complexes.

Asymmetric Pt(IV) complexes allow for further fine tuning of the pharmacokinetics of a cytotoxic Pt(II) drug. Asymmetric complexes may be advantageous in one of two ways. Firstly, using two different cytotoxic axial ligands in a multi-action prodrug means a greater amount of different mechanisms of action per complex relative to one with two of the same axial ligand. Secondly, the use of two different axial ligands can profoundly affect the reduction potential of a platinum(IV) complex. The reduction potential is important because the activation of Pt(IV) prodrugs relies on the intracellular reduction of the complex, which is modulated by the nature of the axial ligands. The axial ligands must have a reduction potential high enough that it is

chemically inert extracellularly, providing the aforementioned advantages of Pt(IV) drugs such as being orally active. The reduction potential must also be low enough that it can be reduced once inside the cell, initiating its cytotoxic action.⁷⁷

When it comes to the reduction potential of Pt(IV) analogues, there are several variables that must be accounted for to elucidate any correlation between cytotoxicity and reduction potential. The reactivity of Pt(IV) is enhanced in the presence of intracellular reducing agents, ascorbic acid,⁸⁸ glutathione⁸⁹ and protein sulfhydryl.⁹⁰ Pt(IV) complexes may bind differently to DNA depending on these reaction conditions and the nature of the axial ligands.⁹¹ When the equatorial ligands are kept approximately the same and the axial ligands are varied a correlation between the electronegativity of the axial ligands and the speed of reduction is revealed. In general the more electronegative the ligands, the more destabilised the Pt(IV) state, resulting in faster reduction.⁹¹ In general this translates to hydroxyl ligands axial ligands reducing the slowest followed by acetate chloride and fluoroacetate. Rate of reduction is also dependant on the bulkiness of the axial ligands, with more bulky ligands reducing faster than smaller ligands. In this case the bulkiness of the equatorial ligands also contributes to the speed of reduction. The bulky ligands destabilise the octahedral Pt(IV) structure resulting in faster reduction to the more stable square planar structure.⁹¹ Everything else equal, cytotoxicity and reduction have a positive correlation, and thus the rate of reduction is an important consideration in the design of Pt(IV) pro-drugs. This conclusion leads to the understanding that in some cases binding two bioactive or targeting ligands may negatively affect the reduction rate and thus negatively affect the prodrugs cytotoxicity. It may therefore be essential for the efficiency of the drug to have two different axial ligands, one to enhance the efficiency of the cytotoxic mechanism and the other to ensure the timely reduction of the prodrug to release said cytotoxic agents.⁷⁷

Asymmetric ligands also offer a large library of potential prodrugs, where bioactive and targeting ligands can be mixed and matched to find the most efficient prodrug. This avenue also leads to dinuclear Pt(IV) compounds, which

combine two different Pt(II) analogues. For example, a dinuclear Pt(IV) compound was synthesised comprising of 56MESS and cisplatin joined by a linker, with two different cytotoxic agents covalently bound to each Pt centre; phenylbutyrate (PhB) and dichloroacetate (DCA) (Figure 1.3.5.1).⁹² This “quadruple action” complex was shown to have DNA binding, mitochondrial action as well as inhibition of histone deacetylase inhibitor, and it is suggested to have further action through the multiple possible cellular processes of each component i.e. the bioactive ligands and PCs way work via more than one mechanism. The combined mechanisms resulted in the GI₅₀ being higher than that of any of the individual components, and the complex is active in cisplatin resistant cells.⁹² These complexes have shown good activity in KRAS mutated cells, which is exciting as KRAS mutated cancers have been previously described as “undrugable”.⁹³ The KRAS gene is responsible for the activation of number of signalling molecules that affect cell differentiation, growth, chemotaxis and apoptosis.⁹⁴ It is a part of the RAS class of oncogenes meaning that their mutations are likely to become cancerous. KRAS mutations are the most common mutation to cause cancer, and occur in particularly high rates in some of the most deadly cancers, 97.7% of pancreatic ductal adenocarcinomas, 44.7% of colorectal adenocarcinomas and 30.9% of lung adenocarcinomas.⁹³ the multi-action dinuclear complexes mentioned above were tested against several lines of aggressive KRAS mutated cells and showed promising activity, significantly higher than that of cisplatin.⁹²

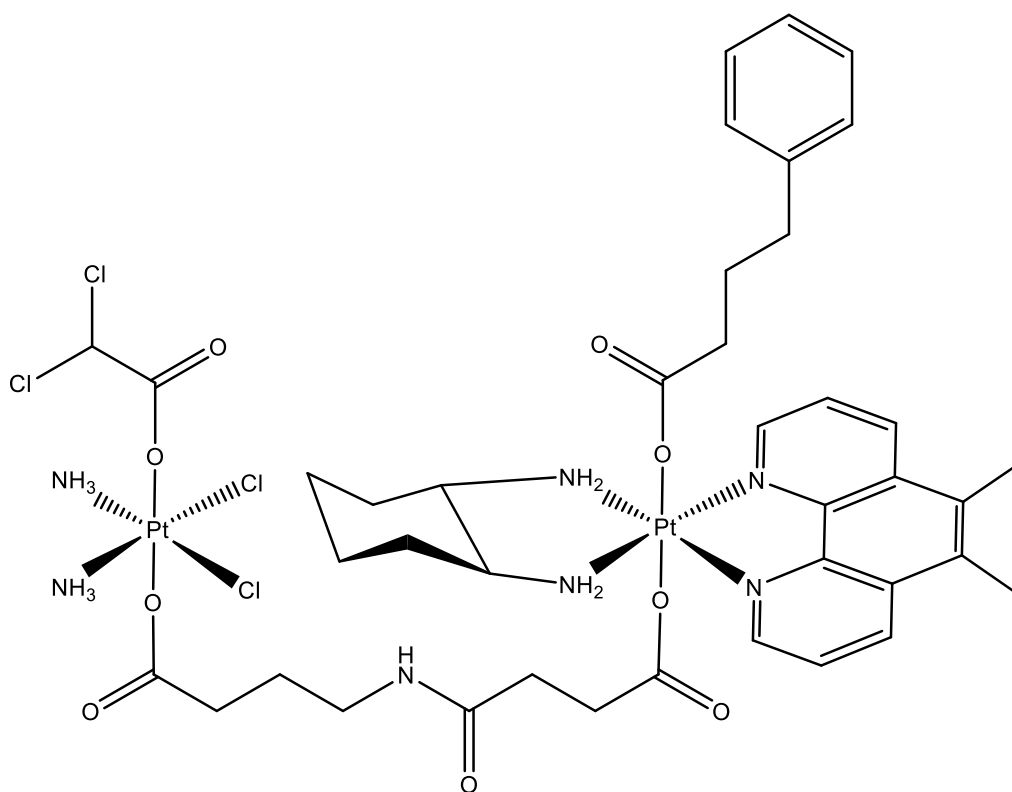


Figure 1.3.5.1: An example of an asymmetric dinedicarbonyl anticancer agent made up of 56MESS, cisplatin, PhB and DCA.⁹²

1.4 New synthetic procedures: continuous flow chemistry

Continuous flow chemistry refers to reactions that occur in a stream rather than in a batch as used in traditional synthesis chemistry. This usually involves pumping solutions through tubes containing reagents or catalysts bound to a solid phase. The stream can flow under pressure or at temperature and can be run with minimal supervision for extended periods of time. As exemplified in Figure 1.4.1 continuous flow chemistry set ups can include a multitude of parameters and intermediates which unlike in batch are undertaken as a part of a continuous system rather than purifying intermediates after each reaction as typically seen in batch chemistry.

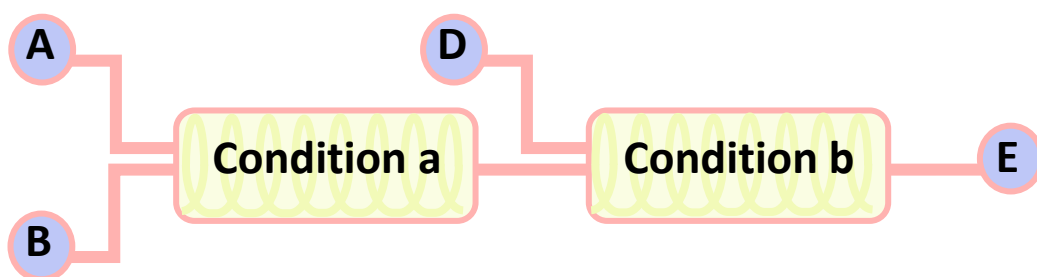


Figure 1.4.1: An example of a flow chemistry set up, where reactants A and B are combined under condition a to create the intermediate C before undergoing condition b and the addition of D to finally produce the final product E.

Continuous flow chemistry has many advantages over batch chemistry: it allows for more precise control of variables such as temperature and pressure, more efficient use of reagents and solvents, as well as reduction of reaction and purification time.⁹⁵ This leads to reduced cost of production as well as creating a safer work space, as the reaction is contained and minimal handling is necessary.⁹⁶ Continuous flow chemistry can also increase the sustainability of the synthesis by reducing waste and increasing the reproducibility of the results.⁹⁷ The current synthesis of 56MESS and analogues using batch chemistry is relatively time consuming with an average time for 2 days with an average yield of ~80% (Figure 2.4.1). Developing a continuous flow protocol for the synthesis of these PCs would reduce the amount of time and resources used during synthesis and purification. The development of such a protocol would be particularly significant as there are currently no reported applications of flow chemistry in the field of inorganic syntheses.

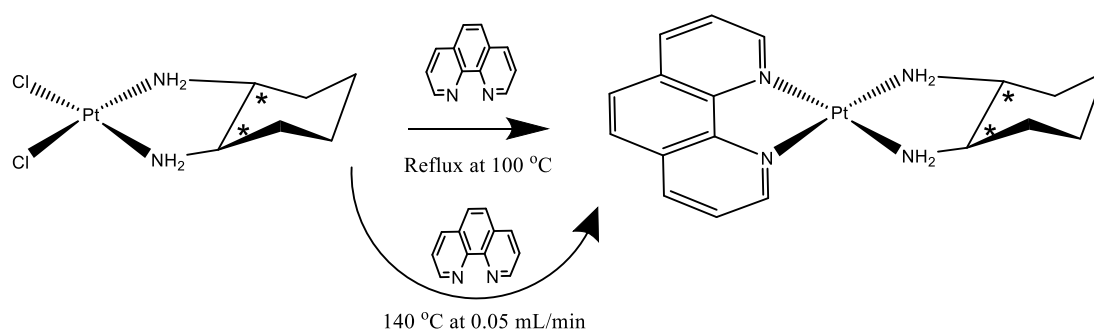


Figure 1.4.2: Reaction scheme for the batch chemistry method (top) and the flow chemistry method (bottom).

1.5 Project Aims

- **To produce a new protocol for the synthesis of $[\text{Pt}(\text{P}_L)(\text{A}_L)]^{2+}$ type complexes, that is more efficient than the current method. Continuous flow chemistry will be investigated to meet this aim which may produce novel findings in the use of flow chemistry for inorganic synthesis protocols.**

Pt(IV) polyaromatic complexes are producing promising preliminary *in vivo* results.³⁴ Further development of these compounds would be significantly assisted if their synthesis were to be automated using flow chemistry protocol. Another exciting aspect of the development of such a protocol is the novelty of using what is currently a technique used for purely organic chemistry and apply it to an inorganic synthesis. The main aim of this aspect of the project is to develop a synthesis that is straightforward and less time consuming than the batch synthesis while achieving the same if not better yields. This will be done by developing the flow protocol using much of the same strategy for optimisation of any other flow system, focusing on each reaction variable in turn until optimal results are achieved. Thus the aim is; to produce a new protocol for the synthesis of $[\text{Pt}(\text{P}_L)(\text{A}_L)]^{2+}$ type complexes, where (P_L) is an analogue of 1,10-phenanthroline (phen) and (A_L) is diaminocyclohexane (dach), that is more efficient than the current method.

- **To effectively oxidise Pt(II) complexes with halides Cl, Br, and I on the axial positions to produce $[\text{Pt}(\text{P}_L)(\text{A}_L)(\text{X}_2)]^{2+}$. The resulting compounds will be characterised and their biological activity determined.**

The coordination of halides (X) in the axial positions of the platinum(IV) complex $(c,c,t\text{-}[\text{Pt}(5,6\text{-dimethyl-1,10-phenanthroline}(56\text{Me}_2\text{phen}))(\text{SS-dach})(\text{X})_2]^{2+})$ will be investigated as a part of this project. It has been previously observed that reduction to platinum(II) occurs faster when the axial ligand is chlorine rather than oxygen, and thus it is hypothesized that the other halides will similarly affect the reduction rate and the pharmacology of these complexes.⁹ To explore their effect on cytotoxicity and pharmacokinetics, a

series of compounds with axially coordinated Cl, Br or I will be synthesised. They will be utilised as an intermediate to more efficiently coordinate other ligands onto the axial positions that can be targeting factors or have anticancer properties themselves. Using the resulting complexes, the effectiveness of substitution in the axial position by various ligands will be assessed, as well as the cytotoxicity of the resulting compounds in cell lines. The main aim of the synthesis of $[\text{Pt}(\text{A}_\text{L})(\text{P}_\text{L})(\text{X})_2]$ complexes is to identify a more efficient method of substitution onto the axial positions, which could be incredibly useful for attaching targeting groups such as folic acid and glucose.⁹⁸ The protocol used will be a modification of a previously described method which has already proven successful.⁹⁹

- **To develop a method for the synthesis of asymmetric compounds of the type $[\text{Pt}(\text{P}_\text{L})(\text{A}_\text{L})(\text{OH})(\text{C}_2\text{H}_3\text{O}_2)]^{2+}$.**

The third aim of the project is to develop a method for the synthesis of asymmetric Pt(IV) compounds which will offer further diversification of the platinum compounds able to be synthesised. These Pt(IV) compounds will incorporate acetate and hydroxido ligands to produce compounds of the type $[\text{Pt}(\text{P}_\text{L})(\text{A}_\text{L})(\text{OH})(\text{C}_2\text{H}_3\text{O}_2)]^{2+}$. The asymmetric design of these compounds will allow further asymmetric derivatisation of the Pt(IV) which may be advantageous in the design and synthesis of multi action drugs.

- **To investigate the substitution of targeting vectors onto $[\text{Pt}(\text{P}_\text{L})(\text{A}_\text{L})(\text{X}_2)]^{2+}$ as a potential method for more efficient cancer cell selectivity.**

The third aim of the project is to develop a method for the synthesis of asymmetric Pt(IV) compounds which will offer further diversification of the platinum compounds able to be synthesised. These Pt(IV) compounds will incorporate acetate and hydroxido ligands to produce compounds of the type $[\text{Pt}(\text{P}_\text{L})(\text{A}_\text{L})(\text{OH})(\text{C}_2\text{H}_3\text{O}_2)]^{2+}$. The asymmetric design of these compounds will allow further asymmetric derivatisation of the Pt(IV) which may be advantageous in the design and synthesis of multi action drugs.

- **To collaborate with other research labs, producing complexes that have the potential to increase targeting.**

The fourth aim of this project is to bind targeting ligands provided by international and local collaborators to PPCs of the type $[\text{Pt}(\text{P}_L)(\text{A}_L)(\text{OH})_2]^{2+}$ to determine their effectiveness. The synthesis of these compounds will further diversify the synthetic methods available to the research team at WSU, expanding the number and type of compounds able to be synthesised. These complexes have the potential to increase the viability of 56MESS (and analogues) as a drug, targeting specific types of cancers and reducing its systemic toxicity. As these targeting ligands will be developed with international and local collaborators; this project also serves to strengthen our position in the research field and our connections with these valuable collaborators.

- **To prepare manuscripts for publication: 1) Modifying the Pharmacokinetics of Platinum(IV) Complexes via Halogenation at axial positions and, 2/3) Substitution of Targeting Vectors Pt(IV) compounds.**

The first paper will be a synthesis and characterisation paper in which nine novel complexes will be synthesised, characterised using a combination of HPLC, NMR, ESI-MS, CD, SRCD microanalysis and biological testing. These complexes should have some interesting activity in cancer cell lines and have characterisation data different to other complexes of the same type which will be a point of interest for the paper. The second and third papers will be in collaboration with other researchers who have provided ligands which I will attach to our lab's complexes. These complexes will be novel and are hypothesised to have improved activity and pharmacokinetics.

Chapter 2 Materials and Methodology

2.1 Materials

Reagents were used as received unless otherwise specified. All solvents used were of analytical grade or higher. Potassium tetrachloroplatinate (K_2PtCl_4) was purchased from Precious Metals Online. Acetone, acetic acid, acetonitrile, dichloromethane (DCM), diethyl ether, ethyl acetate, hexane, hydrochloric acid, silver acetate, silver nitrate, *N*-iodosucinamide, *N*-chlorosucinamide, *N*-bromosucinamine, and sodium chloride were obtained from Sigma-Aldrich. Hydrogen peroxide was obtained from VWR. Methanol was obtained from Honeywell. DCL was purchased from Tokyo Chemical Industry and DCL was synthesised by B. Pages.¹⁰⁰ Deuterated solvents d_7 -Dimethylformamide (99.5%), d_6 -dimethylsulphoxide (99.9%), deuterium oxide (99.9%) and deuterated acetonitrile (99.8%) were purchased from Cambridge Isotope Laboratories. Acetone ($\geq 99.5\%$) was purchased from Biolab.

2.2 Instrumentation

1H NMR experiments were performed on a Bruker Avance 400 MHz NMR spectrometer. Using this instrument ^{13}C NMR experiments were performed at 101 MHz and ^{195}Pt NMR at 86 MHz. All compounds were dissolved in one of the following: D_2O , d_7 -DMF, d_3 - CD_3CN , d_2 - CD_2Cl_2 or d_6 -DMSO. The temperature in the probe was maintained at 25 °C. Spectra are referenced to the residual deuterated solvent peak. The following abbreviations apply to spin multiplicity: s (singlet), d (doublet), dd (doublet of doublets) t (triplet), q (quartet) and m (multiplet).

UV spectra were recorded on a Cary 1E spectrophotometer at room temperature in the 200–400 nm range, using a 10 mm quartz cell. All samples were automatically corrected for solvent baseline. Titration of a stock solution into a known volume of solvent allowed the calculation of the extinction coefficient, a measure of the absorbance at a given wavelength per mass density.

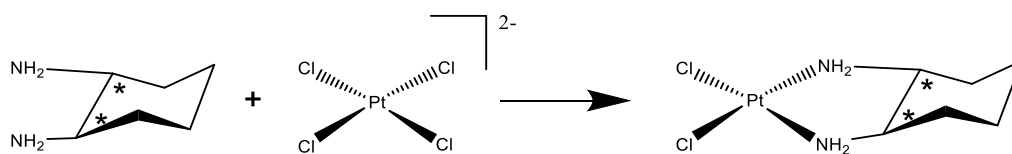
CD spectra were obtained using a Jasco-810 spectropolarimeter at room temperature. The instrument was left to equilibrate for 30 minutes prior to use. Spectra were obtained in a 10 mm quartz cell, and were measured from 400–200 nm with a data pitch of 1 nm, bandwidth of 1 nm and response time of 1 second. For each spectrum, 40 accumulations were collected and a water baseline was subtracted

Electrospray ionisation mass spectrometry (ESIMS) experiments, in the positive mode, were performed using a Waters TQ-MS triple quadrupole mass spectrometer. Sample solutions were made up to 0.5 mM in H₂O and flowed at 0.1 mL/min. A desolvation temperature of 300 °C, desolvation flow rate (nitrogen) of 500 L/hr remained consistent whilst the cone voltage and capillary voltage were varied for each sample in order to adjust for fragmentation. Spectra were collected over varied m/z ranges depending on the target mass.

Samples were purified using the Reveleris® X2 flash chromatography system fitted with a Reveleris® reverse phase C₁₈ 4 g column. The column was equilibrated to 3% MeOH in water for 2.4 min at 8 mL/min, and the samples run for 9 minutes with the UV detector sensitivity on high and detecting at 230, 254 and 280 nm. Samples between 20 and 100 mg were prepared in ~1-2 mL H₂O injected and eluted with a flow rate of 8 mL/min. The column was eluted with 3% MeOH for 6 minutes then MeOH was increased to 100% over 1 minute, kept steady for 1 minute before returning to 3% over another minute. Only one product peak was detected and this was collected in 10 mL fractions.

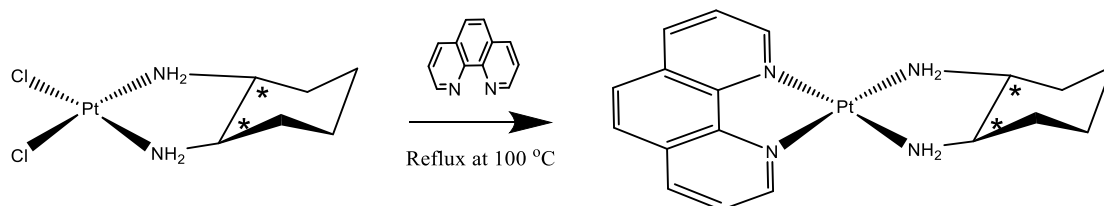
2.3 Synthesis

2.3.1 Synthesis of $[\text{Pt}(1\text{S},2\text{S-diaminocyclohexane})\text{Cl}_2]^{2+}$



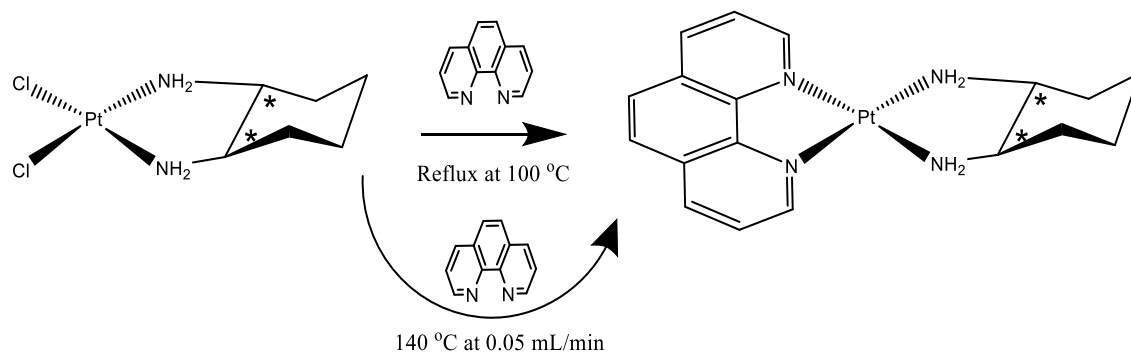
The synthesis of $\text{Pt}(1\text{S},2\text{S-diaminocyclohexane})\text{Cl}_2$ and $\text{Pt}(1\text{R},2\text{R-diaminocyclohexane})\text{Cl}_2$ was achieved using the published method.¹⁰¹ Potassium tetrachloroplatinate (307.5 mg; 7.41 mmol; 1 equiv.) was dissolved in 30 mL of deionized water and filtered using a 45 micrometre syringe filter. Then either 1S,2S-diaminocyclohexane (*SS-dach*) or 1R,2R-diaminocyclohexane (*RR-dach*) (350.2 mg; 3.05 mmol ;1.1 equiv.) was added to the solution which was then sealed and cooled to 4 °C for approximately 48 hrs, at which point the solution turned an opaque pale orange and a yellow precipitate had formed. The solution was then filtered and washed three times with 3 mL aliquots of deionized water. The pure product was then dried in a desiccator for several days. $[\text{Pt}(\text{SS-dach})\text{Cl}_2]$, yield 254.7 mg, 90.0 %: ^1H NMR (400 MHz, $\text{d}_6\text{-DMSO}$) δ 5.56 (d, $J = 8.2\text{Hz}$, 1H), 5.03 (s, 1H), 2.08 (s, 1H), 1.85 (d, 1H, $J = 12.6\text{ Hz}$), 1.44 (d, 1H, $J = 8.4\text{ Hz}$), 1.24 (s, 1H), 0.96 (t, 1H, $J = 9.7\text{ Hz}$). $\text{Pt}(\text{RR-dach})\text{Cl}_2$, yield 254.7 mg, 90.0 %: ^1H NMR (400 MHz, $\text{d}_6\text{-DMSO}$) δ 5.56 (d, 1H, $J = 8.2\text{Hz}$), 5.03 (s, 1H), 2.08 (s, 1H), 1.85 (d, 1H, $J = 12.6\text{ Hz}$), 1.44 (d, 1H, $J = 8.4\text{ Hz}$), 1.24 (s, 1H), 0.96 (t, 1H, $J = 9.7\text{ Hz}$).

2.3.2 Synthesis of [Pt(1,10phenanthroline)(1S,2S-diaminocyclohexane)]²⁺ (Batch)



The batch synthesis of [Pt(phen)(SS-dach)]²⁺ (PHENSS) was achieved using the published method.¹⁰¹ [Pt(SS-dach)Cl₂] (307.5 mg; 85.4 mmol: 1 equiv.) and phen (164.5 mg : 91.3 mmol: 1.1 equiv.) were refluxed for 24 hrs, resulting in the solution transforming from an opaque pale yellow to a clear yellow-orange solution. The volume was then reduced to allow purification *via* a Vac 20cc (5 g) C₁₈ Sep-Pak® column connected to a pump apparatus with UV detector (Bio-Rad, EM-1 Econo™ UV Monitor). The column was activated with methanol (20 mL) and then flushed with water (~40 mL) until the UV absorbance equilibrated. The purified solution was then reduced under vacuum and freeze dried. Yield 393.6 mg, 86.5 %. ¹H NMR (400 MHz, D₂O) δ 8.88 (m, 4H, CH), 8.13 (s, 2H, CH), 7.98 (dd, 2H, CH, *J* = 8.36, 8.50 Hz), 2.70 (m, 2H, CH), 2.20 (d, 2H, CH, *J* = 10.97), 1.62(m, 2H, CH), 1.46 (m, 2H, CH), 1.23 (m, 2H, CH).

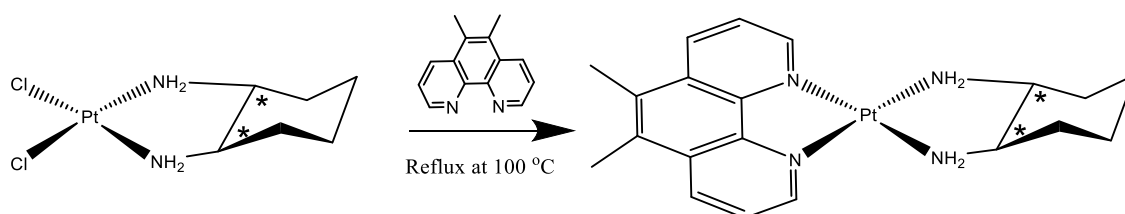
2.3.3 Synthesis of [Pt(1,10-phenanthroline)(1S,2S-diaminocyclohexane)]²⁺ (Flow)



The flow synthesis of PHENSS was developed and optimized to be as follows. [Pt(SS-dach)Cl₂]²⁺ (118.0 mg; 47.35 mmol: 1.1 equiv.) and phen (78.8

mg : 43.72 mmol: 1.equiv.) were heated in a 10 x 100 mm Omnifit column to 140 °C under 100 PSI. The reaction ran for 1.5 hrs at 0.05 mL/min. The crude product was purified *via* a Vac 20cc (5 g) C₁₈ Sep-Pak® column as per the methods in the batch synthesis. The purified solution was then freeze dried in a minimal volume of deionized water (~2 mL). Yield 91.1 mg, 49.6%. ¹H NMR (400 MHz, D₂O) δ 8.92 (m, 4H: CH), 8.11 (s, 2H: CH), 7.98 (dd, 2H: CH, *J* = 8.3, 5.4 Hz), 2.70 (dd, 2H: CH, *J* = 12.2, 8.3 Hz), 2.21 (d, 2H: CH, *J* = 12.7 Hz), 1.83 (s, 6H: CH₃), 1.65 (d, 2H: CH, *J* = 8.9 Hz), 1.46 (d, 2H: CH, *J* = 8.6 Hz), 1.13 (m, 2H: CH).

2.3.4 Synthesis of Pt(II) complexes of the type [Pt(P_L)(A_L)]²⁺



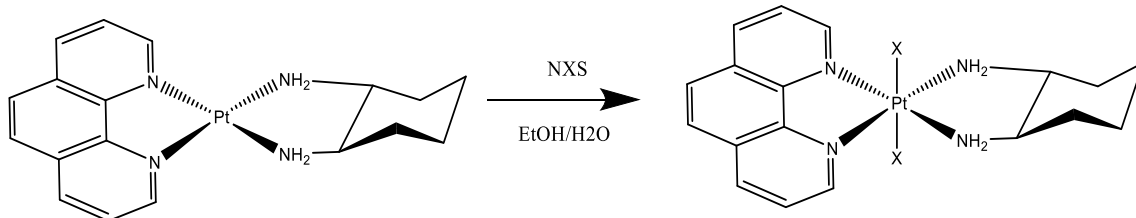
Pt(II) complexes of the type [Pt(P_L)(A_L)]²⁺ was achieved using the method described in B.Pages *et al* 2014.¹⁰¹ P_L (1 equiv) and A_L (1.1 equiv) were refluxed for 48 hrs, resulting in the solution transforming from an opaque pale yellow to a clear yellow orange. The volume was then reduced to allow purification via a Vac 20cc (5 g) C₁₈ Sep-Pak® column connected to a pump apparatus with UV detector (Bio-Rad, EM-1 Econo™ UV Monitor). The column was activated with methanol (20 mL) and then flushed with water (~40 mL) until the UV absorbance equilibrated.. The purified solution was then freeze dried in a minimal volume of deionized water (~2 mL) to produce a pale yellow solid.

This method was utilised to synthesise; [Pt(56Me₂phen)(SS-dach)]²⁺ (56MESS), [Pt(56Me₂phen)(RR-dach)]²⁺ (56MERR), [Pt(phen)(SS-dach)]²⁺ (PHENSS), [Pt(phen)(RR-dach)]²⁺(PHENRR), [Pt(5-methyl-1,10-phenanthroline(5Mephen))(SS-dach)]²⁺ (5MESS), [Pt(5Mephen)(RR-dach)]²⁺ (5MERR), [Pt(4-methyl-1,10-phenanthroline(4Mephen))(SS-dach)]²⁺ (4MESS), [Pt(4Mephen)(RR-dach)]²⁺(4MERR), [Pt(4,4'-Dimethyl-2,2'-dipyridyl(44BPY))(SS-dach)]²⁺(44BPYSS), and [Pt(44BPY)(RR-dach)]²⁺(44BPYRR). Yields and NMR data are displayed in Table 2.3.4.1

Table 2.3.4.1 Summary of NMR data of Pt(II) complexes of the type [Pt(P_L)(A_L)]²⁺ complexes, showing chemical shift (ppm) with integration, multiplicity and coupling constants. Experiments were performed in D₂O, so amine resonances were not observed due to proton exchange.

Label	Complex									
	PHENSS	PHENRR	56MESS	56MERR	5MESS	5MERR	4MESS	4MERR	44BPYSS	44BPYRR
H4	8.87 (d, 2H: CH, k J= 5.35 Hz)	8.88 (d, 2H: CH, k = 5.58 Hz)	8.78 (d, 1H: CH, J= 5.32Hz)	8.78 (d, 1H: CH, J= 4.87 Hz)	8.66 (d, 1H: CH, J= 8.29 Hz)	8.69 (d, 1H: CH, J= 8.44 Hz)	-	-	-	-
H7	-	-	-	-	8.5 (d, 1H: CH, J= 8.90 Hz)	8.89 (d, 1H: CH, J= 8.63 Hz)	8.86 (d, 1H: CH, J= 5.34 Hz)	8.87 (d, 1H: CH, J= 5.48 Hz)	-	-
H3	7.97 (dd, 2H: CH, J= 8.37, 8.46 Hz)	7.98 (dd, 2H: CH, J= 8.44, 8.47 Hz)	7.94 (dd, 1H: CH, J=8.48, 8.37 Hz)	7.95 (dd, 1H: CH, J=8.71, 8.58 Hz)	7.92 (dd, 1H: CH, J= 7.98, 8.29 Hz)	7.92 (dd, 1H: CH, J= 5.57, 8.32Hz)	7.80 (d, 1H: CH, J= 5.64 Hz)	7.81 (d, 1H: CH, J= 5.65 Hz)	8.11 (s, 2H: CH)	8.13 (s, 2H: CH)
H8	-	-	-	-	7.97 (dd, 1H: CH, J= 8.34, 8.44 Hz)	7.98 (dd, 1H: CH, J= 5.57, 8.44 Hz)	7.95 (dd, 1H: CH, J= 8.34, 8.26 Hz)	7.95 (dd, 1H: CH, J= 8.54, 8.26 Hz)	-	-
H2	8.48 (d, 2H: CH, J= 8.50 Hz)	8.86 (d, 2H: CH, J= 8.28 Hz)	8.90 (d, 1H: CH, J= 8.76 Hz)	8.89 (d, 1H: CH, J= 8.72Hz)	8.77 (d, 1H: CH, J= 5.36 Hz)	8.78 (d, 1H: CH, J= 5.72Hz)	8.84 (d, 1H: CH, J= 8.93 Hz)	8.84 (d, H: CH, J= 8.54 Hz)	-	-
H9	-	-	-	-	8.83 (d, 1H: CH, J= 5.04 Hz)	8.85 (d, 1H: CH, J= 5.49 Hz)	8.67 (d, 1H: CH, J= 5.55 Hz)	8.68 (d, 1H: CH, J= 5.82Hz)	-	-
H5	8.07 (s,2H; CH)	8.11 (s,2H; CH)	-	-	-	-	8.18 (d, 1H: CH, J= 9.26 Hz)	8.19 (d, 1H: CH, J= 9.29 Hz)	7.49 (d, 1H: CH, J= 6.12Hz)	7.48 (d, 1H: CH, J= 5.51Hz)
H6	-	-	-	-	7.73 (s,1H; CH)	8.09 (s,1H; CH)	8.07 (d, 1H: CH, J= 9.26 Hz)	8.08 (d, 1H: CH, J= 8.22Hz)	8.29 (d, 1H: CH, J= 5.51Hz)	8.28 (d, 1H: CH, J= 5.90 Hz)
CH ₃	-	-	2.64 (s, 6H; CH ₃)	2.63 (s, 6H; CH ₃)	2.72 (s, 3H; CH ₃)	2.85 (s, 3H; CH ₃)	2.85 (s, 3H; CH ₃)	2.86 (s, 3H; CH ₃)	2.49 (s, 6H; CH ₃)	2.49 (s, 6H; CH ₃)
H1'/2'	2.71 (m, 2H; CH ₂)	2.70 (m, 2H; CH ₂)	2.70 (m, 2H; CH ₂)	2.70 (m, 2H; CH ₂)	2.70 (m, 2H; CH ₂)	3.35 (m, 2H; CH ₂)	2.69 (m, 2H; CH ₂)	2.69 (m, 2H; CH ₂)	2.59 (m, 2H; CH ₂)	2.59 (m, 2H; CH ₂)
H3'/6'	2.21 (d, 2H; CH ₂ , J=14.86 Hz)	2.20 (d, 2H; CH ₂ , J=13.37 Hz)	2.21 (d, 2H; CH ₂ J= 12.57 Hz)	2.21 (d, 2H; CH ₂ J= 12.57 Hz)	2.21 (d, 2H; CH ₂ J= 13.44 Hz)	2.36 (d, 2H; CH ₂ J= 12.09 Hz)	2.20 (d, 2H; CH ₂ J= 13.18 Hz)	2.19 (d, 2H; CH ₂ J= 13.18 Hz)	2.14 (d, 2H; CH ₂ J= 13.00 Hz)	2.14 (d, 2H; CH ₂ J= 13.00 Hz)
H4'/5'	1.46 (m, 2H; CH ₂)	1.65 (m, 2H; CH ₂)	1.65 (m, 2H; CH ₂)	1.1.66 (m, 2H; CH ₂)	1.65 (m, 2H; CH ₂)	1.72 (m, 2H; CH ₂)	1.61 (m, 2H; CH ₂)	1.64 (m, 2H; CH ₂)	1.61 (m, 2H; CH ₂)	1.61 (m, 2H; CH ₂)
H3'/6'	1.65 (m, 2H; CH ₂)	1.46 (m, 2H; CH ₂)	1.46 (d, 2H; CH ₂ J= 12.49 Hz)	1.45 (d, 2H; CH ₂ J= 12.03 Hz)	1.47 (d, 2H; CH ₂ J= 10.90 Hz)	1.66 (d, 2H; CH ₂ J= 10.90 Hz)	1.45 (m, 2H; CH ₂)	1.44 (m, 2H; CH ₂)	1.39 (m, 2H; CH ₂)	1.39 (m, 2H; CH ₂)
H4'/5'	1.23 (m, 2H; CH ₂)	1.23 (m, 2H; CH ₂)	1.23 (m, 2H; CH ₂)	1.23 (m, 2H; CH ₂)	1.23 (m, 2H; CH ₂)	1.30 (m, 2H; CH ₂)	1.22 (m, 2H; CH ₂)	1.23 (m, 2H; CH ₂)	1.19 (m, 2H; CH ₂)	1.19 (m, 2H; CH ₂)
¹ H/ ¹⁹⁵ Pt	8.96/-2823.4	8.97/-2823.6	9.66/-2759.2	9.05/-2753.7	8.92/-2757.8	8.94/-2757.9	9.64/-3189.2	9.59/-3120.5	8.36/-2811.8	8.36/-2814.4
%Yield	90	89	90	85	87	88	78	81	75	76

2.3.5 Synthesis of complexes of the type $[\text{Pt}(\text{P}_L)(\text{A}_L)] \text{X}_2]^{2+}$



The synthesis of $[\text{Pt}(\text{A}_L)(\text{P}_L)\text{X}_2]^{2+}$ (where $\text{X} = \text{Cl}, \text{Br}$ or I , $\text{P}_L = \text{Phen}, 56\text{Me}_2\text{phen}$ or 5Mephen and $\text{A}_L = \text{SS-dach}$) was achieved using the following method. The Pt(II) complex (1 equiv) and *N*-halogensuccinimide (2.4 equiv) were combined and left to react in a 9 mL solution of 1:1:1 $\text{H}_2\text{O}:\text{EtOH}:1 \text{ M HCl}$. After approximately 2 hr the reaction was stopped by evaporation under vacuum. To purify the product, the reaction was redissolved in water and eluted through a Vac 2Occ (5 g) C_{18} Sep-Pak[®] column connected to a pump apparatus with UV detector (Bio-Rad, EM-1 Econo[™] UV Monitor). The column was activated with methanol (20 mL) and then flushed with water (~40 mL) until the UV absorbance equilibrated. The first and last band of three to elute were identified as impurities whilst the second band contained the major product. The compound was further purified using toluene in a soxhlet apparatus. If impurities remained after this process, the sample was further purified using the Reveleris[®] X2 flash chromatography system fitted with a Reveleris[®] reverse phase C_{18} 4 g column and eluted with MeOH and H_2O (see Section 2.2 Instrumentation for details).

$[\text{Pt}(\text{phen})(\text{SS-dach})\text{Cl}_2]^{2+}$ (PHENSSCl₂), $[\text{Pt}(\text{phen})(\text{SS-dach})\text{Br}_2]^{2+}$ (PHENSSBr₂), $[\text{Pt}(\text{phen})(\text{SS-dach})\text{I}_2]^{2+}$ (PHENSSI₂), $[\text{Pt}(56\text{Me}_2\text{phen})(\text{SS-dach})\text{Cl}_2]^{2+}$ (56MESSCl₂), $[\text{Pt}(56\text{Me}_2\text{phen})(\text{SS-dach})\text{Br}_2]^{2+}$ (56MESSBr₂), $[\text{Pt}(56\text{Me}_2\text{phen})(\text{SS-dach})\text{I}_2]^{2+}$ (56MESSI₂), $[\text{Pt}(5\text{Mephen})(\text{SS-dach})\text{Cl}_2]^{2+}$ (5MESSCl₂), $[\text{Pt}(5\text{Mephen})(\text{SS-dach})\text{Br}_2]^{2+}$ (5MESSBr₂), and $[\text{Pt}(5\text{Mephen})(\text{SS-dach})\text{I}_2]^{2+}$ (5MESSI₂), were all synthesised using this method.

Table 2.3.5.1: Summary of NMR data of complexes of the type $[\text{Pt}(\text{A}_L)(\text{P}_L)\text{X}_2]^2$, showing chemical shift (ppm) with integration, multiplicity and coupling constants. Experiments were performed in D_2O , so amine resonances were not observed due to proton exchange.

Label	Complex No.								
	PHENSSCl ₂	PHENSSBR ₂	PHENSSI ₂	5MESSCl ₂	5MESSBR ₂	5MESSI ₂	56MESSCl ₂	56MESSBR ₂	56MESSI ₂
H4	9.07 (d, 2H: CH, <i>k</i> <i>J</i> = 8.31Hz)	9.03 (d, 2H: CH, <i>J</i> = 8.17 Hz)	9.04 (d, 2H: CH, <i>J</i> = 8.43 Hz)	8.90 (d, 1H: CH, <i>J</i> = 8.28 Hz)	8.89 (d, 1H: CH, <i>J</i> = 8.50 Hz)	8.91 (d, 1H: CH, <i>J</i> = 8.44 Hz)	9.14 (d, 1H: CH, <i>J</i> = 8.42 Hz)	9.13 (d, 1H: CH, <i>J</i> = 8.65 Hz)	9.07 (d, 1H: CH, <i>J</i> = 8.58 Hz)
H7	-	-	-	9.13 (d, 1H: CH, <i>J</i> = 8.37 Hz)	9.11 (d, 1H: CH, <i>J</i> = 8.50 Hz)	9.14 (d, 1H: CH, <i>J</i> = 8.72Hz)	-	-	-
H3	8.27 (dd, 2H: CH, <i>J</i> = 5.52, 8.35 Hz)	8.26 (dd, 2H: CH, <i>J</i> = 5.47, 8.17 Hz)	8.27 (dd, 2H: CH, <i>J</i> = 5.41, 8.22Hz)	8.20 (dd, 1H: CH, <i>J</i> = 5.57, 8.32Hz)	8.17 (dd, 1H: CH, <i>J</i> = 5.83, 7.85 Hz)	8.20 (dd, 1H: CH, <i>J</i> = 5.26, 8.21Hz)	8.24 (dd, 1H: CH, <i>J</i> =5.48, 8.56 Hz)	8.21 (dd, 1H: CH, <i>J</i> = 5.55, 8.55 Hz)	8.20 (dd, 1H: CH, <i>J</i> = 5.56, 8.56 Hz)
H8	-	-	-	8.29 (dd, 1H: CH, <i>J</i> = 5.57, 8.44 Hz)	8.25 (dd, 1H: CH, <i>J</i> = 5.60, 8.56 Hz)	8.29 (dd, 1H: CH, <i>J</i> = 2.44, 5.62Hz)	-	-	-
H2	9.09 (d, 2H: CH, <i>J</i> = 5.56 Hz)	9.07 (d, 2H: CH, <i>J</i> = 5.56 Hz)	9.11 (d, 2H: CH, <i>J</i> = 5.55 Hz)	9.01 (d, 1H: CH, <i>J</i> = 5.32Hz)	8.97 (d, 1H: CH, <i>J</i> = 5.33 Hz)	9.00 (d, 1H: CH, <i>J</i> = 5.58 Hz)	9.02 (d, 1H: CH, <i>J</i> = 5.42Hz)	8.99 (d, 1H: CH, <i>J</i> = 5.43 Hz)	9.00 (d, 1H: CH, <i>J</i> = 5.47 Hz)
H9	-	-	-	9.10 (d, 1H: CH, <i>J</i> = 5.49 Hz)	9.05 (d, 1H: CH, <i>J</i> = 5.42Hz)	9.09 (d, 1H: CH, <i>J</i> = 5.58 Hz)	-	-	-
H5	8.33 (s,2H; CH)	8.33 (s,2H; CH)	8.31 (s,2H; CH)	-	-	-	-	-	-
H6	-	-	-	8.09 (s,1H; CH)	8.12 (s,1H; CH)	8.12 (s,1H; CH)	-	-	-
CH ₃	-	-	-	2.85 (s, 3H; CH ₃)	2.89 (s, 3H; CH ₃)	2.86 (s, 3H; CH ₃)	2.77 (s, 6H; CH ₃)	2.79 (s, 6H; CH ₃)	2.67 (s, 6H; CH ₃)
H1'/2'	3.35 (m, 2H; CH ₂)	3.39 (m, 2H; CH ₂)	3.35 (m, 2H; CH ₂)	3.35 (m, 2H; CH ₂)	3.33 (m, 2H; CH ₂)	3.34 (m, 2H; CH ₂)	3.33 (m, 2H; CH ₂)	3.35 (m, 2H; CH ₂)	3.30 (m, 2H; CH ₂)
H3'/6'	2.35 (d, 2H; CH ₂ , <i>J</i> =15.56 Hz)	3.34 (d, 2H; CH ₂ , <i>J</i> =11.00 Hz)	2.36 (d, 2H; CH ₂ , <i>J</i> = 12.13 Hz)	2.36 (d, 2H; CH ₂ , <i>J</i> = 12.09 Hz)	2.32 (d, 2H; CH ₂ , <i>J</i> = 11.55 Hz)	2.36 (d, 2H; CH ₂ , <i>J</i> = 12.05 Hz)	2.36 (d, 2H; CH ₂ , <i>J</i> = 12.57 Hz)	2.33 (d, 2H; CH ₂ , <i>J</i> = 11.53 Hz)	2.33 (d, 2H; CH ₂ , <i>J</i> = 12.08 Hz)
H4'/5'	1.72 (m, 2H; CH ₂)	1.69 (m, 4 H; CH ₂)	1.73 (m, 2H; CH ₂)	1.72 (m, 2H; CH ₂)	1.67 (m, 4 H; CH ₂)	1.72 (m, 2H; CH ₂)	1.72 (m, 2H; CH ₂)	1.67 (m, 4 H; CH ₂)	1.62 (m, 2H; CH ₂)
H3'/6'	1.66 (d, 2H; CH ₂ , <i>J</i> =10.92Hz)	-	1.66 (d, 2H; CH ₂ , <i>J</i> =10.40 Hz)	1.66 (d, 2H; CH ₂ , <i>J</i> = 10.90 Hz)	-	1.66 (d, 2H; CH ₂ , <i>J</i> = 11.02Hz)	1.66 (d, 2H; CH ₂ , <i>J</i> = 10.71Hz)	-	1.69 (d, 2H; CH ₂ , <i>J</i> = 9.50 Hz)
H4'/5'	1.30 (m, 2H; CH ₂)	1.30 (m, 2H; CH ₂)	1.30 (m, 2H; CH ₂)	1.30 (m, 2H; CH ₂)	1.29 (m, 2H; CH ₂)	1.30 (m, 2H; CH ₂)	1.30 (m, 2H; CH ₂)	1.30 (m, 2H; CH ₂)	1.26(m, 2H; CH ₂)
¹ H/ ¹⁹⁵ Pt	9.19/-645.8	9.12/-964.3	9.02/-635.2	9.1/-643.1	9.10/ -649.7	9.17/ -640.7	9.15/-653.5	9.1/ -969	9.09/ -648
Yield %	30.4	21.2	16.3	52.9	19.9	9.16	34.7	45.9	10.9

Table 2.3.5.2: Summary of the characterisation data of complexes of the type [Pt(PL)(AL)(X)₂]²⁺

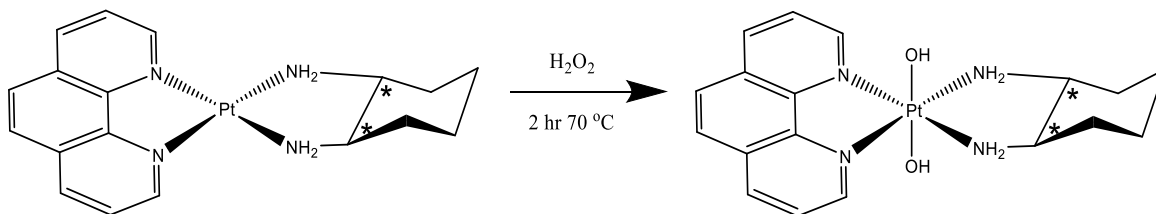
Complex	Molecular Formula	Yield (%)	ESI-MS (<i>m/z</i>) [M-Cl] ⁺ Calc. (Found)	Microanalysis			UV / λ _{max} (nm) (ε/mol ⁻¹ .dm ³ .cm ⁻¹) × 10 ²	CD / λ _{max} (nm) (Θ) × 10 ⁻⁸
				N	C	H		
PHENSSCl ₂	C ₁₈ H ₂₂ Cl ₂ N ₄ Pt	30.4	279.54(280.03)	8.40 (8.40)	33.40 (33.36)	3.93 (37.47)	278 (579), 208 (243)	268(3.85), 216(-25.5), 183(-1.08)
PHENSSBr ₂	C ₁₈ H ₂₂ Br ₂ N ₄ Pt	21.2	323.49(323.35)	7.41 (7.45)	28.59 (28.85)	3.47 (3.39)	277 (310), 207 (168)	279(7.14),226(-20.2),183(-1.04)
PHENSSI ₂	C ₁₈ H ₂₂ I ₂ N ₄ Pt	16.3	371.48(372.10)	8.53 (8.55)	32.17 (32.76)	3.68 (3.72)	277(375), 208 (159)	270(3.19), 217(-24.3),181(-1.38)
5MESSCl ₂	C ₁₉ H ₂₄ Cl ₂ N ₄ Pt	52.9	286.55(285.54)	7.81 (7.72)	31.81 (31.94)	4.50 (4.27)	283 (189), 210 (80)	255(0.93),215(-3.60), 185(-0.45)
5MESSBr ₂	C ₁₉ H ₂₄ Br ₂ N ₄ Pt	19.9	330.50(332.99)	6.51 (6.41)	26.53 (26.83)	3.68 (3.57)	282 (165), 228 (113)	282 (-0.12), 229(-6.80), 185(-2.31)
5MESSI ₂	C ₁₉ H ₂₄ I ₂ N ₄ Pt	9.16	378.48(377.81)	NA	NA	NA	282 (337), 209 (154)	282(2.19), 217(-23.9), 304(-1.18)
56MESSCl ₂	C ₂₀ H ₂₆ Cl ₂ N ₄ Pt	34.7	293.56(294.07)	7.66 (7.52)	32.84 (32.71)	4.69 (4.61)	289 (238), 211(102)	290(4.66), 255(8.56), 214(-3.94)
56MESSBr ₂	C ₂₀ H ₂₆ Br ₂ N ₄ Pt	45.9	337.51(337.07)	7.14 (6.98)	30.63 (30.26)	3.86 (3.70)	289 (227), 210 (121)	292(6.10), 224(-20.8)
56MESSI ₂	C ₂₀ H ₂₆ I ₂ N ₄ Pt	10.9	385.49(385.89)	7.91 (7.43)	32.55 (32.53)	4.33 (4.51)	289 (281), 211 (119)	209(-6.29), 251(1.63)

Table 2.3.5.3: Summary of cytotoxicity results in GI₅₀ = Concentration (μM) that inhibits cell growth by 50%*

Complex	HT29 <i>Colon</i> <i>n=3-4</i>	U87 <i>Glioblastoma</i> <i>n=3-4</i>	MCF-7 <i>Breast</i> <i>n=3-4</i>	A2780 <i>Ovarian</i> <i>n=3-4</i>	H460 <i>Lung</i> <i>n=3-4</i>	A431 <i>Skin</i> <i>n=3-4</i>	Du145 <i>Prostate</i> <i>n=3-4</i>	BE2-C <i>Neuroblasto</i> <i>ma</i> <i>n=3-4</i>	SJ-G2 <i>Glioblastoma</i> <i>n=3-4</i>	MIA <i>Pancreas</i> <i>n=3-4</i>	MCF10A <i>Breast</i> <i>(Normal)</i> <i>n=3-4</i>	ADDP <i>Ovarian</i> <i>n=3-4</i>
PHENSSCl ₂	0.11 ± 0.028	0.81 ± 0.15	0.46 ± 0.069	0.23 ± 0.0058	0.33 ± 0.0088	0.44 ± 0.045	0.11 ± 0.033	0.44 ± 0.050	0.34 ± 0.063	0.21 ± 0.029	0.30 ± 0.0033	0.23 ± 0.026
PHENSSBr ₂	0.16 ± 0.015	0.82 ± 0.090	0.53 ± 0.10	0.27 ± 0.023	0.36 ± 0.029	0.68 ± 0.023	0.18 ± 0.010	0.52 ± 0.025	0.42 ± 0.071	0.25 ± 0.010	0.36 ± 0.032	0.28 ± 0.017
PHENSSI ₂	0.10 ± 0.0033	0.70 ± 0.055	0.46 ± 0.10	0.24 ± 0.059	0.32 ± 0.031	0.44 ± 0.021	0.11 ± 0.0033	0.37 ± 0.00000	0.31 ± 0.031	0.20 ± 0.013	0.29 ± 0.032	0.25 ± 0.020
5MESSCl ₂	0.032 ± 0.0036	0.23 ± 0.033	0.22 ± 0.13	0.25 ± 0.18	0.089 ± 0.018	0.13 ± 0.028	0.023 ± 0.0030	0.25 ± 0.060	0.18 ± 0.034	0.044 ± 0.0045	0.094 ± 0.024	0.056 ± 0.0032
5MESSBr ₂	0.035 ± 0.0058	0.20 ± 0.029	0.087 ± 0.032	0.044 ± 0.012	0.070 ± 0.0091	0.11 ± 0.015	0.025 ± 0.0053	0.20 ± 0.010	0.16 ± 0.044	0.037 ± 0.0046	0.062 ± 0.0083	0.048 ± 0.0046
5MESSI ₂	0.032 ± 0.0035	0.22 ± 0.030	0.091 ± 0.026	0.046 ± 0.010	0.065 ± 0.0061	0.10 ± 0.0123	0.027 ± 0.0027	0.20 ± 0.00000	0.16 ± 0.040	0.032 ± 0.0022	0.061 ± 0.0082	0.044 ± 0.0058
56MESSCl ₂	0.025 ± 0.0020	0.12 ± 0.018	0.060 ± 0.010	0.037 ± 0.0067	0.048 ± 0.012	0.062 ± 0.013	0.012 ± 0.0017	0.12 ± 0.00000	0.092 ± 0.039	0.028 ± 0.0021	0.044 ± 0.0062	0.036 ± 0.0041
56MESSBr ₂	0.021 ± 0.0023	0.090 ± 0.012	0.11 ± 0.056	0.035 ± 0.013	0.032 ± 0.0020	0.061 ± 0.011	0.011 ± 0.0031	0.34 ± 0.18	0.074 ± 0.033	0.024 ± 0.0026	0.034 ± 0.0038	0.033 ± 0.0023
56MESSI ₂	0.019 ± 0.0032	0.074 ± 0.014	0.033 ± 0.0068	0.032 ± 0.017	0.027 ± 0.0032	0.037 ± 0.0054	0.025 ± 0.017	0.087 ± 0.063	0.067 ± 0.028	0.022 ± 0.0022	0.030 ± 0.0039	0.027 ± 0.0007

*Incubated for 72 hr

2.3.6 Synthesis of Pt(IV) complexes of the type $[\text{Pt}(\text{P}_L)(\text{A}_L)(\text{OH})_2]^{2+}$

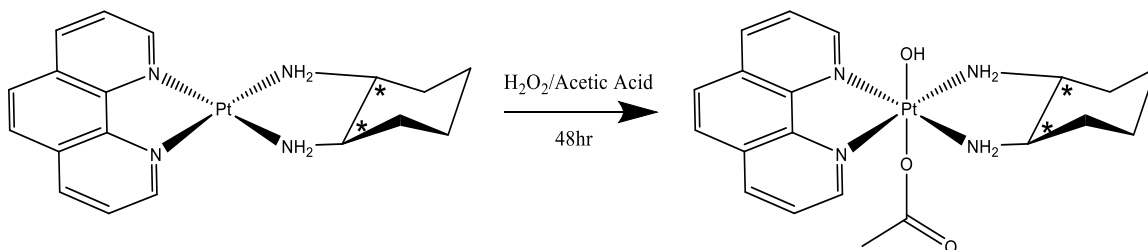


Pt(II) complex (1 equiv) was dissolved in the minimum amount of water and silver nitrate (2 equiv) was added. The solution was stirred in the dark overnight, and then filtered to produce the Pt(II) nitrate salt. This product was then dissolved in water (5.8 mL) and heated to 70 °C on a water bath. 30% hydrogen peroxide solution (10 equiv peroxide) was added and the solution stirred for 2H in the dark at 70 °C. Still in the dark, the reaction solution was immediately frozen and lyophilised. Purification was achieved through a Sep-Pak® (20 cc, 5 g) C-18 column connected to a pump apparatus with UV detector (Bio-Rad, EM-1 Econo™ UV Monitor). The column was activated with methanol (20 mL) and then flushed with water (~40 mL) until the UV absorbance equilibrated. The crude lyophilised platinum(IV) product was dissolved in the minimum amount of water, loaded onto the column, and eluted with water at a flow rate of 1 mL/min. Once absorbance began to increase, the first 2-3 mL to elute were collected and discarded. The rest of the product was collected together as a colourless band. The product solution was reduced to approx. 1-2 mL and was purified through the Sep-Pak® process twice more. The product solution was reduced to approx. 3-5 mL and lyophilised to produce a white solid. This method was utilised to synthesise; $[\text{Pt}(56\text{Me}_2\text{phen})(SS\text{-dach})(\text{OH})_2]^{2+}$ (56MESS(OH)₂), $[\text{Pt}(56\text{Me}_2\text{phen})(RR\text{-dach})(\text{OH})_2]^{2+}$ (56MERR(OH)₂), $[\text{Pt}(\text{phen})(SS\text{-dach})(\text{OH})_2]^{2+}$ (PHENSS(OH)₂), $[\text{Pt}(\text{phen})(RR\text{-dach})(\text{OH})_2]^{2+}$ (PHENRR(OH)₂), $[\text{Pt}(5\text{Mephen})(SS\text{-dach})(\text{OH})_2]^{2+}$ (5MESS(OH)₂), $[\text{Pt}(5\text{Mephen})(RR\text{-dach})(\text{OH})_2]^{2+}$ (5MERR(OH)₂), $[\text{Pt}(4\text{Mephen})(SS\text{-dach})(\text{OH})_2]^{2+}$ (4MESS(OH)₂), $[\text{Pt}(4\text{Mephen})(RR\text{-dach})(\text{OH})_2]^{2+}$ (4MERR(OH)₂), $[\text{Pt}(44\text{BPY})(SS\text{-dach})(\text{OH})_2]^{2+}$ (44BPYSS(OH)₂), and $[\text{Pt}(44\text{BPY})(RR\text{-dach})(\text{OH})_2]^{2+}$ (44BPYRR(OH)₂). Yields and NMR data are displayed in Table 2.3.8.1

Table 2.3.6.1. Summary of NMR data of dihydroxido complexes, showing chemical shift (ppm) with integration, multiplicity and coupling constants. Experiments were performed in D₂O, so amine resonances were not observed due to proton exchange.

Label	Complex									
	PHENSS(OH) ₂	PHENRR(OH) ₂	56MESS(OH) ₂	56MERR(OH) ₂	5MESS(OH) ₂	5MERR(OH) ₂	4MESS(OH) ₂	4MERR(OH) ₂	44BPYSS(OH) ₂	44BPYRR(OH) ₂
H4	9.09 (d, 2H: CH, <i>k</i> <i>J</i> = 5.46 Hz)	9.09 (d, 2H: CH, <i>k</i> <i>J</i> = 6.12 Hz)	9.20 (d, 1H: CH, <i>J</i> = 8.67 Hz)	9.21 (d, 1H: CH, <i>J</i> = 8.39 Hz)	8.96 (d, 1H: CH, <i>J</i> = 8.75 Hz)	8.96 (d, 1H: CH, <i>J</i> = 8.20 Hz)	-	-	-	-
H7	-	-	-	-	9.17 (d, 1H: CH, <i>J</i> = 8.37 Hz)	9.18 (d, 1H: CH, <i>J</i> = 8.31 Hz)	9.20 (d, 1H: CH, <i>J</i> = 5.65 Hz)	8.87 (d, 1H: CH, <i>J</i> = 5.48 Hz)	-	-
H3	8.27 (dd, 2H: CH, <i>J</i> = 8.19, 8.44 Hz)	8.27 (dd, 2H: CH, <i>J</i> = 8.53, 8.65 Hz)	8.24 (dd, 1H: CH, <i>J</i> = 8.50, 8.63 Hz)	8.24 (dd, 1H: CH, <i>J</i> = 8.20, 8.56 Hz)	8.20 (dd, 1H: CH, <i>J</i> = 8.31, 8.54 Hz)	8.20 (dd, 1H: CH, <i>J</i> = 8.34, 8.35 Hz)	8.10 (d, 1H: CH, <i>J</i> = 5.64 Hz)	7.81 (d, 1H: CH, <i>J</i> = 5.82 Hz)	8.12 (s, 2H: CH)	8.12 (s, 2H: CH)
H8	-	-	-	-	8.28 (dd, 1H: CH, <i>J</i> = 8.60, 8.65 Hz)	8.29 (dd, 1H: CH, <i>J</i> = 8.70, 8.65 Hz)	8.25 (dd, 1H: CH, <i>J</i> = 8.50, 8.34 Hz)	7.95 (dd, 1H: CH, <i>J</i> = 8.54, 8.26 Hz)	-	-
H2	9.22 (d, 2H: CH, <i>J</i> = 8.32 Hz)	9.23 (d, 2H: CH, <i>J</i> = 5.49 Hz)	9.12 (d, 1H: CH, <i>J</i> = 5.71 Hz)	9.13 (d, 1H: CH, <i>J</i> = 5.53 Hz)	9.20 (d, 1H: CH, <i>J</i> = 5.65 Hz)	9.13 (d, 1H: CH, <i>J</i> = 5.61 Hz)	9.08 (d, 1H: CH, <i>J</i> = 8.24 Hz)	8.84 (d, 1H: CH, <i>J</i> = 8.54 Hz)	-	-
H9	-	-	-	-	9.12 (d, 1H: CH, <i>J</i> = 5.62 Hz)	9.20 (d, 1H: CH, <i>J</i> = 5.73 Hz)	9.02 (d, 1H: CH, <i>J</i> = 5.92 Hz)	9.02 (d, 1H: CH, <i>J</i> = 5.82 Hz)	-	-
H5	8.35 (s, 2H; CH)	8.35 (s, 2H; CH)	-	-	-	-	8.46 (d, 1H: CH, <i>J</i> = 9.13 Hz)	8.19 (d, 1H: CH, <i>J</i> = 9.29 Hz)	7.48 (d, 1H: CH, <i>J</i> = 5.89 Hz)	7.48 (d, 1H: CH, <i>J</i> = 5.79 Hz)
H6	-	-	-	-	8.16 (s, 1H; CH)	8.16 (s, 1H; CH)	8.35 (d, 1H: CH, <i>J</i> = 9.13 Hz)	8.08 (d, 1H: CH, <i>J</i> = 8.22 Hz)	8.28 (d, 1H: CH, <i>J</i> = 6.01 Hz)	8.28 (d, 1H: CH, <i>J</i> = 5.79 Hz)
CH ₃	-	-	2.85 (s, 6H; CH ₃)	2.84 (s, 6H; CH ₃)	2.91 (s, 3H; CH ₃)	2.90 (s, 3H; CH ₃)	3.08 (s, 3H; CH ₃)	2.86 (s, 3H; CH ₃)	2.49 (s, 6H; CH ₃)	2.50 (s, 6H; CH ₃)
H1'2'	3.18 (m, 2H; CH ₂)	3.19 (m, 2H; CH ₂)	3.17 (m, 2H; CH ₂)	3.15 (m, 2H; CH ₂)	3.17 (m, 2H; CH ₂)	3.18 (m, 2H; CH ₂)	3.17 (m, 2H; CH ₂)	2.69 (m, 2H; CH ₂)	2.58 (m, 2H; CH ₂)	2.58 (m, 2H; CH ₂)
H3'6'	2.39 (d, 2H; CH ₂ , <i>J</i> = 11.07 Hz)	3.39 (d, 2H; CH ₂ , <i>J</i> = 12.26 Hz)	2.38 (d, 2H; CH ₂ , <i>J</i> = 10.99 Hz)	2.37 (d, 2H; CH ₂ , <i>J</i> = 12.45 Hz)	2.38 (d, 2H; CH ₂ , <i>J</i> = 11.11 Hz)	2.38 (d, 2H; CH ₂ , <i>J</i> = 10.75 Hz)	2.38 (d, 2H; CH ₂ , <i>J</i> = 11.53 Hz)	2.19 (d, 2H; CH ₂ , <i>J</i> = 13.18 Hz)	2.13 (d, 2H; CH ₂ , <i>J</i> = 13.24 Hz)	2.13 (d, 2H; CH ₂ , <i>J</i> = 13.00 Hz)
H4'5'	1.69 (m, 4 H; CH ₂)	1.69 (m, 4 H; CH ₂)	1.72 (m, 4 H; CH ₂)	1.68 (m, 4 H; CH ₂)	1.69 (m, 4 H; CH ₂)	1.68 (m, 4 H; CH ₂)	1.68 (m, 4 H; CH ₂)	1.64 (m, 4 H; CH ₂)	1.61 (m, 2H; CH ₂)	1.60 (m, 2H; CH ₂)
H3'6'	-	-	-	-	-	-	-	-	1.38 (m, 2H; CH ₂)	1.37 (m, 2H; CH ₂)
H4'5'	1.31 (m, 2H; CH ₂)	1.31 (m, 2H; CH ₂)	1.31 (m, 2H; CH ₂)	1.30 (m, 2H; CH ₂)	1.31 (m, 2H; CH ₂)	1.31 (m, 2H; CH ₂)	1.30 (m, 2H; CH ₂)	1.23 (m, 2H; CH ₂)	1.18 (m, 2H; CH ₂)	1.18 (m, 2H; CH ₂)
¹ H/ ¹⁹⁵ Pt	9.78/428.8	9.65/429.6	9.68/426.5	9.34/430.1	9.43/429.6	9.45/428.9	9.05/428.5	9.12/432.4	8.69/434.1	8.56/433.6
% Yield	87	85	87	72	85	88	74	79	74	73

2.3.7 Synthesis of Pt(IV) complexes of the type $[\text{Pt}(\text{P}_L)(\text{A}_L)(\text{OH})(\text{C}_2\text{H}_3\text{O}_2)]^{2+}$



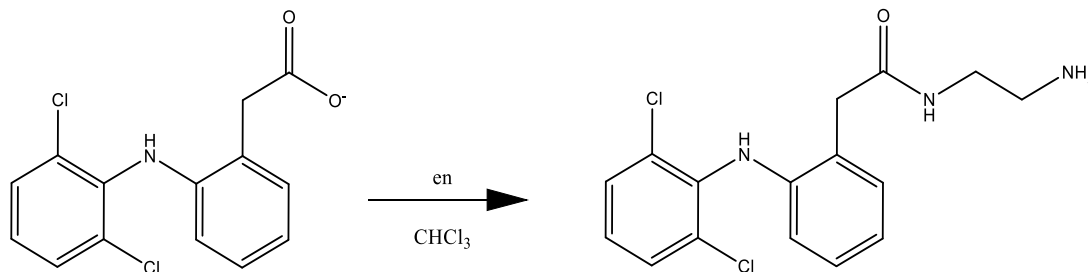
The Pt(II) complex (1 equiv) was dissolved in water (20 mL) and silver acetate (2 equiv) was added. The solution was stirred in the dark overnight, and then filtered to produce the Pt(II) acetate salt. This complex (1 equiv) was dissolved in acetic acid (1.5 mL). 30% hydrogen peroxide solution (3.5 equiv of peroxide) was added and the solution stirred in the dark for 48 h. The solution was precipitated in diethyl ether (~100 mL) and cooled to ~4 °C for 16 h, at which point the product had redissolved in an immiscible solution which was separated and reduced to a minimal volume.

This method was utilised to synthesise; $[\text{Pt}(56\text{Me}_2\text{phen})(SS\text{-dach})(\text{OH})(\text{C}_2\text{H}_3\text{O}_2)]^{2+}$ (56MESS(OH)(OAc)), $[\text{Pt}(56\text{Me}_2\text{phen})(RR\text{-dach})(\text{OH})(\text{C}_2\text{H}_3\text{O}_2)]^{2+}$ (56MERR(OH)(OAc)), $[\text{Pt}(\text{phen})(SS\text{-dach})(\text{OH})(\text{C}_2\text{H}_3\text{O}_2)]^{2+}$ (PHENSS(OH)(OAc)), $[\text{Pt}(\text{phen})(RR\text{-dach})(\text{OH})(\text{C}_2\text{H}_3\text{O}_2)]^{2+}$ (PHENRR(OH)(OAc)), $[\text{Pt}(5\text{Mephen})(SS\text{-dach})(\text{OH})(\text{C}_2\text{H}_3\text{O}_2)]^{2+}$ (5MESS(OH)(OAc)), $[\text{Pt}(5\text{Mephen})(RR\text{-dach})(\text{OH})(\text{C}_2\text{H}_3\text{O}_2)]^{2+}$ (5MERR(OH)(OAc)), $[\text{Pt}(4\text{Mephen})(SS\text{-dach})(\text{OH})(\text{C}_2\text{H}_3\text{O}_2)]^{2+}$ (4MESS(OH)(OAc)), $[\text{Pt}(4\text{Mephen})(RR\text{-dach})(\text{OH})(\text{C}_2\text{H}_3\text{O}_2)]^{2+}$ (4MERR(OH)(OAc)), $[\text{Pt}(44\text{BPY})(SS\text{-dach})(\text{OH})(\text{C}_2\text{H}_3\text{O}_2)]^{2+}$ (44BPYSS(OH)(OAc)), and $[\text{Pt}(44\text{BPY})(RR\text{-dach})(\text{OH})(\text{C}_2\text{H}_3\text{O}_2)]^{2+}$ (44BPYRR(OH)(OAc)). Yields and NMR data are displayed in Table 2.3.10.1

Table 2.3.7.1. Summary of NMR data of Asymmetric (OH)(OAc) complexes, showing chemical shift (ppm) with integration, multiplicity and coupling constants. Experiments were performed in D₂O, so amine resonances were not observed due to proton exchange.

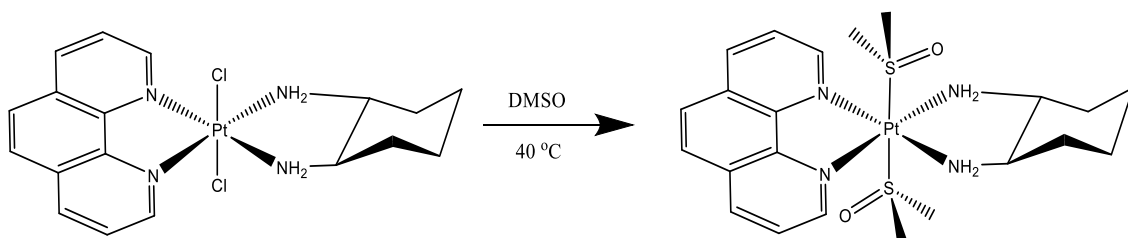
Label	Complex									
	PHENSS(OH)(OAc)	PHENRR(OH)(OAc)	56MESS(OH)(OAc)	56MERR(OH)(OAc)	5MESS(OH)(OAc)	5MERR(OH)(OAc)	4MESS(OH)(OAc)	4MERR(OH)(OAc)	44BPYSS(OH)(OAc)	44BPYRR(OH)(OAc)
H4	9.24 (d, 2H: CH _k , <i>J</i> = 6.12Hz)	9.25 (d, 2H: CH _k , <i>J</i> = 6.67 Hz)	8.73 (m, 4H: CH)	9.16 (d, 1H: CH, <i>J</i> = 8.52 Hz)	8.75 (d, 1H: CH, <i>J</i> = 8.19 Hz)	8.90 (d, 1H: CH, <i>J</i> = 8.28 Hz)	-	-	-	-
H7	-	-	-	-	9.13 (d, 1H: CH, <i>J</i> = 8.37 Hz)	8.79 (d, 1H: CH, <i>J</i> = 4.81Hz)	9.04 (d, 1H: CH, <i>J</i> = 5.65 Hz)	8.82 (d, 1H: CH, <i>J</i> = 5.24 Hz)	-	-
H3	8.24 (dd, 2H: CH, <i>J</i> = 8.16, 8.34 Hz)	8.25 (dd, 2H: CH, <i>J</i> = 5.87, 7.35 Hz)	7.89 (dd, 2H: CH, <i>J</i> =13.63, 11.46 Hz)	8.20 (dd, 1H: CH, <i>J</i> =8.80, 8.93 Hz)	7.89 (dd, 1H: CH, <i>J</i> = 8.66, 8.64 Hz)	8.75 (dd, 1H: CH, <i>J</i> = 5.57, 8.32Hz)	7.71 (d, 1H: CH, <i>J</i> = 5.64 Hz)	7.75 (d, 1H: CH, <i>J</i> = 5.82Hz)	8.09 (s, 2H: CH)	8.41 (s, 2H: CH)
H8	-	-	-	7.89 (dd, 1H: CH, <i>J</i> =8.38, 8.52Hz)	8.20 (dd, 1H: CH, <i>J</i> = 8.69, 8.83 Hz)	8.29 (dd, 1H: CH, <i>J</i> = 5.57, 8.44 Hz)	7.91 (dd, 1H: CH, <i>J</i> = 8.50, 8.34 Hz)	7.91 (dd, 1H: CH, <i>J</i> = 8.47, 8.22Hz)	-	-
H2	9.06 (d, 2H: CH _k , <i>J</i> = 5.57 Hz)	9.05 (d, 2H: CH _k , <i>J</i> = 6.34 Hz)	-	8.74 (d, 1H: CH, <i>J</i> = 5.24 Hz)	7.95 (d, 1H: CH, <i>J</i> = 5.32Hz)	7.91 (d, 1H: CH, <i>J</i> = 5.32Hz)	8.82 (d, 1H: CH, <i>J</i> = 8.24 Hz)	8.78 (d, 1H: CH, <i>J</i> = 8.65 Hz)	-	-
H9	-	-	-	-	8.72 (d, 1H: CH, <i>J</i> = 5.49 Hz)	8.72 (d, 1H: CH, <i>J</i> = 5.49 Hz)	8.75 (d, 1H: CH, <i>J</i> = 5.92Hz)	8.64 (d, 1H: CH, <i>J</i> = 5.82Hz)	-	-
H5	8.31 (s,2H; CH)	8.31 (s,2H; CH)	-	-	-	-	8.61 (d, 1H: CH, <i>J</i> = 9.13 Hz)	8.09 (d, 1H: CH, <i>J</i> = 5.85 Hz)	7.75 (d, 1H: CH, <i>J</i> = 6.16 Hz)	7.74 (d, 1H: CH, <i>J</i> = 5.67 Hz)
H6	-	-	-	-	7.67 (s,1H; CH)	7.60 (s,1H; CH)	8.03 (d, 1H: CH, <i>J</i> = 9.13 Hz)	8.00 (d, 1H: CH, <i>J</i> = 6.06 Hz)	8.60 (d, 1H: CH, <i>J</i> = 6.01Hz)	8.60 (d, 1H: CH, <i>J</i> = 6.15 Hz)
CH ₃	-	-	1.86 (s, 6H; CH ₃)	1.85 (s, 6H; CH ₃)	2.45 (s, 3H; CH ₃)	2.36 (s, 3H; CH ₃)	1.86 (s, 3H; CH ₃)	1.86 (s, 3H; CH ₃)	2.26 (s, 6H; CH ₃)	2.45 (s, 6H; CH ₃)
H1'/2'	3.18 (m, 2H; CH ₂)	3.18 (m, 2H; CH ₂)	2.70 (m, 2H; CH ₂)	2.70 (m, 2H; CH ₂)	2.69 (m, 2H; CH ₂)	2.70 (m, 2H; CH ₂)	2.68 (m, 2H; CH ₂)	2.69 (m, 2H; CH ₂)	3.06 (m, 2H; CH ₂)	2.57 (m, 2H; CH ₂)
H3'/6'	3.38 (d, 2H; CH ₂ , <i>J</i> =10.64 Hz)	3.38 (d, 2H; CH ₂ , <i>J</i> =15.56 Hz)	2.21 (d, 2H; CH ₂ , <i>J</i> = 12.08 Hz)	2.21 (d, 2H; CH ₂ , <i>J</i> = 12.02Hz)	2.21 (d, 2H; CH ₂ , <i>J</i> = 12.09 Hz)	2.20 (d, 2H; CH ₂ , <i>J</i> = 12.31Hz)	2.19 (d, 2H; CH ₂ , <i>J</i> = 11.53 Hz)	2.19 (d, 2H; CH ₂ , <i>J</i> = 13.18 Hz)	2.30 (d, 2H; CH ₂ , <i>J</i> = 11.41Hz)	2.11 (d, 2H; CH ₂ , <i>J</i> = 13.39 Hz)
H4'/5'	1.69 (m, 2H; CH ₂)	1.69 (m, 2H; CH ₂)	1.66 (m, 2H; CH ₂)	1.66 (m, 2H; CH ₂)	1.66 (m, 2H; CH ₂)	1.65 (m, 2H; CH ₂)	1.66 (m, 2H; CH ₂)	1.65 (m, 2H; CH ₂)	1.62 (m, 2H; CH ₂)	1.62 (m, 2H; CH ₂)
H3'/6'	-	-	1.47 (m, 2H; CH ₂)	1.48 (m, 2H; CH ₂)	1.47 (m, 2H; CH ₂)	1.45 (m, 2H; CH ₂)	1.45 (m, 2H; CH ₂)	1.45 (m, 2H; CH ₂)	1.37 (m, 2H; CH ₂)	1.37 (m, 2H; CH ₂)
H4'/5'	1.29 (m, 2H; CH ₂)	1.29 (m, 2H; CH ₂)	1.24 (m, 2H; CH ₂)	1.23 (m, 2H; CH ₂)	1.23 (m, 2H; CH ₂)	1.22 (m, 2H; CH ₂)	1.22 (m, 2H; CH ₂)	1.22 (m, 2H; CH ₂)	1.24 (m, 2H; CH ₂)	1.17 (m, 2H; CH ₂)
¹ H/ ¹⁹⁵ Pt	9.54/543.9	9.35/564.5	9.13/572.6	9.16/544.6	9.25/551.9	9.25/531.9	8.72/539.5	8.75/543.4	8.72/536.6	8.75/540.8
%Yield	54	43	52	48	46	57	55	47	46	49

2.3.8 Synthesis of 2-aminoethyldiclofenacamide (enDCF)



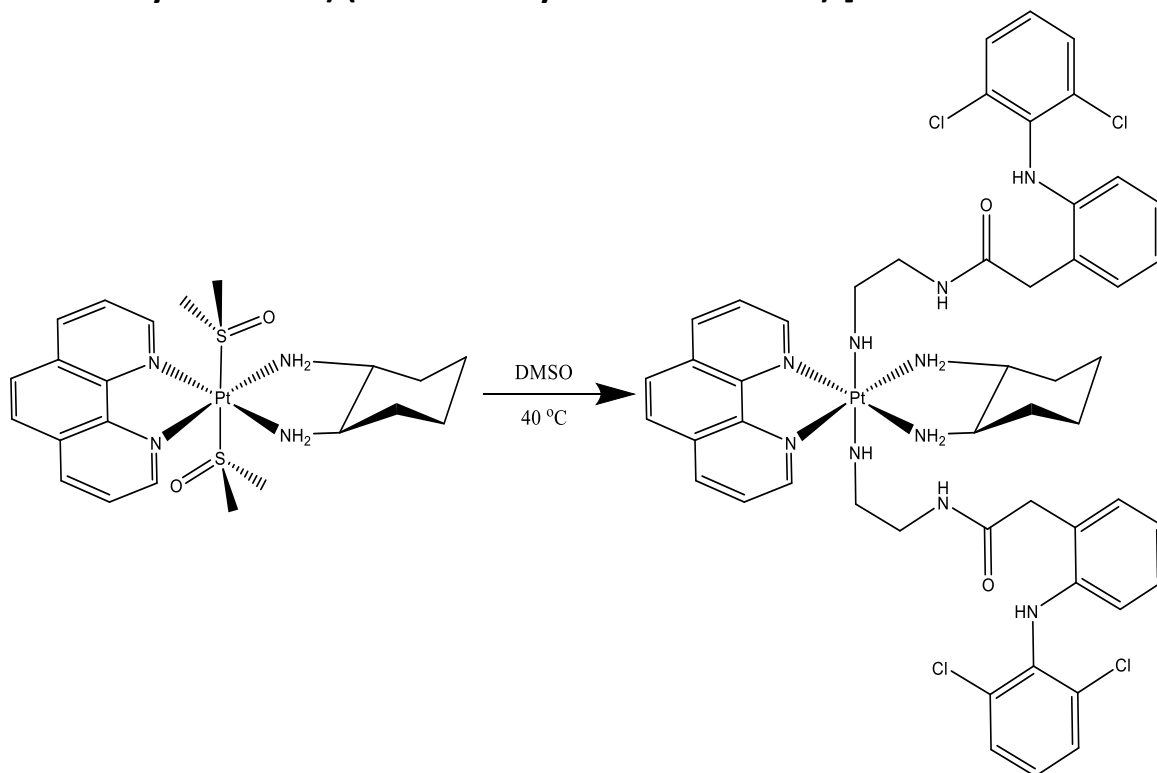
2-(2,6-Dichloroanilino)-phenylacetic acid (DCF) was dissolved in a minimal amount of chloroform before 2 equivalents of 1,2-ethylenediamine (en) were added at room temperature. The solution was left to sit overnight after which it produced large clear crystals which were filtered and washed with chloroform. Yield 95 %. ^1H NMR (400 MHz, d-DMSO) δ 7.37 (d, 2H: CH, J = 8.34 Hz), 7.20 (d, 1H: CH, J = 7.14 Hz), 7.00 (m, 2H; CH), 6.82 (t, 1H, CH, J = 7.74 Hz), 6.37(d, 1H: CH, J = 8.19 Hz), 0.92 (m, H; NH), 4.1(m, H; NH).

2.3.9 Synthesis of [Pt(1,10-phenanthroline)(1S,2S-diaminocyclohexane) (DMSO) $_2$] $^{2+}$



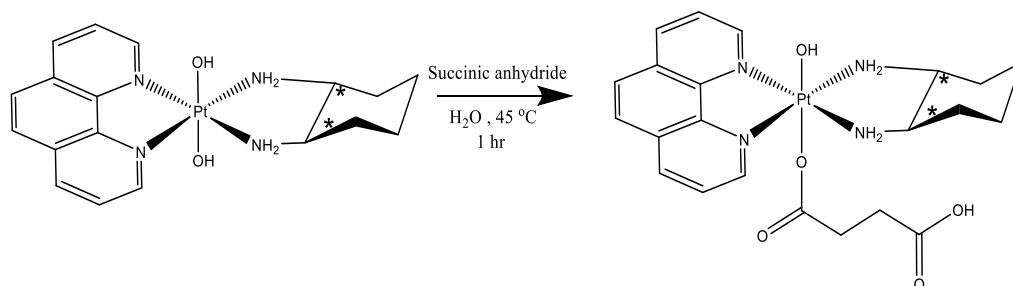
PHENSSCl $_2$ (50 mg) was dissolved in 10 mL of DMSO and stirred at 40 °C overnight at which point the suspension had fully dissolved. The crude product was then either used for further synthesis or extracted using 6 washes of 25 mL Chloroform. Yield 96 %. ^1H NMR (400 MHz, d-DMSO) δ 11.85 (d, 2H: CH, J =5.40 Hz), 11.58 (d, 2H: CH, J = 8.55), 10.79 (m, 4H: CH/ CH $_3$), 5.30 (m, 2H: CH), 4.72 (m, 12H: CH $_3$), 4.57 (m, 2H: CH), 3.96 (m, 2H: CH), 3.83 (m, 2H: CH), 3.53 (m, 2H: CH), ^{195}Pt -600.8 ppm.

2.3.10 Synthesis of [Pt(1,10-phenanthroline)(1S,2S-diaminocyclohexane) (2-aminoethylchlorfenacamide)₂]²⁺



PHENSS(DMSO)₂ (100 mg, 1 equiv) and 2.2 equivalents of 2-Aminoethylchlorfenacamide (DCF-en) were dissolved in 30 mL water and stirred at 70 °C for 20 min before being taken to dryness under vacuum, producing a pale yellow residue. Then 50 mL of absolute ethanol was added to the flask and let to stir at 40 °C for a further 12 hr. The grey suspension was filtered and the filtrate reduced under pressure to ~ 3 mL. The crude product was then precipitated with 20 mL diethyl ether. The precipitate was filtered and washed thrice with ether (3 mL). To remove all traces of solvent, the produce was taken up in ~5 mL of water and freeze dried to produce a plate yellow powder. Yield 85 %, ¹H NMR (400 MHz, d-Acetone) δ (PHENSS peaks) 8.89 (d, 2H: CH, *J* = 8.42Hz), 8.01 (dd, 2H: CH, *J* = 8.13, 8.41Hz), 9.11 (d, 2H: CH, *J* = 5.26 Hz), 8.13 (s, 2H; CH), 2.69, (m, 2H; CH₂), 2.25 (d, 2H; CH₂, *J* = 12.81Hz), 1.69 (m, 2H; CH₂), 1.54 (m, 2H; CH₂), 1.29 (m, 2H; CH₂): (enDCF peaks) 7.23 (d, 2H: CH, *J* = 8.08 Hz), 7.12 (d, 2H: CH, *J* = 7.50 Hz), 6.91 (t, 4 H: CH, *J* = 8.03 Hz), 6.85 (t, 4 H: CH, *J* = 7.72 Hz), 6.70 (t, 2H: CH, *J* = 7.54 Hz), 6.21 (d, 4 H: CH, *J* = 7.95 Hz), ¹⁹⁵Pt -2820.1.

2.3.11 Synthesis of Pt(IV) complexes of the type $[\text{Pt}(\text{P}_L)(\text{A}_L)(\text{OH})(\text{succinimide})]^{2+}$

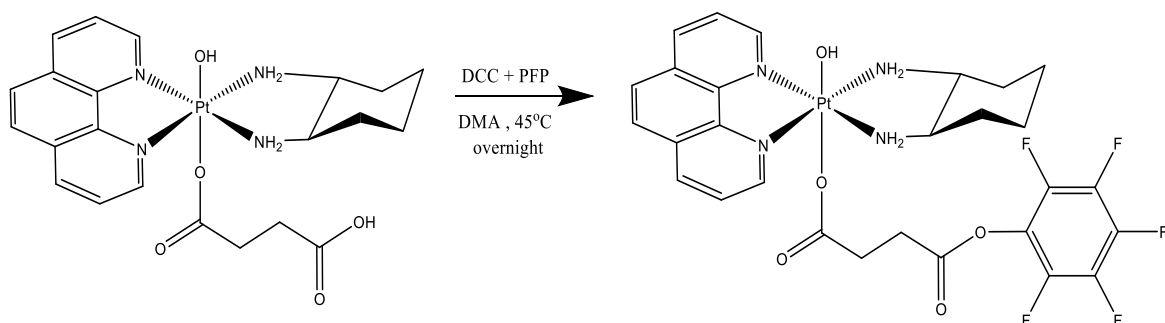


PHENSS(OH)₂ (1 equiv) was stirred in a minimal amount of water (~1 mL per 150 mg) with succinic anhydride (5 equiv) for 1 hr at 45 °C. The product was then precipitated in diethyl ether, then filtered and washed with more ether (3 mL). The product was then dissolved in water and freeze dried to produce a pale yellow powder. This method was repeated for 5MESS and 56MESS with no modifications.

Table 2.3.7.1. Summary of NMR data of $[\text{Pt}(\text{P}_L)(\text{A}_L)(\text{OH})(\text{Succ})]$ complexes, showing chemical shift (ppm), integration, multiplicity and coupling constants. Experiments were performed in D₂O, so amine resonances were not observed.

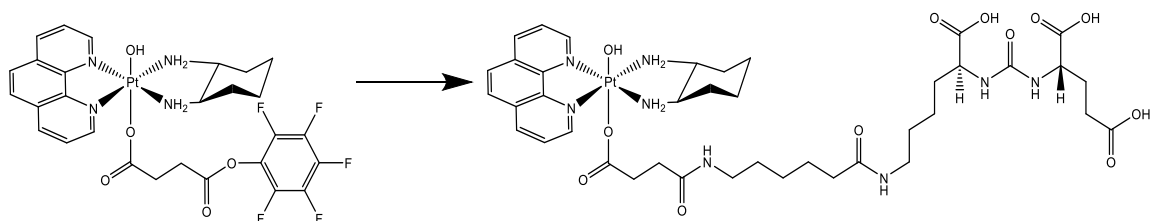
Label	Complexes		
	PHENSS(OH)(Succ)	5MESS(OH)(Succ)	56MESS(OH)(Succ)
H4	9.07 (d, 2H; CH, $J=8.13\text{Hz}$)	9.15 (d, 1H; CH, $J=8.45\text{ Hz}$)	9.08(m, 4H; CH)
H7	-	8.93 (d, 1H; CH, $J=8.45\text{ Hz}$)	-
H3	8.25 (dd, 2H; CH, $J=8.16, 8.34\text{ Hz}$)	8.18 (dd, 1H; CH, $J=8.46, 8.64\text{ Hz}$)	8.35 (dd, 2H; CH, $J=8.45, 8.42\text{ Hz}$)
H8	-	8.26 (dd, 1H; CH, $J=8.69, 8.83\text{ Hz}$)	-
H2	9.27 (dd, 2H; CH, $J=5.71\text{ Hz}, 8.37\text{ Hz}$)	9.26 (dd, 1H; CH, $J=5.50\text{Hz}, 8.64\text{Hz}$)	9.31 (dd, 2H; CH, $J=5.51\text{ Hz}, 8.47\text{ Hz}$)
H9	-	9.18 (dd, 1H; CH, $J=5.45\text{ Hz}, 8.33\text{ Hz}$)	-
H5	8.33 (s, 2H; CH)	-	-
H6	-	8.12 (s, 1H; CH)	-
CH ₃	-	2.89 (s, 3H; CH ₃)	8.21 (s, 6H; CH ₃)
H1'/2'	3.19 (m, 2H; CH ₂)	3.17 (m, 2H; CH ₂)	3.15(m, 2H; CH ₂)
H3'/6'	2.39 (m, 2H; CH ₂)	2.38 (m, 2H; CH ₂ $J=$)	2.38(m, 2H; CH ₂)
H4'/5'	1.68 (m, 2H; CH ₂)	1.65 (m, 2H; CH ₂)	1.66 (m, 2H; CH ₂)
H3'/6'	-	-	-
H4'/5'	1.29 (m, 2H; CH ₂)	1.29 (m, 2H; CH ₂)	1.29 (m, 2H; CH ₂)
H1*	2.22 (m, 2H; CH ₂)	1.20 (m, 2H; CH ₂)	1.22 (m, 2H; CH ₂)
H2*	2.16 (m, 2H; CH ₂)	2.14 (m, 2H; CH ₂)	2.13 (m, 2H; CH ₂)
¹ H/ ¹⁹⁵ Pt	9.37/542.1	9.32/543.6	9.46/ 546.5
% Yield	85	80	86

2.3.12 Synthesis of [Pt(1,10-phenanthroline)(1S,2S-diaminocyclohexane) (OH)(succinatePFP)]²⁺



This synthesis is a modified version of the method of Yuan et al.⁷⁴ PHENSS(Succ)(OH) (1.46 mg, 1 equiv.), DCC (122.6 mg, 3 equiv.) and pentafluorophenol (PFP) (110.4 mg, 3 equiv.) were added to 3 mL dry DMA. This solution was then stirred at room temperature for 14 hr after which it was filtered and washed with DMA. The product was then taken up in water and freeze dried to produce a yellow solid, yield 54.8 mg, 29.5%. ¹H NMR (400 MHz, D₂O) δ 9.09 (d, 2H: CH, *k* *J* = 8.45 Hz), 8.31 (dd, 2H: CH, *J* = 8.16, 8.34 Hz), 9.37 (dd, 2H: CH, *J* = 5.31 Hz, 8.37 Hz), 8.39 (s, 2H; CH), 3.23 (m, 2H; CH₂), 2.35 (m, 2H; CH₂), 1.68 (m, 2H; CH₂), 1.29 (m, 2H; CH₂), 2.22 (m, 2H; CH₂), 2.16 (m, 2H; CH₂).

2.3.13 Synthesis of [Pt(1,10-phenanthroline)(1S,2S-diaminocyclohexane) (OH)(PSMA)]²⁺



PhenSS(OH)(SuccPFP) (1 equiv) was dissolved in 4 mL of dry DMA, then 2 equiv of DCL was added. This solution was stirred at room temperature for 5 minutes before *N,N*-diisopropylethylamine (DIPEA) (6 equiv) was added. The solution was then dried

under vacuumed and purified using the Reveleris® X2 flash chromatography system fitted with a Reveleris® reverse phase C₁₈ 4 g column and eluted with MeOH and H₂O (see 2.2 Instrumentation for details). The product was then taken up in water and freeze dried to produce a yellow solid, yield 32.4 mg, 23%. ¹H NMR (400 MHz, D₂O) δ (PHENSS peaks) 8.87 (d, 2H: CH, *J*= 8.30 Hz), 7.98 (dd, 2H: CH, *J*= 8.30, 13.80 Hz), 8.47 (d, 2H: CH, *J*= 5.39 Hz), 8.11 (s, 2H; CH), 2.70, (m, 2H; CH₂), 2.20 (m, 2H; CH₂), 1.69 (m, 2H; CH₂), 1.22 (m, 2H; CH₂): (DCL peaks): 4.02 (dd, 1H, CH, *J*= 5.13 Hz), 3.98 (dd, 1H, CH, *J*= 5.23 Hz), 3.09 (t, 2H, CH₂, *J*= 7.13 Hz), 2.91 (t, 2H, CH₂, *J*= 7.18 Hz), 2.32 (t, 2H, CH₂, *J*= 5.43 Hz), 2.16 (t, 2H, CH₂, *J*= 5.45 Hz), 1.99 (m, 2H; CH₂), 1.82 (m, 2H; CH₂), 1.68 (m, 2H; CH₂), 1.56 (m, 6H; CH₂), 1.43 (m, 2H; CH₂), 1.28 (m, 4H; CH₂).

2.4 Cytotoxicity methodology

Cytotoxicity assay studies were performed at Calvary Mater Newcastle Hospital, Waratah, NSW Australia. In vitro studies were performed according to described methods in literature and from Calvary Mater facility. N₄-T₁S were prepared in DMSO as stock treatment (30 mM) solutions and stored at -20 °C. All of the cell lines were cultured in a humidified atmosphere with 5 % CO₂ at 37 °C. The cancer cell lines were maintained in Dulbecco's modified eagle's medium (DMEM; Trace Biosciences, Australia) supplemented with 10 % fetal bovine serum, sodium bicarbonate (10 mM), penicillin (100 IU mL⁻¹), streptomycin (100 µg mL⁻¹), and L-glutamine (4 mM). The non-cancer MCF10A cell line was cultured in DMEM.F12 (1:1) cell culture media, 5% heat-inactivated horse serum, supplement with penicillin (50 IU mL⁻¹), streptomycin (50 µg mL⁻¹), HEPES (20 mM), L-glutamine (2 mM), epidermal growth factor (20 ng mL⁻¹), hydrocortisone (500 ng mL⁻¹), cholera toxin (100 ng mL⁻¹), and insulin (10 µg mL⁻¹). Cytotoxicity was determined by plating cells in duplicate in 100 mL medium at a density of 2500-4000 cells per well in 96-well plates. On day 0, (24 hr after plating) when cells were in logarithmic growth, medium (100 µL) or without the test agent was added to each well. After 72 hr ligand exposure growth inhibitory (GI) effects were evaluated by MTT (3-[4,5-dimethylthiazol-2-yl]-2,5-diphenyltetrazolium bromide) assay, and

absorbance was read at 540 nm. An eight-point dose-response curve was produced, from which the GI₅₀ value was calculated, representing the drug concentration at which cell growth is inhibited by 50% based on the difference between the optical density values on day 0 and those at the end of drug exposure. Cell lines MCF10A, MCF7, MIA PaCa-2, BE(2)-C, U-87, NCI-H460, HT-29, and DU 145 are from ATCC (American Type Culture Collection); A2780 and, A431 are from ECACC (European Collection of Authenticated Cell Cultures) and; SJ-G2 are from St Jude's childrens hospital (Australia).

Chapter 3 Results and Discussion

3.1 Synthesis

3.1.1 Synthesis of [Pt(1,10-phenanthroline)(1S,2S-diaminocyclohexane)]²⁺

PHENSS was synthesised as an intermediate to form [Pt(1,10-phenanthroline)(1S,2S-diaminocyclohexane)₂]²⁺ and to assess the efficiency of synthesis using flow. All of the optimization of the flow procedure was accomplished using PHENSS. When synthesised using batch chemistry, phen and [Pt(1S,2S-diaminocyclohexane)Cl₂]²⁺ were suspended in 50 mL of deionized water in a 1.1:1 molar ratio and refluxed for 24 hours. During this time the chlorine ligands dissociate from the platinum complex and the 1,10-phenanthroline coordinates the nitrogen forming the soluble product PHENSS. As both starting materials are insoluble in water while the product is soluble, the reaction turns initially from an opaque to clear solution upon completion, making it an easy reaction to monitor. The volume of the crude solution is then reduced under pressure so that it may be purified using a Vac 20cc (5 g) C₁₈ Sep-Pak[®] column connected to a pump apparatus with UV detector (Bio-Rad, EM-1 Econo™ UV Monitor). The column was activated with methanol (20 mL) and then flushed with water (~40 mL) until the UV absorbance equilibrated. Any platinum-diaminocyclohexane impurities elute first through the column followed by the product which is bright yellow in colour. Phen and other impurities do not flow through the column when eluted with water, and remain in the top few millimetres of the column. The pure sample collected is reduced in volume to roughly 2 mL whereupon it is frozen and dried *via* sublimation (86.5 % yield).

For the continuous flow synthesis of PHENSS the column was fitted sealed and the outlet fitted with a 100 psi pressure adaptor before being filled with water and heated to 140 °C. Once heated, deionized water was then eluted through the vessel at a flow rate 0.05 mL/min for 1.5 hrs (Figure 3.1.1.1). The volume of the crude solution is then reduced under pressure so that it may be filtered. The pure sample collected is

reduced in volume to roughly 2 mL whereupon it is frozen and dried *via* sublimation. This method relies on both starting materials being insoluble so that they do not flow through the glass frit fitted at the end of the column whereas the product is soluble and can flow through the frit into the collection vessel, avoiding a further purification step. Phen is moderately soluble in water at high temperatures, so at moderate temperatures it was hypothesised that the reagents would react while only dissolving a minimal amount of phen. However, this was not the case; instead the yield rose steadily as temperature increased, with the yield doubling every 20 °C increase until 140 °C (Figure 3.1.1.4) at which point experiments were stopped due to safety concerns with the high pressure and temperature in the glass column. It is also interesting to note that the optimal temperature (140 °C) is significantly higher than the temperature used in the batch synthesis (100 °C).

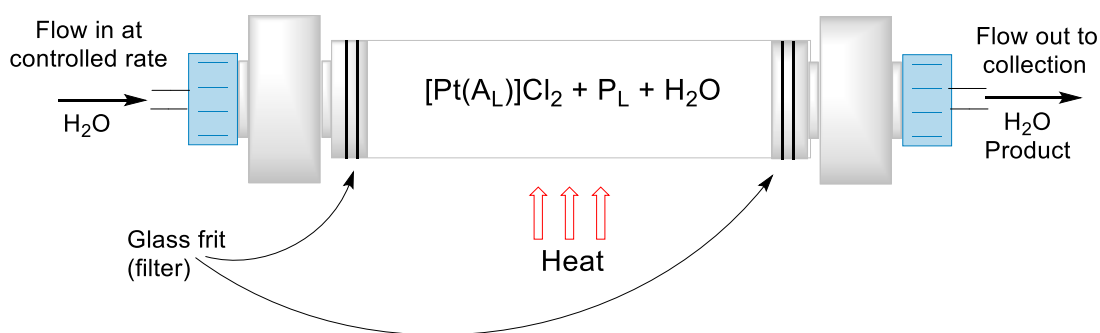


Figure 3.1.1.1: Set up for flow chemistry synthesis of $[\text{Pt}(\text{P}_L)(\text{A}_L)]^{2+}$

Optimization

PhenSS was chosen as the target product for the optimization process due to its relative simplicity and inexpensiveness of the starting materials. The product of the batch synthesis of PhenSS was used to produce a standard HPLC curve so that the fractions off the flow apparatus (Figure 3.1.1.2) could be quantitatively analysed. The retention time was ~ 3.7 min when using gradient elution from 10% acetonitrile to 100% over 15 minutes.

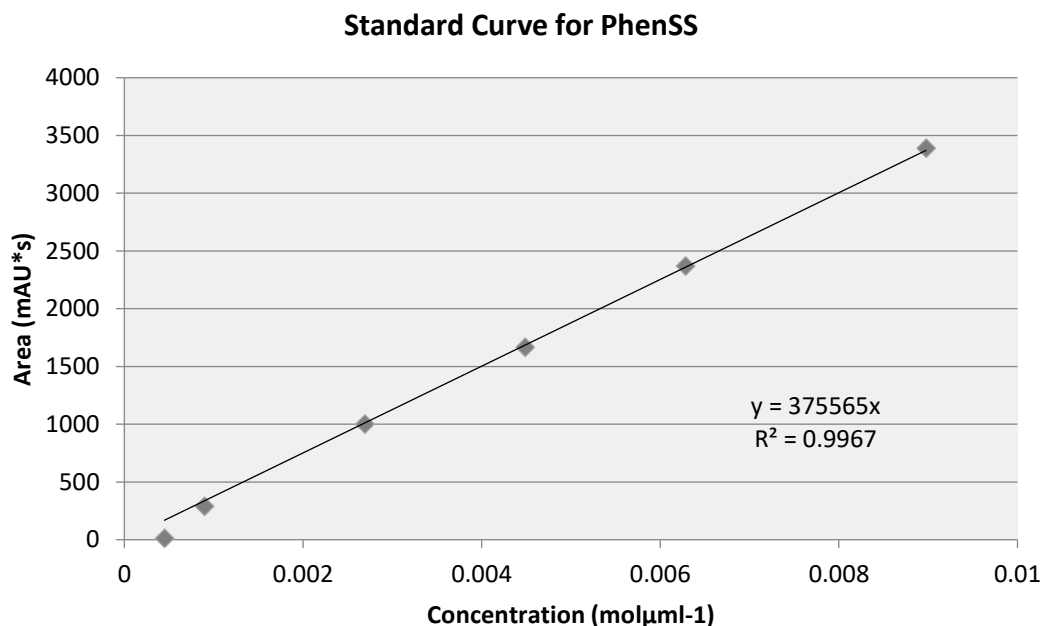


Figure 3.1.1.2: Standard HPLC curve for PhenSS from gradient elution of acetonitrile.

Optimisation of Time

Using the apparatus depicted in Figure: 3.1.1.1, deionised water was run through the reaction column containing [Pt(dach)Cl₂] and phen (1:1.1 mole ratio) for three hours at a flow rate of 0.25 mL/min at 80 °C. Every 15 min a 3 mL sample was collected for analysis. These fractions were then assessed by HPLC and their concentration calculated using the standard curve. The resulting curve of concentration output over 3 hrs (Figure 3.1.1.3) suggests that the product starts forming in between t_{15} and t_{30} and reaches its maximum rate at t_{60} before slowly declining right up until t_{180} .

From this it was ascertained that 1.5 hrs was the optimal reaction time, and consequently all subsequent optimisation reactions went for 1.5 h. Later this time was reconsidered after reviewing the area under the curve between t_{90} and t_{180} . Another experiment was conducted for 2.5 hrs which resulted in an average percent yield of 18.9% which is significantly lower than the average percent yield gained from the same reaction conditions run for only 1.5 hr, 28.1 %. These results appear to be contradictory and suggest that the use of continuous flow chemistry for the synthesis of these

inorganic compounds does not produce the reproducible results reported for organic synthesis.

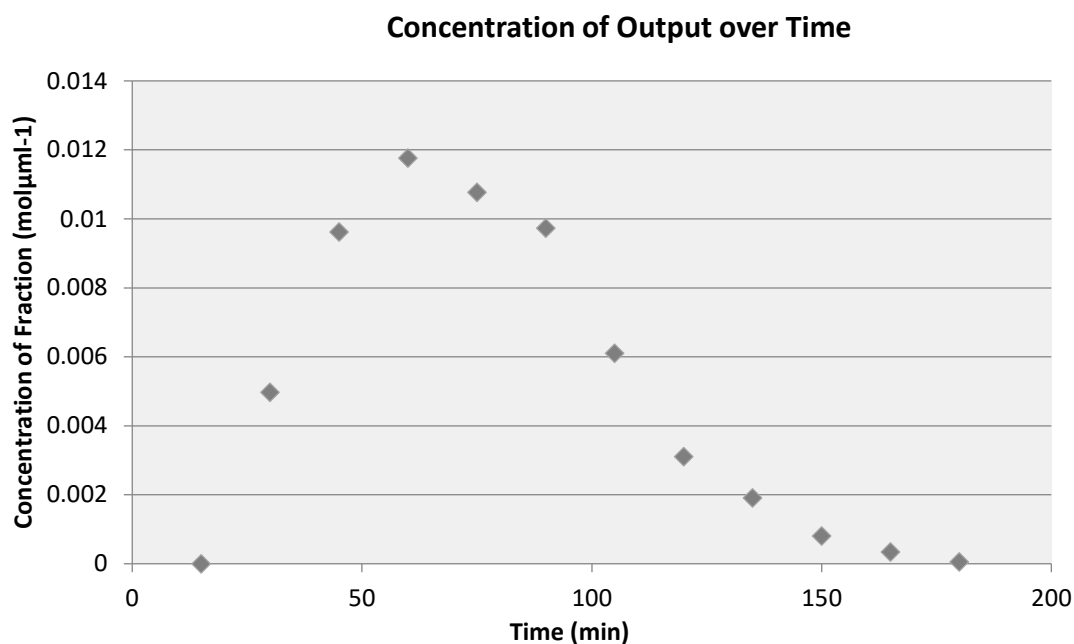


Figure 3.1.1.3: Concentration of fractions collected off the column containing [Pt(dach)Cl₂] and 1,10-Phenanthroline (1:1.1 mole ratio) every 15 minutes for three hours at a flow rate of 0.25 mL/min at 80 °C.

Optimisation of Temperature

The experiment was repeated, this time running for 1.5 hrs with the temperature changing for each run. Experiments were run for 20, 40, 60, 80 100 and 120 °C. To quickly find the yield of each run, a small sample of each was analysed using the HPLC. The HPLC data and the standard curve for PhenSS concentration vs temperature was used to calculate the concentration of PhenSS in the crude product which subsequently allowed the yield to be calculated. When analysed by HPLC it was found that no significant product formation occurred until 80 °C was reached, and appeared to increase at higher temperatures. The experiment was repeated twice more, this time only with the temperatures 80, 100 and 120 °C so as not to waste reagents. The results revealed that the yield increased exponentially as temperature increased (Figure 3.1.1.4).

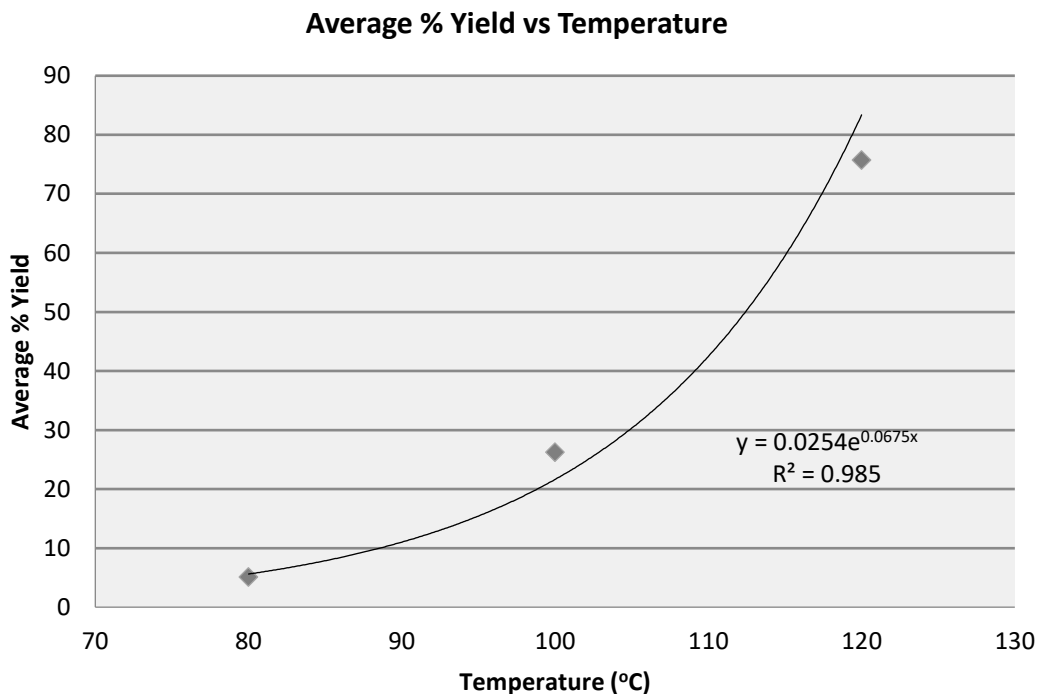


Figure: 3.1.1.4: Average percentage yield of PhenSS calculated based on HPLC trace, synthesised at 80, 100 and 120 °C, with a flow rate of 0.25 mL/min with a [Pt(DACH)Cl₂] to 1,10-phenanthroline more ratio of 1:1.1.

These results were very promising and in order to confirm this trend and produce a higher yield, 140 °C was also assessed. To reach this temperature a pressure adapter was fitted to the 'out' tubing that brought the pressure inside the column to 100 PSI, which prevented the water from evaporating. The resulting yield (calculated using the HPLC-standard curve method) was far above 100% and this brought the reliability of the yield calculation method into question. The reactions were repeated however, this time the crude product was purified using Vac 20cc (5 g) C₁₈ Sep-Pak® columns and the product was weighed. The result of this data series (Figure 3.1.15) clearly shows that the yields calculated *via* the HPLC-standard curve method were vastly exaggerated. Each subsequent yield was calculated using the new method as it was more accurate and more appropriate to compare to the yield gained from the batch chemistry method.

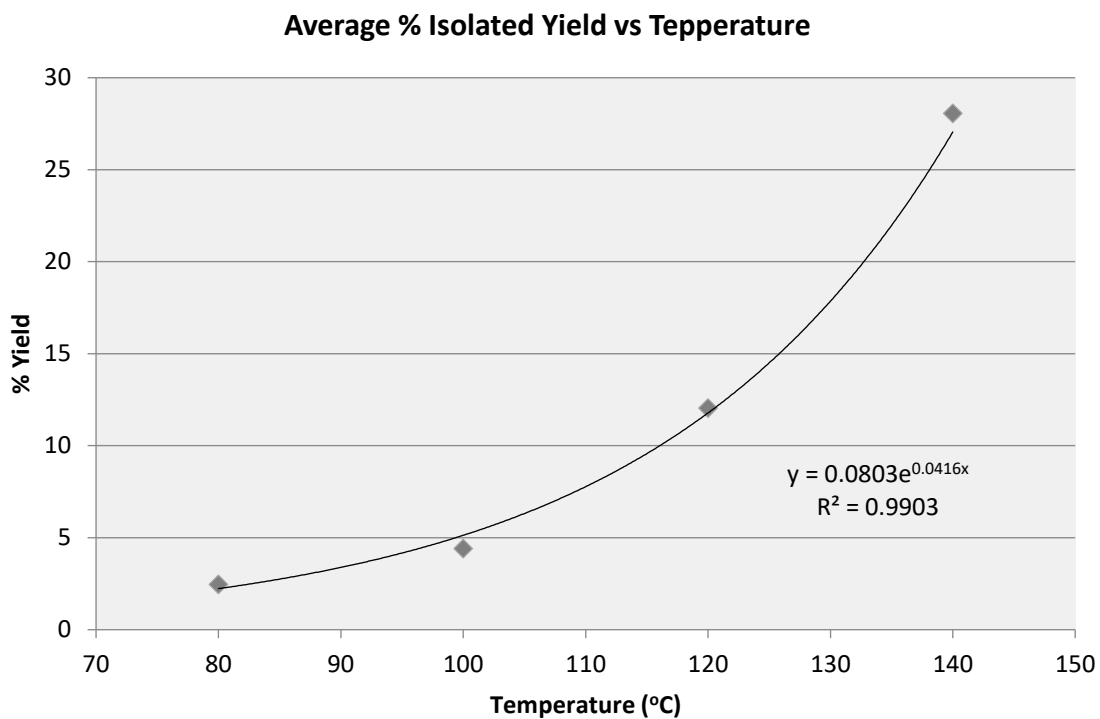


Figure: 3.1.1.5: Average percentage yield of PhenSS calculated based on isolated pure complex, synthesised at 80, 100 and 120 °C, with a flow rate of 0.25 mL/min and a [Pt(dach)Cl₂] to phen ratio of 1:1.1.

To find the optimal flow rate, a single run at 0.10 mL/min was undertaken and the % yield was determined to be higher than that of 0.25 mL/min; a faster flow rate was not assessed as it was predicted that the relationship would be linear and thus such a run would be a waste of resources. The reaction was repeated for 0.25, 0.10, 0.05 and 0.02 mL/min in duplicate (Table 3.3.1). It is suspected that the partial solubility of the phen was the reason that a reduced flow rate is beneficial; if the flow rate was too high, a solid white phen precipitate formed in the collection vessel. Thus it was concluded that the 1,10-phenanthroline had reached a high enough temperature to become soluble, and so could flow through the glass frit of the outlet; reducing the flow rate increases the chance of reaction as the 1,10-phenanthroline has more of a chance to react with the [Pt(dach)Cl₂] before leaving the reaction vessel.

Table 3.3.1: Percent yield of [Pt(1,10-phenanthroline)(1S,2S-diaminocyclohexane)]²⁺

Flow Rate	[Pt(SSDACH)Cl ₂] (mg)	1,10-PHEN (mg)	Predicted yield	Actual Yield	Yield (%)
0.25	98.0	53.2	144.5	43.8	30.3
0.25	108.4	54.2	159.8	41.3	25.8
0.10	97.8	51.5	144.1	53.2	37.1
0.10	118.2	65.3	183.9	61.5	33.4
0.05	110.2	73.2	162.4	59.0	36.3
0.05	118.0	78.8	183.6	91.1	49.6
0.02	101.9	53.5	150.2	24.4	16.3
0.02	76.7	43.4	174.2	65.7	37.7

Table 3.3.1 shows that the yield increases as the flow rate drops, the yield reaches a maximum at 0.05 mL/min before dropping off at 0.02 mL/min. This indicated that the optimal flow rate is 0.05 mL/min; however, it was noticed that when the flow rate was 0.05 mL/min the water level within the reaction vessel dropped slightly and even more so when the flow rate was 0.02 mL/min. The reaction vessel was standing upright with the inlet at the base, and so a drop in the water level means that the water was leaving the vessel as a gas, preventing the product from being filtered out of the reaction solution into the collection vessel. Thus the drop in yield after 0.05 mL/min could be due to the fact that the product was unable to leave the reaction vessel rather than because the product was only being synthesised at a small yield. This theory is supported by the inconsistency of the yields calculated for flow rates of 0.05 and 0.02 mL/min. When the materials remaining inside the vessel were prepared for NMR it was revealed that only the starting products remained, there was no trace of PhenSS; thus the inconsistency of the results was not due to the positioning of the vessel.

The continuous flow method is not advantageous over the traditional batch method. Although the flow method produced PhenSS in just one 16th of the time of batch method; at its best the flow method produced just half the predicted yield compared with 80-85% from the batch method. Continuous flow chemistry typically produces consistent reliable results however this was not the case when used to

synthesise PhenSS. Due to poor yields and inconsistent results, the continuous flow method development was terminated. Despite being unsuccessful, this is as far as I am aware, first time continuous flow chemistry has been used for the synthesis of this type of coordination compound, as there are no other references to such methods in the literature.

3.1.2 Synthesis of [Pt(1,10-phenanthroline)(1*S*,2*S*-diaminocyclohexane)]²⁺, [Pt(1,10-phenanthroline)(1*R*,2*R*-diaminocyclohexane)]²⁺, [Pt(5 methyl-1,10-phenanthroline)(1*S*,2*S*-diaminocyclohexane)]²⁺, [Pt(5-methyl-1,10-phenanthroline)(1*R*,2*R*-diaminocyclohexane)]²⁺ [Pt(5,6 dimethyl-1,10-phenanthroline)(1*S*,2*S*-diaminocyclohexane)]²⁺, [Pt(5,6 dimethyl-1,10-phenanthroline)(1*R*,2*R*-diaminocyclohexane)]²⁺

PHENSS, PHENRR, 5MESS, 5MERR, 56MESS and 56MERR were synthesised as intermediates to form platinum(IV) complexes and to assess the efficiency of batch synthesis compared to using flow and, as a part of a series of compounds of which the dihydroxy and asymmetric (OH)(OAc) complexes were made. When synthesised using batch chemistry, phen and [Pt(SS-dach)Cl₂]²⁺ were suspended in 50 mL of deionized water in a 1.1:1 molar ratio and refluxed for 24 hours. During this time the chlorine ligands dissociate from the platinum complex and the Pt coordinates the atomic nitrogen forming the soluble product [Pt(56Me₂phen)(SS-dach)]²⁺. As both starting materials are insoluble and the product soluble, the reaction turns initially from an opaque to clear solution at completion, making it an easy reaction to monitor. The volume of the crude solution is then reduced under pressure so that it may be filtered using a Vac 20cc (5 g) C₁₈ sep-pak column connected to a pump apparatus with UV detector (Bio-Rad, EM-1 Econo™ UV Monitor). The column was activated with methanol (20 mL) and then flushed with water (~40 mL) until the UV absorbance equilibrated. Any dach impurities elute first through the column followed by the

product which is bright yellow in colour. The 5,6-dimethyl-1,10-phenanthroline and any other impurities do not flow through the column when eluted with water, and remain in the top few millimetres of the column. The pure sample collected is reduced in volume to roughly 2 mL whereupon it is frozen and dried *via* sublimation. The purity of these compounds was confirmed using NMR and HPLC.

3.1.3 The Synthesis of [Pt(1,10-phenanthroline)(1S,2S-diaminocyclohexane)X₂]²⁺

For the synthesis of [Pt(phen)(SS-dach)X₂]²⁺ there are two reported methods, both of which were modified to suit this type of complex and trialled for the synthesis of [Pt(phen)(SS-dach)Cl₂]²⁺. The first synthetic method was a combination of the procedure described in Symal A. *et al.*¹⁰² and Yamanda M. *et al.*¹⁰³ This procedure required the *in situ* generation of the halide gas (in this case Cl₂) from the combination of the halide salt and a mixture of concentrated sulphuric and nitric acids. The gas produced was then passed through a vessel containing PHENSS dissolved in dilute HCl (Figure 3.1.4.1). This reaction was left until the gas ceased to form (~3 h) at which point the apparatus was flushed with N₂ for several hours to remove any excess chlorine. The crude product neutralized and produced chlorine gas when the volume was reduced under pressure which is highly unfavourable as chlorine gas is highly toxic and cause severe respiratory damage. The chlorine gas produced during this reaction corroded all of the plastic tubing and the plastic joint clips, demonstrating that the gas was not sufficiently contained within the glassware. These observations provide evidence that the safety precautions undertaken may not be adequate and thus the *N*-halogensuccinimide reaction is preferable.

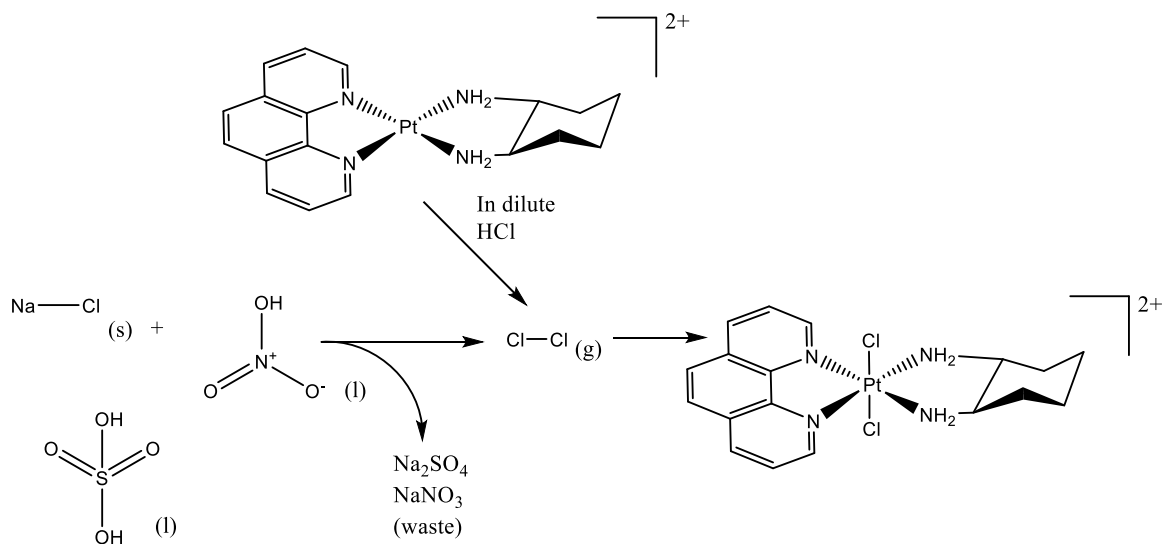


Figure 3.1.4.1: Reaction scheme for the formation of $[\text{Pt}(\text{Phen})(\text{SS-dach})\text{Cl}_2]^{2+}$ using the *in situ* formation of Cl_2 gas.

The second method (NXS method) utilises the oxidating property of *N*-halogensuccinimides in order to oxidise platinum whilst also binding halogens to the platinum centre. This method achieved oxidation in less than five minutes and is significantly less hazardous than the first method, whilst producing the same yield of product. Half of the NXS reacts with ethanol to produce HX (where X is Br, Cl, or I) which then reacts with the second half of NXS to produce halogen radicals which attack the platinum centre;¹⁰⁴ reducing it to Pt(IV) to produce the desired product $[\text{Pt}(1,10\text{-phenanthroline})(1S,2S\text{-diaminocyclohexane})\text{X}_2]^{2+}$ (Figure 3.1.4.2). However, the introduction of the succinimide resulted in the synthesis of impurities where one of the axial ligands is succinimide bound via the nitrogen (Figure 3.1.4.3).

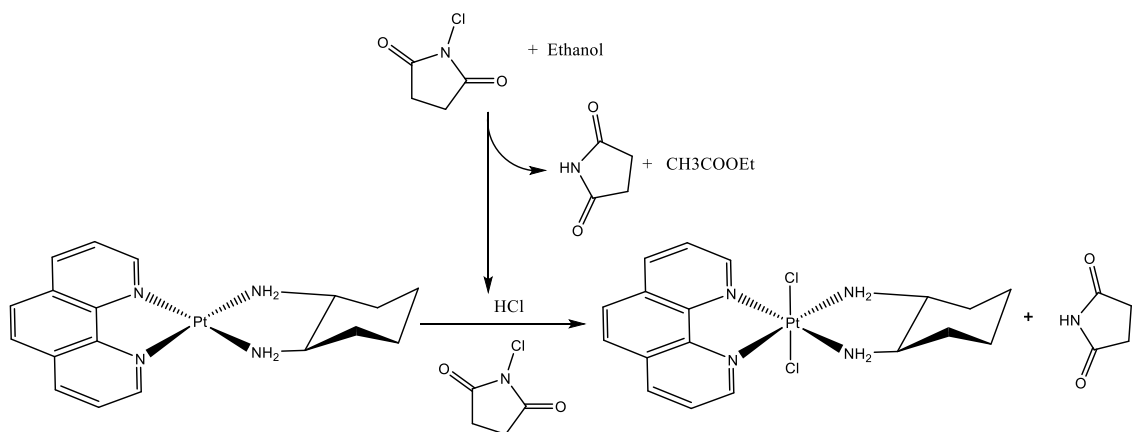


Figure 3.1.4.2: Reaction scheme for the formation of [Pt(1,10phenanthroline)(1S,2S-diaminocyclohexane)Cl₂]²⁺ using NCS.

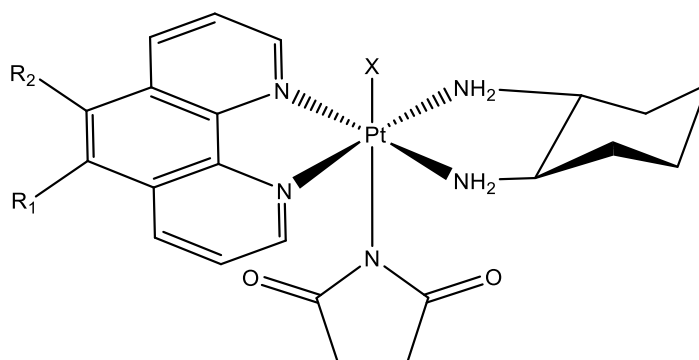


Figure 3.1.4.3: Suggested impurity synthesised using the NXS method. Where X is Br, Cl, or I. and where R₁ and R₂ are either H or CH₃.

The presence of this impurity was confirmed both by NMR and Mass spectrometry. In proton NMR spectra there is a large peak at 2.7 ppm, which is very easily identifiable. A ¹H/¹H homonuclear correlation spectroscopy (COSY) spectra confirmed that this impurity was succinimide; the 2.7 ppm ¹H peak corresponded to a carbon peak at 29 ppm, which is likely to be a carbon adjacent to a ketone. Computational models (completed using Avogadro) were made to predict how binding of the halogens and the succinimide were affecting the structure and consequently the NMR (Figure 3.1.4.3). These models suggest that the configuration of PhenSS is not

changed from their typical planar structure with the addition of bromine on the axial ligands. When a succinimide is bound in one of the axial positions there is a significant bend in the overall structure and this pushes the dach region toward the halide, which explains why there is a shift in the proton NMR peaks in the dach region when the impurity is present. Analysis of mass spectra of these complexes revealed that the succinimide binds directly to the Pt centre via the nitrogen, and that there are no instances of two succinimide binding. Several attempts were made to separate the di-halogenated product from the mono-halogenated succinimide impurity; however, it appeared that the two major products have the same solubilities and chromatographic retention times and thus cannot be separated by filtration, crystallisation, precipitation or by changing the counter ions. Standard crystallisation methods did not produce crystals or produced crystals which were in low yields and which were inappropriate of x-ray crystallography.

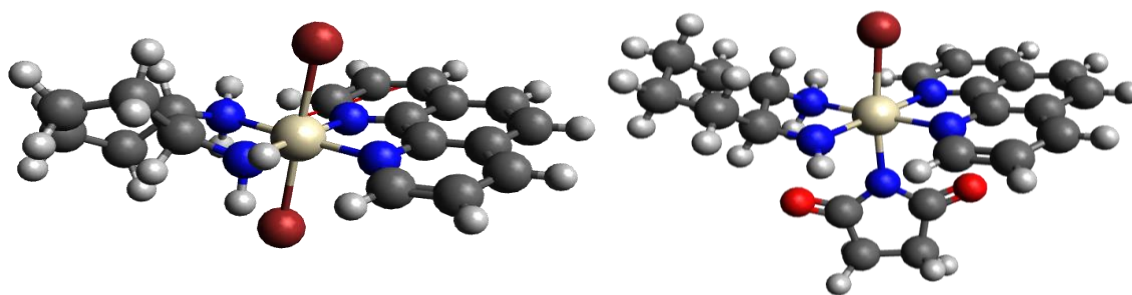


Figure 3.1.4.3: Structure of PHENSSX₂ and PhenSSX(succinimide), showing the distortion of the DACH region.

Due to these issues with purification, the reaction conditions were revisited to attempt to favour the formation of one product over another. It was found that a pure PhenSSXsuccinimide could be synthesised by refluxing 1 mol equiv of PhenSS with 2.4 mol equiv of NXS in a solution of 50:50 (v:v) ethanol and water at 78 °C. The purity of these compounds was confirmed by NMR and the structure confirmed by mass spectrometry. Interestingly, the addition of hydrochloric acid pushed the reaction to favour the dihalogen product. Presumably this is due to the interaction between the succinimide by-product and the acid, preventing the coordination of the succinimide.

Perhaps due to the high concentration of ions in the solution encouraging the halogen to remain bound to the Pt. This method resulted in the successful synthesis of PHENSSCl₂, PHENSSBr₂, PHENSSI₂, 5MESSCl₂, 5MESSBr₂, 5MESSI₂, 56MESSCl₂, 56MESSBr₂, and 56MESSI₂.

Another hurdle that needed to be surmounted was the purification of these complexes. The presence of unbound succinimide remained in all samples both asymmetric and symmetric, which was easily seen in the NMR spectra. Again the products and the succinimide have almost the same solubility and could not be separated by filtration, precipitation or Sep-Pak C₁₈ column. However, free succinimide is mildly soluble in toluene, and so if the crude complex was washed 5 times with toluene only a small amount of succinimide removed. It was concluded that extended washing could considerably improve the purity of the sample so a soxhlet apparatus was set up. The soxhlet needed to be run for a minimum of two weeks before the impurity was undetectable. In some cases the soxhlet resulted in the appearance of other small unidentified impurities but, these were easily removed using flash chromatography. The soxhlet and the flash chromatography both contributed to the overall loss of yield (16.3- 30.4%). The identity and purity of the compounds was confirmed using NMR spectra, elemental microanalysis, circular dichroism (CD), synchrotron radiation circular dichroism (SRCD), UV spectra and HPLC.

3.1.4 Synthesis of [Pt(5,6-dimethylphenanthroline)(1*S*,2*S*-diaminocyclohexane)X₂]²⁺ and [Pt(5-methylphenanthroline)(1*S*,2*S*-diaminocyclohexane)X₂]²⁺

The synthesis of 56MESSX₂ and 5MESSX₂ was much the same as for PhenSSX₂ however; they tended to need slightly more time to react and produced more darkly coloured products in lower yields. The complexes were also much harder to purify in most cases which also contributed to a lower average yield. Some compounds however, such as 5MESSCl₂ (yield of 52.9%), separated more cleanly in the flash chromatography system resulting in a significantly higher yield overall than complexes

that were run through the soxhlet then the flash. None of these complexes were completely purified during the two week soxhlet and they all had to be run through the flash chromatography needing a minimum of 5 runs each. Each flash chromatography elution resulted in approximately 5 mg of compound being lost, only some of which can be attributed to the removal of the impurity. The 5MESSX₂ complexes were slightly more pure after the soxhlet and were pure after fewer runs through the flash chromatography system than the 56MESSX₂ complexes. The number of methyl substituents appears to influence the ease of purification in this case. Interestingly, despite the succinimide impurity having a white appearance, as the purity of the desired complex improved, it became lighter in colour. This was particularly the case for the iodo complexes which turned from a dark brown crude product to pale yellow when pure. There may have been some traces of the halogen which would not be picked up in a proton NMR, which are removed by either the toluene wash or through flash chromatography. The yellow colour may also be due to an unidentified impurity that was also present during the previous synthesis of platinum(IV) dihydroxido complexes, which were yellow/cream coloured at first but then white after extensive chromatography purification.¹⁰⁰ The extensive chromatography did not result in a white final product, and so these complexes may just be yellow. The range of yields for these complexes was 9.16 - 52.9% due to the extensive amount of purification required. The identity and purity of the compounds was confirmed using NMR, microanalysis, CD, synchrotron CD, UV spectra and HPLC.

3.1.5 Synthesis of Pt(IV) complexes of the type [Pt(P_L)(A_L)(OH)₂]²⁺

56MESS(OH)₂, 56MERR(OH)₂, PHENSS(OH)₂, PHENRR(OH)₂, 5MESS(OH)₂, 5MERR(OH)₂, 4MESS(OH)₂, 4MERR(OH)₂, 44BPYSS(OH)₂, and 44BPYRR(OH)₂ were synthesised as a part of a series of compounds of which the dihydroxido and asymmetric (hydroxide-acetato) compounds were made. To synthesise these complexes, the complementary Pt(II) complex was first converted to the nitrate salt. This was achieved through the addition of silver nitrate, which removes chloride from

solution as silver chloride, allowing nitrate to become the counter-ion. Once filtered, the Pt(II) is dried via sublimation, ready to be converted to Pt(IV). 1 equiv. of $[\text{Pt}(\text{P}_L)(\text{A}_L)]\text{NO}_3$ was dissolved in a minimal amount of water and stirred at 70 °C with 10 equiv. of H_2O_2 for 2 h, after which the solution was immediately frozen and dried *via* sublimation. Within the 2 h, the free radicals of the peroxide react with the Pt centre, forming a co-ordinate bond in the axial position allowing the addition of the solvent (in this case acetic acid) in the remaining axial position. If the reaction is left to heat for too long, heated on the hot plate rather than in a water bath or, exposed to light before completely dry; there is a risk that some of the newly formed Pt(IV) being reduced to platinum(0) (Pt(0)) which appears in the form of a black precipitate. The complex when removed from the freeze dryer is pale yellow, fluffy and highly sensitive to static due to its 2+ charge. The lyophilised solid is then dissolved in a minimal volume of water and filtered using a Vac 2Occ (5 g) C_{18} sep-pak column connected to a pump apparatus with UV detector (Bio-Rad, EM-1 Econo™ UV Monitor). The column was activated with methanol (20 mL) and then flushed with water (~40 mL) until the UV absorbance equilibrated. Pt(0) and other impurities remain at the head of the column. The aliquots containing the pure sample are combined and reduced in volume to roughly 2 mL whereupon it is frozen and dried *via* sublimation again. If after one run through the column the sample is still quite yellow, this process was repeated but at a slower elution rate until the complex is almost completely white; with the exception of $\text{BPYSS}(\text{OH})_2$ and $\text{BPYRR}(\text{OH})_2$ which remained bright yellow after several elutions through a column, suggesting that this is its characteristic colour rather than evidence of an impurity. The purity of these compounds was confirmed using NMR and HPLC.

3.1.6 Synthesis of Pt(IV) complexes of the type $[\text{Pt}(\text{P}_L)(\text{A}_L)(\text{OH})(\text{C}_2\text{H}_3\text{O}_2)]^{2+}$

56MESS(OH)(OAc), 56MERR(OH)(OAc), PHENSS(OH)(OAc), PHENRR(OH)(OAc), 5MESS(OH)(OAc), 5MERR(OH)(OAc), 4MESS(OH)(OAc), 4MERR(OH)(OAc), 44BPYSS(OH)(OAc), and 44BPYRR(OH)(OAc) were synthesised as a part of a series of complexes of which the dihydroxy and asymmetric (OH)(OAc) compounds were made.

This method was adopted from that used by B. Pages to synthesise PHENSS(OH)(OAc).¹⁰⁰ Although successfully synthesised, method difficulties were encountered when attempting to purify the final product. As a result only partial characterisation was achieved, and only for one complex, PHENSS.

Although in the aforementioned paper the Pt(II) was first converted to the acetate salt, the standard method on converting to the nitrate salt as described in Section 3.1.6, was trailed with PHENSS however the resulting complex was a mix of Pt(II) dihydroxy and asymmetric compounds so the remainder of the complexes were made by first converting to the acetate salt. To convert to the acetate salt, Pt(II) chloride (1 equiv) was dissolved in a minimal amount of water with 2 equiv of silver acetate, and stirred overnight in the dark. As the reaction is stirred, the acetate ions from the silver acetate exchange with the chloride from the Pt salt, producing silver chloride and the nitrate salt of the Pt(II) complex. The silver chloride precipitates out as a very fine white precipitate which must be filtered with membrane filters with a pore size of 45 micrometres or less. As mentioned previously the solution must be kept in darkness as the silver chloride is photosensitive. Once filtered the Pt(II) is dried via sublimation, it is ready to be converted to Pt(IV). Due to the use of acetic acid in the Pt(IV) synthesis, the Pt(II) chloride was converted to the acetate salt, rather than the nitrate salt, prior to oxidation. To oxidise, 1 equiv. of Pt(II) acetate was stirred in the dark at room temperature for two days with 3.5 equiv. of hydrogen peroxide and 25 equiv of acetic acid (as a 1.5 mL solution). The reaction was kept at room temperature to prevent rapid activation of the peroxide and coordination of two hydroxide ligands, in order to allow time for the acetate ligands to coordinate. It was determined that even a mild heat (45 °C) resulted in an NMR with many impurities. The acetic acid is added in excess to maximise binding as the hydroxyl ligands tend to be more reactive, thus the peroxide volume must be kept to a minimum in order to avoid the synthesis of the dihydroxy product. After 48 hrs the solution was added dropwise to diethyl ether, resulting in a very fine precipitate formed which was then refrigerated in an attempt to increase the yield. After 24 hrs more precipitate formed and collected in a fluffy

aggregate toward the bottom of the flask. Some of the precipitation had also adhered to the flask. Water (2 mL) was added to increase the volume of the small immiscible layer that formed so that the ether could be removed (along with any Pt(II) impurities) *via* separation rather than by filtration. This was beneficial as the presence of water from the acetic acid solution would contribute to the low yield and, the precipitate adhered to the flask could also be collected. The next step was to evaporate the solution to obtain a NMR spectrum; however, drying resulted in the formation of Pt(II) and Pt(0) and an impure NMR spectra, instead the volume was reduced to 0.5 mL and the complexes stored in solution. In solution, the Pt(II) concentration increased slightly over a period of 3 months but, the majority of the solution remained as Pt(IV). It is hypothesised that the acetate ligands are in constant exchange with the solvent, and when the solvent is removed, the acetate ligands are removed along with it. Despite being unable to isolate the complexes for characterisation, the complexes in solution could still be used to build further asymmetric Pt(IV) complexes.

3.1.7 Synthesis of 2-aminoethyldiclofenamide

Diclofenamide (DCF) was dissolved in a minimal amount of chloroform before 2 equivalents of 1,2-ethylenediamine (en) were added at room temperature. This reaction appeared to occur instantaneously in quantitative yields. The solution was left to sit overnight, after which large clear crystals were obtained, which were filtered and washed with chloroform. The crystals were large, completely clear, and colourless; in some instances there was a slight beige colour to the crystals at which point they were recrystallised in ethanol to produce colourless crystals. (95 % yield)

3.1.8 Synthesis of [Pt(1,10-phenanthroline)(1S,2S-diaminocyclohexane)(DMSO)₂]²⁺

PhenSS(DMSO)₂ was synthesised as a part of a reaction scheme used to attach DCF to platinum, the concept being that DMSO would be such a good leaving group that any other potential ligands in solution would bind in preference. Based on

methods previously published, stirring a Pt complex solution that has chloride ligands with a DMSO solvent at a low temperature, will result in the synthesis of a DMSO ligated complex.¹⁰⁵ PHENSSCl₂ was synthesised as per the method described in Section 2.3.5. However, the purification steps were not undertaken in order to save time and with the understanding that upon precipitation, the succinimide by-product from the synthesis of the dichlorido intermediate would be separated from the final product. The crude solution was instead dried under vacuum and added as is to 16 mL of DMSO. The reaction can be easily monitored visually as the starting reagent is not soluble in DMSO; thus a clear solution indicates that the chlorido ligands have exchanged with the solvent. In the first attempt 100 mg of PHENSS was used to synthesise the dichlorido intermediate, which was then dissolved in 16 mL of solvent, as per the literature method. In an attempt to reduce the amount of DMSO used, this volume was reduced to 2 mL per 100 mg starting material, this reaction did not turn clear, indicating that the desired product was not formed. The sample was heated incrementally over a period of a week to see if this would allow the ligands to exchange without increasing the volume of DMSO. A temperature of up to 120 °C was used without the observation of a clear solution, at which point the idea was scrapped and more DMSO was added. Optimisation revealed that a minimum of 7 mL DMSO is required for every 100 mg of starting reagent. In the published method mentioned above the final product was precipitated in diethyl ether; this method was unsuccessful using PHENSS, which would not precipitate even when cooled to 4 °C with excess ether. In order to extract the product from DMSO, the solution was washed with 5 x 50 mL of dichloromethane (DCM). Although the DCM layer appeared to go cloudy when dried there was no trace of Pt complex in the NMR spectrum. Extraction with a mixture of briny water with DCM or ether were attempted but, when these methods could not remove the DMSO, elution through a flash chromatography C₁₈ column was trailed. However, multiple runs were required, removing less than 1 mL of DMSO per run. Because continued runs through the flash would result in lost product, a chloroform extraction was trailed and successfully separated the Pt(IV) complex from DMSO;

however the ^{195}Pt NMR signal was suspiciously similar to that of $\text{PHENSS}(\text{Cl})_2$, as was the ^1H spectra. The compound was consequently made in deuterated DMSO so that the final product could be characterised without the axial ligand exchanging. The resulting solution had no trace of $\text{Pt}(\text{II})$ nor the dichloro starting materials. Although all the peaks could be assigned the amine peaks appear much further upfield than expected, resonating close to the phenanthroline peaks. For reaction with DCF, the crude solution was used and the final product precipitated out of the DMSO solution so it could be characterised as per usual. (96 % yield)

3.1.9 Synthesis of $[\text{Pt}(\text{1,10-phenanthroline})(\text{1S,2S-diaminocyclohexane})(\text{2-aminoethyldiclofenacamide})_2]^{2+}$

As mentioned previously, the starting reagent for this method $\text{PHENSS}(\text{DMSO})_2$ was not isolated from the reaction solvent before being used. 5 equiv. of en-DCF was added directly into the DMSO solution, at which point the colour changed from pale yellow to dark orange, back to almost clear before becoming dark green, all within the space of a minute; after several minutes the solution had turned to a purple black colour. The reaction was then stirred at $70\text{ }^\circ\text{C}$ for 20 minutes. The 20 minute stir time was increased in instances where the en-DCF crystals had not fully dissolved, and this had no noticeable impact on the purity or quantity of the yield. Once the en-DCF had dissolved (or after at least 20 minutes) the DMSO was diluted by a factor of 4 with absolute ethanol and stirred overnight at $40\text{ }^\circ\text{C}$. The ethanol was then removed *via* evaporation and the remaining liquid was filtered before being eluted through the flash chromatography unit using a C_{18} reverse phase column using a low water to methanol gradient. Two peaks eluted through the column; one did not contain anything recognisable on a proton NMR and the other contained the final product along with some impurities. This fraction was reduced to a minimal volume and run through the same column again at a higher gradient to remove these impurities. The final product was an off white powder that was slightly soluble in water and very soluble in

methanol. The typical yield from this reaction scheme (Figure 3.1.10.1) is about 50% of the PHENSS starting material. (85 % yield)

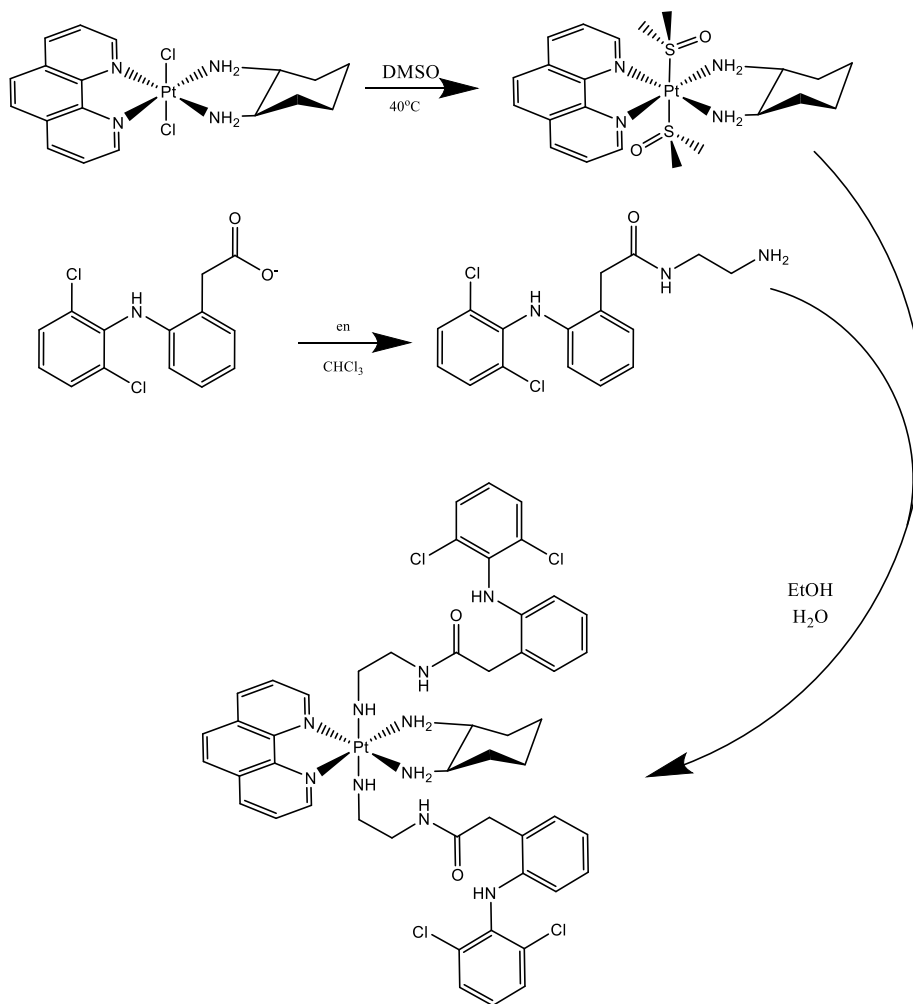
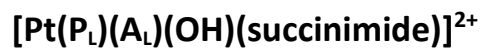


Figure 3.1.10.1: Reaction scheme for the synthesis of PHENSS(enDCF).

3.1.10 Synthesis of of Pt(IV) complexes of the type



This is a general method that was developed to work with all compounds developed in the lab of the type in order to offer new synthetic pathways. This unpublished method was in part developed by Krishant Deo who developed how to selectively synthesise the mono and di-succinate analogues.¹⁰⁶ This process appears to

be time dependant which explains why preliminary testing resulted in the near pure synthesis of the mono succinate product. Mild conditions were used to prevent reduction and diethyl ether was used to wash the product clean of any Pt(II) or succinate impurities.

3.1.11 Synthesis of [Pt(1,10-phenanthroline)(1S,2S-diaminocyclohexane)(OH)(succinatePFP)]²⁺

[Pt(1,10-phenanthroline)(1S,2S-diaminocyclohexane)(OH)(succinatePFP)]²⁺ was synthesised as an intermediate for PHENSS(OH)(DCL) synthesis, to facilitate the formation of the amide bond. DCC (dicyclohexylcarbodiimide) was used as a coupling agent ensuring that the addition occurred on the carboxylic acid and not the hydroxide ligand. The DCC temporarily bonds to the carboxylic acid, and then leaves upon nucleophilic substitution. During this reaction dicyclohexylcarbodiimide is transformed to dicyclohexylurea which is insoluble in water and can thus be removed by washing with organic solvents. The solvent was dried to prevent water disturbing the reaction. The reaction worked on the first attempt and further development was not undertaken as the product was produced in good yield and purity. (29.5 % yield)

3.1.12 Synthesis of [Pt(1,10-phenanthroline)(1S,2S-diaminocyclohexane)(OH)(DCL)]²⁺

The conjugation of DCL to the asymmetric PHENSS(IV) has been attempted previously.¹⁰⁰ However, the final product was unable to be isolated in sufficient quantities to be characterised aside from evidence of the product in a mass spectrum. The method of DCL-platinum conjugation has advanced since this attempt,¹⁰⁷ and so there is cause to revisit this reaction in the context of polyaromatic platinum complexes. DIPEA was used as a coupling reagent and when added to the solution resulted in near immediate precipitation. The PFP moiety is an excellent leaving group and was attached so that this step would have a higher yield. The reaction solution was filtered and washed with ether, however upon investigation the precipitate was not

pure and had traces of both Pt(II) and unbound DCL. The flash chromatography unit was employed to separate the three complexes which resulted in good separation after 2 elutions through the C₁₈ column. The overall yield was very low, which can be attributed to several factors; firstly there was not full conversion with a significant portion of the Pt(IV) being reduced in solution to Pt(II), during filtration the filtrate was not passed through the filter a second time to avoid contamination however some product was probably lost here, and each elution through the chromatography unit results in approximately 5 mg of lost product. (23 % yield)

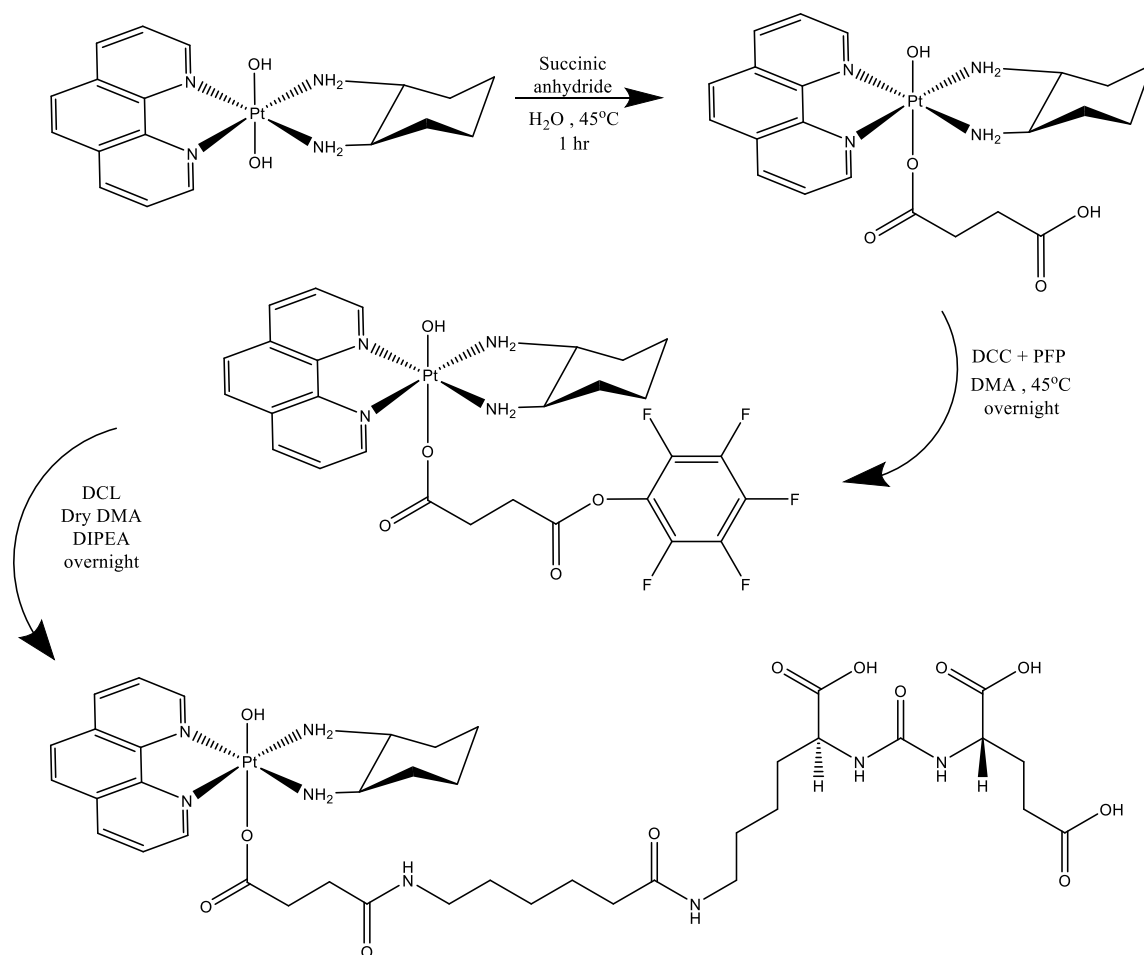


Figure 3.1.13.1: Reaction scheme for the synthesis of PHENSS(OH)(DCL).

3.2 Characterisation

NMR is a technique used to measure the energy released when the magnetic spin on particular atoms in a molecule returns to its ground state after being stimulated to a higher spin state. The energy profile of the solution is displayed in an NMR spectrum. When an atom is close to another that is electronegative, it becomes de-shielded and its magnetic spin is more easily reversed. Thus if an atom were to bind to a complex there would be a quantitative change in the NMR spectra and the site of binding could be determined by noting where on the spectrum variations occur.¹⁰⁸ The NMR spectrometers can measure the spin change of different elements including ^1H , ^{195}Pt and, ^{13}C . An NMR spectrum of hydrogen atoms is called a proton or ^1H NMR which was used in this spectrum due to the relative abundance of this atom in the compounds being characterised and in any impurities, thus making it perfect for confirming the structure and determining the purity.

UV absorbance spectroscopy can be used to determine the characteristic absorbance spectra of complexes which provide structural information as well as information about the colour. UV spectra were recorded on a Cary 1E spectrophotometer at room temperature in the 200–400 nm range, using a 10 mm quartz cell. All samples were automatically corrected for solvent baseline. Titration of a stock solution into a known volume of solvent allowed the calculation of the extinction coefficient, a measure of the absorbance at a given wavelength per mass density.

Circular dichroism (CD) is a technique used to measure chirality. This is achieved by measuring the absorption of elliptically polarised light traveling normal through the sample. The chirality of the compound can be determined by comparing the CD spectra of two enantiomers which will have spectra that are mirror images to each other: this occurs because one will absorb the right handed polarised light whilst the other absorbs left-handed polarised light. CD spectra were obtained using a Jasco-810 spectropolarimeter at room temperature. The instrument was left to equilibrate for 30 minutes prior to use. Spectra were obtained in a 10 mm quartz cell, and were measured from 400–200 nm with a data pitch of 1 nm, bandwidth of 1 nm and

response time of 1 second. For each spectrum, 40 accumulations were collected and a water baseline was subtracted

Synchrotron Radiation Circular Dichroism (SRCD) experiments were performed at the Centre for Storage Ring Facilities, Aarhus, Denmark (ASTRID and ASTRID2). The instrument was calibrated for magnitude and polarisation daily, using D-10-camphorsulfonic acid (CSA, 7.4 mg mL⁻¹). For all experiments the ratio of the 192.5 : 290 nm peaks ranged between 2.07 and 2.09. Data as averaged triplicate scans were collected from 170-350 nm in 1 nm steps. Samples were loaded into a circular sealed 0.1 mm pathlength quartz cuvette. A water baseline was run prior to each new complex run and subtracted from each data set.

Flash Chromatography, samples were purified using the Reveleris® X2 flash chromatography system fitted with a Reveleris® reverse phase C₁₈ 4 g column. The column was equilibrated to 3% MeOH for 2.4 min at 8 mL/min, and the samples eluted for 9 minutes with the UV detector sensitivity on high and detecting at 230, 254 and 280 nm. Samples between 20 and 100 mg were prepared in ~1-2 mL H₂O, injected and eluted at a flow rate of 8 mL/min. The column was eluted with 3% MeOH for 6 minutes then MeOH was increased to 100% over 1 minute, kept steady for 1 minute before returning to 3% over another minute. Only one peak was detected and this was collected in 10 mL fractions.

3.2.1 The characterisation of Pt(II) complexes of the type [Pt(P_L)(A_L)]²⁺

The characterisation of PHENSS, PHENRR, 56MESS, 56MERR, 5MESS, 5MERR, 4MESS, 4MERR, 44BPYSS and, 44BPYRR was achieved using a combination of ¹H proton NMR spectra and ¹H ¹⁹⁵Pt heteronuclear multiple quantum correlation (HMQC) spectra. These complexes have been characterised in previously published papers.³⁴ The NMR characterization of Pt(II) complexes of the type [Pt(P_L)(A_L)]²⁺ was achieved using a combination of ¹H proton NMR spectra and ¹H/¹⁹⁵Pt heteronuclear multiple quantum correlation (HMQC) spectra. The HMQC peak was the same as other platinum complexes of the same type reported in the literature.¹⁰⁹ An example of the HMQC

spectra is shown in Figure 3.3.1.1, the ^{195}Pt chemical shift of -2823.4 ppm is significantly different to the two starting Pt complexes $[\text{Pt}(\text{SS-dach})\text{Cl}_2]$ and K_2PtCl_4 (-3282 and -1650 ppm, respectively). The correlation between the Pt centre and the aromatic resonance 8.96 ppm confirms the coordination of the 1,10-phenanthroline.

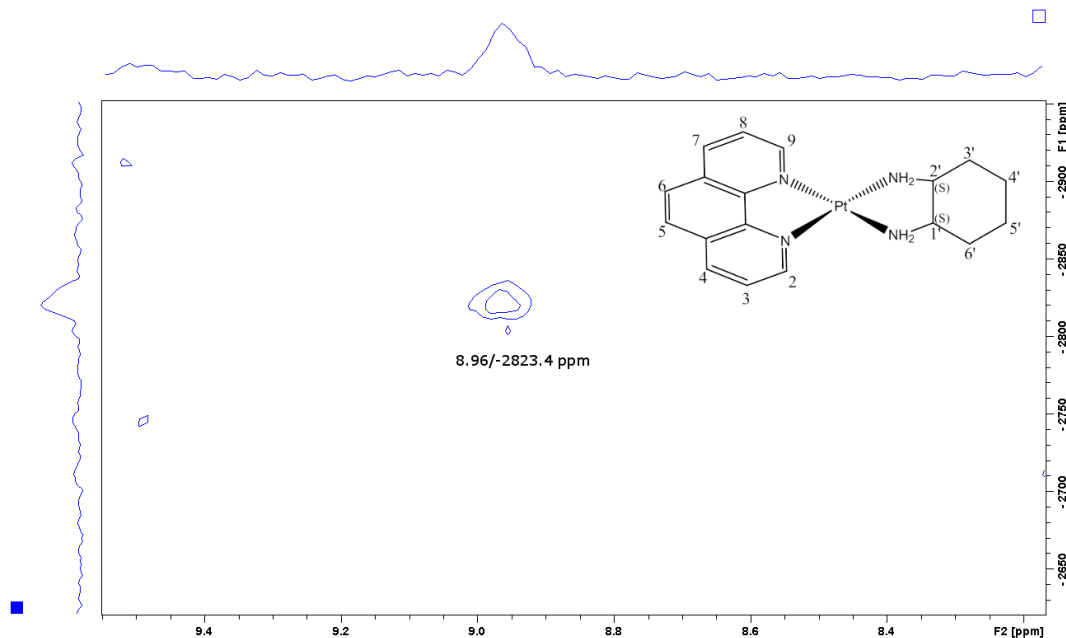


Figure 3.2.1.1: The ^1H - ^{195}Pt HMQC spectrum of PHENSS in D_2O , performed on a Bruker Avance 400 MHz NMR spectrometer.

The proton spectra were almost identical the literature with very minor chemical shifts which occur due to stacking of the 1,10-phenanthroline ligands in solution.¹¹⁰ Figure 3.2.1.2 shows the ^1H spectra of PHENSS with the peaks labelled with the corresponding proton. The aromatic region for PHENSS was assigned as follows: the singlet at 8.07 ppm was assigned to H5 and H6 as the two protons will share the peak location due to the symmetry of the complex and there are no protons on the adjacent carbons. The doublet of doublets (dd) at 7.97 ppm was assigned to H3 and H8, again the symmetry resulted in the combining of the two peaks and the presence of the protons on the adjacent carbons resulting in a dd splitting pattern due to coupling. The remaining two doublet (d) peaks in the aromatic region were merged in the spectra; however, they could still be distinguished due to the larger coupling constant of H2 and H9 due to the proximity to the nitrogen. Thus the 8.48 ppm doublet $J = 8.50$ Hz was

assigned to H4 and H7 and the doublet at 8.87 ppm $J= 5.35$ Hz was assigned to H2 and H9. The resonances for the aliphatic region were consistent with NMR spectra reported in the literature with the same axillary ligands. The aliphatic peaks were assigned as follows: the multiplet at 2.71 ppm was assigned to H1' and H2' as the two protons closest to the amine. The remaining protons do not display symmetry due to the conformation of the dach ring. Consequently each of the remaining peaks corresponds to 2 protons and can be assigned based on their proximity to the Pt(II) centre and amine groups. H3' and H6' are the next closed and were consequently assigned to the multiples at 2.21 and 1.65 ppm. The remaining two peaks at 1.46 and 1.24 ppm were assigned to H4'' and H5'. The amine proton resonances were not visible due to exchange with D₂O.

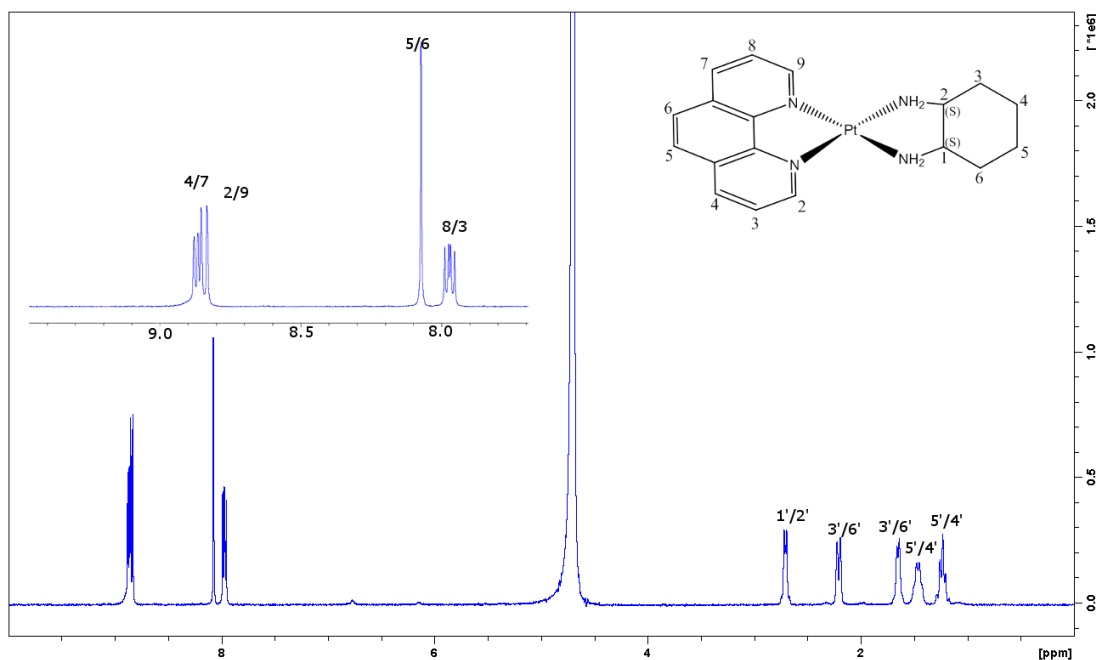


Figure 3.2.1.2: The ¹H NMR spectra of PHENSS in D₂O, showing proton assignment; performed on a Bruker Avance 400 MHz NMR spectrometer.

The above assignment was repeated for the NMR spectra of PHENSS, PHENRR, 56MESS, 56MERR, 5MESS, 5MERR, 4MESS, 4MERR, 44BPYSS, and 44BPYRR, the results are summarised in Table 2.3.4.1 (Chapter two). There were some minor differences in the resonances for these complexes, particularly in the aromatic region where the

relative concentration of each solution affects the stacking of the phenanthroline region and thus affects the resonance of the H2, 9 and H4,7 peaks; and the symmetry of the complexes changed the splitting pattern for complexes with ligands in the 4 and 5 positions.

3.2.2 The characterisation of complexes of the type $[\text{Pt}(\text{P}_L)(\text{A}_L)]\text{X}_2]^{2+}$

Each complex was characterised using a combination of NMR spectroscopy, HPLC, circular dichroism (CD spectroscopy), UV spectroscopy, micro analysis and ESI-MS. The NMR spectra produced peaks consistent with those seen in the literature for similar compounds with little to no impurities detected.³² The compound broke down in the HPLC column producing 2 by-products. It was hypothesised that this was due to the trifluoroacetic acid (TFA) however the elution profiles did not improve when TFA was removed from the mobile phase or when formic acid was used. The benchtop CD spectra confirmed that the chirality of the starting materials was retained during synthesis; whilst the synchrotron spectra provided additional information about the structure revealing dramatic differences from similar, previously published Pt(IV) complexes. ESI-MS also resulted in significant fracturing of the compounds; although the correct mass peak could be identified in all samples, in some spectra this was not the main peak.

The NMR characterization of PHENSSCl₂, PHENSSBr₂ and PHENSSI₂ was achieved using a combination of ¹H proton NMR spectra and ¹H ¹⁹⁵Pt heteronuclear multiple quantum correlation (HMQC) spectra. The HMQC peak was significantly different to other platinum complexes of the same type reported in the literature.¹⁰⁹ Typically a Pt(IV) complex of the type $[\text{Pt}(\text{P}_L)(\text{A}_L)(\text{OH})_2]^{+2}$ will demonstrate a ¹⁹⁵Pt resonance at 450 ppm whereas the complexes synthesised in this work have ¹⁹⁵Pt resonate at approximately -630 ppm, this confirms the presence of the halide ligands in place of the typical hydroxyl ligands seen in the literature.⁴⁰ An example of the HMQC spectra is shown in Figure 3.2.2.1, the ¹⁹⁵Pt chemical shift of -645.8 ppm is significantly different to the two starting Pt complexes $[\text{Pt}(\text{SS-dach})\text{Cl}_2]$ and K_2PtCl_4 (-3282 and -1650 ppm,

respectively). The correlation between the Pt centre and the aromatic resonance 9.19 ppm confirms the coordination of the 1,10-phenanthroline.

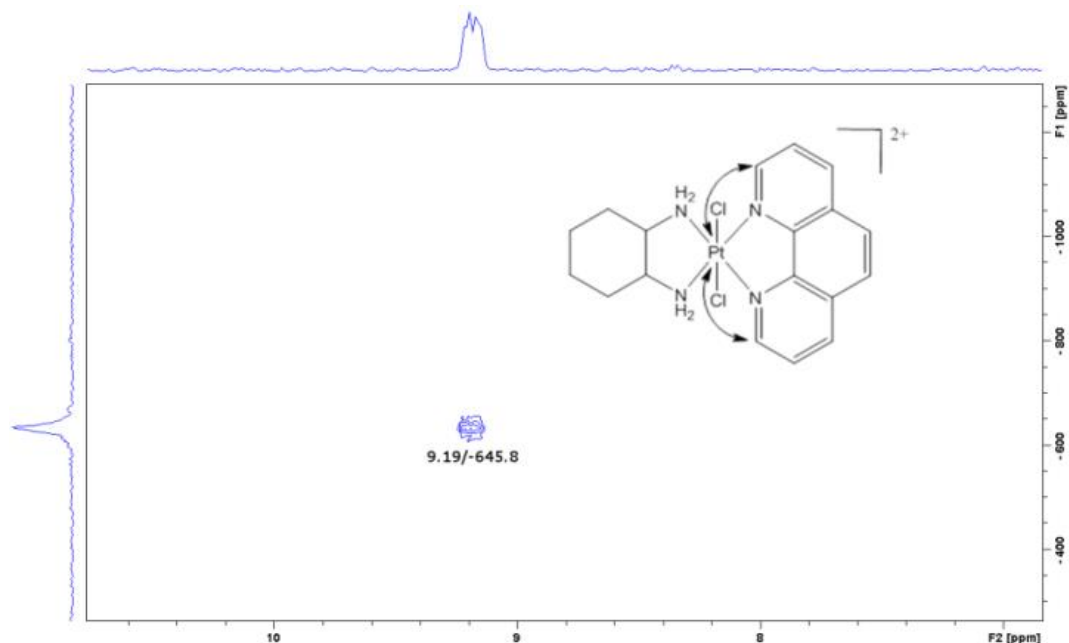


Figure 3.2.2.1: The ^1H - ^{195}Pt HMQC spectrum of PHENSSCl₂ in D₂O, displaying the correlations between the platinum centre and the protons from each ligand; performed on a Bruker Avance 400 MHz NMR spectrometer.

The proton spectra were almost identical to similar complexes in the literature with very minor chemical shifts which occur due to stacking of the 1,10-phenanthroline ligands stacking in solution.¹¹⁰ Figure 3.3.2.2 shows the ^1H spectra of PHENSSCl₂ with the peaks labelled with the corresponding proton. The aromatic region for PHENSSCl₂ was assigned as follows: the singlet at 8.33 ppm was assigned to H5 and H6 as the two protons will share the peak location due to the symmetry of the complex and there are no protons on the adjacent carbons. The doublet of doublets (dd) at 8.27 ppm was assigned to H3 and H8, again the symmetry resulted in the combining of the two peaks and the presence of the protons on the adjacent carbons resulting in a dd splitting pattern due to coupling. The remaining two doublet (d) peaks in the aromatic region were merged in the spectra; however, they could still be distinguished due to the smaller coupling constant of H2 and H9 due to the proximity to the nitrogen. Thus the 9.03 ppm doublet $J = 8.31$ Hz was assigned to H4 and H7 and the doublet at 9.09 ppm $J =$

5.56 Hz was assigned to H2 and H9. The resonances for the aliphatic region were consistent with NMR spectra reported in the literature with the same axillary ligands. The peaks were almost identical with only slight variants in the ppm. The amine proton resonances were not visible due to exchange with D₂O.

The above was repeated for the NMR spectra of PHENSSBr₂ and PHENSSI₂, the results of which are summarised in Table 2.3.5.1 (Chapter two). There were some minor differences in the resonances for these complexes, particularly in the aromatic region where the relative concentration of each solution affects the stacking of the phenanthroline region and thus affects the resonance of the H_{2,9} and H_{4,7} peaks.

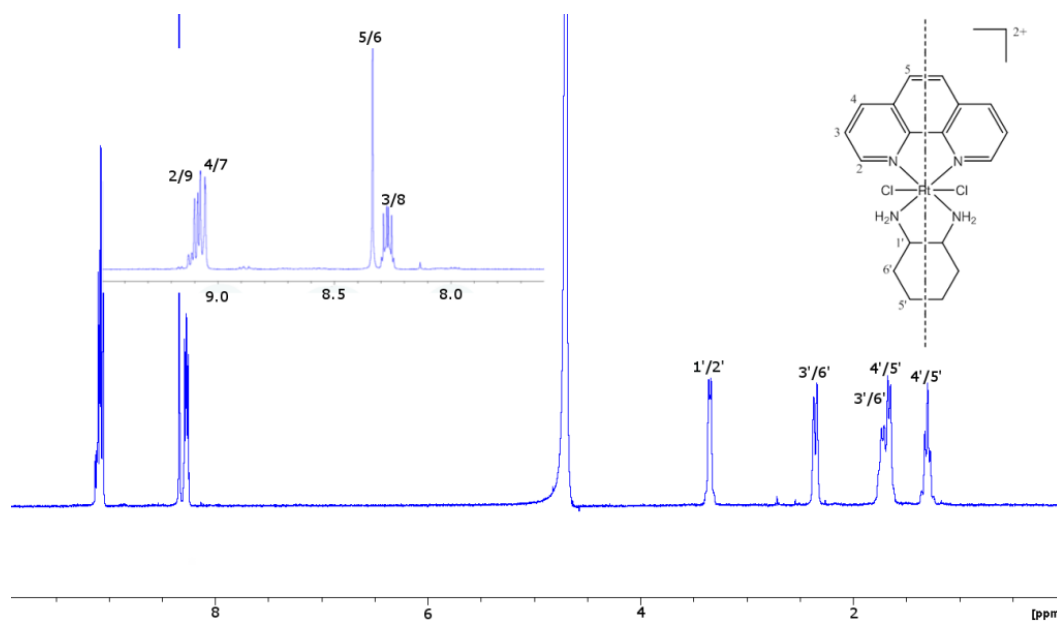


Figure 3.3.2.2: The ¹H NMR spectra of PHENSSCl₂ in D₂O, showing proton assignment; performed on a Bruker Avance 400 MHz NMR spectrometer.

The NMR characterization of 56MESSCl₂, 56MESSBr₂ and 56MESSI₂ was achieved using a combination of ¹H proton NMR spectra and ¹H ¹⁹⁵Pt heteronuclear multiple quantum correlation (HMQC) spectra. The spectra were analysed in the same way as for complexes PhenSSX₂, however, in the aliphatic region for complexes had an additional peak due to the presence of the methyl group on the 1,10-phenanthroline, apart from this there were no changes in the region and peaks were assigned using the same rational. The results of the NMR spectra are summarised in Table 2.3.5.1 (Chapter

two), the ^1H and ^{195}Pt spectra of 56MESSCl_2 are shown in Figures 3.2.2.3 and 3.2.2.4, respectively.

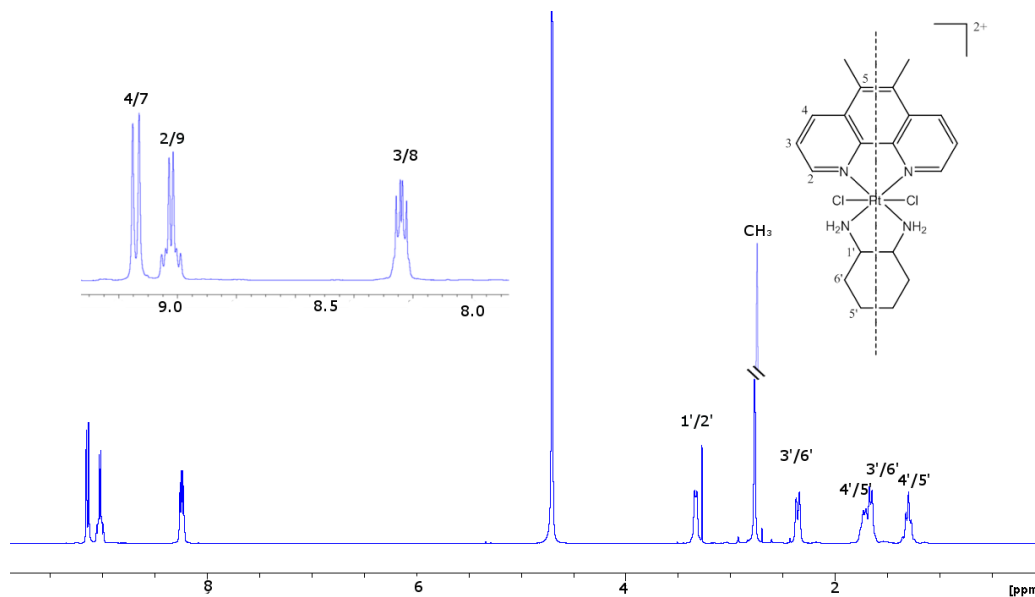


Figure 3.2.2.3: The ^1H NMR spectra of 56MESSCl_2 in D_2O , showing proton assignment; performed on a Bruker Avance 400 MHz NMR spectrometer.

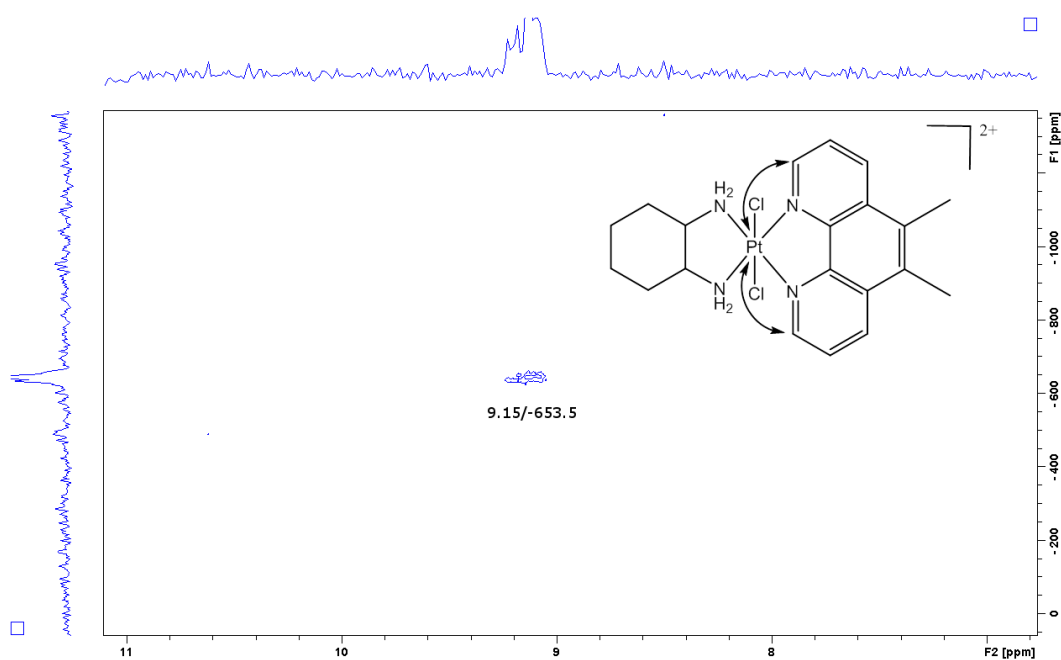


Figure 3.2.2.4: The ^1H - ^{195}Pt HMQC spectrum of 56MESSCl_2 in D_2O , displaying the correlations between the platinum centre and the protons from each ligand; performed on a Bruker Avance 400 MHz NMR spectrometer.

The NMR characterization of 5MESSCl₂, 5MESSBr₂ and 5MESSI₂ was achieved using a combination of ¹H proton NMR spectra and ¹H ¹⁹⁵Pt heteronuclear multiple quantum correlation (HMQC) spectra. The spectra were analysed in the same way as above however, these complexes are split due to their asymmetry. The aliphatic region for complexes 4-9 had an additional peak due to the presence of the methyl group on the 1,10-phenanthroline but again the remaining peaks were assigned using the same rationale described above. The results of the NMR spectra are summarised in Table 2.3.5.1 (Chapter two), the ¹H and ¹⁹⁵Pt spectra of 56MESSCl₂ are shown in Figures 3.2.2.5 and 3.2.2.6, respectively. The relative ¹⁹⁵Pt resonances of these complexes appear to be more dependent on the halide ligand than the variations in the PL. For example complexes with bromo ligands tended to have a much lower ppm of around -960 ppm and those with iodo ligands tended to have the highest ¹⁹⁵Pt peak of approximately -640 ppm.

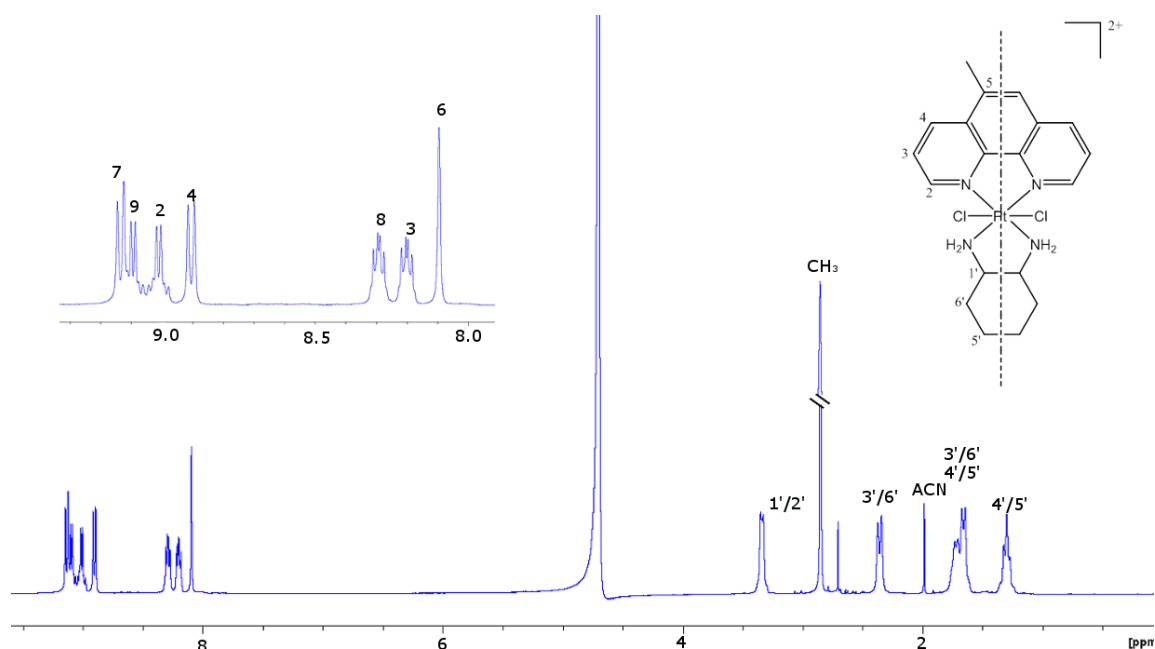


Figure 3.2.2.5: The ¹H NMR spectra of 5MESSCl₂ in D₂O, showing proton assignment; performed on a Bruker Avance 400 MHz NMR spectrometer.

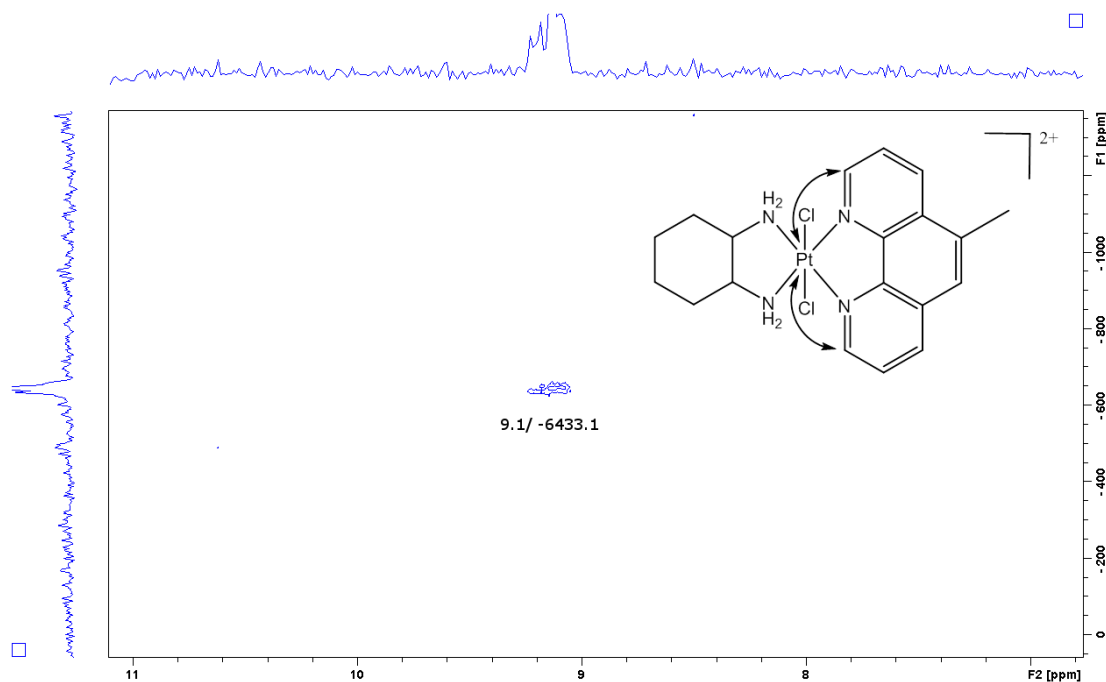


Figure 3.2.2.6: The ^1H - ^{195}Pt HMQC spectrum of 5MESSCl₂ in D₂O, displaying the correlations between the platinum centre and the protons from each ligand; performed on a Bruker Avance 400 MHz NMR spectrometer.

The UV characterisation of PHENSSCl₂, PHENSSBr₂ and PHENSSI₂ was achieved titration of a stock solution into a known volume of solvent allowed the calculation of the extinction coefficient (ϵ). Figure 3.2.2.7 shows the titration curves and the extinction coefficient calculation of PHENSSCl₂, achieved by plotting the absorbance against concentration change at each of the two peaks (278 and 208 nm). The UV spectra of each PHENSSX₂ compound is compared in Figure 3.2.2.8, allowing the analysis of the structural change of the molecule caused by each halide ligand. The spectra of complexes where the axial ligands are chloro or iodo complexes are similar to the spectra of Pt(IV)PHENSS complexes with hydroxido axial ligands reported in the literature.⁴⁰ Complexes with bromo axial ligands are easily distinguishable with distinctive broad, shoulder band between 220 and 250 nm. Despite the appearance of this shoulder the change in axial ligand did not result in a change in absorbance i.e. the peaks had almost identical wavelengths. The UV data for PHENSSCl₂, PHENSSBr₂ and PHENSSI₂ is summarised in Table 3.2.4.1 in Section 3.2.4.

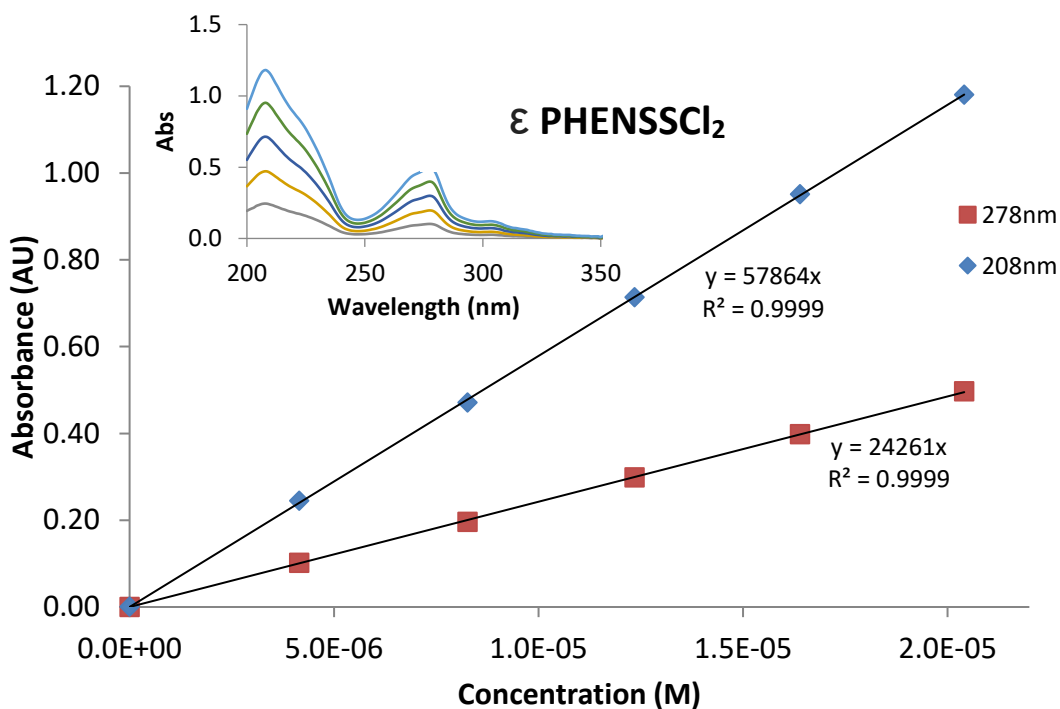


Figure 3.2.2.7: Titration of a stock solution of PHENSSCl₂ into a known concentration of H₂O and the resulting extinction coefficient calculated based on the two main peaks at 278 (red) and 208 nm (blue).

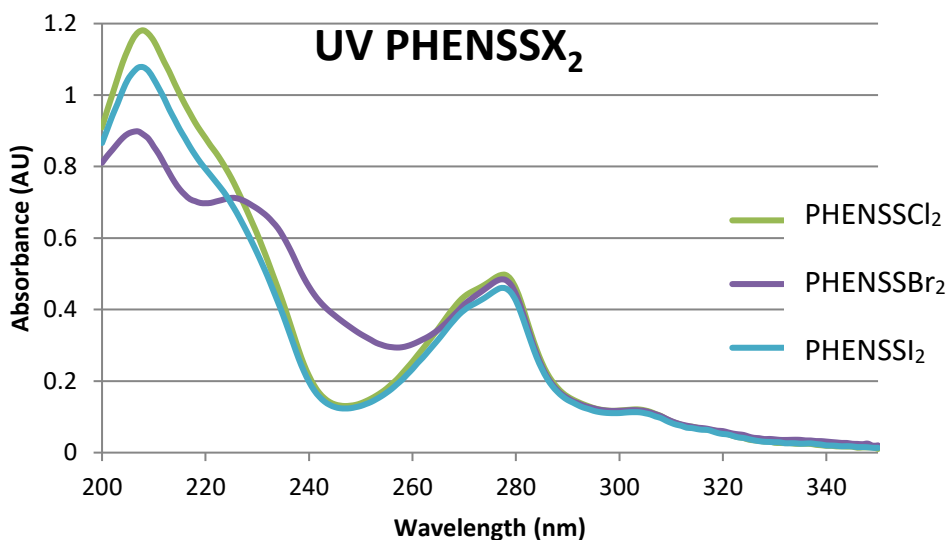


Figure 3.2.2.8: UV spectra of PHENSSCl₂ (green), PHENSSBr₂ (purple) and, PHENSSI₂ (blue); at room temperature in the 200–350 nm range, using a 10 mm quartz cell, corrected for solvent baseline (H₂O).

The UV characterisation of 56MESSCl₂, 56MESSBr₂ and 56MESSI₂ was achieved titration of a stock solution into a known volume of solvent allowed the calculation of ϵ . Figure 3.3.2.9 shows the titration curves and the extinction coefficient calculation of 56MESSCl₂, achieved by plotting the absorbance against concentration change at each of the two peaks (289 and 211 nm). The UV spectra of each 56MESSX₂ compound is compared in Figure 3.2.2.10, allowing the analysis of the structural change of the molecule caused by each halide ligand. The spectra of complexes where the axial ligands are chloro or iodo complexes are similar to the spectra of Pt(IV)PHENSS complexes with hydroxido axial ligands reported in the literature.¹⁰⁹ Complexes with bromo axial ligands are easily distinguishable with distinctive broad, shoulder band between 220 and 30 nm on top of the shoulders appearing between 250 and 230 nm which are present in all three spectra. Despite the appearance of this shoulder the change in axial ligand did not result in a change in absorbance i.e. the peaks had almost identical wavelengths. The UV data for 56MESSCl₂, 56MESSBr₂ and 56MESSI₂ is summarised in Table 3.2.4.1 in Section 3.2.4.

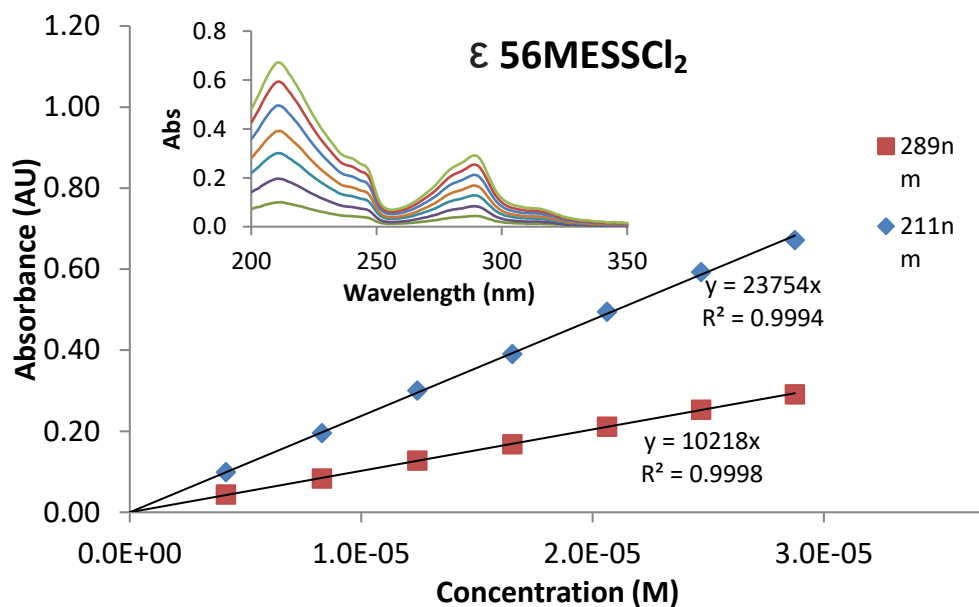


Figure 3.2.2.9: Titration of a stock solution of 56MESSCl₂ into a known concentration of H₂O and the resulting extinction coefficient calculated based on the two main peaks at 289 (red) and 211 nm (blue).

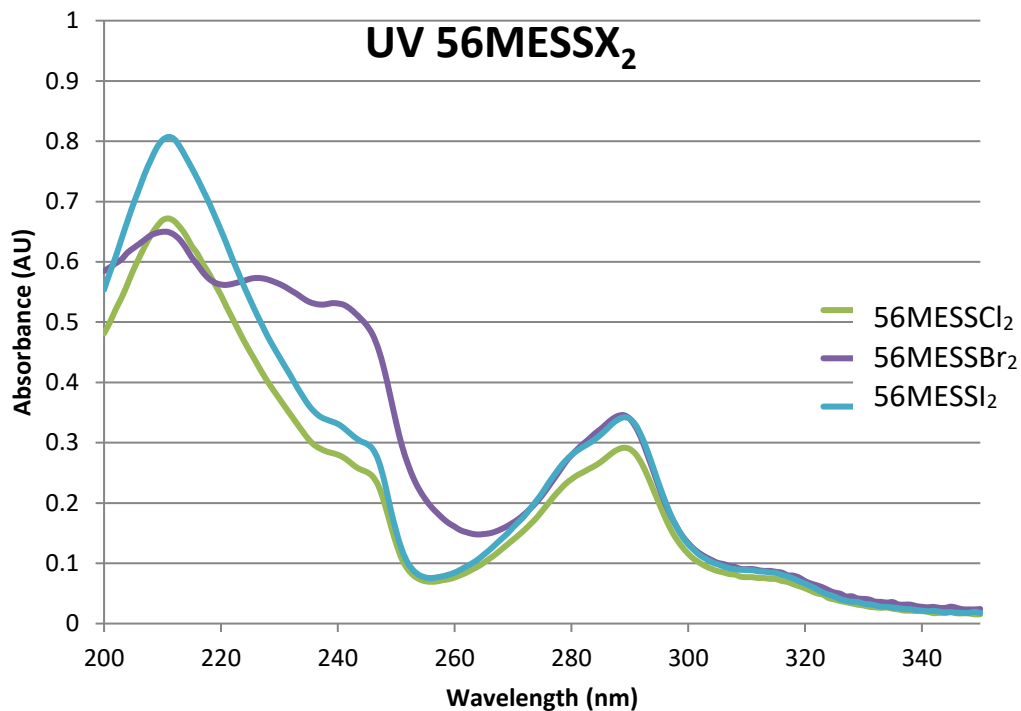


Figure 3.2.2.10: UV spectra of 56MESSCl₂ (green), 56MESSBr₂ (purple) and, 56MESSI₂ (blue); at room temperature in the 200–350 nm range, using a 10 mm quartz cell, corrected for solvent baseline (H₂O).

The UV characterisation of 5MESSCl₂, 5MESSBr₂ and 5MESSI₂ was achieved titration of a stock solution into a known volume of solvent allowed the calculation of ϵ . Figure 3.2.2.11 shows the titration curves and the ϵ calculation of 5MESSCl₂, achieved by plotting the absorbance against concentration change at each of the two peaks (283 and 210 nm). The UV spectra of each 56MESSX₂ compound is compared in Figure 3.2.2.12, allowing the analysis of the structural change of the molecule caused by each halide ligand. The spectra of complexes where the axial ligands are chloro or iodo complexes are similar to the spectra of Pt(IV)PHENSS complexes with hydroxido axial ligands reported in the literature.⁴⁰ Complexes with bromo axial ligands are easily distinguishable with distinctive broad shoulder band between 220 and 250 nm. The bromo ligand for 5MESSX₂ complexes has a hypsochromic effect significant enough that the peak is outside of the measured wavelengths (less than 200 nm) while the other two 5MESSX₂ complexes peak at ~280 nm well within the measured wavelength. Despite

the appearance of this shoulder the change in axial ligand did not result in a change in absorbance i.e. the peaks had almost identical wavelengths. The UV data for 56MESSCl₂, 56MESSBr₂ and 56MESSI₂ is summarised in Table 3.2.4.1 in Section 3.2.4.

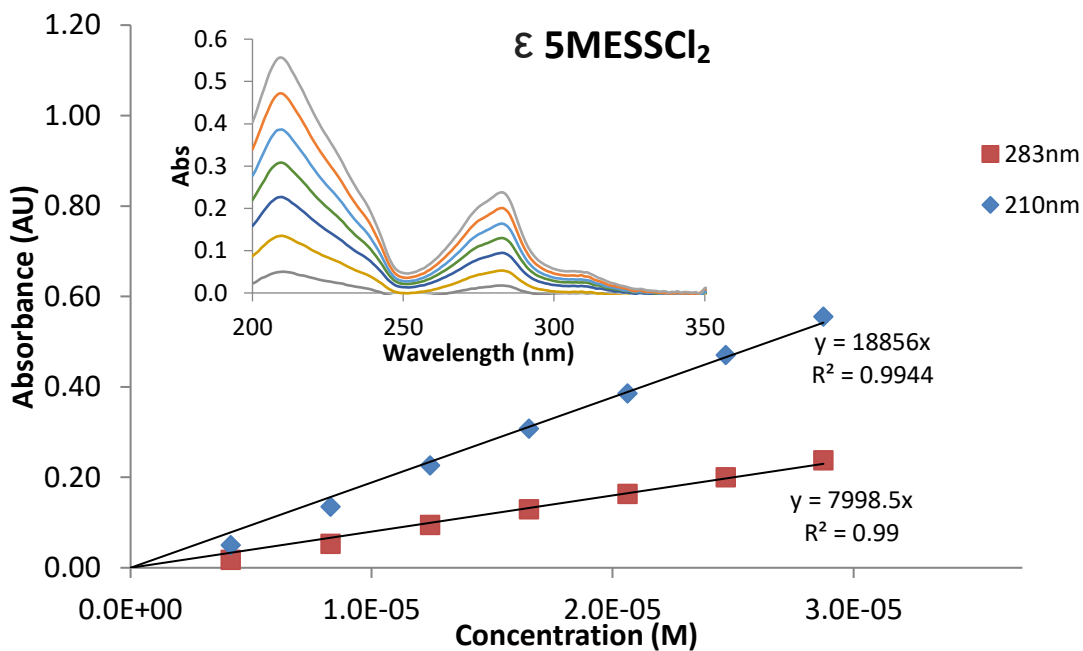


Figure 3.2.2.11: Titration of a stock solution of 5MESSCl₂ into a known concentration of H₂O and the resulting extinction coefficient calculated based on the two main peaks at 283 (red) and 210 nm (blue).

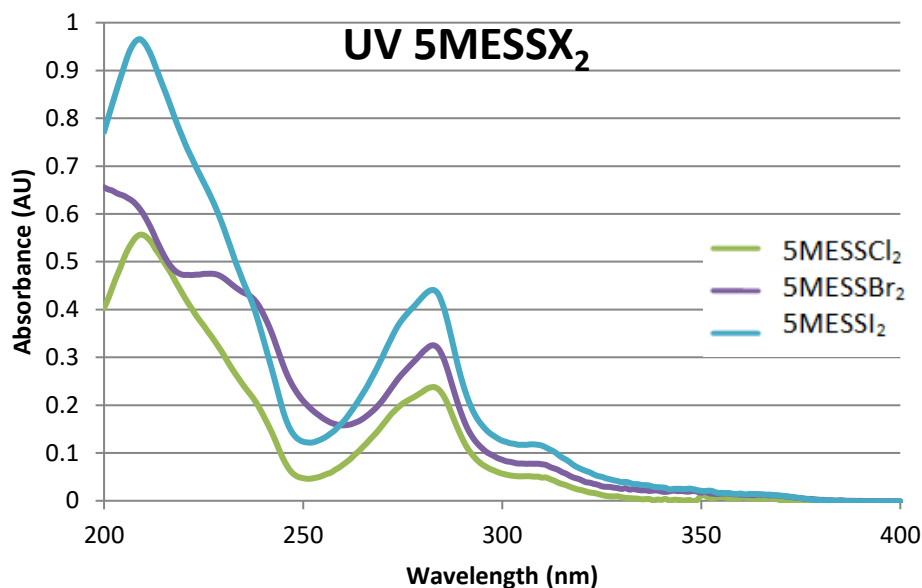


Figure 3.2.2.12: UV spectra of 5MESSCl₂ (green), 5MESSBr₂ (purple) and, 5MESSI₂ (blue); at room temperature in the 200–350 nm range, using a 10 mm quartz cell, corrected for solvent baseline (H₂O).

If the complexes of the type $[Pt(P_L)(A_L)(X)_2]^{2+}$ are compared in terms of the polypyridyl ligands another trend appears; the transitions of the phenanthroline ligand produce a consistent difference in the bands with the band at 280-290 nm which then shifts (blue) in order of the number of methyl groups (i.e. PhenSS(X)₂ complexes followed by 5MeSS(X)₂ and then 56MeSS(X)₂ complexes). A similar trend is observed for the weak bands above 300 nm. The 56MeSS(X)₂ compounds also display a shoulder at approximately 240 nm which is not present for 5MeSS(X)₂ and PhenSS(X)₂. Figure 3.2.2.13 illustrates the effect the polypyridal ligand has on the di-chloro complexes. All complexes were measured at 24.7 μM and thus the decrease in absorption intensity from PHENSS to 56MESS followed by 5MESS can be attributed to hypochromic effect. Interestingly the same trend is followed for the bathochromic effect (red shift) in the peaks between 250 and 300 nm, where PHENSS < 56MESS < 5MESS. For the shoulder between 260 and 280 nm, 5 and 56MESSCl₂ have much broader shoulders than PHENSSCl₂. This trend continues for the shoulder between 220 and 250 nm where

PhenSS has the narrowest peak while 5MESS has a slight shoulder and 56MESS has a significant board shoulder.

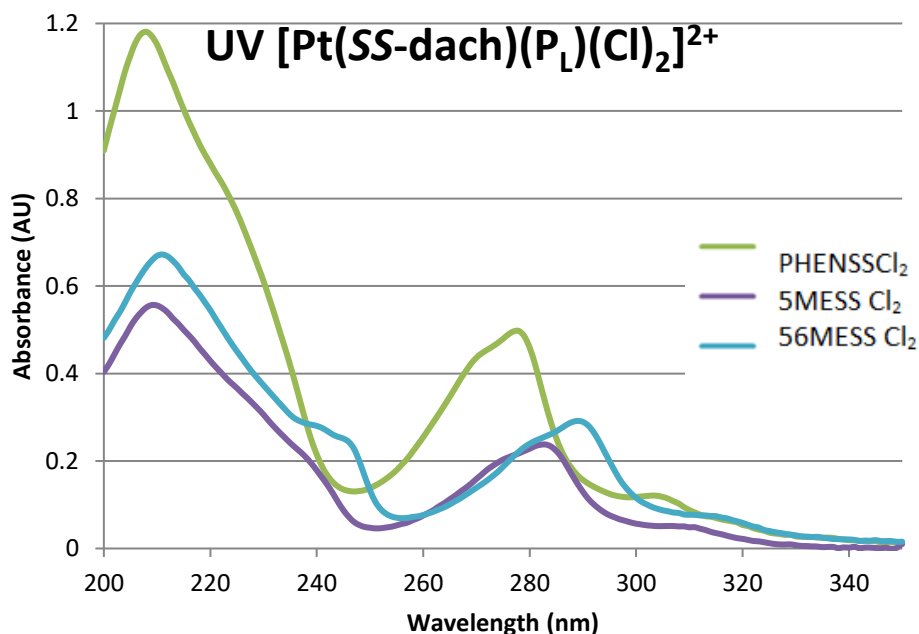


Figure 3.2.2.13: UV spectra of PHENSSCl₂ (green), 5MESSCl₂ (purple) and, 56MESSCl₂ (blue); at room temperature in the 200–350 nm range, using a 10 mm quartz cell, corrected for solvent baseline (H₂O).

Figure 3.2.2.14 illustrates the effect the polypyridal ligand has on the di-bromo complexes. All complexes were measured at 28.7 μM and thus the decrease in absorption intensity from PHENSS to 5MESS followed by 56MESS for the peak between 260 and 300 nm can be attributed to hypochromic effect; interestingly following a different trend to the di-chloro complexes. Unlike the di-chloro complexes the hypochromic effect for the peak between 200 and 230 nm did not follow the same trend: instead 5MESS had the highest absorption intensity (had a hyperchromic effect) followed by PHENSS and lastly 56MESS which had the lowest intensity (had a hypochromic effect). As with the di-chloro complexes the trend in hypochromic effect was the same as that for the red shift for the peak between 250 and 300 nm i.e. wavelength increased from PHENSS to 5MESS followed by 56MESS. The order so the

most t least broad shoulder for the peak between 200 and 250 nm is also different to that of the di-chloro complexes; PHENSS has the broadest shoulder followed by 56MESS and lastly 5MESS which barely has a shoulder at all.

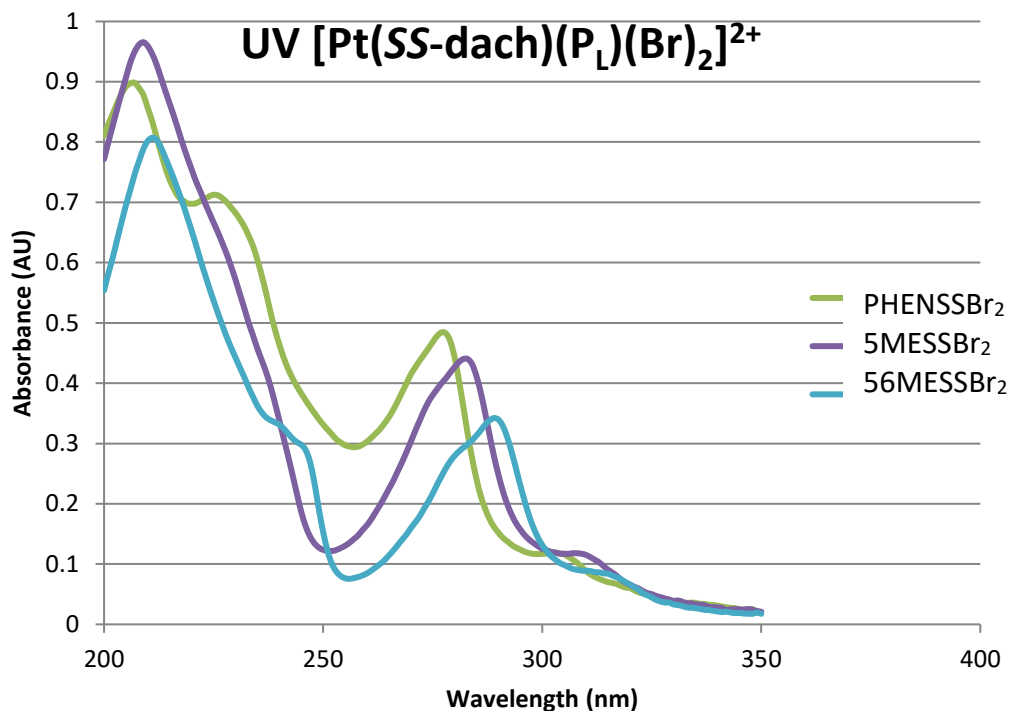


Figure 3.2.2.14: UV spectra of PHENSSBr₂ (green), 5MESSBr₂ (purple) and, 56MESSBr₂ (blue); at room temperature in the 200–350 nm range, using a 10 mm quartz cell, corrected for solvent baseline (H₂O).

Figure 3.2.2.15 illustrates the effect the polypyridal ligand has on the di-iodo complexes. All complexes were measured at 28.7 μM and thus the decrease in absorption intensity from PHENSS to 5MESS followed by 56MESS for the peak between 260 and 300 nm can be attributed to hypochromic effect; interestingly following the same trend as the di-bromo complexes and a different trend to the di-chloro complexes. Unlike the di-bromo complexes the trend in hypochromic effect is the same for the two main peaks. The blue shift trend 56MESS>5MESS>PHENSS is followed for both peaks however, the hypochromic effect is more extreme in the peak between 200 and 300 nm.

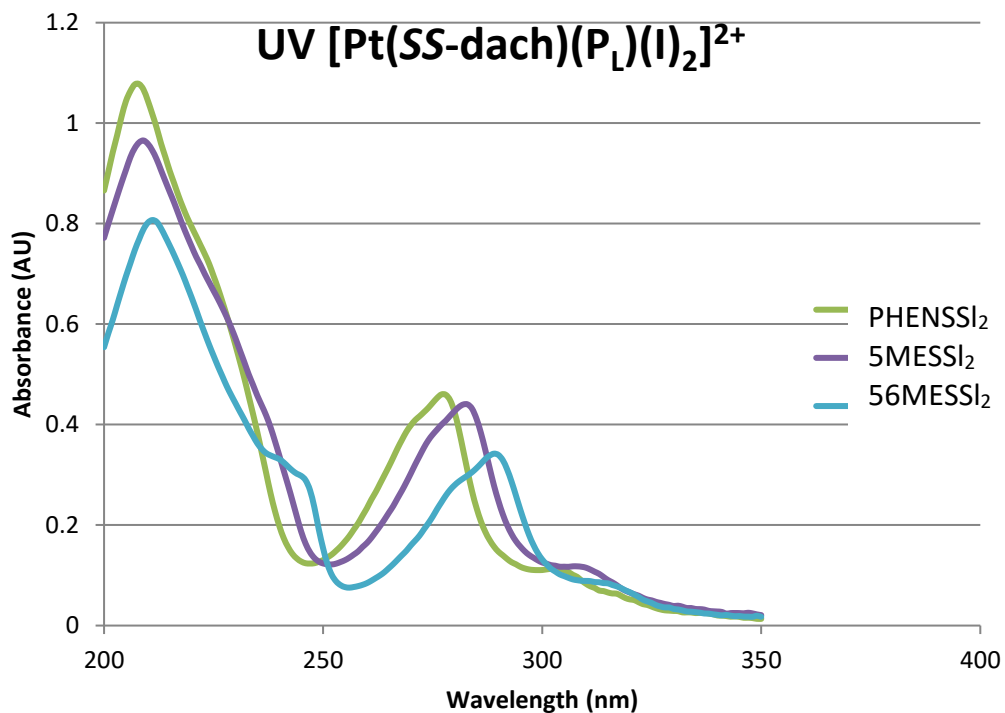


Figure 3.2.2.15: UV spectra of PHENSSI₂ (green), 5MESSI₂ (purple) and, 56MESSI₂ (blue); at room temperature in the 200–350 nm range, using a 10 mm quartz cell, corrected for solvent baseline (H₂O).

The benchtop CD spectra of all 9 complexes were taken first as a simple characterisation process. It was hypothesised that these spectra would be relatively basic similarly to the PHENSS(OH)₂ benchtop CD spectra which showed only very small peaks from ~270 nm to 400 nm with a sharp drop off starting at ~270 nm which continues downward until 200 nm (the lowest wavelength that can be reached with a standard benchtop machine). The spectra for the PHENSSX₂ complexes were very similar to this as seen in Figure 3.2.2.16. The CD spectra for the 56MESSX₂ (Figure 3.2.2.17) and 5MESSX₂ (Figure 3.2.2.18) a similar trend occurred between 250 and 400 nm however at wavelengths below this point there are one or two peaks and although the spectra has a similar drop off, it appeared as though it might be on an upward trend.

Figure 3.2.2.16 illustrates the effect of the halogen axial ligand on PHENSS. The three spectra are very similar up until 320 nm at which point the spectra for PHENSSBr₂ varies significantly. Both PHENSSCl₂ and PHENSSI₂ have an absorption band at 226 nm but for PHENSSBr₂ this absorption band is red shifted to 280 nm indicating a clockwise/ positive chirality shift. The height of the band followed by a much sharper drop off compared to the two other compounds also suggests that PHENSSBr₂ have significantly different velocities due to different indices of refraction for left or right polarised light. It appears that all three spectra have another band that is reaching its minimum just before 200 nm but this cannot be relied upon due to the limitations of the benchtop spectrometer.

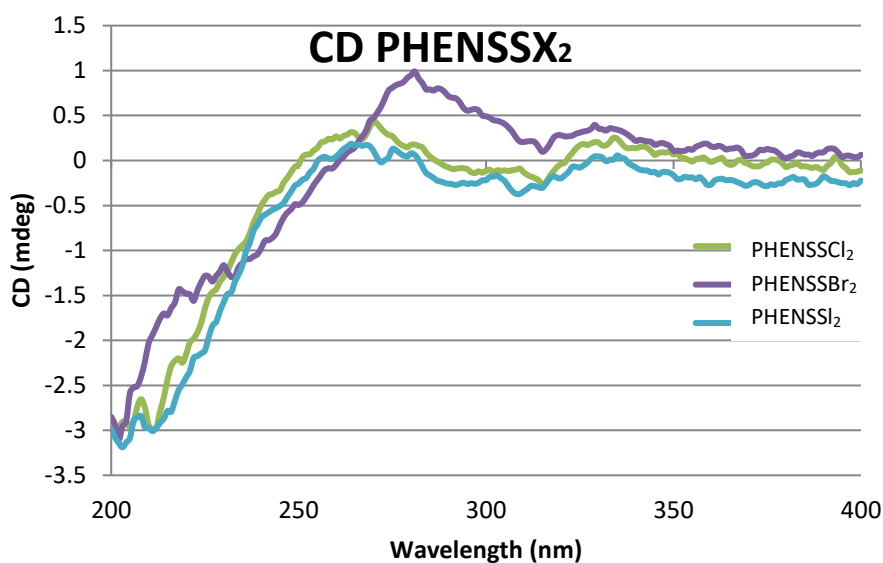


Figure 3.2.2.16: CD spectra of PHENSSCl₂ (green), PHENSSBr₂ (purple) and, PHENSSI₂ (blue); at room temperature in the 200–350 nm range, using a 10 mm quartz cell, corrected for solvent baseline (H₂O).

Figure 3.2.2.17 illustrates the effect of the halogen axial ligand on 56MESS complexes. Interestingly these complexes do not follow the same trends as the PHENSS complexes for which the bromo complex showed the most deviation. For the 56MESS complexes the chloro ligands appear to have the most significant effect on the absorption of polarised light. The three spectra are very similar up until ~250 nm; at

which point both the 56MESSBr₂ and 56MESSI₂ start on an upward trend towards another peak at 332 nm whereas, 56MESSCl₂ continues on its downward trend until 210 nm where it reaches a minimum and begins to rise again. There appears to be a shoulder along this downward trend that has a similar shape to the two peaks seen in the other spectra, this suggests that although the indices of refraction are different there are still structural similarities causing similar absorption of polarised light. The absorption band at 210 nm is shared between the three complexes although the intensity is different for each. 56MESSCl₂ has the most negative value followed by 56MESSBR₂ and lastly 56MESSI₂. This trend follows the same trend as both the electronegativity and size of these ligands and thus it can be hypothesised that at one or both of these factors are effecting the structure of 56MESS such that their absorption of polarised light is effected at this wavelength.

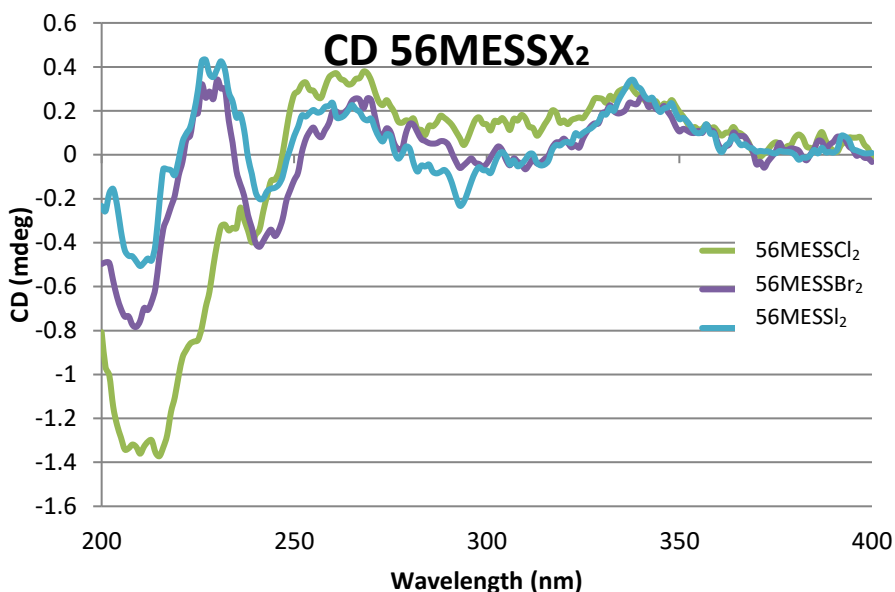


Figure 3.2.2.17: CD spectra of 56MESSCl₂ (green), 56MESSBr₂ (purple) and, 56MESSI₂ (blue); at room temperature in the 200–350 nm range, using a 10 mm quartz cell, corrected for solvent baseline (H₂O).

Figure 3.2.2.18 illustrates the effect of the halogen axial ligands on 5MESS complexes. These complexes showed the least consistency in their spectra. Similarly to the complexes previously seen the spectra are very similar and almost flat up unit ~ 230

nm at which point there are some major variations. The spectra of 5MESSI₂ appears to be similar to that of the PHENSS complexes whereas, the spectra of 5MESSBr₂ appears to be similar to those of the 56MESS complexes while 5MESSCl₂ has a unique spectra. One of the key differences between 5MESS and both 56MESS and PHENSS is its asymmetry. Thus it can be hypothesised that the asymmetry of the phen is affecting the conformation of the molecule when the halogen ligands are coordinated. Interestingly the magnitude of effect cannot be correlated to the size or electronegativity of the halides unlike the 56MESS complexes.

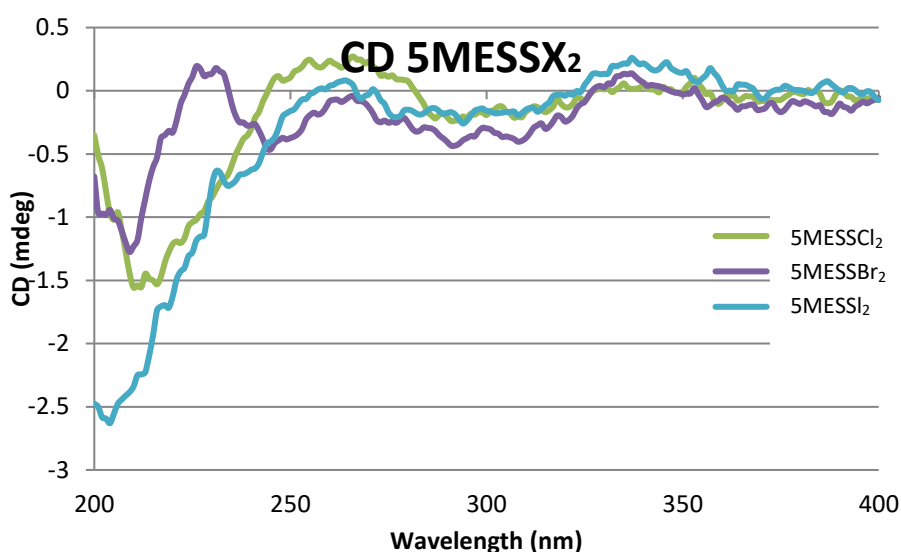


Figure 3.2.2.18: CD spectra of 5MESSCl₂ (green), 5MESSBr₂ (purple) and, 5MESSI₂ (blue); at room temperature in the 200–350 nm range, using a 10 mm quartz cell, corrected for solvent baseline (H₂O).

The SRCD spectra for the dihydroxy Pt(IV) spectra were obtained to see if the absorbance would increase at lower nm. This was not the case and the larger nm range did not result in any extra characterisation data the spectra simply continued on a downward slope. The SRCD spectra of the [Pt(A_L)(P_L)X₂]²⁺ complexes was collected as they showed some promise of having additional peaks below 200 nm. These experiments were successful in observing additional peaks for which there were some interesting trends when comparing based on the axial ligands or the polyaromatic ligand which helps to give some insight into the band systems.

The SRCD data was processed using OriginPro8.5, all spectra were smoothed using 11 point smoothing which ensured a clean line without disturbing any of the peak intensities or shapes (Figure 3.2.2.20). The units were then changed to molar ellipticity ($[\theta]$); this normalises the data based on their concentration, molecular mass and, the difference between the pathlengths of the two cells used to obtain the spectra (difference of 0.00029 cm). Molar ellipticity makes comparison between the spectra more valid.

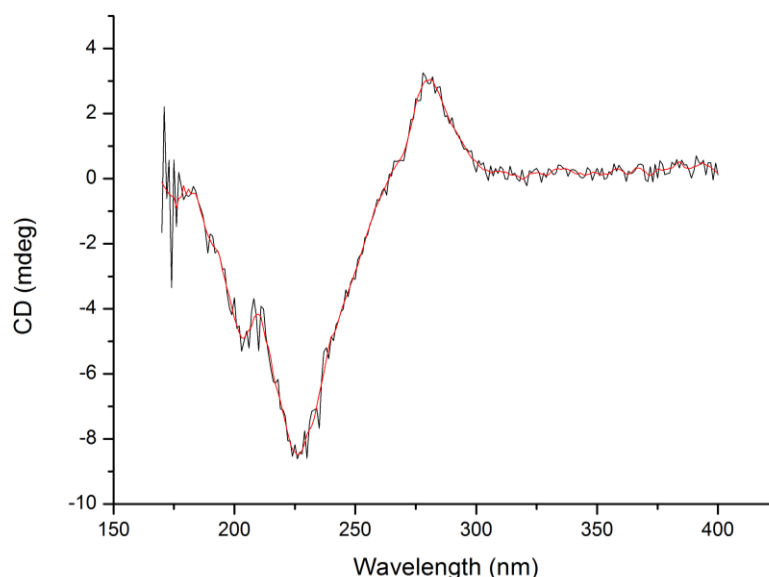


Figure 3.2.2.20: SRCD spectra of PHENSSBr₂ showing the raw data (black) and the 11 point smoothed data (red) at room temperature in the 170-400 nm range, using a 0.1 mm cell, corrected for solvent baseline (H₂O).

Figure 3.2.2.21 similarly to Figure 3.2.2.16, shows the effect of the halogen axial ligand on the PHENSS complexes. The spectra from 400 to 200 nm has already been discussed, the SRCD spectra allows us to see that the similarity in polarised light absorption between PHENSSCl₂ and PHENSSI₂ continues, with the only differential factor being the slightly more intense band at 216 nm for PHENSSCl₂. The equivalent peak for PHENSSBr₂ is red shifted, appearing at 226 nm and thus has a more positive

chirality shift. The second peak revealed by the SRCD at ~ 180 nm was similar for the three compounds however, PHENSSCl₂ had a large shoulder at 212 nm.

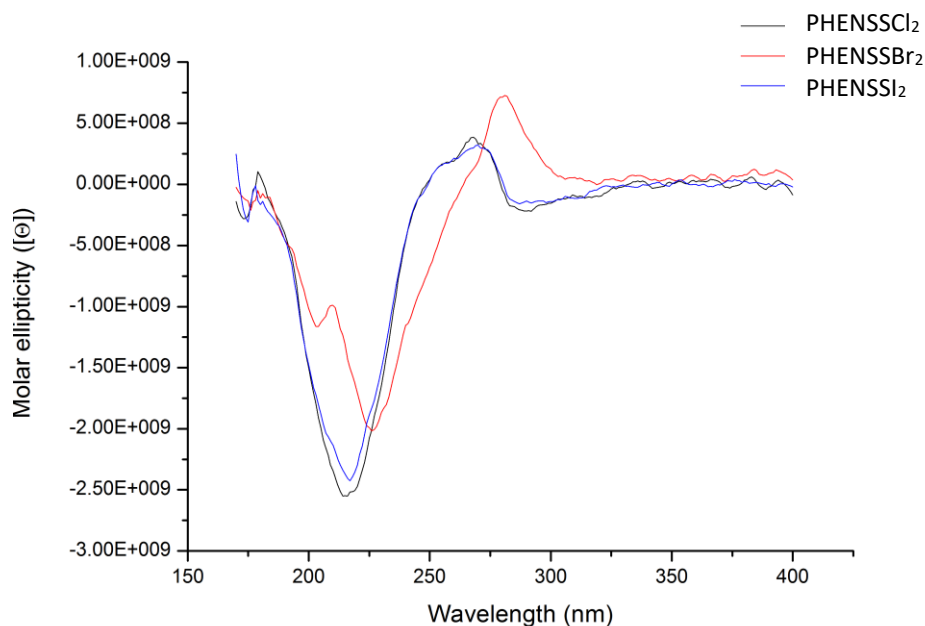


Figure 3.2.2.21: SRCD spectra of PHENSSCl₂ (black), PHENSSBr₂ (red) and, PHENSSI₂ (blue); at room temperature in the 170-400 nm range, using a 0.1 mm cell, corrected for solvent baseline (H₂O).

Figure 3.2.2.22 similarly to Figure 3.2.2.18, shows the effect of the halogen axial ligand on the 5MESS complexes. The spectra from 400 to 200 nm has already been discussed, the SRCD spectra allows us to see the similarity in polarised light absorption between the three complexes more easily. At this scale the spectra appear more similar and a trend appears. Similarly to the PHENSS complexes the intensity of the band increases as the size of the ligand increases and as the electronegativity decreases, that is 5MESSI₂ has the most intense band followed by 5MESSBr₂ and then 5MESSCl₂. Thus it can be hypothesised that either the size of the ligand or the electronegativity affect the conformation of the complex such that they have indices or refraction for left and/or right polarised light. The spectra of 5MESSI₂ has by far the more intense absorption

band as well as the sharpest, indicating that the iodo ligands have a stronger effect on the structure than the other two ligands.

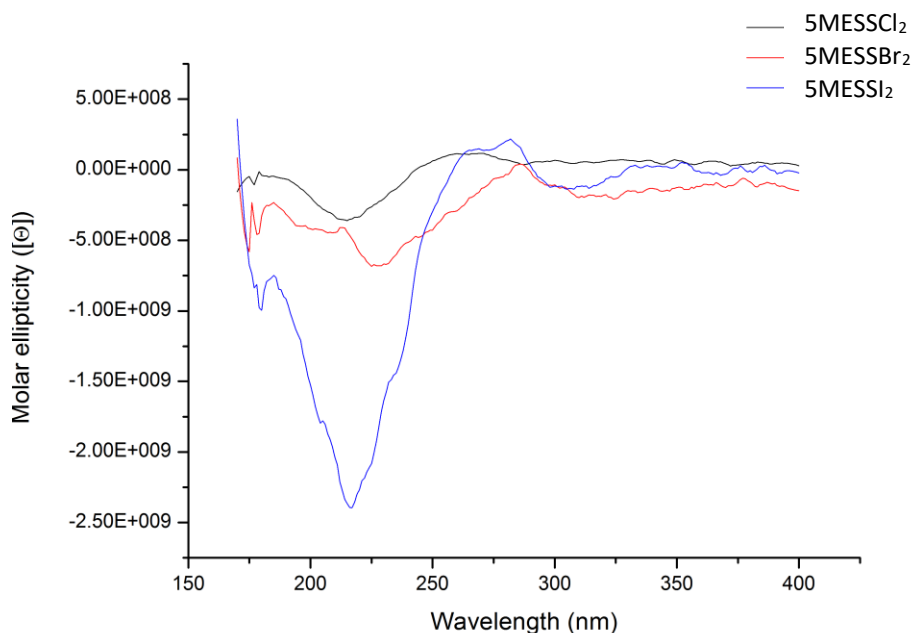


Figure 3.2.2.22: SRCD spectra of 5MESSCl₂ (black), 5MESSBr₂ (red) and, 5MESSI₂ (blue); at room temperature in the 170-400 nm range, using a 0.1 mm cell, corrected for solvent baseline (H₂O).

Figure 3.2.2.23 similarly to Figure 3.2.2.17, shows the effect of the halogen axial ligand on the 56MESS complexes. The spectrum from 400 to 200 nm has already been discussed but, the SRCD spectra reveal further differences between the three complexes. The red shift seen in the spectra of 56MESSBr₂ continues into the lower wavelengths, indicating a positive chirality shift. The negative absorption band at 225 nm for 56MESSBr₂ is also much stronger than the blue shifted bands of 56MESSCl₂ and 56MESSI₂. 56MESSCl₂ appears to have two peaks more than that of 56MESSBr₂ with additional peaks at 184 and 302 nm. The opposite is true of 56MESSI₂ which has only one true peak which is blue shifted to the equivalent peaks of the bromo and chloro complexes. This indicates that this compound overall absorbs somewhat even amounts

of left and right polarised light. As noted earlier the intensity of the peaks for the 56MESS complexes does not follow a trend that correlates to either size or electronegativity and thus more complex factors are at play.

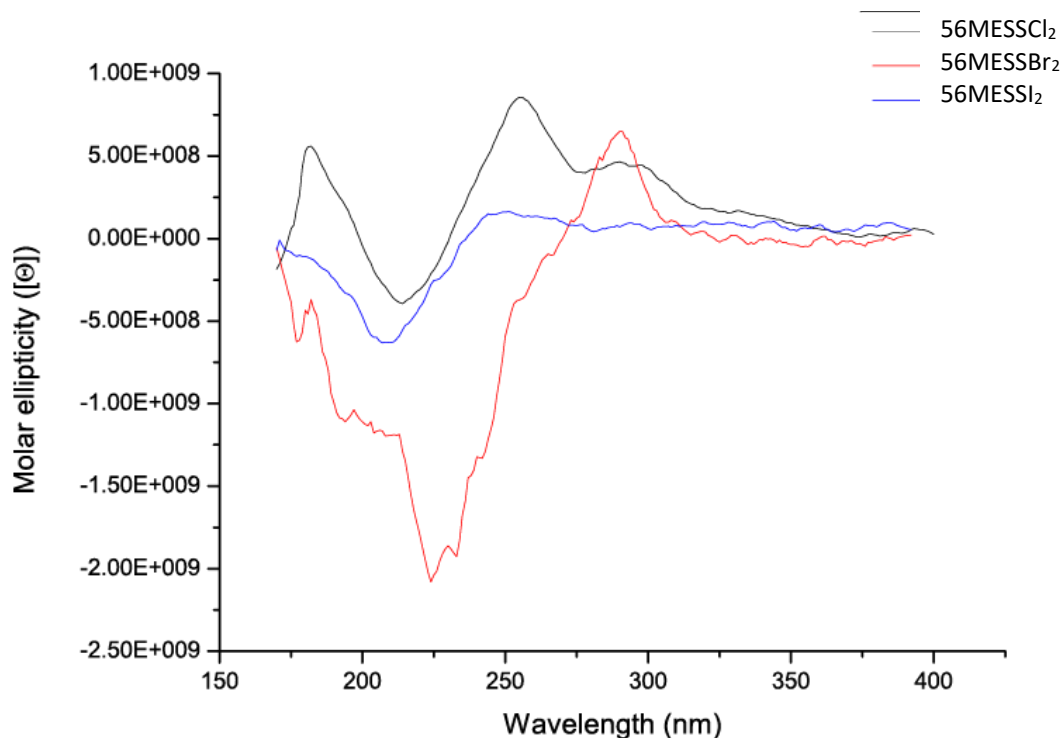


Figure 3.2.2.23: SRCD spectra of 56MESSCl₂ (black), 56MESSBr₂ (red) and, 56MESSI₂ (blue); at room temperature in the 170-400 nm range, using a 0.1 mm cell, corrected for solvent baseline (H₂O).

As with the UV data the SRCD spectra of complexes with the same polyaromatic region were also compared. Figure 3.2.2.24 illustrates the effect of the polyaromatic ligand on dichlorinated complexes. The spectra for PHENSSCl₂ and 56MESSCl₂ are quite similar in terms of their intensity where as 5MESSCl₂ has a comparatively flat spectra. As mentioned previously the difference in the spectra is most likely due to the asymmetry of 5MePhen effecting the conformation and thus the absorption of polarised light. Although the spectra for 56MESSCl₂ and PHENSSCl₂ are very similar their bands between 275 and 325 nm are in opposition with PHENSSCl₂ having a positive maxim and 56MESSCl₂ having a negative maxim. For the remaining peaks 56MESSCl₂ was red shifted to the peaks of PHENSSCl₂ which has almost identical peak locations to

5MESSCl₂. Interestingly the Cl₂ complexes had the least similar SRCD spectra, which is unexpected due to the smaller size of the chloro ligand, which strengthens the hypothesis that changes in spectra are due to the electronegativity of the ligands.

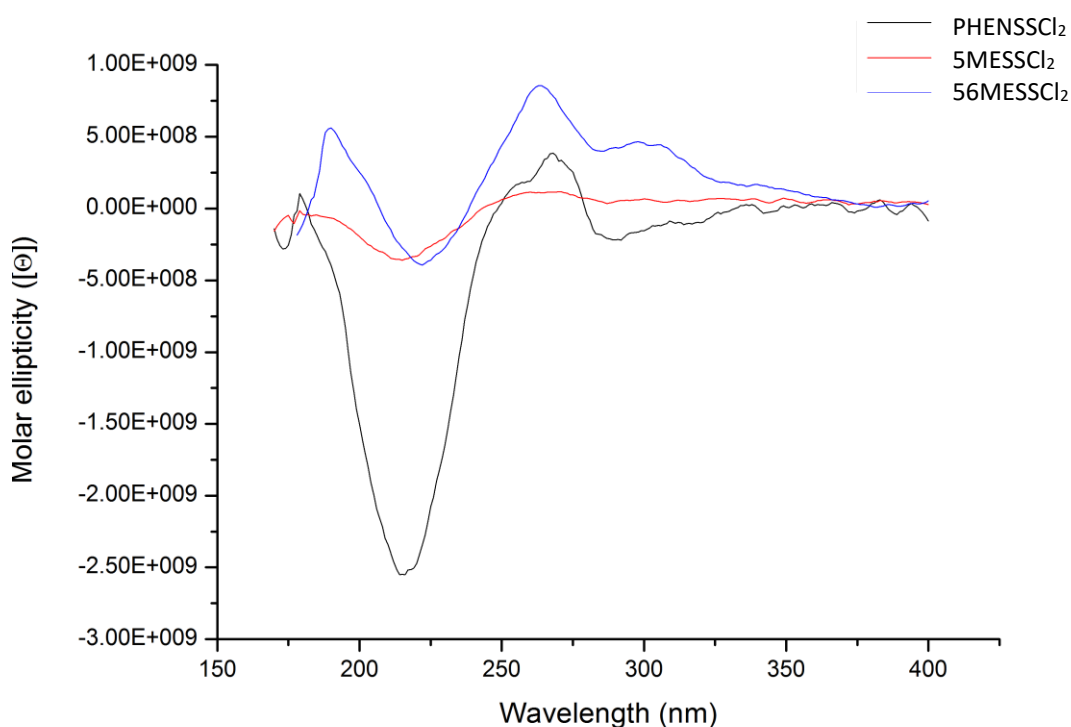


Figure 3.2.2.4: SRCD spectra of PHENSSCl₂ (black), 5MESSCl₂ (red) and, 56MESSCl₂ (blue); at room temperature in the 170-400 nm range, using a 0.1 mm cell, corrected for solvent baseline (H₂O).

Figure 3.2.2.25 illustrates the effect of the polyaromatic ligand on dibrominated complexes. Similarly to the dechlorinated complexes 5MePhen had the flattest spectra, providing more evidence for the hypothesis that asymmetry results in more even absorbance of right and left polarised light. For all three peaks visible in the spectra 56MESSBr₂ is the most red shifted followed by 5MESSBr₂ and lastly PHENSSBr₂. This suggests that the more methyl groups or the larger the polyaromatic ligand the more positive the chiral shift of the molecule however, the intensity of the bands is determined by other factors such as symmetry.

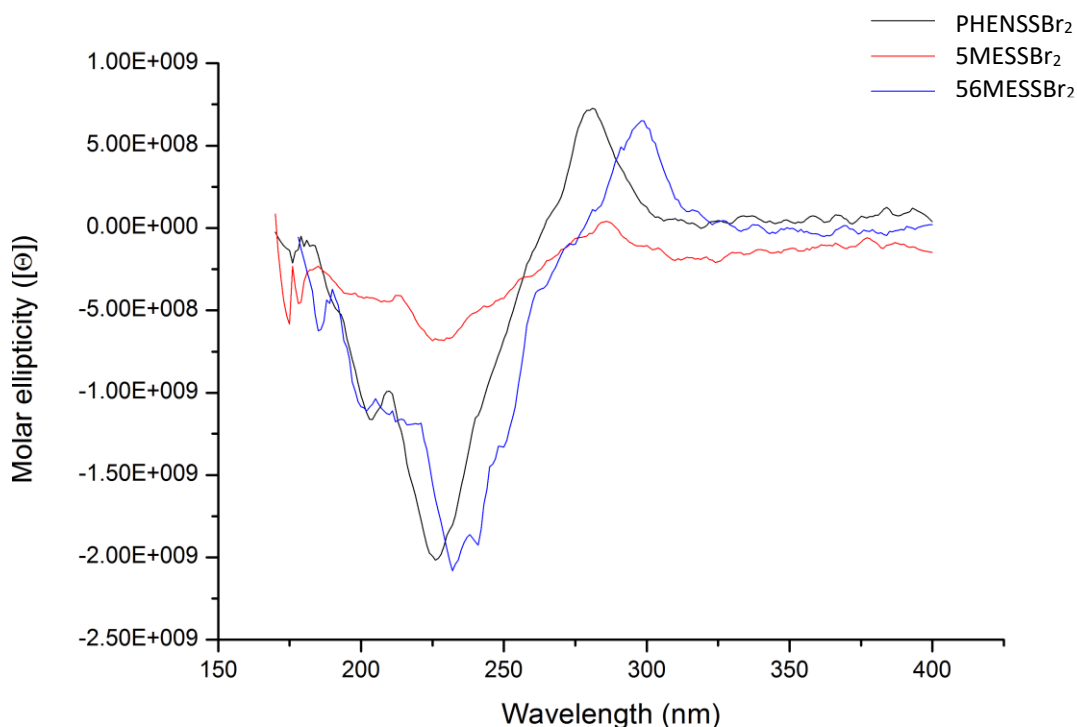


Figure 3.2.2.25: SRCD spectra of PHENSSBr₂ (black), 5MESSBr₂ (red) and, 56MESSBr₂ (blue); at room temperature in the 170-400 nm range, using a 0.1 mm cell, corrected for solvent baseline (H₂O).

Figure 3.2.2.26 illustrates the effect of the polyaromatic ligand on diiodo complexes. Unlike the dibromo and dichloro complexes 56Me₂Phen has the flattest spectra not the 5MePhen complex. These three complexes had the most similar spectra out of any of the comparisons made so far, the main difference being the flatness of the spectra of 56MESSI₂. A possible explanation for this is that the iodo ligands have a stronger influence on chirality than the polyaromatic ligand and thus the spectra emulate the changes made by the iodo ligands that they have in common with only minor differences due to the influence of the polyaromatic ligand.

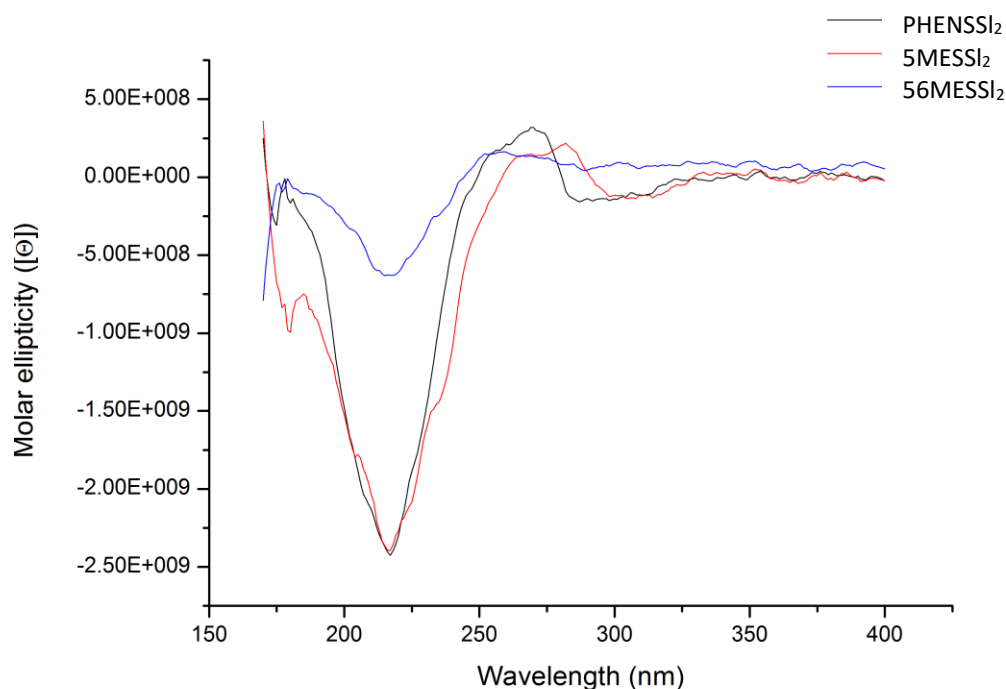


Figure 3.2.2.26: SRCD spectra of PHENSSI₂ (black), 5MESSI₂ (red) and, 56MESSI₂ (blue); at room temperature in the 170-400 nm range, using a 0.1 mm cell, corrected for solvent baseline. (H₂O).

3.2.3 The characterisation of Pt(IV) complexes of the type



The NMR characterisation of 56MESS(OH)(OAc), 56MERR(OH)(OAc), PHENSS(OH)(OAc), PHENRR(OH)(OAc), 5MESS(OH)(OAc), 5MERR(OH)(OAc), 4MESS(OH)(OAc), 4MERR(OH)(OAc), 44BPYSS(OH)(OAc) and, 44BPYRR(OH)(OAc); was achieved using a combination of ¹H proton NMR spectra, ¹H ¹⁹⁵Pt heteronuclear multiple quantum correlation (HMQC) spectra and, ¹H/ ¹H COSY spectra. As mentioned in previous spectra, a Pt(IV) complex of the type [Pt(P_L)(A_L)(OH)₂]^{+2H} as a ¹⁹⁵Pt resonance at 450 ppm and so deviation from this trend can help to identify the coordination of the axial ligands. For these asymmetric complexes the ¹⁹⁵Pt shift was hypothesised to be similar to the dihydroxy complexes as they have the same coordination sphere and one of the ligands is identical. Complexes of the type [Pt(P_L)(A_L)(OH)(C₂H₃O₂)]²⁺ were

discovered to have a ^{195}Pt resonance approximately 100 ppm higher than that of the dihydroxy counterpart. An example of the HMQC spectra is shown in Figure 3.2.3.1, the ^{195}Pt chemical shift of 543.9 ppm is significantly different to the two starting PCs [Pt(SS-dach)Cl₂] and K₂PtCl₄ (-3282 and -1650 ppm, respectively). The correlation between the Pt centre and the aromatic resonance 9.34 ppm confirms the coordination of the 1,10-phenanthroline.

The proton spectra were similar to the Pt(II) counterparts of these complexes in the literature with the presence of the axial ligands affecting the chemical shifts in both the aromatic and aliphatic regions. In the aromatic region the asymmetric ligands caused splitting of the 2/9 and 4/7 protons as these two protons are closest sterically to the axial ligands. In the aliphatic region the axial ligands caused the merging of the 3'4 and 4'/5' proton peaks, as is typically seen when complexes of this type are oxidised. Figure 3.2.3.2 shows the ^1H spectra of PHENSS(OH)(OAc) with the peaks labelled with the corresponding proton. As discussed in the synthesis chapter the isolation of these complexes was problematic, leading to the presence of Pt(II) in the final compound which is evident in the NMR spectra. The relative integration of peaks

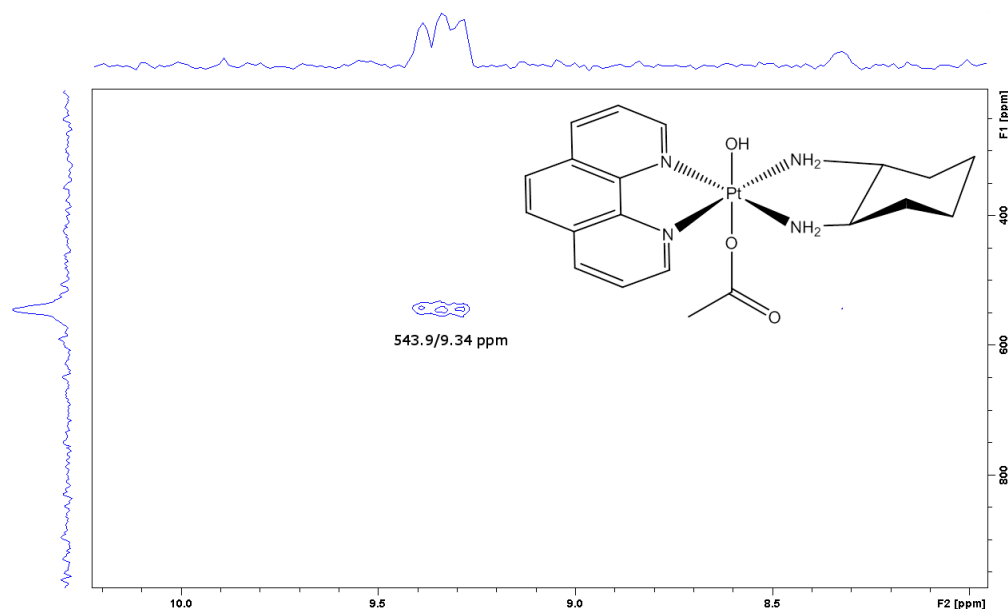


Figure 3.2.3.1: The ^1H - ^{195}Pt HMQC spectrum of PHENSS(OH)(OAc) in D₂O, displaying the correlations between the platinum centre and the protons from each ligand; performed on a Bruker Avance 400 MHz NMR spectrometer.

was used to identify which peaks belonged to the two PCs. The aromatic region for PHENSS(OH)(OAc) was assigned as follows: the singlet at 8.31 ppm was assigned to H5 and H6 as the two protons will share the peak location due to the symmetry of the complex and there are no protons on the adjacent carbons. The doublet of doublets (dd) at 8.24 ppm were assigned to H3 and H8, again the symmetry resulted in the combining of the two peaks and the presence of the protons on the adjacent carbons resulting in a dd splitting pattern due to coupling. The remaining two peaks corresponding to H4/7 and H2/9 usually appear as doublets however, the asymmetry of these complexes caused further splitting. At first glance they appear to be doublets of doublets but, closer inspection reveals further splitting of these peaks. In order to distinguish between the two peaks the *J* coupling was still used as in previous interpretations. H4 and H7 were assigned to the peak at 9.05 ppm had a major coupling constant of 8.63 Hz, and a secondary coupling constant of 1.23 Hz. The smaller coupling constant of the peak at 9.25 ppm was assigned to H2 and H9 is due to the proximity to the nitrogen. The resonances for the aliphatic region were consistent with NMR spectra reported in the literature for Pt(IV) complexes with the same axillary ligands. The peaks were almost identical with only slight variants in the ppm. The amine proton resonances were not visible due to exchange with D₂O.

The above was repeated for the NMR spectra for the remaining (OH)(OAc) complexes the results of which are summarised in Table 2.3.7.1 (Chapter two). There were some minor differences in the resonances for 5MESS and 56MESS, due to the methyl groups, and greater differences were seen in the 4MESS and 44BPYSS spectra in the aromatic region. The RR and SS isomers had almost identical spectra however, the relative concentration of each solution affected the stacking of the phenanthroline region and thus affected the resonance of the H2,9 and H4,7 peaks.

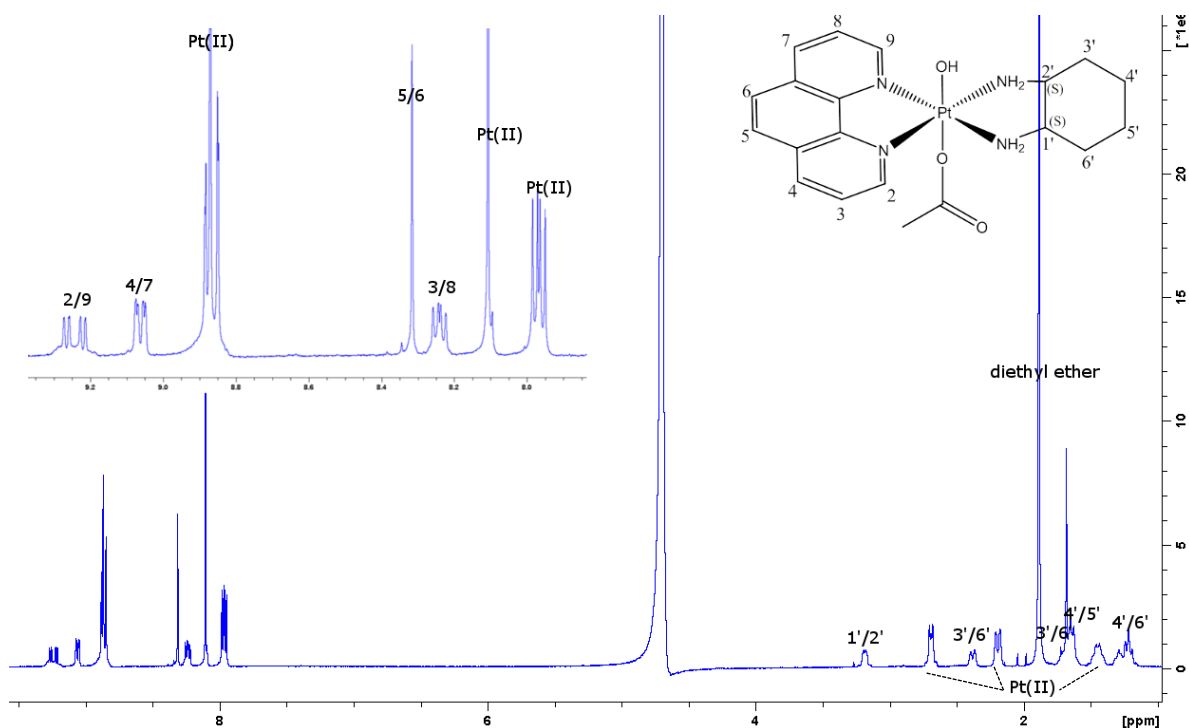


Figure 3.2.3.2: The ^1H NMR spectra of PHENSS(OH)(OAc) in D_2O , showing proton assignment and Pt(II) impurity; performed on a Bruker Avance 400 MHz NMR spectrometer. * indicates stereocenter (SS).

3.2.4 The characterisation 2-aminoethyldiclofenacamide

The NMR characterisation of 2-aminoethyldiclofenacamide was achieved using a ^1H NMR. The NMR characterisation of the starting material was reported previously and this was used as a tool to help check the peak assignments.⁸⁷ The proton assignment of en-DCF is shown in Figure 3.3.4.1. The C-H proton peaks were assigned as follows: the doublet at 7.45 ppm was assigned to H12 and H14 as the two protons will share the peak due to the symmetry of that portion of the complex and there is only one proton on the adjacent carbons. The multiplet at 7.08 ppm was assigned as the peaks from H4 and H13 overlapping. The triplet at 6.95 ppm was assigned to H6 due to the single hydrogens on the two adjacent carbons and the splitting caused by the asymmetry of the ring. The triplet at 6.76 ppm was assigned to H5 for using the same rational, H5 and H6 were distinguished due to the proximity to the amine group which brings H6 further downfield. The doublet at 6.26 ppm was assigned to H7 as it

has only one neighbouring carbon bound to a proton. The two doublets were distinguishable firstly due to the integration which was doubled for the H12/14 peak vs the H7 peak, but also because the proximity of the electronegative chloro groups neighbouring the H12/14 peaks meant that they would be positioned further downfield. The multiplets at 3.01 and 2.51 ppm were assigned to H1* and H2*, respectively where the H2* was assigned to the peak further downfield due to its proximity to the NH₂ group. The N-H peaks were visible although their integrations could not be relied upon due to exchange with water. The peak at 9.89 ppm was assigned to the NH both of the ethylenediamine (en) and the DCF, whereas the peak at 1.09 ppm was assigned to NH₂.

In order to confirm the binding of en to DCF the two proton NMRs were compared as shown in Figure 3.3.4.2. This was essential to the characterisation due to the small differences in ¹H spectra, where the amine peaks were unreliable due to exchange with water and the C-H peaks of en could easily be confused with solvent peaks. The ¹H spectra for en-DCF is shifted downfield and the H13 and H4 peaks are significantly merged whereas in the DCF spectra the two individual peaks can more easily be discerned. This technique was useful for the quick confirmation of the presence and purity of en-DCF so that it could quickly be used for further synthesis.

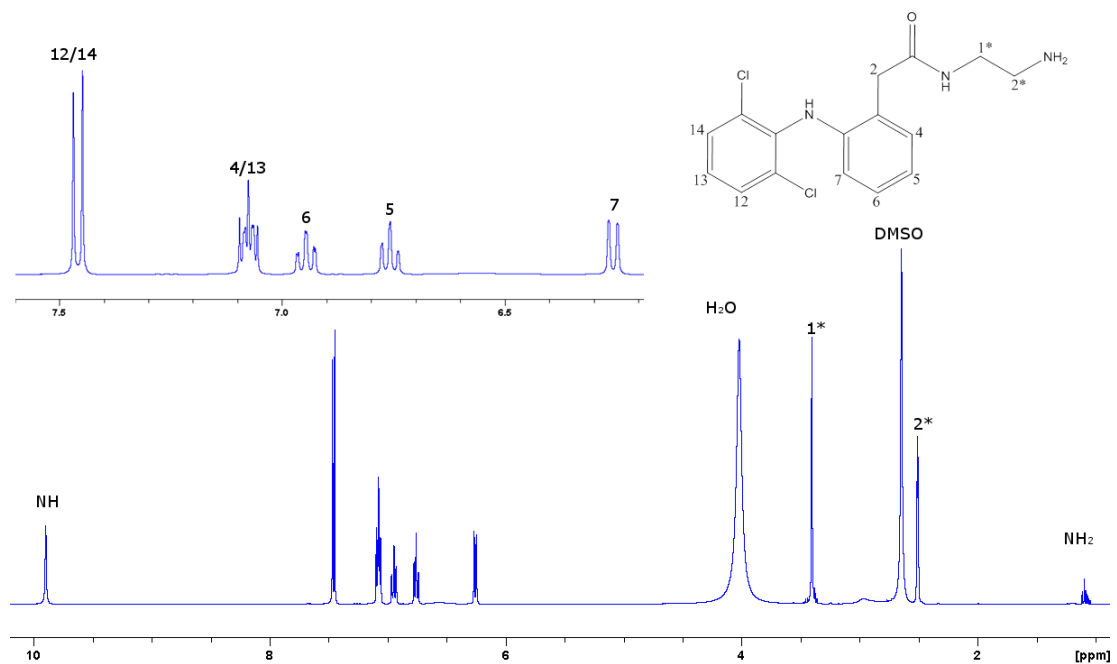


Figure 3.3.4.1: The ¹H NMR spectra of en-DCF in DMSO showing proton assignment; performed on a Bruker Avance 400 MHz NMR spectrometer.

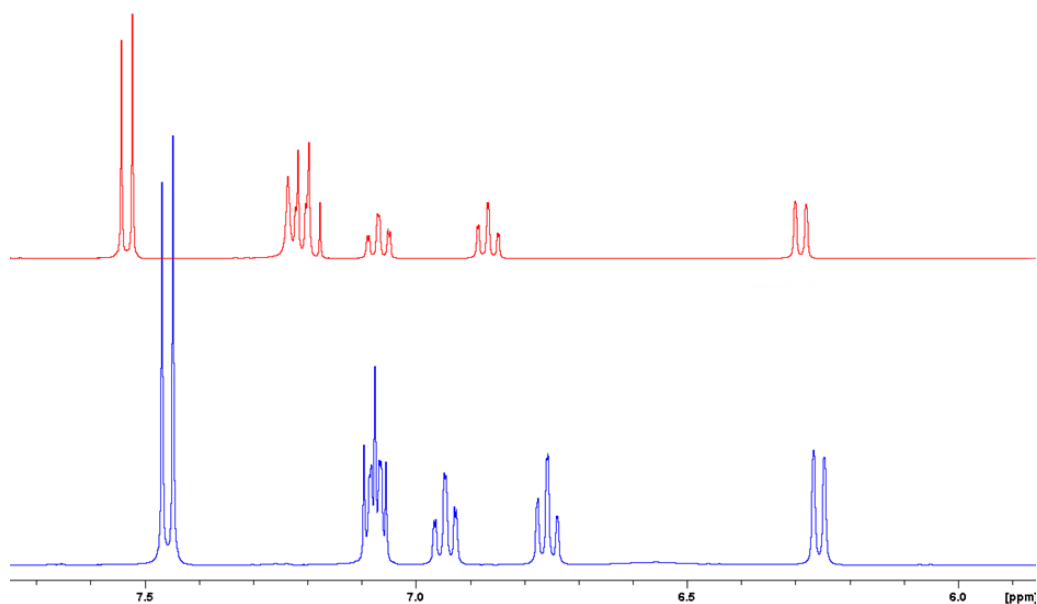


Figure 3.3.4.2: The ¹H NMR spectra of en-DCF in DMSO (blue) in comparison to the ¹H NMR spectra of DCF in DMSO (red) ; performed on a Bruker Avance 400 MHz NMR spectrometer.

3.2.5 The characterisation of [Pt(1,10-phenanthroline)(1S,2S-diaminocyclohexane) (DMSO)₂]²⁺

The NMR characterisation of PHENSS(DMSO)₂ was achieved through a combination of ¹H proton NMR spectra, ¹H ¹⁹⁵Pt heteronuclear multiple quantum correlation (HMQC) spectra and, ¹H/ ¹H COSY spectra. As discussed earlier a typical Pt(IV) complex of the type [Pt(P_L)(A_L)(OH)₂]⁺² will demonstrate a ¹⁹⁵Pt resonance at 450 ppm whereas the [Pt(P_L)(A_L)(X)₂]⁺² type complexes had a ¹⁹⁵Pt resonance at approximately -630 ppm. This information was used to confirm the synthesis of PHENSSDMSO₂ by ruling out that the Pt(IV) complex visible in the ¹H spectra was not the starting reagent and that the Cl ligands had not exchanged with water or hydroxyl ligands. The ¹⁹⁵Pt resonance of PHENSSDMSO₂ was found to be at -600.7 ppm, similar to that of the halide complexes most likely because the coordination spheres are more similar in comparison to the coordination spheres containing oxygen. Both the 1 dimensional ¹⁹⁵Pt spectra and the 2 dimensional HMQC are displayed in the supplementary information. Figure 3.3.5.1 shows the ¹H spectra of PhenSSDMSO₂ with the peaks labelled with the corresponding proton. The aromatic region was significantly different from similar compounds previously reported, they were assigned as follows: the singlet at 10.79 ppm was assigned to H5 and H6 as the two protons will share the peak due to the symmetry of the complex and there are no protons on the adjacent carbons. The doublet of doublets (dd) at 10.78 ppm were assigned to H3 and H8, again the symmetry resulted in the combining of the two peaks and the presence of the protons on the adjacent carbons resulting in a dd splitting pattern due to coupling. The remaining two doublet (d) peaks in the aromatic region were merged in the spectra; however, they could still be distinguished due to the smaller coupling constant of H2 and H9 due to the proximity to the nitrogen. Thus the 11.58 ppm doublet *J*= 8.28 Hz was assigned to H2 and H9 and the doublet at 11.85 ppm *J*= 5.50 Hz was assigned to H4 and H7. The resonances for the aliphatic region were consistent with NMR spectra reported in the literature with the same axillary ligands however, there were some minor differences and all peaks were shifted downfield due the solvent (DMSO). The

multiplet at 5.31 ppm was assigned to H1' and H2' due to the symmetry of the complex and their proximity to the amine groups. The multiplet at 4.56 ppm which presents as a doublet was assigned to H3' and H6' for similar reasoning: despite its appearance the signal must be a multiplet as there are a total of three protons on the adjacent carbons. The multiplet at 3.96 ppm was also assigned to H3' and H6', again the symmetry of the complex resulting in these protons sharing a peak and the boat conformation resulting in two peaks both of an integration of 2. The multimultiplets at 3.84 and 3.53 ppm were assigned to H4' and H5' using the same rationale. The amine proton resonances are usually not reported for this type of complex due to exchange with water, in DMSO they appear in the aromatic region. The two amine peaks are shifted far downfield; at 11 and 12.08 ppm for the SS-Dach and phenanthroline amines, respectively. Despite being shifted further downfield than expected, the integration and shape of the peaks is good evidence that they are accurate and it is known that in hydrogen bonding solvents such as DMSO and acetone the peaks for amine groups are shifted downfield.¹¹¹

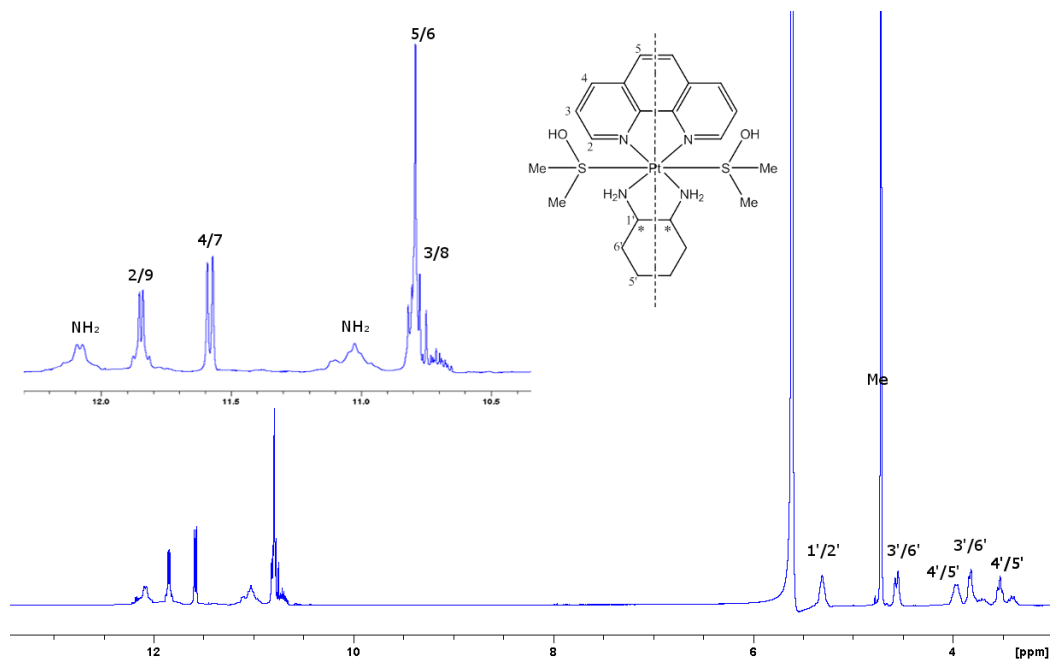


Figure 3.3.5.1: The ^1H NMR spectra of PHENSSDMSO₂ in *d*-DMSO, showing proton assignment; performed on a Bruker Avance 400 MHz NMR spectrometer.

3.2.6 The characterisation of [Pt(1,10-phenanthroline)(1S,2S-diaminocyclohexane)(2-Aminoethylclufenamide)₂]²⁺

The NMR characterisation of PHENSSenDCF₂ was achieved through a combination of ¹H proton NMR spectra, ¹H /¹⁹⁵Pt heteronuclear multiple quantum correlation (HMQC) spectra and, ¹H/ ¹H COSY spectra. Additional confirmation was achieved through a combination of ¹H/¹³C heteronuclear single quantum coherence (HSQC) which allows the inspection of carbon-proton single bond correlations, ¹H/¹³C heteronuclear multiple bond correlation (HMBC) which allows for the inspection of interactions between protons up to four bond lengths away. The ¹⁹⁵Pt peak resonates at – 2820.9 ppm, which is more similar to a typical Pt(II) complex of this type than any previously synthesised Pt(IV) compounds, this was a part of the reason additional spectra were inspected, to confirm the ligand was bound and the ¹H NMR signals were not simply depicting a mixture of PHENSS and enDCF. The aromatic and aliphatic peaks of PHENSS and the peaks of enDCF were similar to those described above with only slight differences. The annotated ¹H NMR spectra is illustrated in Figure 3.3.6.1. The ¹H PHENSS aromatic peaks were assigned as follows: the doublet at 8.89 ppm was assigned to H4 and H7 which were combined due to the symmetry of the complex, the *J* coupling (*J* = 8.42Hz) was used to distinguish it from the other doublet at 9.11 ppm (*J* = 5.26 Hz) that was assigned to H2 and H9 which has a smaller *J* coupling value because of their proximity to the amine. The doublet of doublet at 8.01 ppm was assigned to H3 and H8 which are again combined due to symmetry, the splitting pattern can be attributed to the non-equivalence of the two neighbouring protons (one of which is adjacent to the amine group) and confirmed by the *J* coupling values *J* = 8.13, 8.41 Hz. The singlet at 8.13 ppm was assigned to H6 and H5. The aliphatic region was similar to that of similar compounds previously reported however, unlike previously reported Pt(IV) compounds the merging of the H3'/6' peak with the H4'/5' did not occur similarly to the dihalogen compounds discussed above. The splitting may be due to the solvent, which in this case was MeOH, or the electronegativity of the coordinating atom of the ligand. The aliphatic groups were assigned as follows: the multiplet at 2.69 ppm was

assigned to H1' and H2', although the shape of the peak appeared to be similar to that of previously reported compounds the merging of the DMSO residual solvent peak made integration difficult. The pseudo doublet at 2.25 ppm was assigned to H3' and H6' as was the multiplet at 1.69 ppm. The two multiplets at 1.54 and 1.29 ppm were similarly assigned to H4' and H5'. The enDCF ligand peaks were similar to that described above however, all the intergradations were doubled and a slight downfield shift of all the aromatic peaks as well as a few peaks moving downstream in relation to the others. The enDCF peaks were assigned as follows: the doublet at 7.23 ppm was assigned to H12'' and H14'' which was distinguished from the other doublets due to its integration which is twice that of the others as they are the only two protons which have equivalent chemical environments. The doublet at 7.12 ppm was assigned to H4''; which is distinguishable from the doublet at 7.95 ppm assigned to H7'' due to the *J* couplings $J = 7.50$ Hz and $J = 7.95$ Hz respectively, due to the proximity of H7'' to the amine which shifts it further downfield. The multiplet at ~ 6.9 ppm can be split into a triplet at 6.91 ppm and another triplet at 6.85 ppm which correspond to H13'' and H6'' respectively. Again the relative couplings allowed these two peaks to be distinguished from one another with H13'' $J = 8.03$ Hz and H6'' $J = 7.72$ Hz, at 6.70 ppm where the larger *J* coupling of H13'' can be attributed to its proximity to the two chloro groups. The triplet at 6.21 ppm was assigned to H5'' which is a similar chemical environment to H6'' as evident by their similarity although the H5'' peak is further upfield due to its distance from the electronegative groups. The N-H peaks were visible although their integrations could not be relied upon even less than they could be in DMSO due to exchange with water and MeOH.

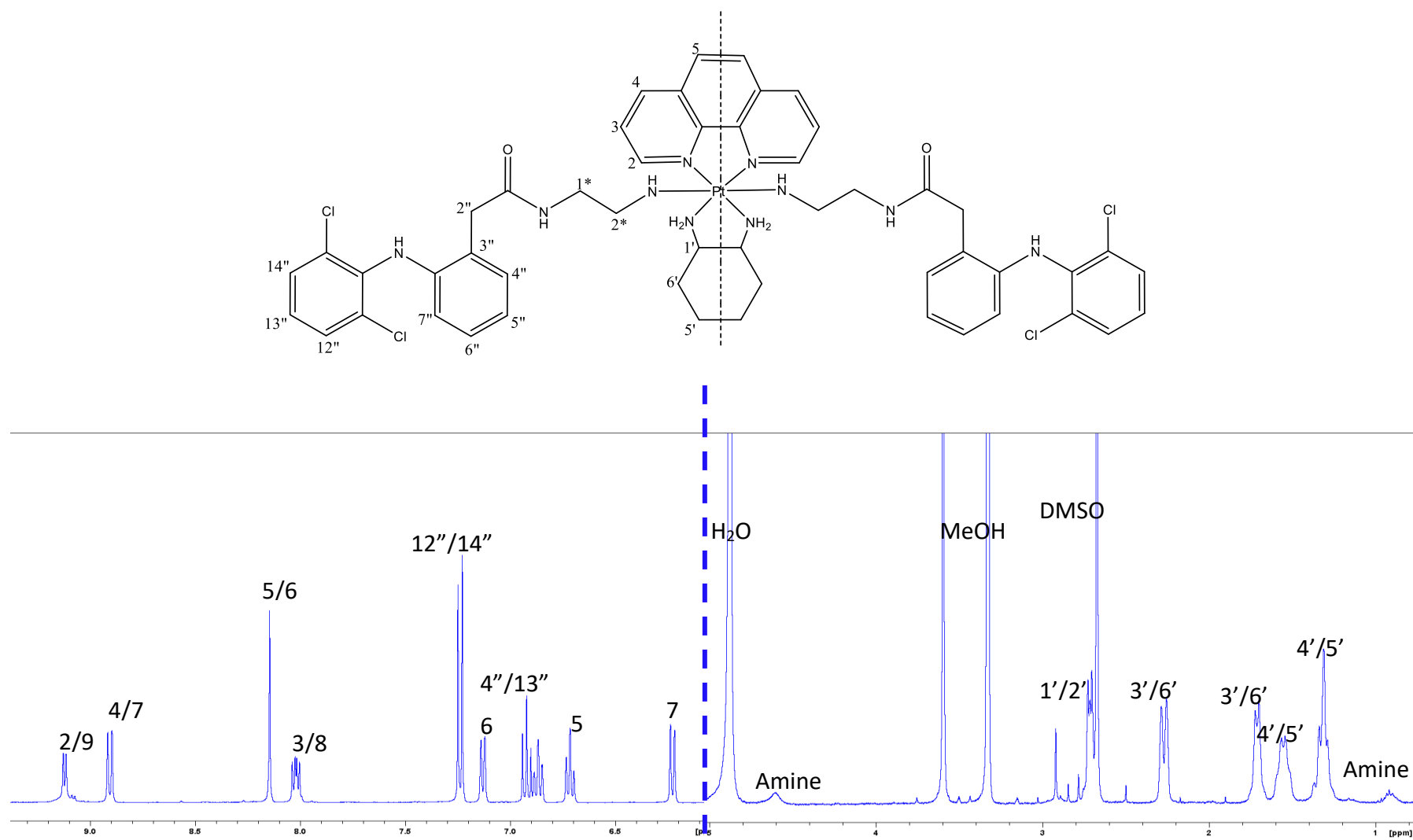


Figure 3.3.6.1: ¹H NMR spectra of PHENSSenDCF₂ in MeOD, showing proton assignment; performed on a Bruker Avance 400 MHz NMR spectrometer.

3.2.7 The characterisation of Pt(IV) complexes of the type $[\text{Pt}(\text{P}_L)(\text{A}_L)(\text{OH})(\text{succinimide})]^{2+}$

The NMR characterization of PHENSS(OH)(Succ), 5MESS(OH)(Succ), and 56MESS(OH)(Succ) was achieved using a combination of ^1H proton NMR spectra and ^1H ^{195}Pt heteronuclear multiple quantum correlation (HMQC) spectra. The HMQC peak was significantly different to other platinum complexes of the same type reported in the literature.¹⁰⁹ Typically a Pt(IV) complex of the type $[\text{Pt}(\text{P}_L)(\text{A}_L)(\text{OH})_2]^{2+}$ will demonstrate a ^{195}Pt resonance at 450 ppm whereas the complexes synthesised in this work have ^{195}Pt resonate at approximately -550 ppm, this confirms the presence of the succinate ligand in place of one of the hydroxyl.⁴⁰ An example of the HMQC spectra is shown in Figure 3.2.7.1, the ^{195}Pt chemical shift of 542.1 ppm is significantly different to the two starting Pt(II) complexes $[\text{Pt}(\text{SS-dach})\text{Cl}_2]$ and K_2PtCl_4 (-3282 and -1650 ppm, respectively). The correlation between the Pt centre and the aromatic resonance 9.37 ppm confirms the coordination of the 1,10-phenanthroline.

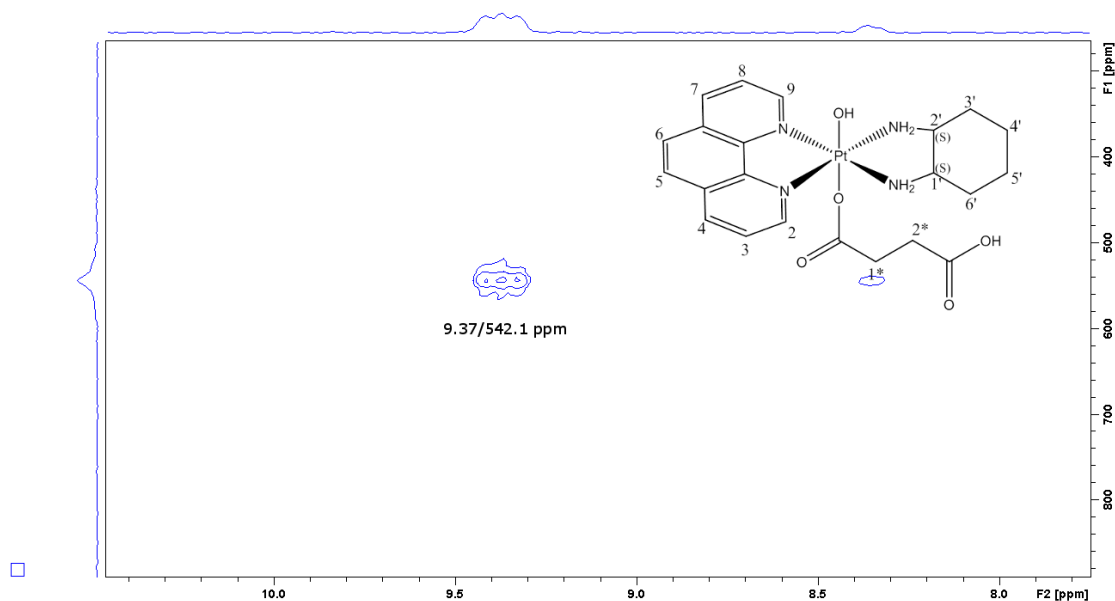


Figure 3.2.7.1: The ^1H - ^{195}Pt HMQC spectrum of PHENSS(OH)(Succ) in D_2O , displaying the correlations between the platinum centre and the protons from each ligand; performed on a Bruker Avance 400 MHz NMR spectrometer.

The proton spectra were almost identical to similar complexes in the literature with very minor chemical shifts which occur due to stacking of the 1,10-phenanthroline ligands stacking in solution.¹¹⁰ Figure 3.3.7.2 shows the ¹H spectra of PHENSS(OH)(Succ) with the peaks labelled with the corresponding proton. The aromatic region for PHENSS(OH)(Succ) was assigned as follows: the singlet at 8.32 ppm was assigned to H5 and H6 as the two protons will share the peak location due to the symmetry of the complex and there are no protons on the adjacent carbons. The doublet of doublets (dd) at 8.25 ppm was assigned to H3 and H8, again the symmetry resulted in the combining of the two peaks and the presence of the protons on the adjacent carbons resulting in a dd splitting pattern due to coupling. The remaining two doublet (d) peaks in the aromatic region, merged in the spectra; however, they could still be distinguished due to the smaller coupling constant of H2 and H9 due to the proximity to the nitrogen. Thus the 9.07 ppm doublet $J = 8.13$ Hz was assigned to H4 and H7 and the doublet at 9.27 ppm $J = 5.77$ Hz was assigned to H2 and H9. The resonances for the aliphatic region were consistent with NMR spectra reported in the literature with the same axillary ligands. The peaks were almost identical with only slight variants in the ppm. The amine proton resonances were not visible due to exchange with D₂O.

The above was repeated for the NMR spectra of 5MESS(OH)(Succ), and 56MESS(OH)(Succ), the results of which are summarised in Table 2.3.11.1 (Chapter two). There were some minor differences in the resonances for these complexes, particularly in the aromatic region where the relative concentration of each solution affects the stacking of the phenanthroline region and thus affects the resonance of the H2, 9 and H4,7 peaks.

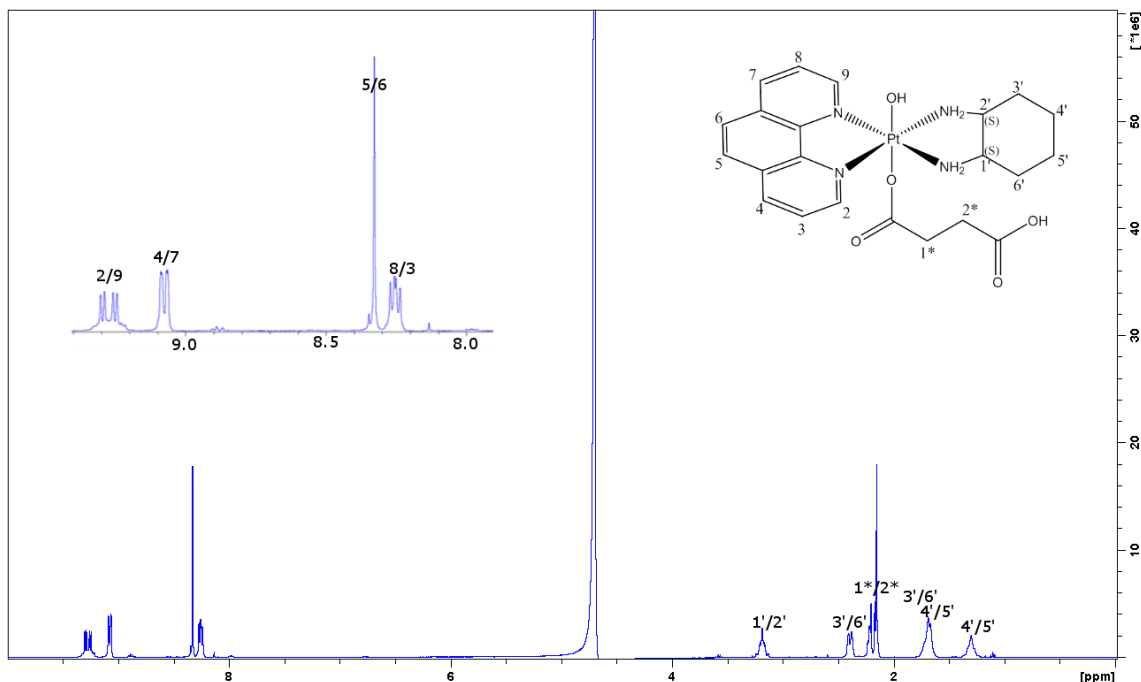


Figure 3.2.7.2: ^1H NMR spectra of PHENSSenDCF₂ in MeOD, showing proton assignment; performed on a Bruker Avance 400 MHz NMR spectrometer.

3.2.8 The characterisation of [Pt(1,10-phenanthroline)(1S,2S-diaminocyclohexane) (OH)(succinatePFP)]²⁺

The NMR characterisation of PHENSS(succinatePFP) was achieved using a combination of ^1H proton NMR spectra, ^1H ^{195}Pt heteronuclear multiple quantum correlation (HMQC) spectra and, $^1\text{H}/^1\text{H}$ COSY spectra. As mentioned in previous characterisation analysis, a Pt(IV) complex of the type $[\text{Pt}(\text{P}_L)(\text{A}_L)(\text{OH})_2]^{+2}$ has a ^{195}Pt resonance at 450 ppm and so deviation from this trend can help to identify the coordination of the axial ligands. An example of the HMQC spectra is shown in Figure 3.2.5.1, the ^{195}Pt chemical shift of 531.5 ppm (Figure 3.2.8.1) is significantly different to the two starting PCs $[\text{Pt}(\text{SS-dach})\text{Cl}_2]$ and K_2PtCl_4 (–3282 and –1650 ppm, respectively). The correlation between the Pt centre and the aromatic resonance 9.34 ppm confirms the coordination of the 1,10-phenanthroline. The addition of the PFP moiety did not significantly alter the ^1H NMR spectra thus the protons were assigned in using the same justification as in Section 3.2.8, the proton assignment is shown in Figure 3.2.8.2.

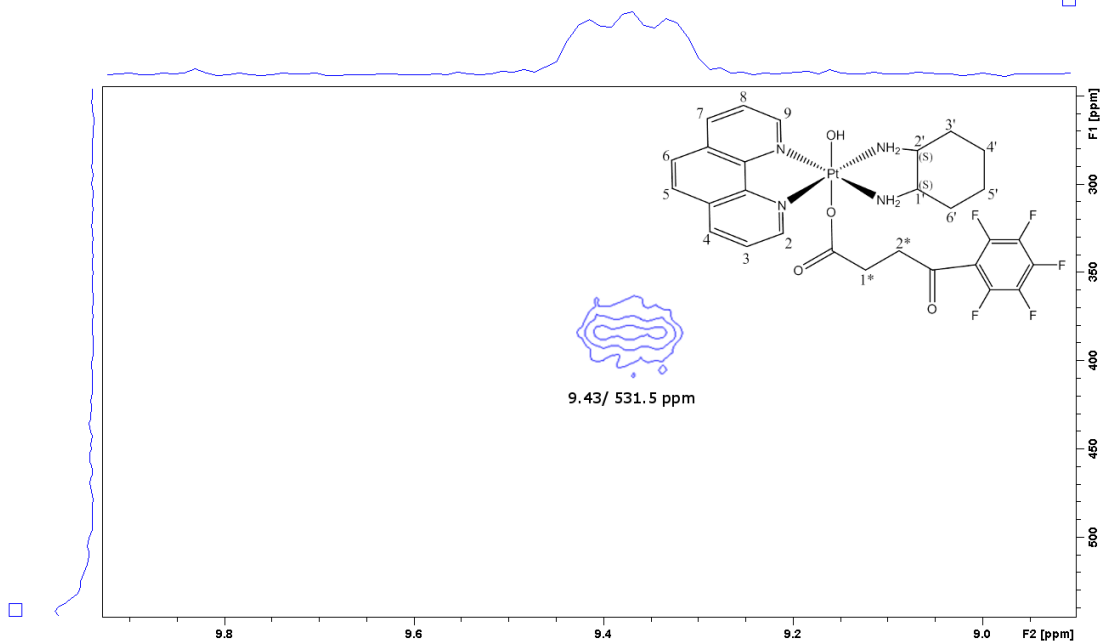


Figure 3.2.8.1: The ^1H - ^{195}Pt HMQC spectrum of PHENSS(OH)(SuccPFP) in D_2O , performed on a Bruker Avance 400 MHz NMR spectrometer.

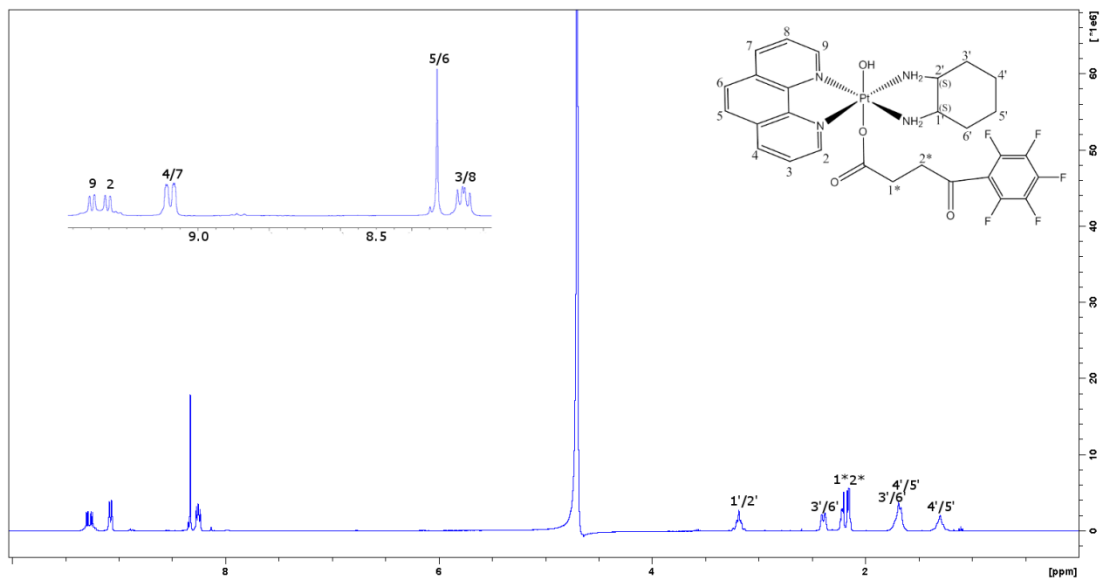


Figure 3.2.8.1: The ^1H spectrum of PHENSS(OH)(SuccPFP) in D_2O , performed on a Bruker Avance 400 MHz NMR spectrometer.

3.2.9 The characterisation of [Pt(1,10-phenanthroline)(1S,2S-diaminocyclohexane)(OH)(PSMA)]²⁺

The NMR characterisation of PHENSS(OH)(PSMA) was achieved using a combination of ¹H proton NMR spectra, ¹H ¹⁹⁵Pt heteronuclear multiple quantum correlation (HMQC) spectra and, ¹H/¹H COSY spectra. As mentioned in previous characterisation analysis, a Pt(IV) complex of the type [Pt(P_L)(A_L)(OH)₂]^{+2H} as a ¹⁹⁵Pt resonance at 450 ppm and so deviation from this trend can help to identify the coordination of the axial ligands. For these asymmetric complexes the ¹⁹⁵Pt shift was hypothesised to be similar to the dihydroxy complexes as they have the same coordination sphere and one of the ligands is identical. Complexes of the type [Pt(P_L)(A_L)(OH)(PSMA)]²⁺ were discovered to have a ¹⁹⁵Pt resonance at 537.1 ppm. An example of the HMQC spectra is shown in Figure 3.3.9.1, the ¹⁹⁵Pt chemical shift of 543.9 ppm is significantly different to the two starting PCs [Pt(SS-dach)Cl₂] and K₂PtCl₄ (−3282 and −1650 ppm, respectively). The correlation between the Pt centre and the aromatic resonance 9.34 ppm confirms the coordination of the phen.

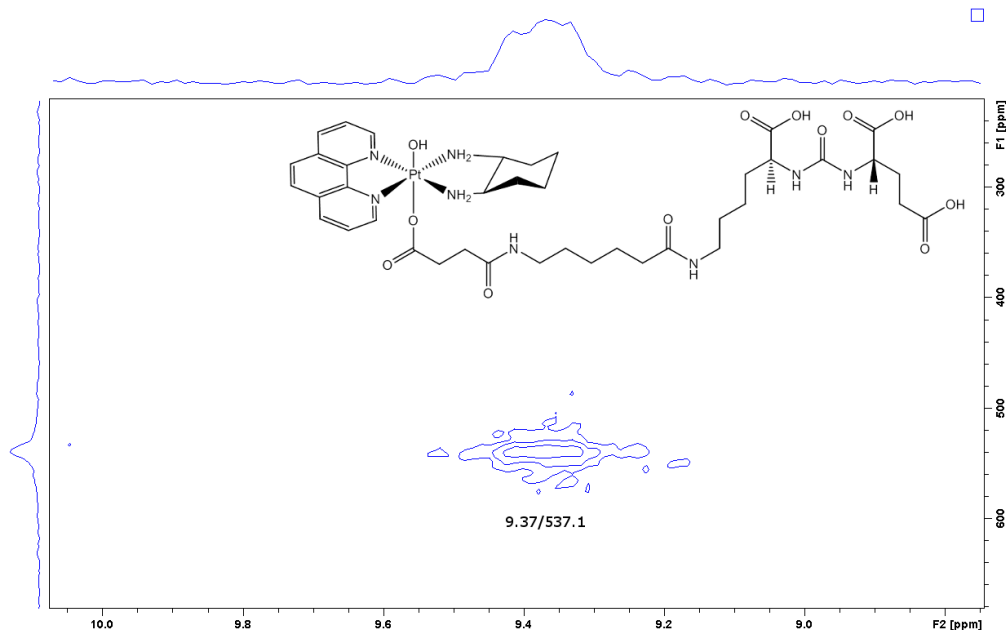


Figure 3.3.9.1: The ¹H–¹⁹⁵Pt HMQC spectrum of PHENSS(OH)(PSMA) in D₂O, displaying the correlations between the platinum centre and the protons from each ligand; performed on a Bruker Avance 400 MHz NMR spectrometer.

The ^1H analysis was significantly more difficult to analyse than the complexes previously mentioned as the DCL peaks resonate in the same region as DACH. An overview of the literature around DCL did not identify an annotated NMR spectra, so in order to fully characterise PHENSS bound DCL the peaks in the spectra of the DCL starting reagent were first analysed (Figure 3.3.9.2)

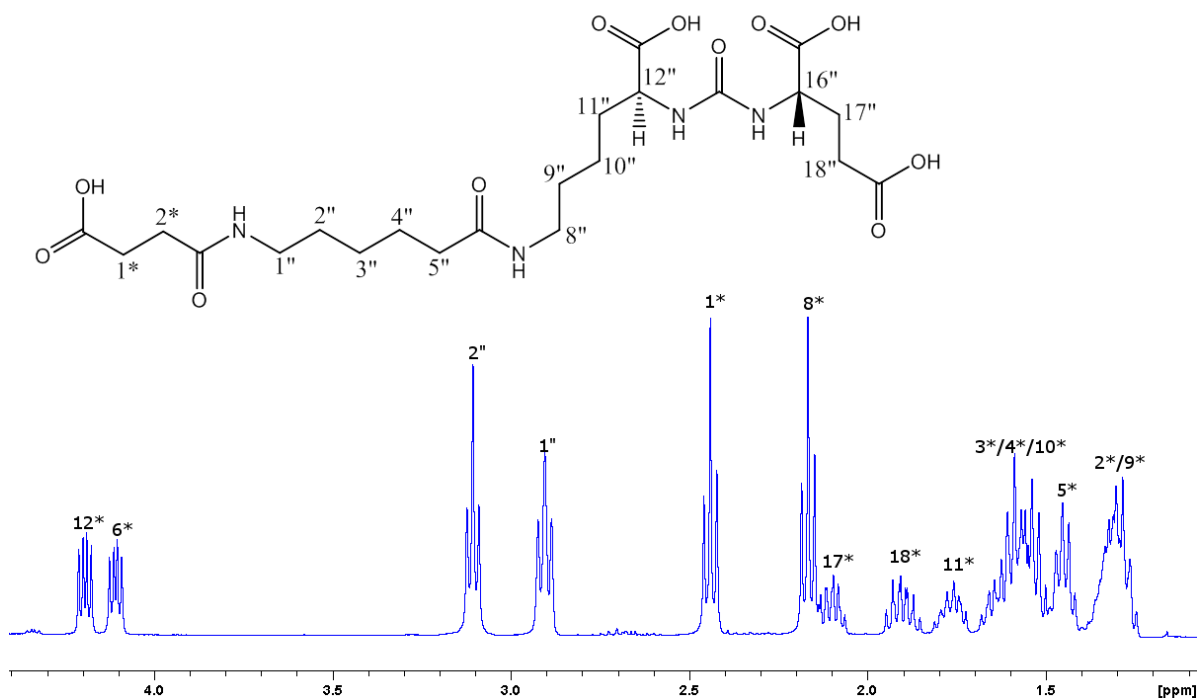


Figure 3.3.9.2: ^1H NMR spectra of DCF in D_2O , showing proton assignment; performed on a Bruker Avance 400 MHz NMR spectrometer.

Figure 3.3.9.3 shows the proton assignment of PHENSS(OH)(PSMA), the analysis of which was confirmed by comparison with PHENSS and DCL spectra (Figure 3.3.9.4). The PHENSS aromatic peaks were assigned as follows: the doublet at 8.87 ppm was assigned to H4 and H7 which were combined due to the symmetry of the complex, the J coupling ($J = 8.30$ Hz) was used to distinguish it from the other doublet at 8.47 ppm ($J = 5.39$ Hz) that was assigned to H2 and H9 which has a smaller J coupling value due to their proximity to the amine. The doublet of doublet at 7.98 ppm was assigned to H3 and H8 which are again combined due to symmetry, the splitting pattern can be attributed to the non-equivalence of the two neighbouring protons (one of which is

adjacent to the amine group) and confirmed by the J coupling values $J = 8.30, 13.80$ Hz. The singlet at 8.11 ppm was assigned to H6 and H5 which was easily identifiable as the only singlet and the only peak with an integration of 6. The aliphatic region for the PHENSS peaks was similar to that of similar compounds previously reported however the DCL peaks hid some of the peaks which usually resonate at ~ 1.5 ppm. The PHENSS aliphatic peaks that are visible were assigned as follows: the multiplet at 2.70 ppm was assigned to H1' and H2', although the shape of the peak appeared to be similar to that of previously reported compounds the merging of the DMSO residual solvent peak made integration difficult. The pseudo doublet at 2.20 ppm was assigned to H3' and H6' and the multiplet 1.22 ppm were similarly assigned to H4' and H5'. These 4 protons typically share an additional peak at ~ 1.5 ppm which was merged with DCL peaks such that an accurate ppm could not be obtained. The DCL peaks were identified in the aromatic region, protons bound to O or N were not visible due to exchange with the protic solvent (D_2O). The DCL peaks were assigned as follows: the dds at 4.02 and 3.98 ppm were assigned to H12'' and H16'' as these protons have very similar environments and would be expected to have the furthest downfield shifts due to their proximity to the amine and carboxylic acid groups. The triplet of doublets at 3.09 ppm was assigned to H2* while the triplet at 2.91 was assigned to H1* because the trace Pt peaks around the peak at 2.91 ppm indicating that it is interacting with the platinum and thus must be assigned to the peaks closest to the Pt centre. The triplets at 2.32 and 2.16 ppm were assigned to H1'' and H8'', respectively. Both protons have similar chemical environments however H1'' has a closer proximity to the Pt centre and thus resonates further downfield. The multiplets at 1.99, 1.82 and, 1.68 ppm were assigned to H17'', H18'' and H11'', respectively they have similar shifts as they are all located adjacent to a carboxylic acid. H17'' is the most down field due to its proximity to both the amine and an additional carboxylic acid whilst H11'' is in a chemically similar environment except for the additional carbocyclic acid group. The remaining peaks are merged with each other and the DACH peaks meaning that only approximate ppm values can be assigned and protons are grouped together despite having slightly

different chemical environments which would have resulted in individual peaks if the spectra had not been so crowded. The multiplet at 1.56 ppm was assigned to H3'', H4' and H10'' from the DCL ligand as well as H3' and H6' from the DACH ligand. These protons were assigned to this multiplet based on the comparison illustrated in Figure 3.2.10.4. The multiplets at 1.43 and 1.28 ppm were assigned to H5'' and H2'/9'', respectively for the same reason.

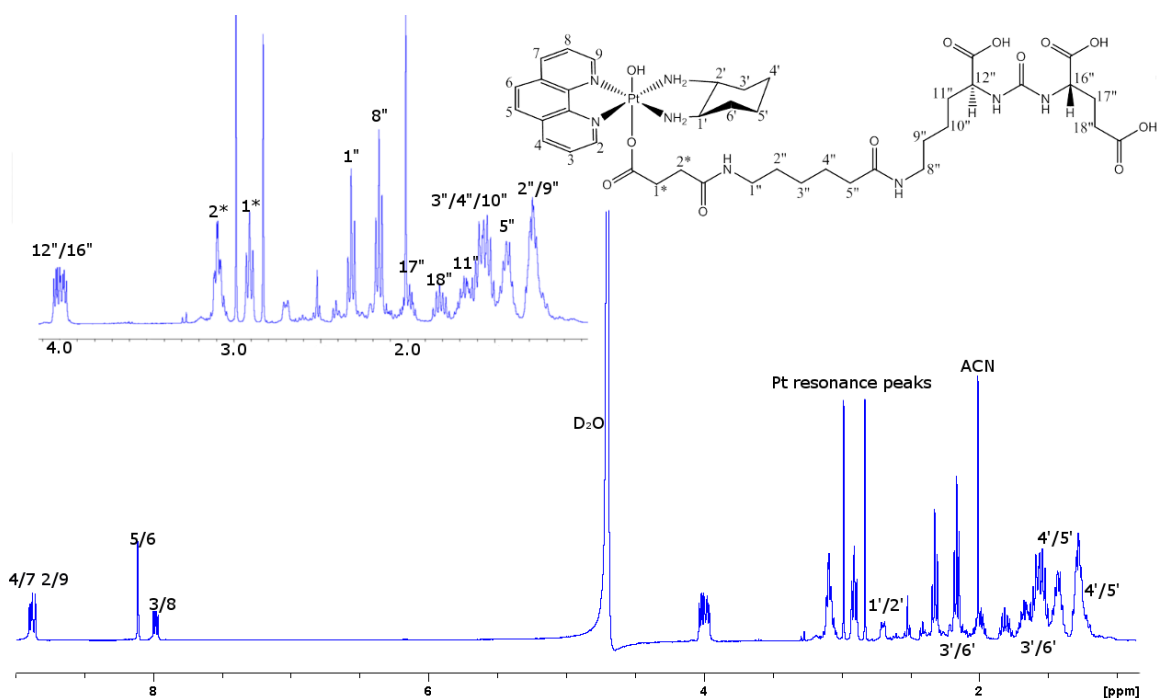


Figure 3.3.9.3: ^1H NMR spectra of PHENSS(OH)(PSMA) in D_2O , showing proton assignment; performed on a Bruker Avance 400 MHz NMR spectrometer.

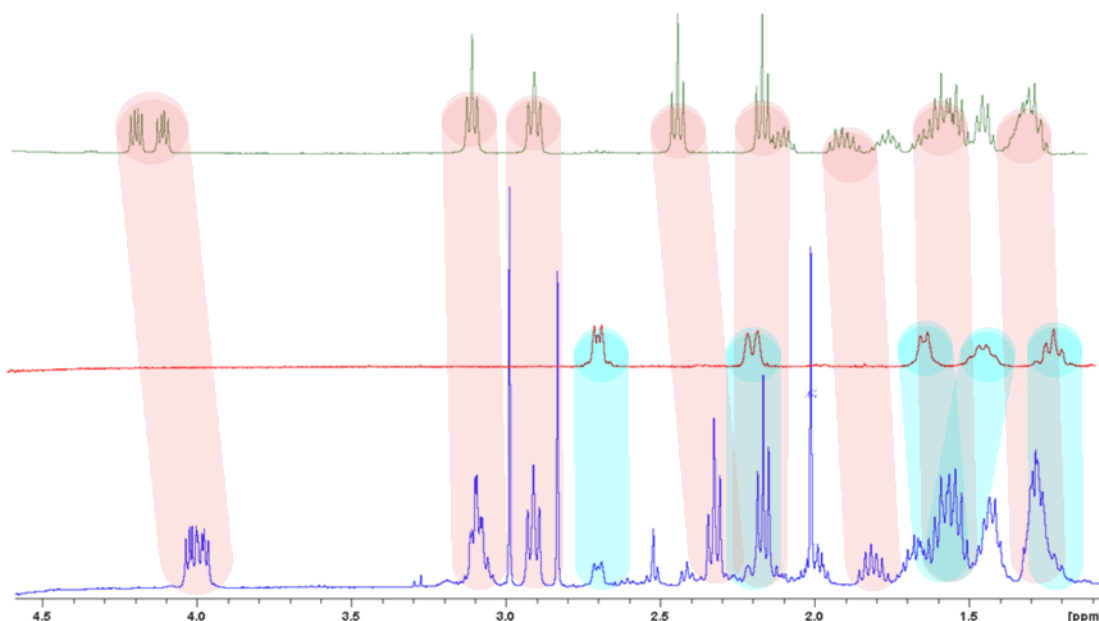


Figure 3.3.9.4: The aliphatic region of the ¹H NMR spectra of PHENSS(OH)(PSMA) in D₂O (blue) in comparison to the ¹H NMR spectra of PHENSS in D₂O (red) and DCL in D₂O (green); performed on a Bruker Avance 400 MHz NMR spectrometer.

3.3 Summary of characterisation: ¹⁹⁵Pt(IV) NMR trends

For complexes such as those synthesised in this thesis, the ¹⁹⁵Pt NMR spectra can be key to the elucidation of the structure. For Pt(II) complexes the ¹⁹⁵Pt shift is well understood and as such it is possible to predict where a peak will appear. This is not the case for polyaromatic Pt(IV) complexes, which means that several spectra need to be taken in order to find the Pt(IV) peak. As our lab synthesise and characterise more of these complexes trends are starting to appear which help speed the elucidation of the structure. For example monosubstituted complexes tend to have higher ppm values than their disubstituted counterparts. Most of the compounds that have been synthesised have an N₄O₂ coordination sphere, new compounds with different coordination spheres appear at different locations. Table 3.3.1 shows the ppm values of the complexes synthesised in this thesis in an attempt to elucidate a trend between the ligand and the location of the ¹⁹⁵Pt chemical shift. In general there appears to be a

Table 3.3.1: ^{195}Pt chemical shift for all PHENSS Pt(IV) complexes synthesised during candidature, illustrating the effect of the axial ligand in the determination of the ppm.

ppm	Coordination sphere	Complex
543	N_4O_2	
537	N_4O_2	
524	N_4O_2	
450	N_4O_2	
-600	N_4S_2	
-635	N_4I_2	
-645	N_4Cl_2	
-964	N_4Br_2	
-2820	N_6	

trend between soft ligands having negative ppm values while hard ligands tend to have positive values. PHENSSS(enDCL)₂ was the exception to this rule with the most negative value of all the compounds synthesised, this could mean that only complexes with N₄O₂ coordination spheres have positive values or that having a coordination sphere containing only one type of atom results in a more negative coordination sphere. Interestingly the ppm value of the halogenated compounds does not correlate to the atomic size or the electronegativity.

3.4 Cytotoxicity

3.4.1 Cytotoxicity of $[\text{Pt}(\text{P}_L)(\text{A}_L)(\text{X})_2]^{2+}$ type complexes

The cytotoxicity of these complexes was determined and compared to the traditional platinum anticancer drugs, cisplatin carboplatin and oxaliplatin; as well as the Pt(II) and Pt(IV) dihydroxide of the most promising candidate designed in our lab 56MESS. Figure 3.5.1.1 shows the relative cytotoxicity of 56MESS, 56MESS(OH)₂, cisplatin carboplatin and oxaliplatin. The GI₅₀ values of 56MESS and 56MESS(OH)₂ are so low (within the μM range) that comparison between them and the traditional anticancer drugs is difficult.

Clearly 56MESS and 56MESS(OH)₂ exhibit promising cytotoxic results with the potential to lower dosage in patients. $[\text{Pt}(\text{P}_L)(\text{A}_L)(\text{X})_2]^{2+}$ had results similar to that of 56MESS and 56MESS(OH)₂ and thus they will be used in place of cisplatin to evaluate the cytotoxicity results. Both the polyaromatic and axial ligands affected the cytotoxicity results. When comparing by polyaromatic ligand the general trend is phen>5Mephen>56Me₂phen. There are several exceptions to this trend; for $[\text{Pt}(\text{P}_L)(\text{A}_L)(\text{Cl})_2]^{2+}$ complexes the trend for the A2780 Ovarian cell line was 5Mephen>phen>56Me₂phen, for $[\text{Pt}(\text{P}_L)(\text{A}_L)(\text{Br})_2]^{2+}$ complexes the trend for MCF-7 Breast and BE2-C Neuroblastoma cell lines the trend was phen>56Me₂phen >5Mephen, there was no deviation from the general trend for the $[\text{Pt}(\text{P}_L)(\text{A}_L)(\text{I})_2]^{2+}$ complexes. The axial ligand appears to have a less consistent effect on the relative cytotoxicity. There is no general order to be allocated to all three polyaromatic ligands; PHENSSX₂ complexes have the general trend Br>Cl>I while both 5MESSX₂ and 56MESSX₂ have the general trend Cl>Br>I. the exceptions for these rules are: for PHENSSX₂ complexes the trend changes to Br>I>Cl for both ovarian cancer cell lines, for 56MESSX₂ the trend is Br>Cl>I for both MCF-7 Breast and BE2-C Neuroblastoma cell lines. For the 5MESSX₂ complexes there were many exceptions to the rule; for Du145 prostate cell line it was I>Cl>Br, for HT29 colon Br>Cl>I for A2780 ovarian, MCF-7 breast, and BE2-C neuroblastoma it was Br>I>Cl. Figures and tables for all data can be found in the supplementary information.

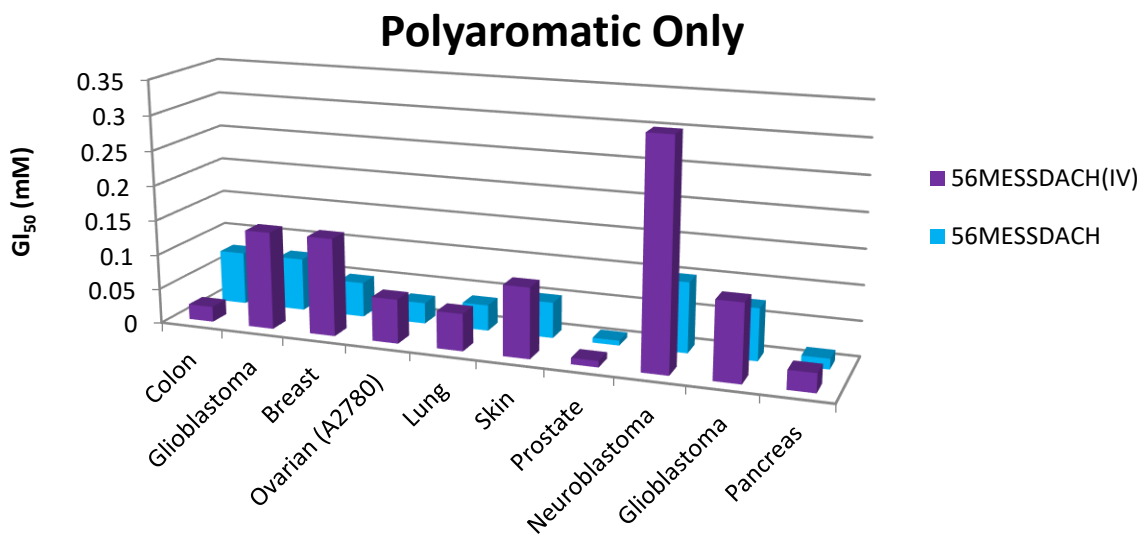
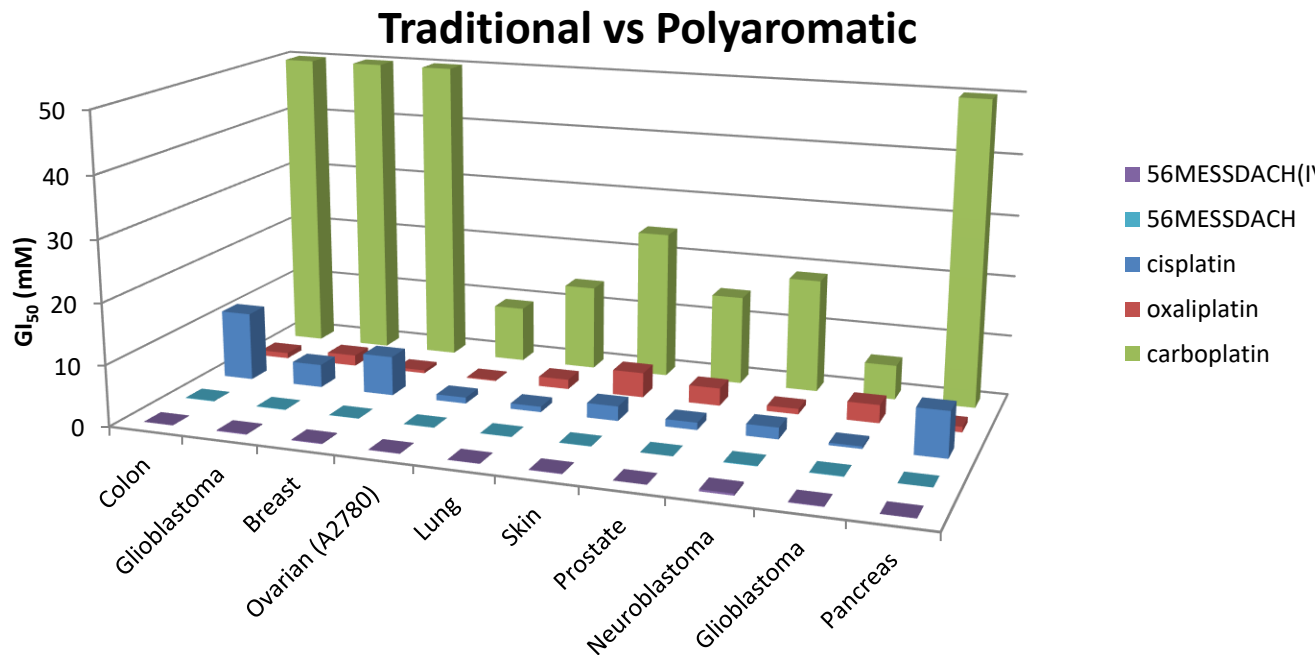


Figure 3.4.1.1: Cytotoxicity of 56MESS, 56MESS(OH)₂, cisplatin carboplatin and oxaliplatin over multiple cell lines: HT29 colon, U87 glioblastoma, MCF-7 breast, A2780 ovarian, H460 lung, A431 skin, Du145 prostate, BE2-C neuroblastoma, SJ-G2 glioblastoma, and MIA pancreas; incubated for 72 hr.

Figure 3.5.1.2 shows the GI_{50} values of 56MESS Cl_2 , 56MESS Br_2 , and 56MESS I_2 in comparison to 56MESS (Pt(II)) and 56MESS OH_2 . These complexes have been selected as they show an interesting trend between the Pt(II) and Pt(IV) results. In most cell lines 56MESS has a much lower GI_{50} than 56MESS OH_2 (all cell lines bar HT29 colon). This is disappointing as the Pt(IV) variant should allow oral administration and improved extracellular stability without affecting the mechanism of action within the cell. The 56MESS X_2 series offers a new perspective on the relationship between oxidation state and cytotoxicity, with the vast majority of compounds having a lower value than that of 56MESS OH_2 and even lower than 56MESS in some cell lines. These results suggest that although reduction may play a role in the cytotoxicity it is not necessarily a negative effect. Perhaps the fast reduction off the halides contributed to their toxicity or perhaps the prodrug was preserved for longer as unlike OH the halides are soft bases and thus Pt(IV) as a soft acid is more stable when bound to them.

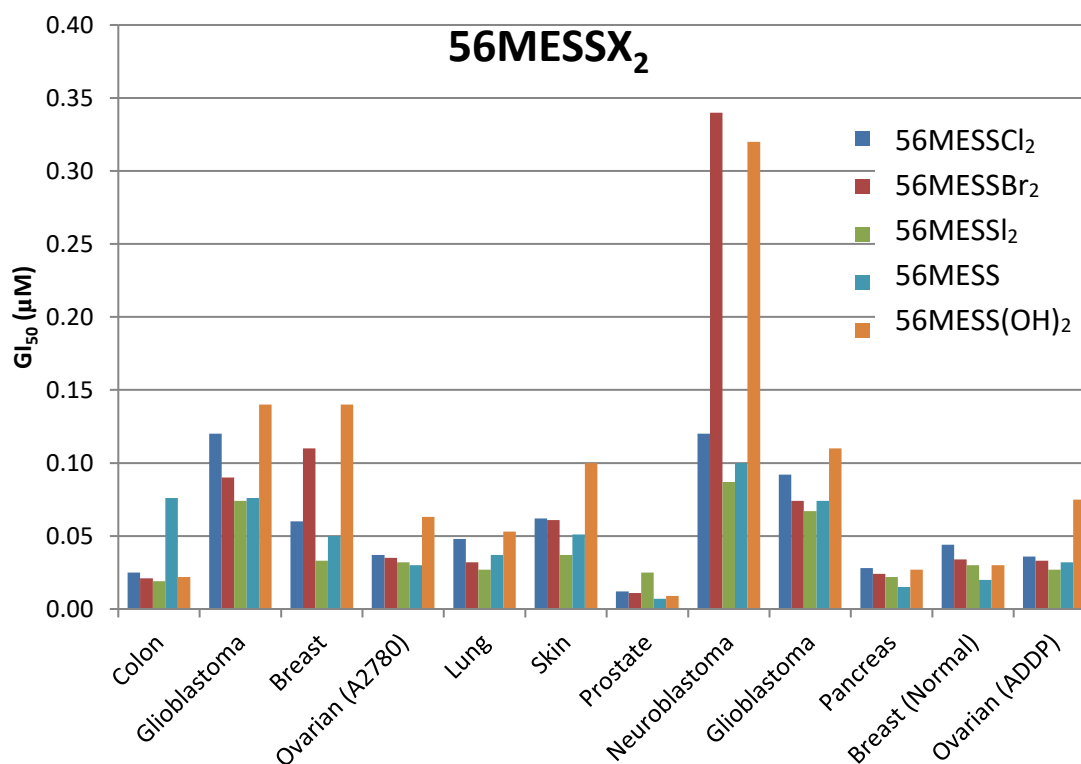


Figure 3.4.1.2: GI_{50} values of 56MESSCl₂, 56MESSBr₂, 56MESSI₂, 56MESS, and 56MESSOH₂ in multiple cell lines: HT29 colon, U87 glioblastoma, MCF-7 breast, A2780 ovarian, H460 lung, A431 skin, Du145 prostate, BE2-C neuroblastoma, SJ-G2 glioblastoma, MIA pancreas, MCF10A breast (normal), and SMA glioblastoma (murine); incubated for 72 hr.

All nine complexes show remarkable results in comparison to cisplatin in terms of their GI_{50} values. Further testing will need to be undertaken to compare the ability of these complexes to target cancer cells in comparison to cisplatin. Comparing the results for the normal and cancerous breast cell lines (MCF-7 and MCF10A respectively) obtained in this study provides hope that these results may be positive, but again further testing is required for confirmation (Figure 3.4.1.3).

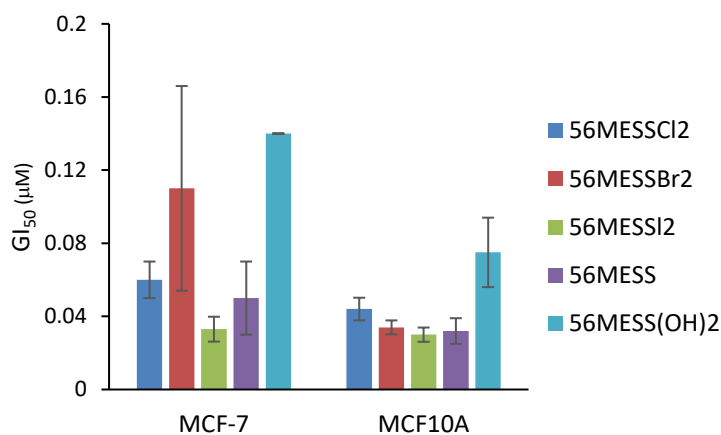


Figure 3.4.1.3: IC_{50} values of 56MESSCl₂, 56MESSBr₂, 56MESSI₂, 56MESS, and 56MESS(OH)₂ in human breast cell lines, MCF-7 (normal) and MCF10A; incubated for 72 hr.

Chapter 4 Conclusions

In this work, 55 complexes were synthesised of which 23 were novel. All Pt(II) complexes were of the type $[\text{Pt}(\text{P}_L)(\text{A}_L)]^{2+}$ and Pt(IV) complexes were of the type $[\text{Pt}(\text{P}_L)(\text{A}_L)(\text{X})_2]^{2+}$; where P_L was either Phen, 4Mephen, 5Mephen, 5Me₂phen or BPY, A_L was either *SS*-dach or *RR*-dach, and X was either, OH, succinimide, Br, I, Cl, en-DCF, DCL or OAc. The synthesis of Pt(II) complexes was achieved using methods in previously published papers, although PHENSS was also synthesised via a novel method developed in this work which utilised flow chemistry techniques. Pt(IV) complexes were synthesised via methods designed and optimised in this work aside from the $[\text{Pt}(\text{P}_L)(\text{A}_L)(\text{OH})_2]^{2+}$ complexes which were synthesised *via* previously published methods.

A series of Pt(IV) polyaromatic complexes with halogenated axial ligands made up for 9 of the novel complexes. These complexes were characterised using ESIMS, UV spectroscopy, CD spectroscopy, SRCD spectroscopy, microanalysis, NMR and HPLC and the cytotoxicity was analysed. For this series only the *SS*-dach isomer was synthesised, the P_L was restricted to Phen, 5Mephen, and 5Me₂phen and the halogens used were Cl, Br and I. This resulted in a family of complexes that could be compared either by their polyaromatic ligand or the halogen of the axial ligand. In general, the halogen axial ligands tended to have a significant impact on the UV absorbance, CD spectra, mass and cytotoxicity of the complexes whilst having a small impact on the NMR spectra. The polyaromatic ligand tended to have more of an effect on the NMR spectra and cytotoxicity, while only some impact on the UV absorbance and CD spectra. The cytotoxicity of these complexes was much better than cisplatin and its derivatives, was comparable to the Pt(II) precursors to these complexes, and more cytotoxic than the dihydroxy analogues. These compounds allow the development of new synthetic methods which were previously closed to these complexes, allowing the synthesis of targeted complexes that have the potential to improve prognosis. The developed method is much less time consuming than the current oxidation methods, reducing

time spent on synthesising intermediates which will maximise outcomes for the synthesis of derivatives.

$[\text{Pt}(\text{P}_L)(\text{A}_L)(\text{OH})_2]^{2+}$ type complexes were synthesised as per previously published methods to be used as a point of comparison for the $[\text{Pt}(\text{P}_L)(\text{A}_L)(\text{OH})(\text{OAc})]^{2+}$ type complexes, whose method was designed as a part of this work. These complexes were found to be highly susceptible to reduction and as a result only NMR characterisation was undertaken. Despite these difficulties with the characterisation it could still be confirmed that the desired complexes were synthesised in good yields and they account for another 10 of the novel complexes synthesised in this work. Further investigation is required to assess if these complexes will make good intermediates for the synthesis of new asymmetric complexes.

The synthesis of Pt(IV) complexes with additional biological design resulted in the synthesis of the remaining four novel complexes for which new methods were designed. The synthesis of PHENSS-enDCF required the synthesis of two Pt(IV) intermediates and the addition of a linker (en) to the ligand (DCF). The addition of an amide to a Pt centre has been achieved previously in the literature however only through substitution of a DMSO ligand, thus the PHENSSDMSO₂ ligand was required. Both PHENSSenDCF and PHENSS(DMSO)₂ were characterised by NMR, confirming the attachment of the ligands. PHENSSenDCF was then sent to our collaborators for biological testing. The attachment of the PSMA targeting ligand DCL also required the synthesis of several Pt(IV) intermediates one of which (PHENSS(OH)(SuccPFP)) was novel. Both the intermediates PHENSS(OH)(Succ) and PHENSS(OH)(SuccPFP) were characterised using NMR along with the final product PHENSS(OH)(DCL). The final product was then sent to our collaborator for further testing and biological analysis. The PHENSS derivatives were sent as for biological assessment with plans to make further derivatives if the biological results are promising.

This project has provided opportunities for future work and further development of methods. The NXS oxidation method has the potential to be used to synthesise intermediates for future complexes, with targeting ligands or bioactive ligands similarly

to how it was used in the development of PHENSS(enDCF)₂ and PHENSS(OH)(DCL). The method for the synthesis of PHENSS(X)(Succinamide) (which was a by-product) could also be developed further to be used as an intermediate and also to test its biological activity to compare to the dihalogenated equivalent. The asymmetric (OH)(OAc) type complexes need similar method development for use as intermediates and also require further characterisation and isolation so that the GI₅₀ value can be determined. Further investigation of the influence of axial ligands on the ¹⁹⁵Pt NMR shift would be very interesting with the potential to elucidate an equation, with which the chemical shift could be determined computationally prior to the synthesis of the complex. The mechanism of action for these complexes is still not completely understood and the design and synthesis of fluorescent molecules may enable the elucidation of the mechanism. Reduction studies on the Pt(IV) complexes would also provide additional information on the mechanism of action; and the influence of redox potential on the GI₅₀ results would be valuable in the design of future potential anticancer complexes.

Other avenues this research could take is looking at the mechanism of action for 56MESS and its analogues, synthesis of quadruplex DNA (QDNA) binding complexes and synthesis of multinuclear dinuclear Pt(IV) complexes. One potential way to further the investigation into the mechanism of action is the synthesis of cyclometallated analogues of 56MESS. These analogues have cyclometallation as the nitrogen of the 56MePhen is replaced by a carbon this typically results in luminescence of PCs. It is hypothesised that the mechanism of action would be the same as they are very structurally similar non-cyclometallated complexes. Thus biological testing of the fluorescent molecules may help to elucidate the mechanism of action. Cyclometallated complexes with QDNA binding potential is another area of interest. It is thought that binding to QDNA may be a good strategy for a new class of anticancer complexes and cyclometallated Pt(II) complexes have been made successfully by other groups.¹¹² Lastly 56MESS dinuclear complexes can be synthesised with multiple targeting and bioactive ligands as mentioned in Section 1.3.5. There are many promising bioactive linkers and ligands that can be attached to such a complex, many of which are already

used in clinics. Figure 4.1 shows some of the complexes that will be potentially synthesised in future works.

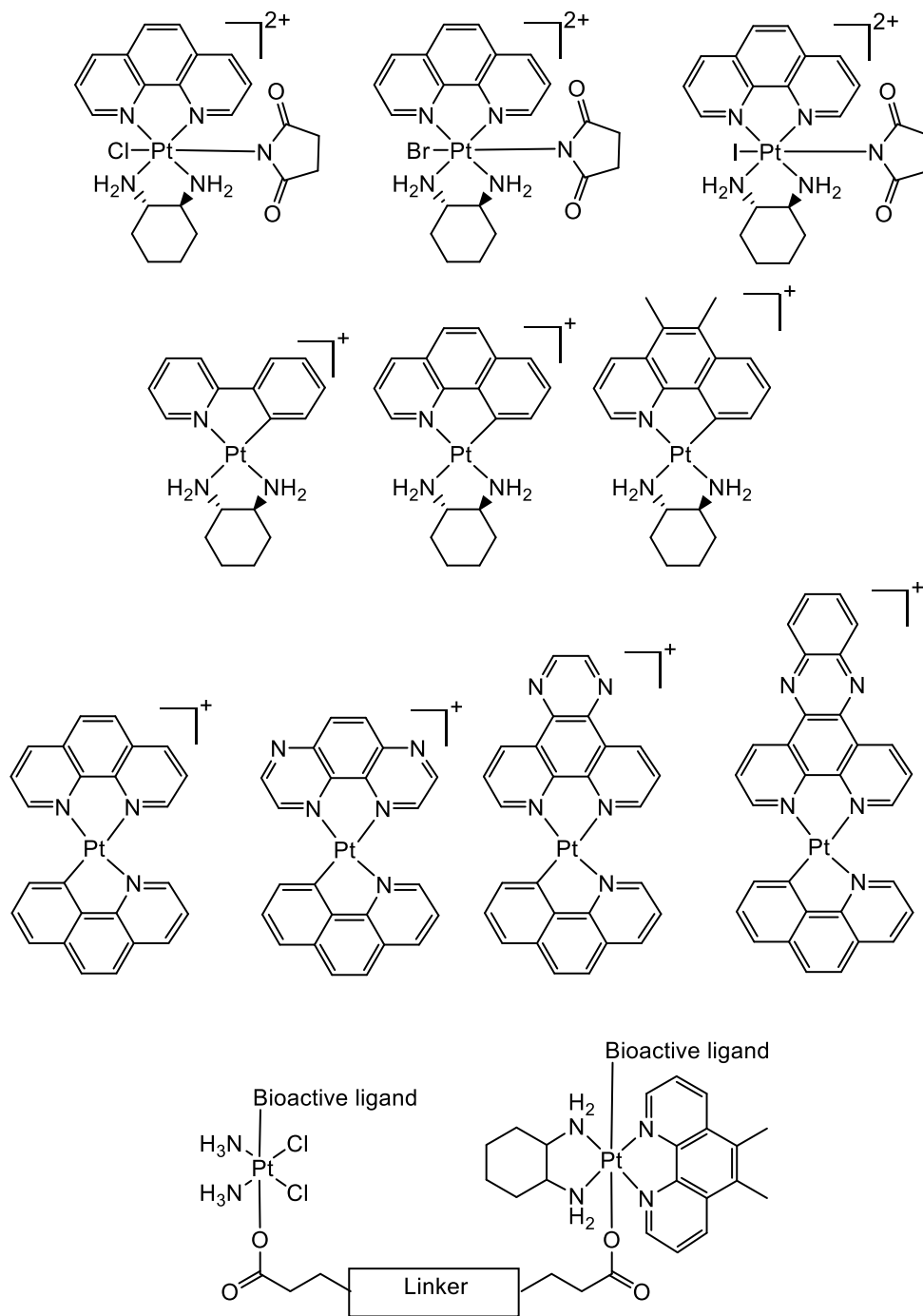


Figure 4.1: Potential complexes to be synthesised in future works.

References

1. B. W. Stewart and C. Wild, *World Health Organization*, 2014, **505**, 77-619.
2. A. I. o. H. a. Welfare and Canberra, 2017.
3. F. Bray, A. Jemal, N. Grey, J. Ferlay and D. Forman, *The lancet oncology*, 2012, **13**, 790-801.
4. N. J. Wheate, S. Walker, G. E. Craig and R. Oun, *Dalton transactions*, 2010, **39**, 8113-8127.
5. S. C. Hayes, R. R. Spence, D. A. Galvão and R. U. Newton, *Journal of Science and Medicine in Sport*, 2009, **12**, 428-434.
6. E. E. Calle, C. Rodriguez, K. Walker-Thurmond and M. J. Thun, *New England Journal of Medicine*, 2003, **348**, 1625-1638.
7. F. Sitas, A. Gibberd, C. Kahn, M. F. Weber, M. Chiew, R. Supramaniam, L. Velentzis, C. Nickson, D. P. Smith and D. O'Connell, *Cancer epidemiology*, 2013, **37**, 780-787.
8. M. Marques, *ISRN Spectroscopy*, 2013, **2013**, 1-29.
9. M. D. Hall, R. C. Dolman and T. W. Hambley, *Metal ions in biological systems*, 2004, **42**, 297-322.
10. B. Rosenberg, *Cancer*, 1985, **55**, 2303-2316.
11. M. G. Apps, E. H. Choi and N. J. Wheate, *Endocrine-related cancer*, 2015, **22**, R219-R233.
12. M. S. Davies, S. J. Berners-Price and T. W. Hambley, *Inorganic chemistry*, 2000, **39**, 5603-5613.
13. E. R. Jamieson and S. J. Lippard, *Chemical Reviews*, 1999, **99**, 2467-2498.
14. A. V. Klein and T. W. Hambley, *Chemical Reviews*, 2009, **109**, 4911-4920.
15. M. D. Hall, M. Okabe, D.-W. Shen, X.-J. Liang and M. M. Gottesman, *Annu. Rev. Pharmacol. Toxicol.*, 2008, **48**, 495-535.
16. M. Fuertes, J. Castilla, C. Alonso and J. Prez, *Current medicinal chemistry*, 2003, **10**, 257-266.
17. Z. H. Siddik, *Oncogene*, 2003, **22**, 7265-7279.
18. T. W. Hambley, *Coordination Chemistry Reviews*, 1997, **166**, 181-223.
19. M. Kartalou and J. M. Essigmann, *Mutation Research/Fundamental and Molecular Mechanisms of Mutagenesis*, 2001, **478**, 23-43.
20. M. Kartalou and J. M. Essigmann, *Mutation Research/Fundamental and Molecular Mechanisms of Mutagenesis*, 2001, **478**, 1-21.
21. A. Shikanov, B. Vaisman, M. Y. Krasko, A. Nyska and A. J. Domb, *Journal of Biomedical Materials Research Part A: An Official Journal of The Society for Biomaterials, The Japanese Society for Biomaterials, and The Australian Society for Biomaterials and the Korean Society for Biomaterials*, 2004, **69**, 47-54.
22. N. J. Wheate, R. I. Taleb, A. M. Krause-Heuer, R. L. Cook, S. Wang, V. J. Higgins and J. R. Aldrich-Wright, *Dalton Transactions*, 2007, 5055-5064.
23. M. J. Schell, V. A. McHaney, A. A. Green, L. E. Kun, F. A. Hayes, M. Horowitz and W. Meyer, *Journal of Clinical Oncology*, 1989, **7**, 754-760.

24. E. Wong and C. M. Giandomenico, *Chemical reviews*, 1999, **99**, 2451-2466.
25. M. Treskes and W. J. van der Vijgh, *Cancer chemotherapy and pharmacology*, 1993, **33**, 93-106.
26. L. Kelland, *Nature Reviews Cancer*, 2007, **7**, 573-584.
27. M. Pavelka, M. F. A. Lucas and N. Russo, *Chemistry—A European Journal*, 2007, **13**, 10108-10116.
28. J. Reedijk, *Proceedings of the National Academy of Sciences*, 2003, **100**, 3611-3616.
29. J. Suryadi and U. Bierbach, *Chemistry-A European Journal*, 2012, **18**, 12926-12934.
30. G. Momekov, A. Bakalova and M. Karaivanova, *Current medicinal chemistry*, 2005, **12**, 2177-2191.
31. S. M. Aris and N. P. Farrell, *European journal of inorganic chemistry*, 2009, **2009**, 1293-1302.
32. K. B. Garbutcheon-Singh, P. Leverett, S. Myers and J. R. Aldrich-Wright, *Dalton Transactions*, 2013, **42**, 918-926.
33. A. Alama, B. Tasso, F. Novelli and F. Sparatore, *Drug discovery today*, 2009, **14**, 500-508.
34. B. J. Pages, K. B. Garbutcheon-Singh and J. R. Aldrich-Wright, *European Journal of Inorganic Chemistry*, 2017, **2017**, 1613-1624.
35. V. Kostjukov, N. Khomytova, A. Hernandez Santiago, R. Licon Ibarra, D. B. Davies and M. Evstigneev, *International Journal of Quantum Chemistry*, 2011, **111**, 711-721.
36. S. Wang, V. J. Higgins, J. R. Aldrich-Wright and M. J. Wu, *Journal of chemical biology*, 2012, **5**, 51-61.
37. G. Housman, S. Byler, S. Heerboth, K. Lapinska, M. Longacre, N. Snyder and S. Sarkar, *Cancers*, 2014, **6**, 1769-1792.
38. J. Moretto, B. Chauffert, F. Ghiringhelli, J. R. Aldrich-Wright and F. Bouyer, *Investigational New Drugs*, 2011, **29**, 1164-1176.
39. M. D. Hall and T. W. Hambley, *Coordination Chemistry Reviews*, 2002, **232**, 49-67.
40. F. J. Macias, K. M. Deo, B. J. Pages, P. Wormell, J. K. Clegg, Y. Zhang, F. Li, G. Zheng, J. Sakoff, J. Gilbert and J. R. Aldrich-Wright, *Chemistry – A European Journal*, 2015, **21**, 16990-17001.
41. B. W. Harper, E. Petruzzella, R. Sirota, F. F. Faccioli, J. R. Aldrich-Wright, V. Gandin and D. Gibson, *Dalton Transactions*, 2017, 7005-7019.
42. Y.-R. Zheng, K. Suntharalingam, T. C. Johnstone, H. Yoo, W. Lin, J. G. Brooks and S. J. Lippard, *Journal of the American Chemical Society*, 2014, **136**, 8790-8798.
43. E. Wexselblatt and D. Gibson, *Journal of Inorganic Biochemistry*, 2012, **117**, 220-229.
44. H. Choy, *Expert review of anticancer therapy*, 2006, **6**, 973-982.
45. K. B. Garbutcheon-Singh, S. Myers, B. W. Harper, N. S. Ng, Q. Dong, C. Xie and J. R. Aldrich-Wright, *Metallomics*, 2013, **5**, 1061-1067.
46. X. Wang and Z. Guo, *Chemical Society Reviews*, 2013, **42**, 202-224.

47. N. P. E. Barry and P. J. Sadler, *ACS Nano*, 2013, **7**, 5654-5659.
48. S. S. Banerjee, N. Aher, R. Patil and J. Khandare, *Journal of Drug Delivery*, 2012, 1-17.
49. F. Kratz, I. A. Müller, C. Ryppa and A. Warnecke, *ChemMedChem*, 2008, **3**, 20-53.
50. S. van Zutphen and J. Reedijk, *Coordination Chemistry Reviews*, 2005, **249**, 2845-2853.
51. M. J. Pisani, N. J. Wheate, F. R. Keene, J. R. Aldrich-Wright and J. G. Collins, *Journal of Inorganic Biochemistry*, 2009, **103**, 373-380.
52. T. C. Johnstone, J. J. Wilson and S. J. Lippard, *Inorg. Chem.*, 2013, **52**, 12234-12249.
53. A. K. Iyer, G. Khaled, J. Fang and H. Maeda, *Drug Discovery Today*, 2006, **11**, 812-818.
54. Y. Matsumura and H. Maeda, *Cancer Research*, 1986, **46**, 6387-6392.
55. J. Fang, H. Nakamura and H. Maeda, *Advanced Drug Delivery Reviews*, 2011, **63**, 136-151.
56. D. R. Rhodes, J. Yu, K. Shanker, N. Deshpande, R. Varambally, D. Ghosh, T. Barrette, A. Pandey and A. M. Chinnaiyan, *Neoplasia* 2004, **6**, 1-6.
57. C. M. Paulos, J. A. Reddy, C. P. Leamon, M. J. Turk and P. S. Low, *Molecular Pharmacology*, 2004, **66**, 1406-1414.
58. M. Srinivasarao, C. V. Galliford and P. S. Low, *Nat Rev Drug Discov*, 2015, **14**, 203-219.
59. L. M. A. Crane, H. J. G. Arts, M. van Oosten, P. S. Low, A. G. J. van der Zee, G. M. van Dam and J. Bart, *Cellular Oncology*, 2012, **35**, 9-18.
60. M. V. Grandal, R. Zandi, M. W. Pedersen, B. M. Willumsen, B. van Deurs and H. S. Poulsen, *Carcinogenesis*, 2007, **28**, 1408-1417.
61. X. Wang, D. Ma, W. C. Olson and W. D. W. Heston, *Molecular Cancer Therapeutics*, 2011, **10**, 1728-1729.
62. K. Zhang, R. Rossin, A. Hagooly, Z. Chen, M. J. Welch and K. L. Wooley, *Journal of Polymer Science Part A: Polymer Chemistry*, 2008, **46**, 7578-7583.
63. A. Sulistio, J. Lowenthal, A. Blencowe, M. N. Bongiovanni, L. Ong, S. L. Gras, X. Zhang and G. G. Qiao, *Biomacromolecules*, 2011, **12**, 3469-3477.
64. P. M. S. D. Cal, R. F. M. Frade, V. Chudasama, C. Cordeiro, S. Caddick and P. M. P. Gois, *Chemical Communications*, 2014, **50**, 5261-5263.
65. I. R. Vlahov and C. P. Leamon, *Bioconjugate Chemistry*, 2012, **23**, 1357-1369.
66. C. P. Leamon, I. R. Vlahov, J. A. Reddy, M. Vetzal, H. K. R. Santhapuram, F. You, A. Bloomfield, R. Dorton, M. Nelson, P. Kleindl, J. F. Vaughn and E. Westrick, *Bioconjugate Chemistry*, 2014, **25**, 560-568.
67. S. D. Weitman, R. H. Lark, L. R. Coney, D. W. Fort, V. Frasca, V. R. J. Zurawski and B. A. Kamen, *Cancer Research*, 1992, **52**, 3396-3401.
68. A. Ghosh and W. D. Heston, *Journal of Cellular Biochemistry*, 2004, **91**, 528-539.
69. M. Hofman, J. Violet, S. Sandhu, J. Ferdinandus, S. P. Thang, A. Iravani, G. Kong, A. R. Kumar, T. Akhurst and P. Jackson, *Journal of Nuclear Medicine*, 2018, **59**, 531-531.

70. S. R. Banerjee, C. A. Foss, M. Castanares, R. C. Mease, Y. Byun, J. J. Fox, J. Hilton, S. E. Lupold, A. P. Kozikowski and M. G. Pomper, *Journal of Medicinal Chemistry*, 2008, **51**, 4504-4517.
71. S. Jayaprakash, X. Wang, W. D. Heston and A. P. Kozikowski, *ChemMedChem: Chemistry Enabling Drug Discovery*, 2006, **1**, 299-302.
72. K. P. Maresca, S. M. Hillier, F. J. Femia, D. Keith, C. Barone, J. L. Joyal, C. N. Zimmerman, A. P. Kozikowski, J. A. Barrett, W. C. Eckelman and J. W. Babich, *Journal of Medicinal Chemistry*, 2009, **52**, 347-357.
73. W. H. Ang, I. Khalaila, C. S. Allardyce, L. Juillerat-Jeanneret and P. J. Dyson, *Journal of the American Chemical Society*, 2005, **127**, 1382-1383.
74. Y. Yuan, Y. Chen, B. Z. Tang and B. Liu, *Chemical Communications*, 2014, **50**, 3868-3870.
75. L. Ma, R. Ma, Y. Wang, X. Zhu, J. Zhang, H. C. Chan, X. Chen, W. Zhang, S.-K. Chiu and G. Zhu, *Chemical Communications*, 2015, **51**, 6301-6304.
76. W. Neumann, B. C. Crews, M. B. Sárosi, C. M. Daniel, K. Ghebreselasie, M. S. Scholz, L. J. Marnett and E. Hey-Hawkins, *ChemMedChem*, 2015, **10**, 183-192.
77. D. Gibson, *Dalton Transactions*, 2016, **45**, 12983-12991.
78. U. Basu, B. Banik, R. Wen, R. K. Pathak and S. Dhar, *Dalton Transactions*, 2016, **45**, 12992-13004.
79. R. Brogden, R. Heel, G. Pakes, T. M. Speight and G. Avery, *Drugs*, 1980, **20**, 24-48.
80. W. R. Waddell and R. W. Loughry, *Journal of Surgical Oncology*, 1983, **24**, 83-87.
81. P. A. Todd and E. M. Sorokin, *Drugs*, 1988, **35**, 244-285.
82. P. Moser, A. Sallmann and I. Wiesenberger, *Journal of Medicinal Chemistry*, 1990, **33**, 2358-2368.
83. F. M. Giardiello, S. R. Hamilton, A. J. Krush, S. Piantadosi, L. M. Hyland, P. Celano, S. V. Booker, C. R. Robinson and G. J. A. Offerhaus, *New England Journal of Medicine*, 1993, **328**, 1313-1316.
84. M. Tsujii, S. Kawano, S. Tsuji, H. Sawaoka, M. Horii and R. N. DuBois, *cell*, 1998, **93**, 705-716.
85. Q. Cheng, H. Shi, H. Wang, J. Wang and Y. Liu, *Metallomics*, 2016, **8**, 672-678.
86. R. K. Pathak, S. Marrache, J. H. Choi, T. B. Berding and S. Dhar, *Angewandte Chemie International Edition*, 2014, **53**, 1963-1967.
87. F. P. Intini, J. Zajac, V. Novohradsky, T. Saltarella, C. Pacifico, V. Brabec, G. Natile and J. Kasparkova, *Inorganic Chemistry*, 2017, **56**, 1483-1497.
88. J. L. van der Veer, A. R. Peters and J. Reedijk, *Journal of Inorganic Biochemistry*, 1986, **26**, 137-142.
89. Y. Kido, A. R. Khokhar and Z. H. Siddik, *Biochemical pharmacology*, 1994, **47**, 1635-1642.
90. G. R. Gibbons, S. Wyrick and S. G. Chaney, *Cancer research*, 1989, **49**, 1402-1407.
91. S. Choi, C. Filotto, M. Bisanzo, S. Delaney, D. Lagasee, J. L. Whitworth, A. Jusko, C. Li, N. A. Wood and J. Willingham, *Inorganic Chemistry*, 1998, **37**, 2500-2504.

92. E. Petruzzella, J. P. Braude, J. R. Aldrich-Wright, V. Gandin and D. Gibson, *Angewandte Chemie International Edition*, 2017, **56**, 11539-11544.
93. A. D. Cox, S. W. Fesik, A. C. Kimmelman, J. Luo and C. J. Der, *Nature Reviews Drug Discovery*, 2014, **13**, 828-826.
94. S. Jančík, J. Drábek, D. Radzioch and M. Hajdúch, *BioMed Research International*, 2010, **2010**.
95. J. Wegner, S. Ceylan and A. Kirschning, *Chemical Communications*, 2011, **47**, 4583-4592.
96. J. C. Pastre, D. L. Browne and S. V. Ley, *Chemical Society Reviews*, 2013, **42**, 8849-8869.
97. P. Van Arnum, *Pharmaceutical Technology*, 2013, **37**, 78-82.
98. M. Patra, T. C. Johnstone, K. Suntharalingam and S. J. Lippard, *Angewandte Chemie International Edition*, 2016, **55**, 2550-2554.
99. Z. Xu, C. Li, Z. Tong, L. Ma, M. K. Tse and G. Zhu, *European Journal of Inorganic Chemistry*, 2017, **2017**, 1706-1712.
100. B. J. Pages, Doctor of Philosophy (Science), Western Sydney University, 2018.
101. B. J. Pages, F. Li, P. Wormell, D. L. Ang, J. K. Clegg, C. J. Kepert, L. K. Spare, S. Danchaiwijit and J. R. Aldrich-Wright, *Dalton Transactions*, 2014, **43**, 15566-15575.
102. A. Syamal and R. C. Johnson, *Inorganic Chemistry*, 1970, **9**, 265-268.
103. M. Yamada, Y. Tanaka, Y. Yoshimoto, S. Kuroda and I. Shima, *Bulletin of the Chemical Society of Japan*, 1992, **65**, 1006-1011.
104. J. Sharma, R. Singh, A. Singh and B. Singh, *Tetrahedron*, 1986, **42**, 2739-2747.
105. S. H. Crosby, G. J. Clarkson, R. J. Deeth and J. P. Rourke, *Organometallics*, 2010, **29**, 1966-1976.
106. K. Deo, Doctor of Philosophy, Western Sydney University, Thesis in process 14/07/2018.
107. T. Cashman, Bachelor of Science (Adv) (Hons.), Sydney University, 2016.
108. P. G. Morris, *INIS*, 1986, **17**, 680-698.
109. F. J. Macias, K. M. Deo, P. Wormell, J. K. Clegg, Y. Zhang, F. Li, G. Zheng, J. Sakoff, J. Gilbert and J. R. Aldrich-Wright, *Chemistry—A European Journal*, 2015, **21**, 16990-17001.
110. A. M. Krause-Heuer, N. J. Wheate, W. S. Price and J. Aldrich-Wright, *Chemical Communications*, 2009, 1210-1212.
111. O. Me, *Reich, U.Wisc. Chem.*, 2010, 22.21-22.26.
112. D.-L. Ma, C.-M. Che and S.-C. Yan, *Journal of the American Chemical Society*, 2009, **131**, 1835-1846.

Supplementary Data

Supplementary Data Table of Contents

NMR Data	8
PHENSS(Cl) ₂ ¹⁹⁵ Pt NMR spectra	8
PHENSS(Cl) ₂ ¹ H NMR spectra	8
PHENSS(Br) ₂ ¹⁹⁵ Pt NMR spectra	9
PHENSS(Br) ₂ ¹ H NMR spectra	9
PHENSS(I) ₂ ¹⁹⁵ Pt NMR spectra	10
PHENSS(I) ₂ ¹ H NMR spectra	10
5MESS(Cl) ₂ ¹⁹⁵ Pt NMR spectra	11
5MESS(Cl) ₂ ¹ H NMR spectra	11
5MESS(Br) ₂ ¹⁹⁵ Pt NMR spectra	12
5MESS(Br) ₂ ¹ H NMR spectra	12
5MESS(I) ₂ ¹⁹⁵ Pt NMR spectra	13
5MESS(I) ₂ ¹ H NMR spectra	13
56MESS(Cl) ₂ ¹⁹⁵ Pt NMR spectra	14
56MESS(Cl) ₂ ¹ H NMR spectra	14
56MESS(Br) ₂ ¹⁹⁵ Pt NMR spectra	15
56MESS(Br) ₂ ¹ H NMR spectra	15
56MESS(I) ₂ ¹⁹⁵ Pt NMR spectra	16
56MESS(I) ₂ ¹ H NMR spectra	16
PHENSS(OH)(DCL) ¹ H NMR spectra	17
DCL ¹ H NMR spectra	17
PHENSS(OH)(PSMA) ¹⁹⁵ Pt NMR spectra	18
PHENSSenDCF ₂ ¹ H NMR spectra	19
PHENSSenDCF ₂ ¹⁹⁵ Pt NMR spectra	20
PHENSS(DMSO) ₂ (in DMSO) ¹ H NMR spectra	20
PHENSS(DMSO) ₂ (in DMSO) ¹⁹⁵ Pt NMR spectra	21
en-DCF ¹ H NMR spectra	21
PHENSS ¹ H NMR spectra	22
PHENSS ¹⁹⁵ Pt NMR spectra	22
PHENRR ¹ H NMR spectra	23
PHENRR ¹⁹⁵ Pt NMR spectra	23
5MESS ¹ H NMR spectra	24
5MESS ¹⁹⁵ Pt NMR spectra	24

5MERR ¹ H NMR spectra	25
5MERR ¹⁹⁵ Pt NMR spectra.....	25
56MESS ¹ H NMR spectra.....	26
56MESS ¹⁹⁵ Pt NMR spectra	26
56MERR ¹ H NMR spectra	27
56MERR ¹⁹⁵ Pt NMR spectra.....	27
4MESS ¹ H NMR spectra.....	28
4MESS ¹⁹⁵ Pt NMR spectra	28
4MERR ¹ H NMR spectra	29
4MERR ¹⁹⁵ Pt NMR spectra	29
44BPYSS ¹ H NMR spectra	30
44BPYSS ¹⁹⁵ Pt NMR spectra.....	30
44BPYRR ¹ H NMR spectra.....	31
BPYRR ¹⁹⁵ Pt NMR spectra	31
PHENSS(OH)(OAc) ¹ H NMR spectra	32
PHENSS(OH)(OAc) ¹⁹⁵ Pt NMR spectra	32
PHENRR(OH)(OAc) ¹ H NMR spectra	33
PHENRR(OH)(OAc) ¹⁹⁵ Pt NMR spectra	33
5MESS(OH)(OAc) ¹ H NMR spectra.....	34
5MESS(OH)(OAc) ¹⁹⁵ Pt NMR spectra	34
5MERR(OH)(OAc) ¹ H NMR spectra	35
5MERR(OH)(OAc) ¹⁹⁵ Pt NMR spectra	35
56MESS(OH)(OAc) ¹ H NMR spectra.....	36
56MESS(OH)(OAc) ¹⁹⁵ Pt NMR spectra.....	36
56MERR(OH)(OAc) ¹ H NMR spectra	37
56MERR(OH)(OAc) ¹⁹⁵ Pt NMR spectra.....	37
4MESS(OH)(OAc) ¹ H NMR spectra.....	38
4MESS(OH)(OAc) ¹⁹⁵ Pt NMR spectra.....	38
4MERR(OH)(OAc) ¹ H NMR spectra	39
4MERR(OH)(OAc) ¹⁹⁵ Pt NMR spectra	39
44BPYSS(OH)(OAc) ¹ H NMR spectra.....	40
BPYSS(OH)(OAc) ¹⁹⁵ Pt NMR spectra	40
44BPYRR(OH)(OAc) ¹ H NMR spectra.....	41
44BPYRR(OH)(OAc) ¹⁹⁵ Pt NMR spectra.....	41

PHENSS(OH) ₂ ¹ H NMR spectra.....	42
PHENSS(OH) ₂ ¹⁹⁵ Pt NMR spectra	42
PHENRR(OH) ₂ ¹ H NMR spectra	43
PHENRR(OH) ₂ ¹⁹⁵ Pt NMR spectra	43
5MESS(OH) ₂ ¹ H NMR spectra	44
5MESS(OH) ₂ ¹⁹⁵ Pt NMR spectra.....	44
5MERR(OH) ₂ ¹ H NMR spectra.....	45
5MERR(OH) ₂ ¹⁹⁵ Pt NMR spectra.....	45
56MESS(OH) ₂ ¹ H NMR spectra	46
56MESS(OH) ₂ ¹⁹⁵ Pt NMR spectra.....	46
56MERR(OH) ₂ ¹ H NMR spectra	47
56MERR(OH) ₂ ¹⁹⁵ Pt NMR spectra.....	47
4MESS(OH) ₂ ¹ H NMR spectra	48
4MESS(OH) ₂ ¹⁹⁵ Pt NMR spectra.....	48
4MERR(OH) ₂ ¹ H NMR spectra.....	49
4MERR(OH) ₂ ¹⁹⁵ Pt NMR spectra	49
44BPYSS(OH) ₂ ¹ H NMR spectra	50
44BPYSS(OH) ₂ ¹⁹⁵ Pt NMR spectra	50
44BPYRR(OH) ₂ ¹ H NMR spectra.....	51
44BPYRR(OH) ₂ ¹⁹⁵ Pt NMR spectra	51
PHENSS(OH)(Succ) ¹ H NMR spectra	52
PHENSS(OH)(Succ) ¹⁹⁵ Pt NMR spectra	52
5MESS(OH)(Succ) ¹ H NMR spectra.....	53
5MESS(OH)(Succ) ¹⁹⁵ Pt NMR spectra	53
56MESS(OH)(Succ) ¹ H NMR spectra.....	54
56MESS(OH)(Succ) ¹⁹⁵ Pt NMR spectra	54
PHENSS(OH)(SuccPFP) ¹ H NMR spectra.....	55
PHENSS(OH)(SuccPFP) ¹⁹⁵ Pt NMR spectra	55
UV Data	56
Spectra by Polypyridyl Ligand	56
UV Spectra of PHENSS(X) ₂ complexes.....	56
UV Spectra of 5MESS(X) ₂ complexes	56
UV Spectra of 56MESS(X) ₂ complexes	57
Spectra by Axial Ligand	57

UV Spectra of Chloro compounds 1,4 and 7	57
UV Spectra of Bromo compounds 2,4, and 8.....	58
UV Spectra of Iodo compounds 3,6 and 9	58
UV Spectra PhenSS(Cl) ₂	59
UV Spectra PhenSS(Br) ₂	59
UV Spectra PhenSS(I) ₂	60
UV Spectra 5MeSS(Cl) ₂	60
UV Spectra 5MeSS(Br) ₂	61
UV Spectra 5MeSS(I) ₂	61
UV Spectra 56MeSS(Cl) ₂	62
UV Spectra 56MeSS(Br) ₂	62
UV Spectra 56MeSS(I) ₂	63
CD Data	64
Spectra by Polypyridyl Ligand	64
CD Spectra of PHENSS(X) ₂	64
CD Spectra of 5MESS(X) ₂	65
CD Spectra of 56MESS(X) ₂	66
Spectra by Axial Ligand	67
CD Spectra of Chloro compounds	67
CD Spectra of Bromo compounds.....	67
CD Spectra of Iodo compounds 3,6 and 9.....	68
Smoothed individual spectra:	68
CD Spectra PHENSS(Cl) ₂	68
CD Spectra PHENSS(Br) ₂	69
CD Spectra PHENSS(I) ₂	69
CD Spectra 5MESS(Cl) ₂	70
CD Spectra 5MESS(Br) ₂	70
CD Spectra 5MESS(I) ₂	71
CD Spectra 56MESS(Cl) ₂	71
CD Spectra 56MESS(Br) ₂	72
CD Spectra 56MeSS(I) ₂	72
SRCD Data	73
Spectra by Polypyridyl Ligand	73
SRCD Spectra of PHENSS(X) ₂	74

SRCD Spectra of 5MESS(X) ₂	75
SRCD Spectra of 56MESS(X) ₂	76
Spectra by Axial Ligand	77
SRCD Spectra of Chloro compounds	77
SRCD Spectra of Bromo compounds.....	78
SRCD Spectra of Iodo compounds	79
SRCD Spectra PHENSS(Cl) ₂	80
SRCD Spectra PHENSS(Br) ₂	80
SRCD Spectra PHENSS(I) ₂	81
SRCD Spectra 5MESS(Cl) ₂	81
SRCD Spectra 5MESS(Br) ₂	82
SRCD Spectra 5MESS(I) ₂	82
SRCD Spectra 56MESS(Cl) ₂	83
SRCD Spectra 56MESS(Br) ₂	83
SRCD Spectra 56MeSS(I) ₂	84
Cytotoxicity	85
Tables	85
DOSE SCREEN:	85
DOSE RESPONONSE:	86
Figures.....	87
Spectra by axial ligand	87
IC ₅₀ values of [Pt(PL)(AL)(Cl) ₂] ²⁺ type complexes.....	87
IC ₅₀ values of [Pt(PL)(AL)(Br) ₂] ²⁺ type complexes.....	88
IC ₅₀ values of [Pt(PL)(AL)(I) ₂] ²⁺ type complexes.....	89
Spectra by polyaromatic ligand.....	90
IC ₅₀ values of PHENSSX ₂ type complexes	90
IC ₅₀ values of 5MESSX ₂ type complexes.....	91
IC ₅₀ values of 56MESSX ₂ type complexes.....	92
ESIMS Data	93
PHENSSCl ₂	93
PHENSSBr ₂	94
PHENSSI ₂	95
5MESSCl ₂	96
5MESSBr ₂	97

5MESSI ₂	98
56MESSCl ₂	99
56MESSBr ₂	100
56MESSI ₂	101

NMR Data

PHENSS(Cl)₂ ¹⁹⁵Pt NMR spectra

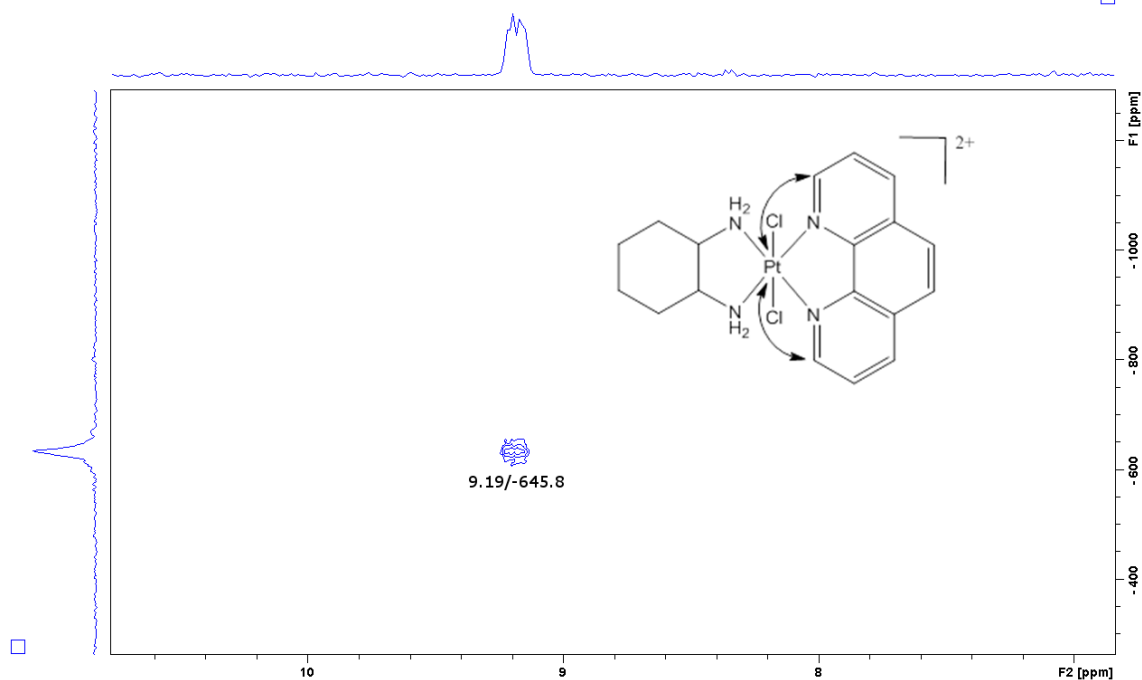


Figure A1: The ¹H-¹⁹⁵Pt HMQC spectrum of PHENSSCl₂ in D₂O, performed on a Bruker Avance 400 MHz NMR spectrometer.

PHENSS(Cl)₂ ¹H NMR spectra

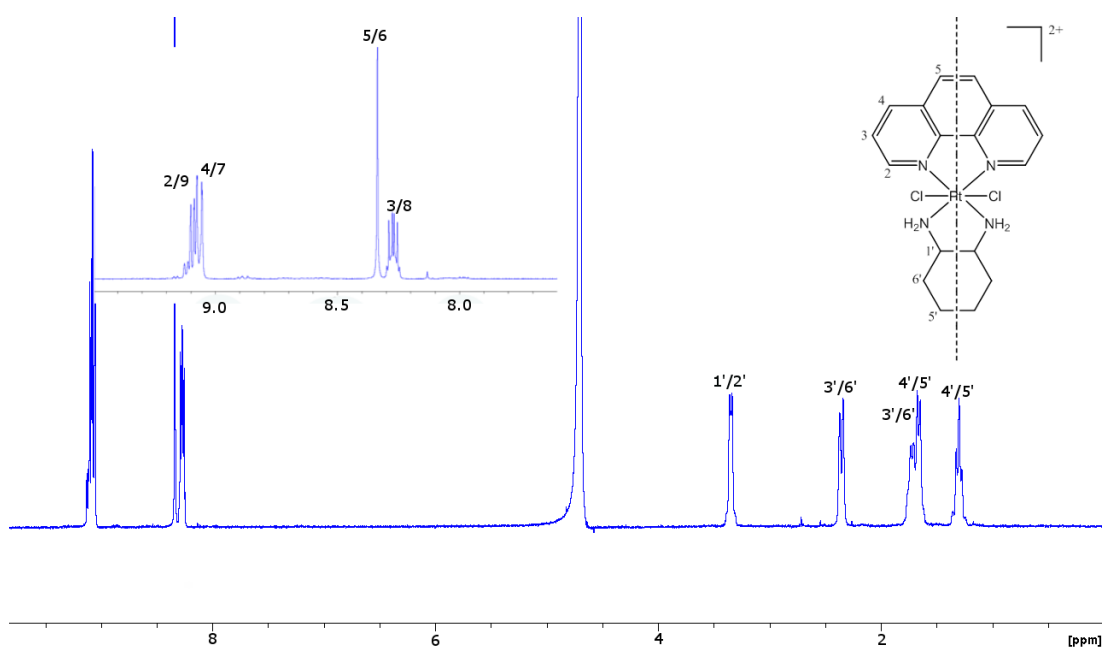


Figure A2: The ¹H spectrum of PHENSSCl₂ in D₂O, performed on a Bruker Avance 400 MHz NMR spectrometer.

PHENSS(Br)₂ ¹⁹⁵Pt NMR spectra

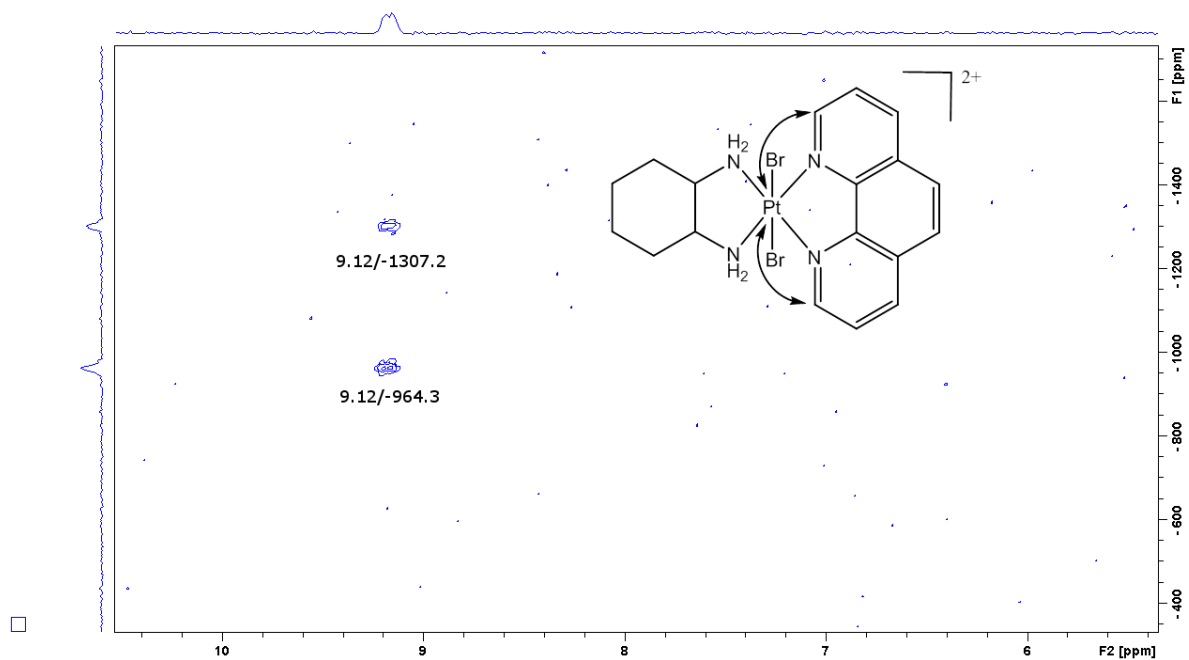


Figure A3: The ¹H-¹⁹⁵Pt HMQC spectrum of PHENSSBr₂ in D₂O, performed on a Bruker Avance 400 MHz NMR spectrometer.

PHENSS(Br)₂ ¹H NMR spectra

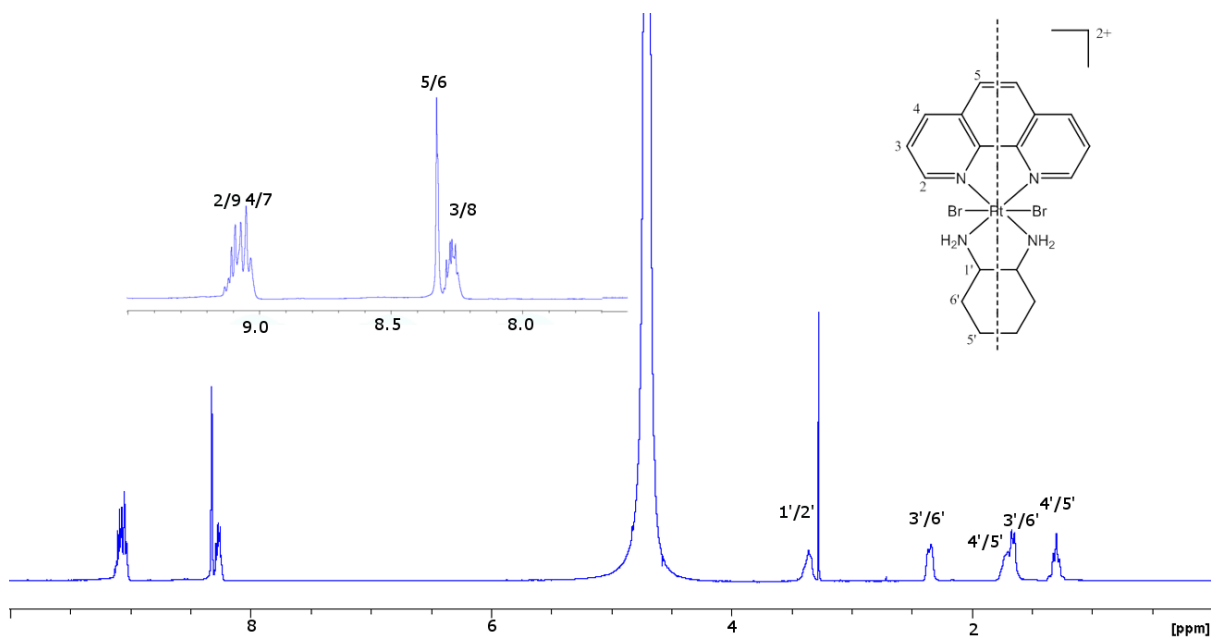


Figure A4: The ¹H spectrum of PHENSSBr₂ in D₂O, performed on a Bruker Avance 400 MHz NMR spectrometer.

PHENSS(I)₂ ¹⁹⁵Pt NMR spectra

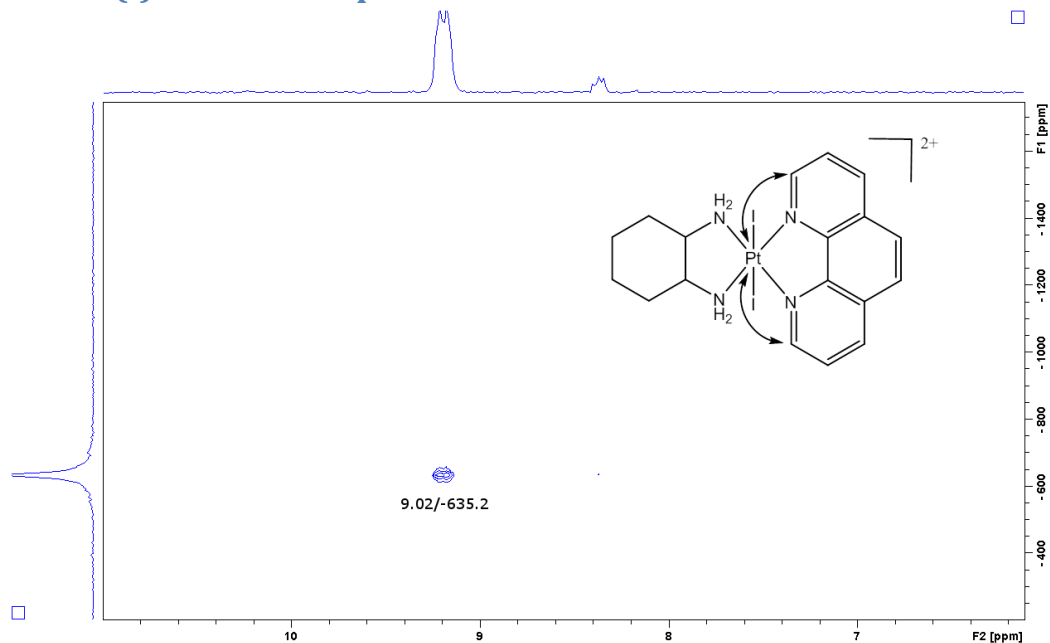


Figure A5: The ¹H-¹⁹⁵Pt HMQC spectrum of PHENSS(I)₂ in D₂O, performed on a Bruker Avance 400 MHz NMR spectrometer.

PHENSS(I)₂ ¹H NMR spectra

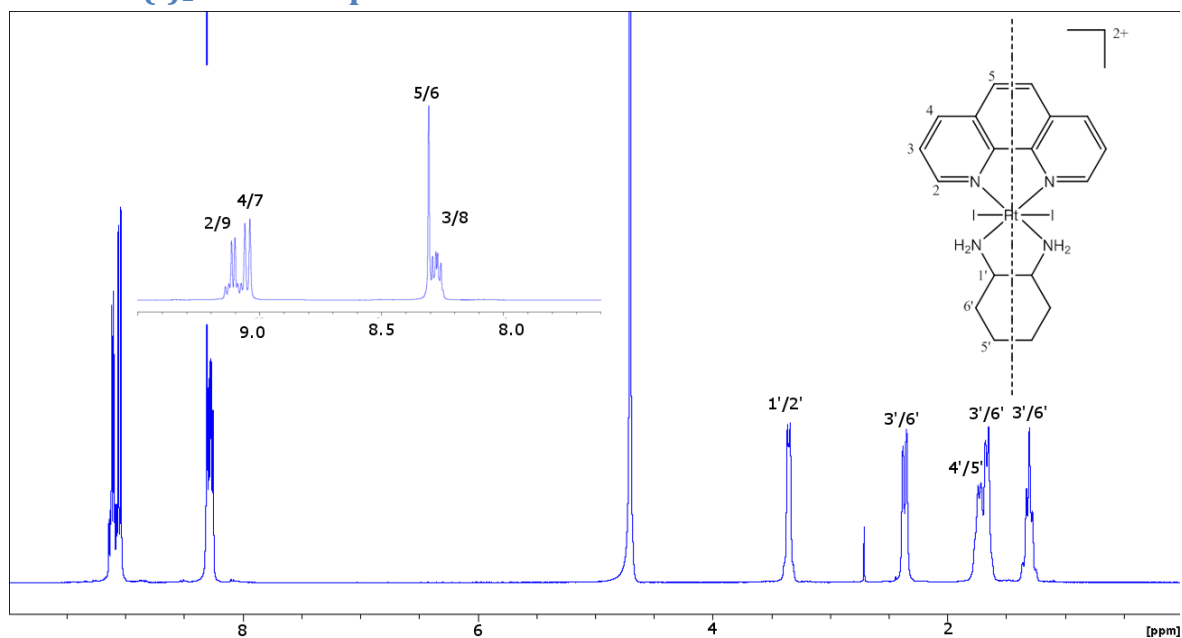


Figure A6: The ¹H spectrum of PHENSSBr₂ in D₂O, performed on a Bruker Avance 400 MHz NMR spectrometer.

5MESS(Cl)₂ ¹⁹⁵Pt NMR spectra

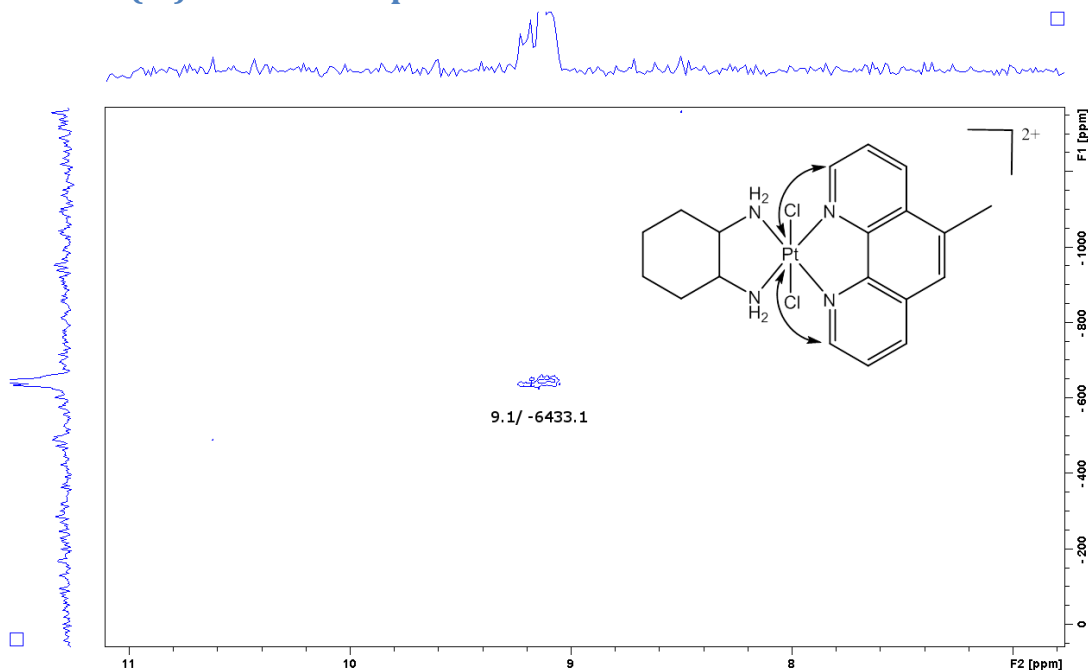


Figure A7: The ¹H-¹⁹⁵Pt HMQC spectrum of 5MESSCl₂ in D₂O, performed on a Bruker Avance 400 MHz NMR spectrometer.

5MESS(Cl)₂ ¹H NMR spectra

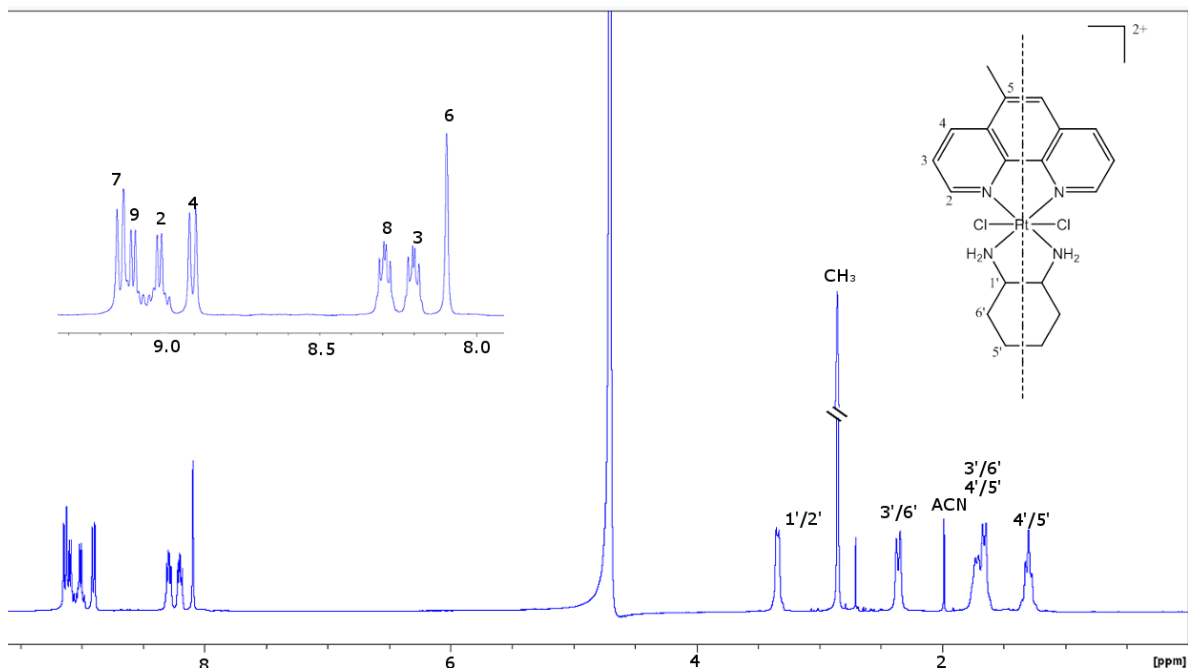


Figure A8: The ¹H spectrum of 5MESSCl₂ in D₂O, performed on a Bruker Avance 400 MHz NMR spectrometer.

5MESS(Br)₂ ¹⁹⁵Pt NMR spectra

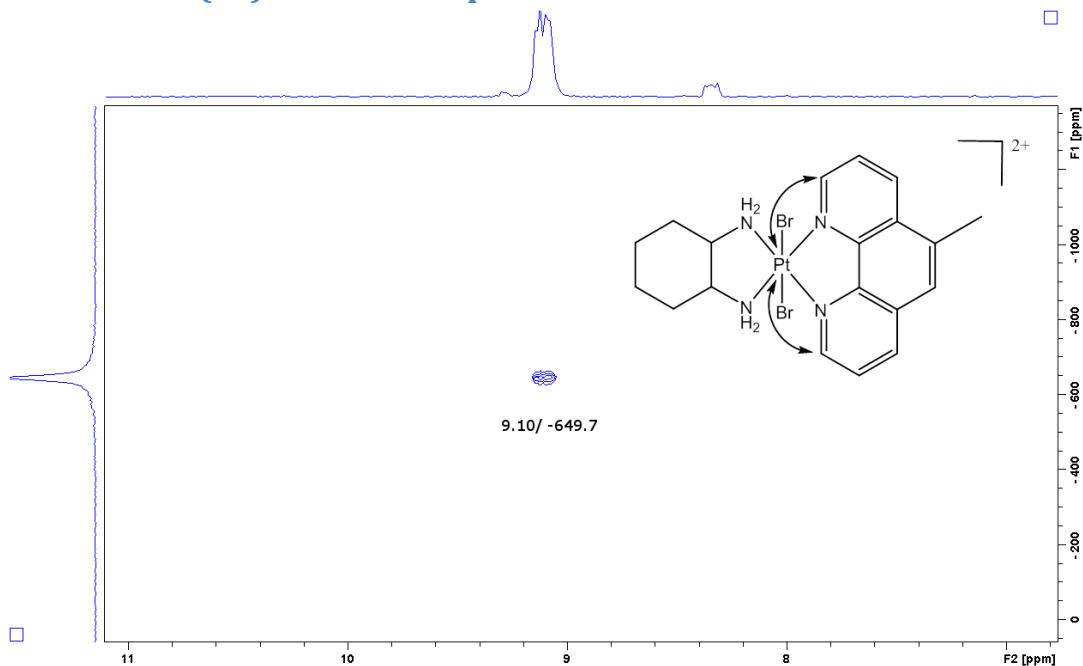


Figure A7: The ¹H-¹⁹⁵Pt HMQC spectrum of 5MESSBr₂ in D₂O, performed on a Bruker Avance 400 MHz NMR spectrometer.

5MESS(Br)₂ ¹H NMR spectra

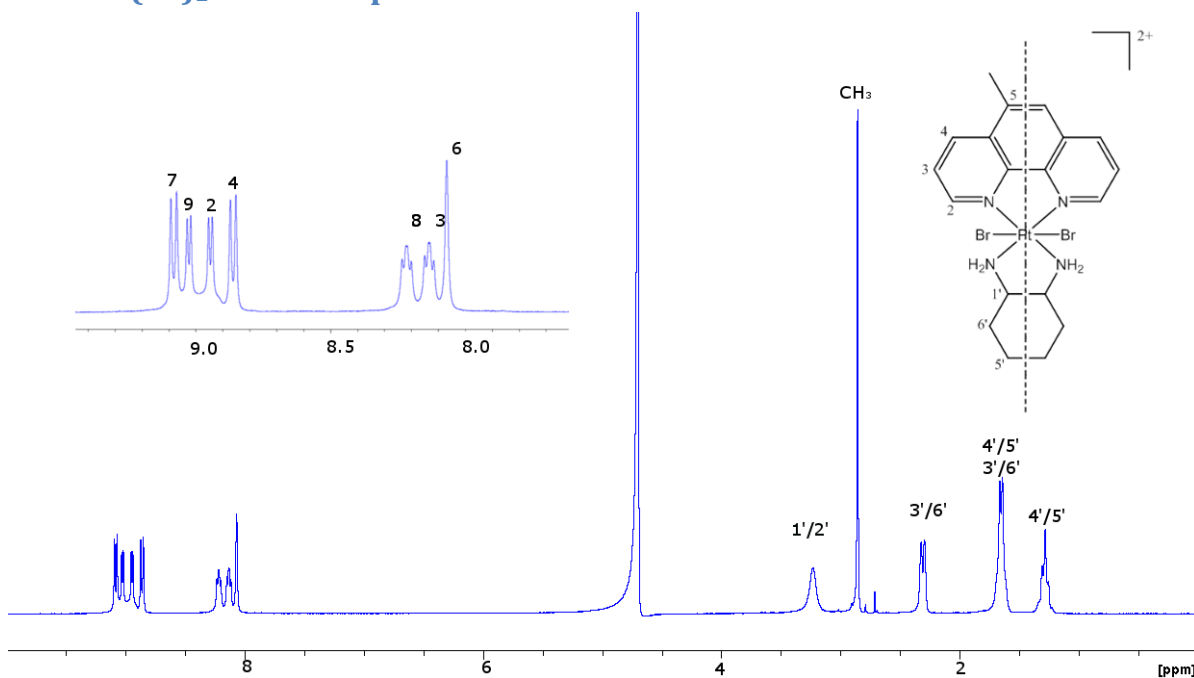


Figure A8: The ¹H spectrum of 5MESSBr₂ in D₂O, performed on a Bruker Avance 400 MHz NMR spectrometer.

5MESS(I)₂ ¹⁹⁵Pt NMR spectra

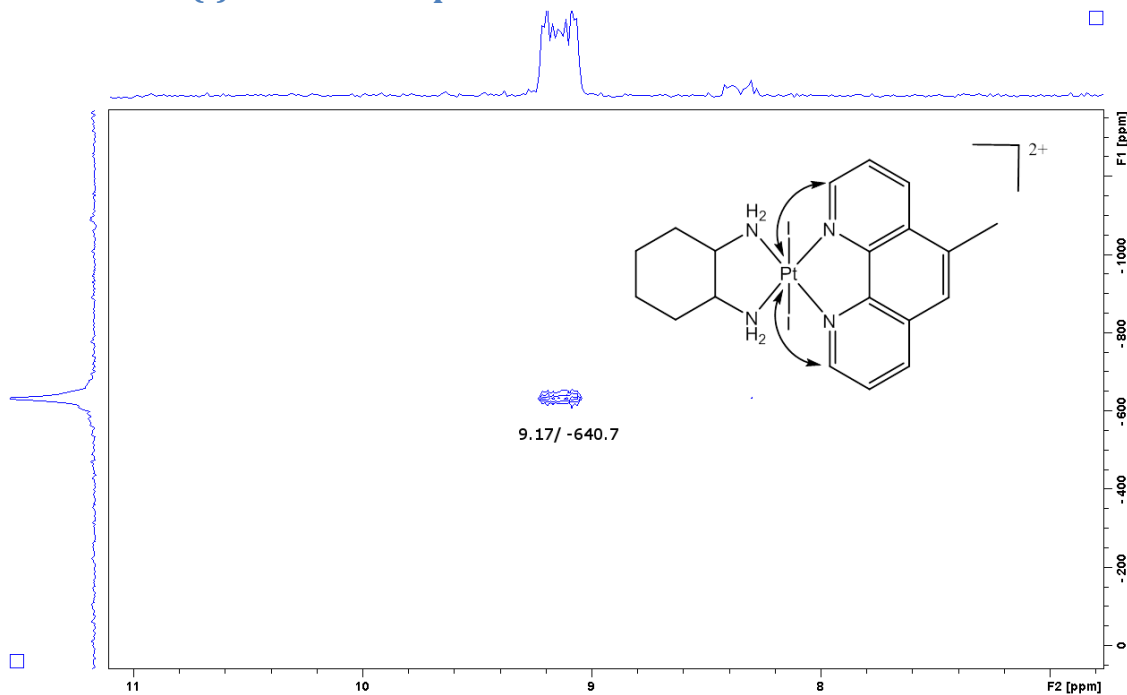


Figure A9: The ¹H-¹⁹⁵Pt HMQC spectrum of 5MESSl₂ in D₂O, performed on a Bruker Avance 400 MHz NMR spectrometer.

5MESS(I)₂ ¹H NMR spectra

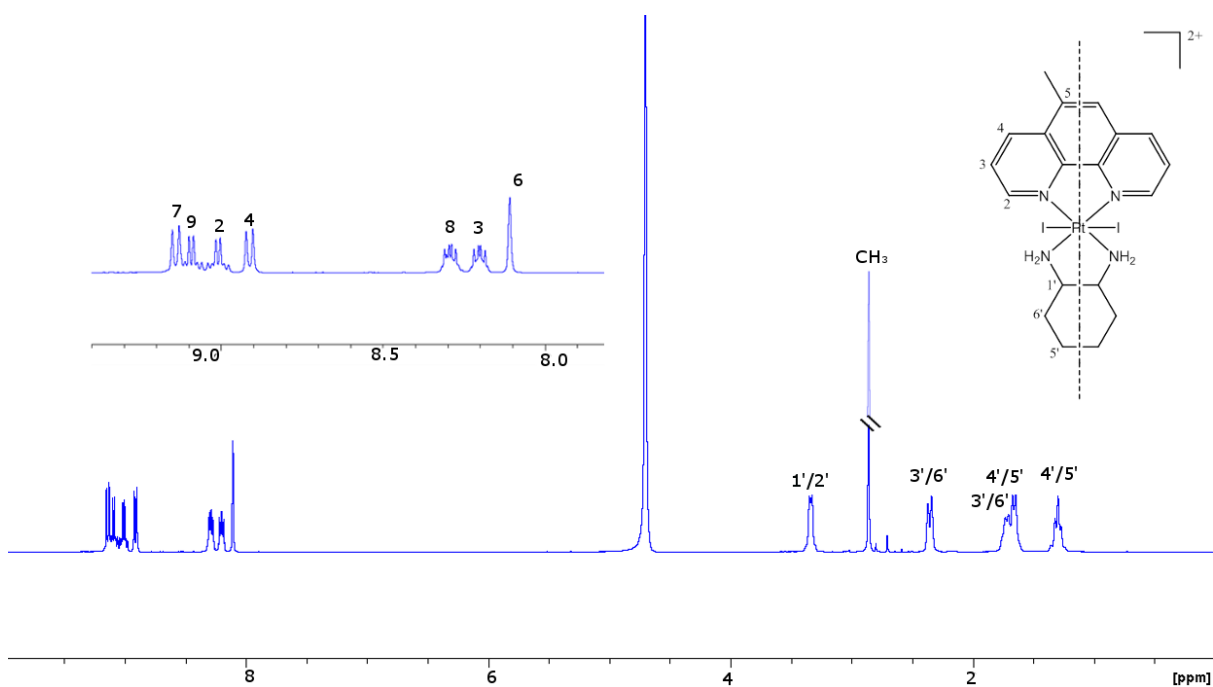


Figure A10: The ¹H spectrum of 5MESSl₂ in D₂O, performed on a Bruker Avance 400 MHz NMR spectrometer.

56MESS(Cl)₂ ¹⁹⁵Pt NMR spectra

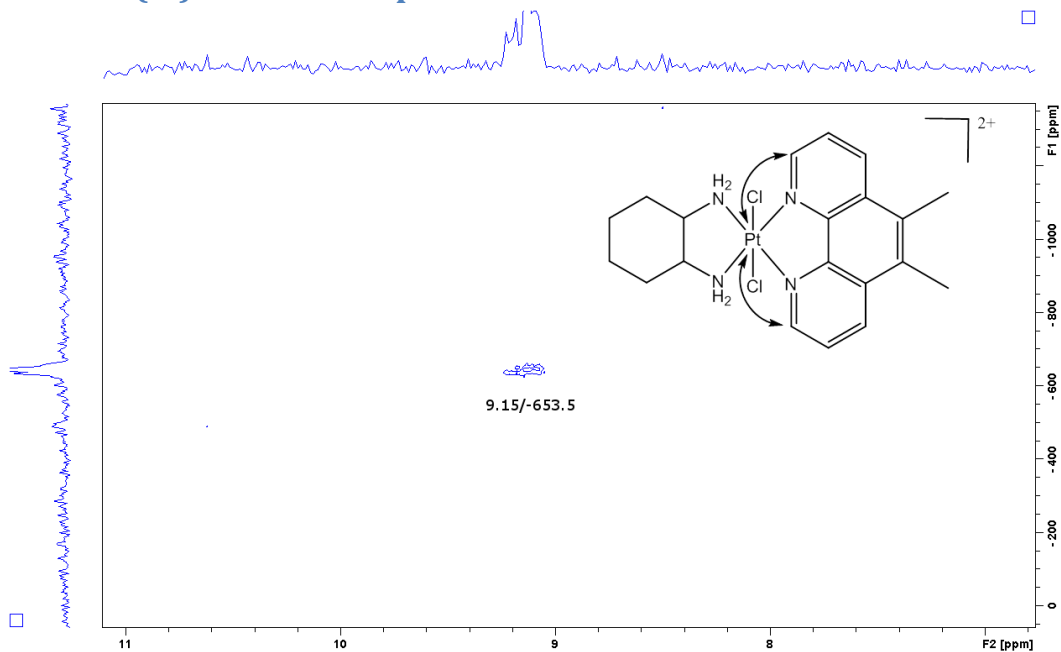


Figure A11: The ¹H-¹⁹⁵Pt HMQC spectrum of 56MESSCl₂ in D₂O, performed on a Bruker Avance 400 MHz NMR spectrometer.

56MESS(Cl)₂ ¹H NMR spectra

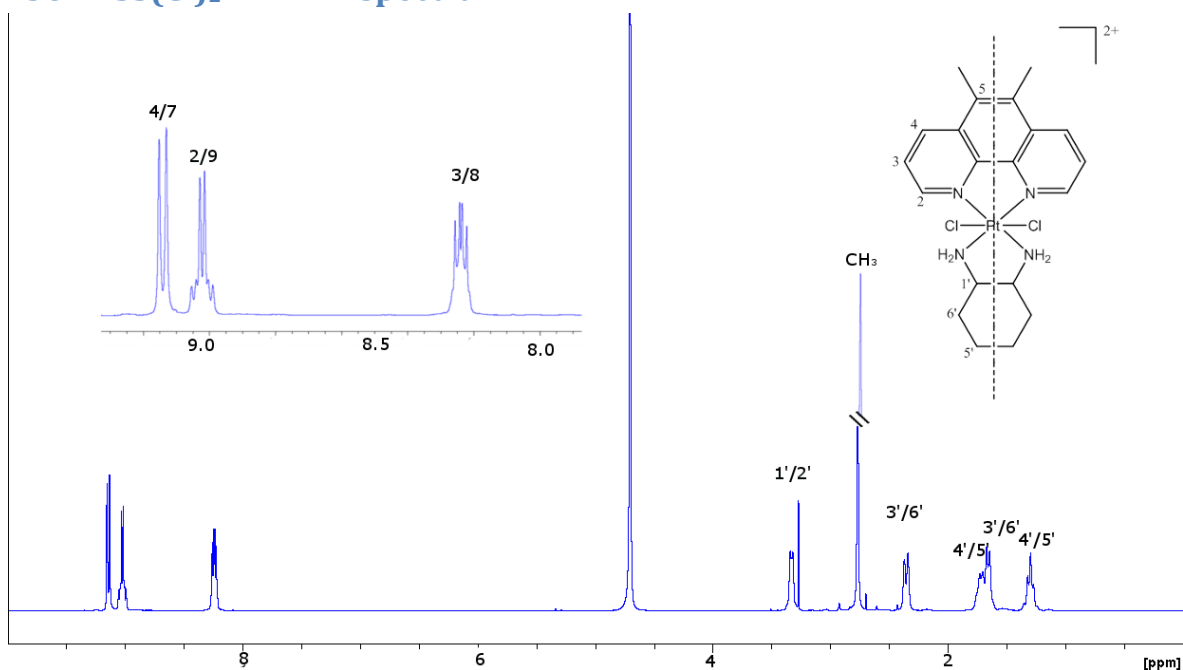


Figure A12: The ¹H spectrum of 56MESSCl₂ in D₂O, performed on a Bruker Avance 400 MHz NMR spectrometer.

56MESS(Br)₂ ¹⁹⁵Pt NMR spectra

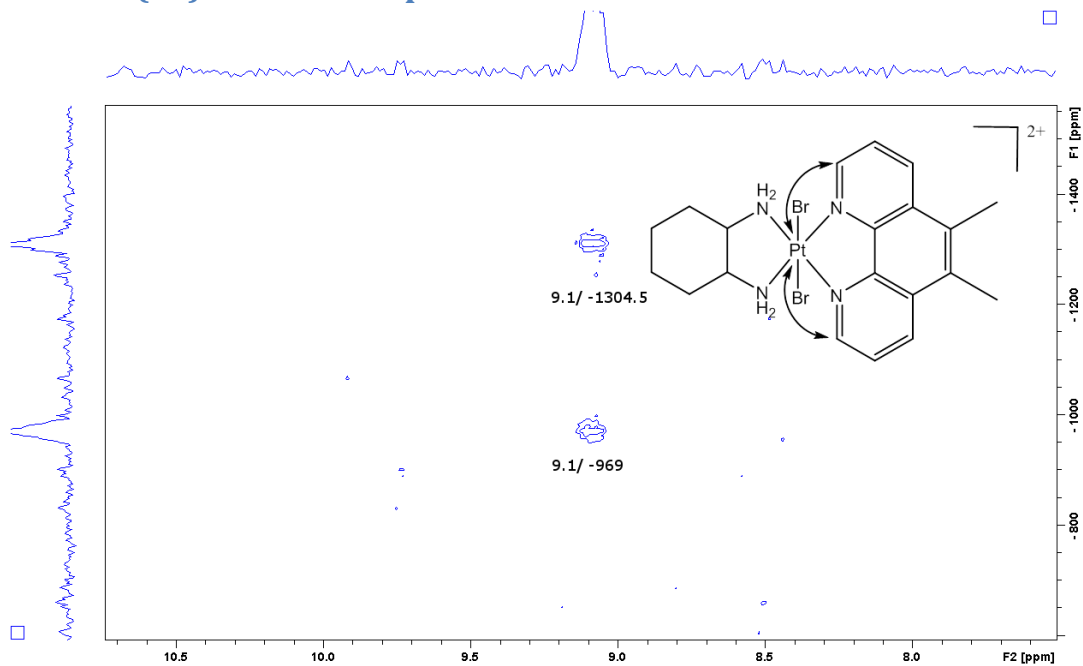


Figure A13: The ¹H–¹⁹⁵Pt HMQC spectrum of 56MESSBr₂ in D₂O, performed on a Bruker Avance 400 MHz NMR spectrometer.

56MESS(Br)₂ ¹H NMR spectra

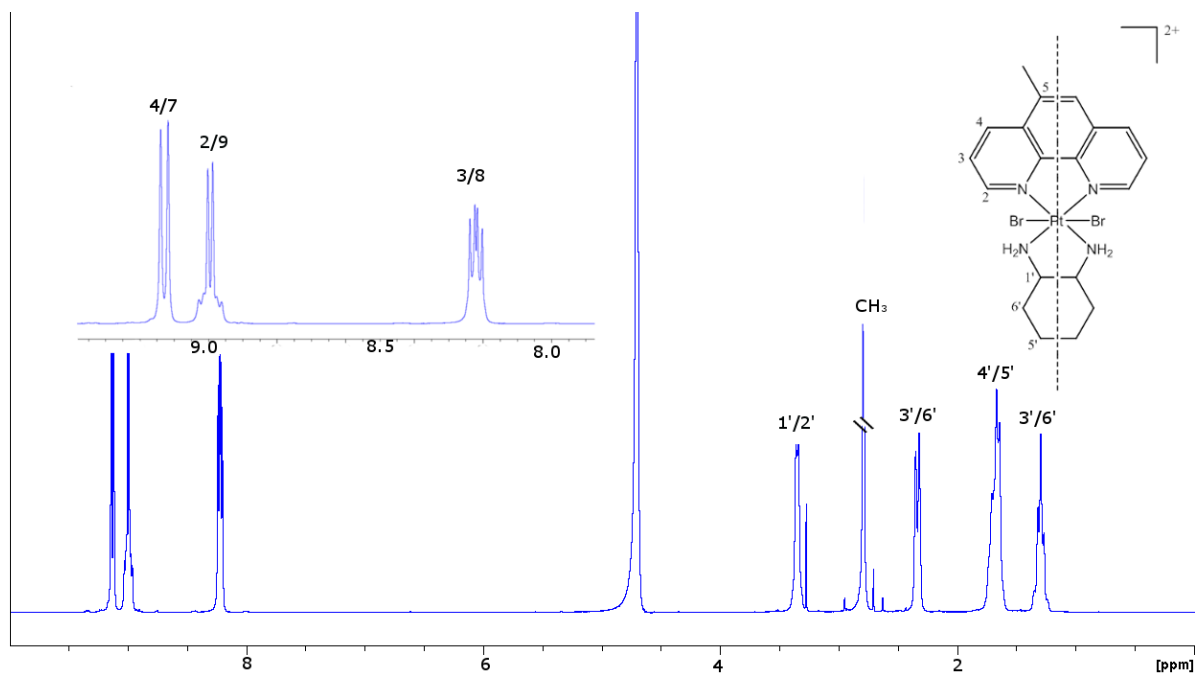


Figure A14: The ¹H spectrum of 56MESSBr₂ in D₂O, performed on a Bruker Avance 400 MHz NMR spectrometer.

56MESS(I)₂ ¹⁹⁵Pt NMR spectra

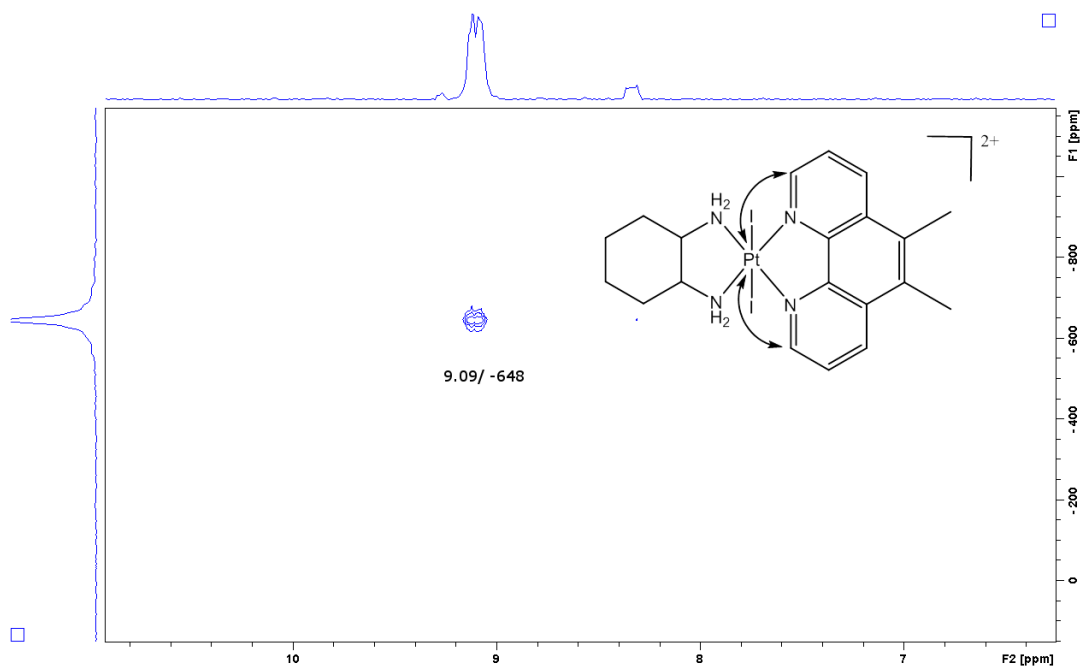


Figure A15: The ¹H-¹⁹⁵Pt HMQC spectrum of 56MESSI₂ in D₂O, performed on a Bruker Avance 400 MHz NMR spectrometer.

56MESS(I)₂ ¹H NMR spectra

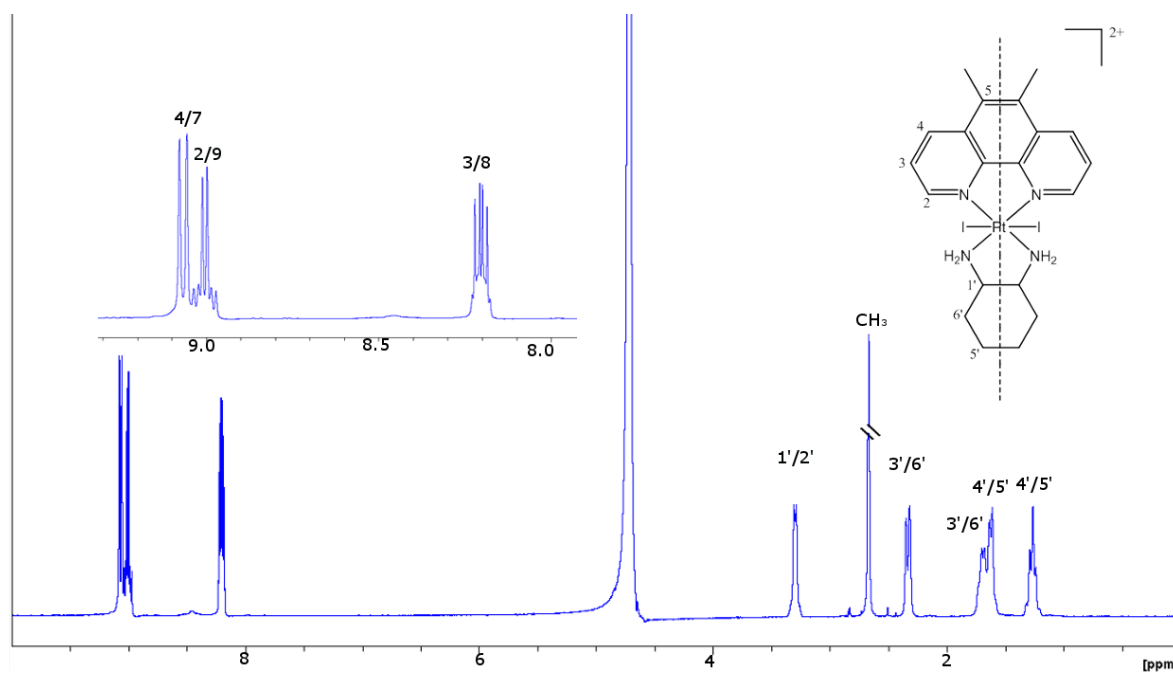


Figure A16: The ¹H spectrum of 56MESSI₂ in D₂O, performed on a Bruker Avance 400 MHz NMR spectrometer.

PHENSS(OH)(DCL) ¹H NMR spectra

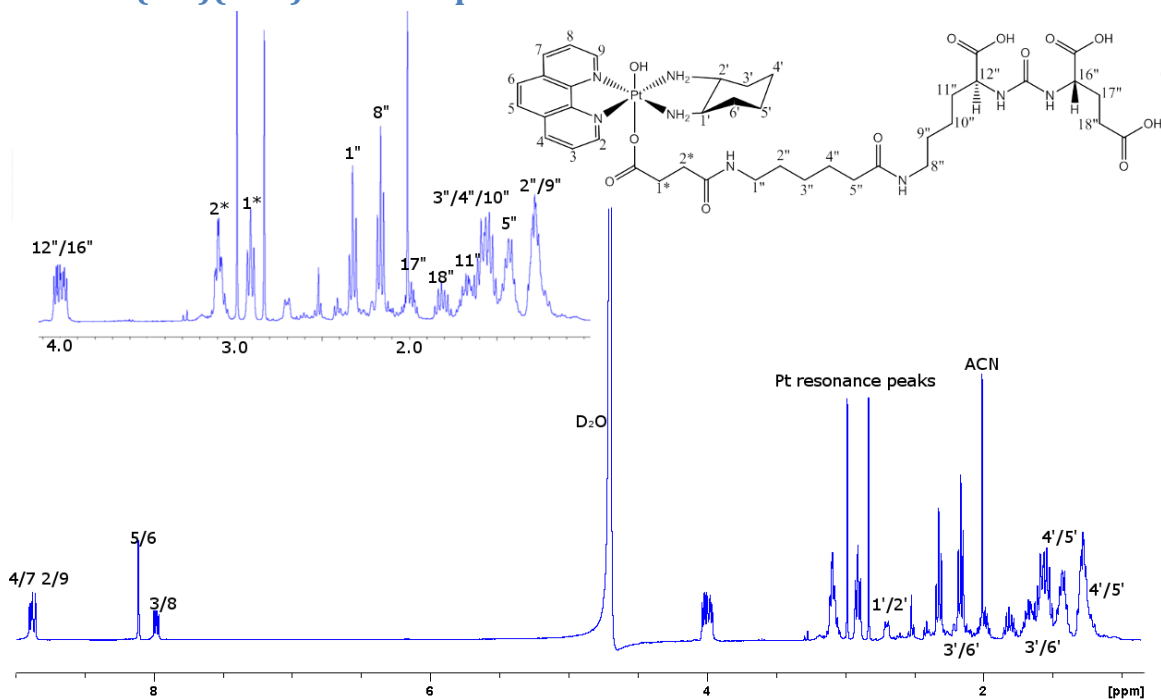


Figure A17: The ¹H spectrum of PHENSS(OH)(DCL) in D₂O, performed on a Bruker Avance 400 MHz NMR spectrometer.

DCL ¹H NMR spectra

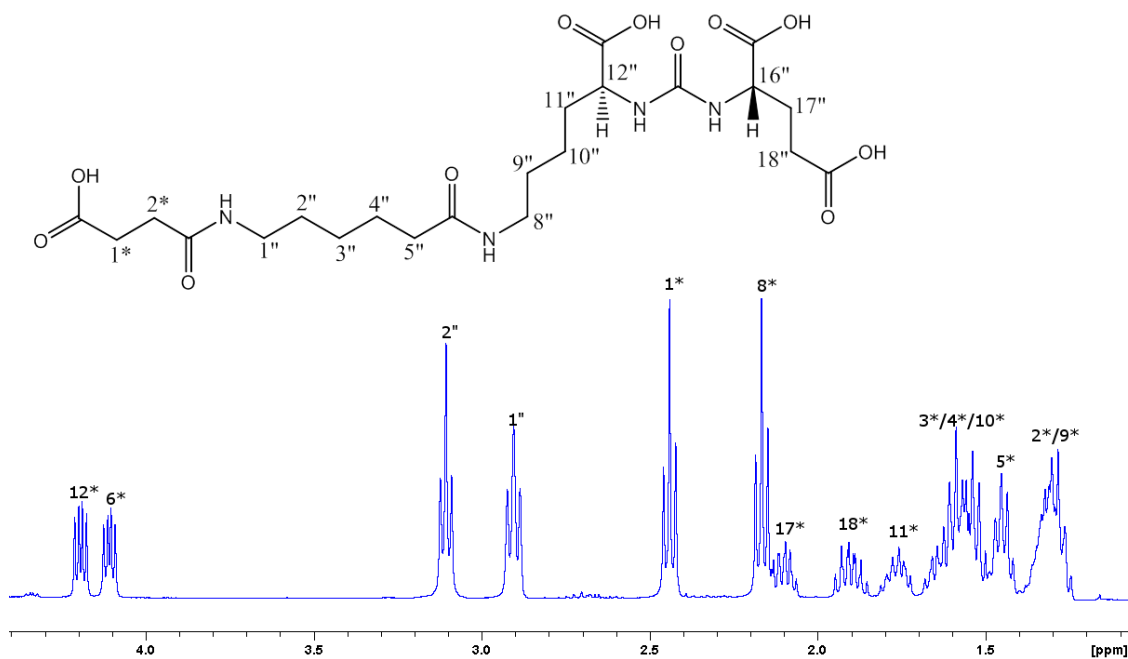


Figure A18: The ¹H spectrum of DCL in MeOD, performed on a Bruker Avance 400 MHz NMR spectrometer.

PHENSS(OH)(PSMA) ^{195}Pt NMR spectra

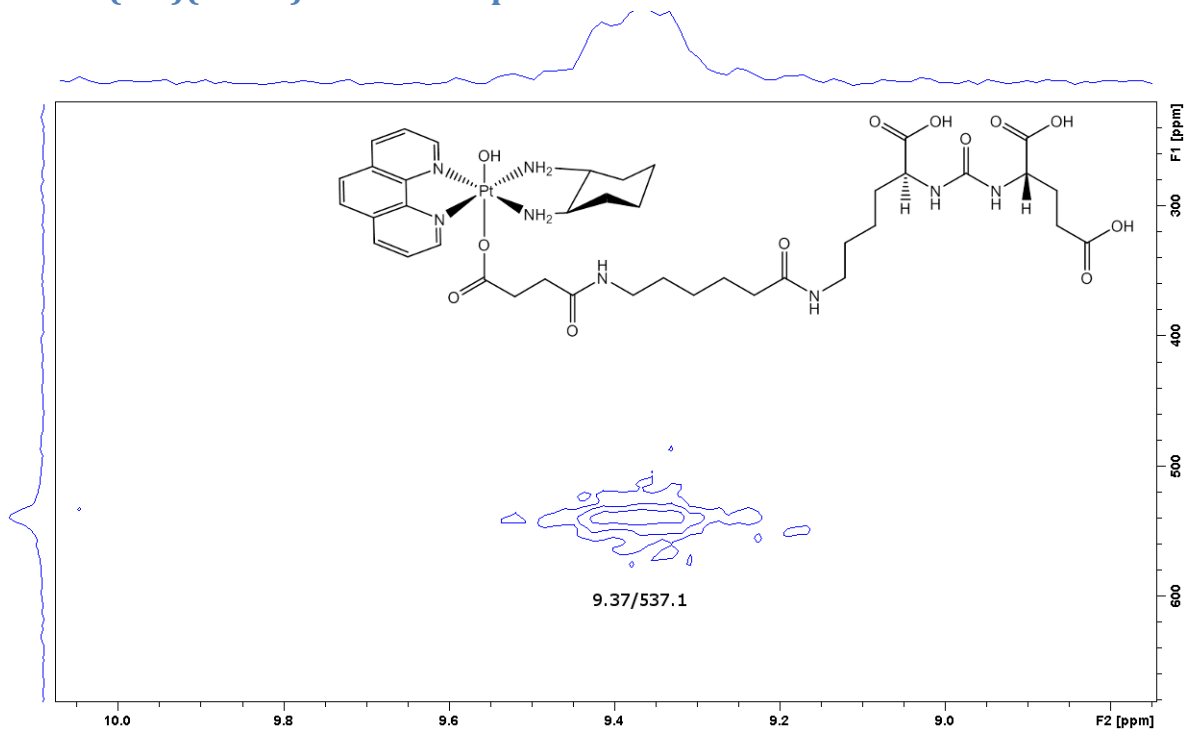


Figure A19: The ^1H - ^{195}Pt HMQC spectrum of PHENSS(OH)(DCL) in D_2O , performed on a Bruker Avance 400 MHz NMR spectrometer.

PHENSSenDCF₂ ¹H NMR spectra

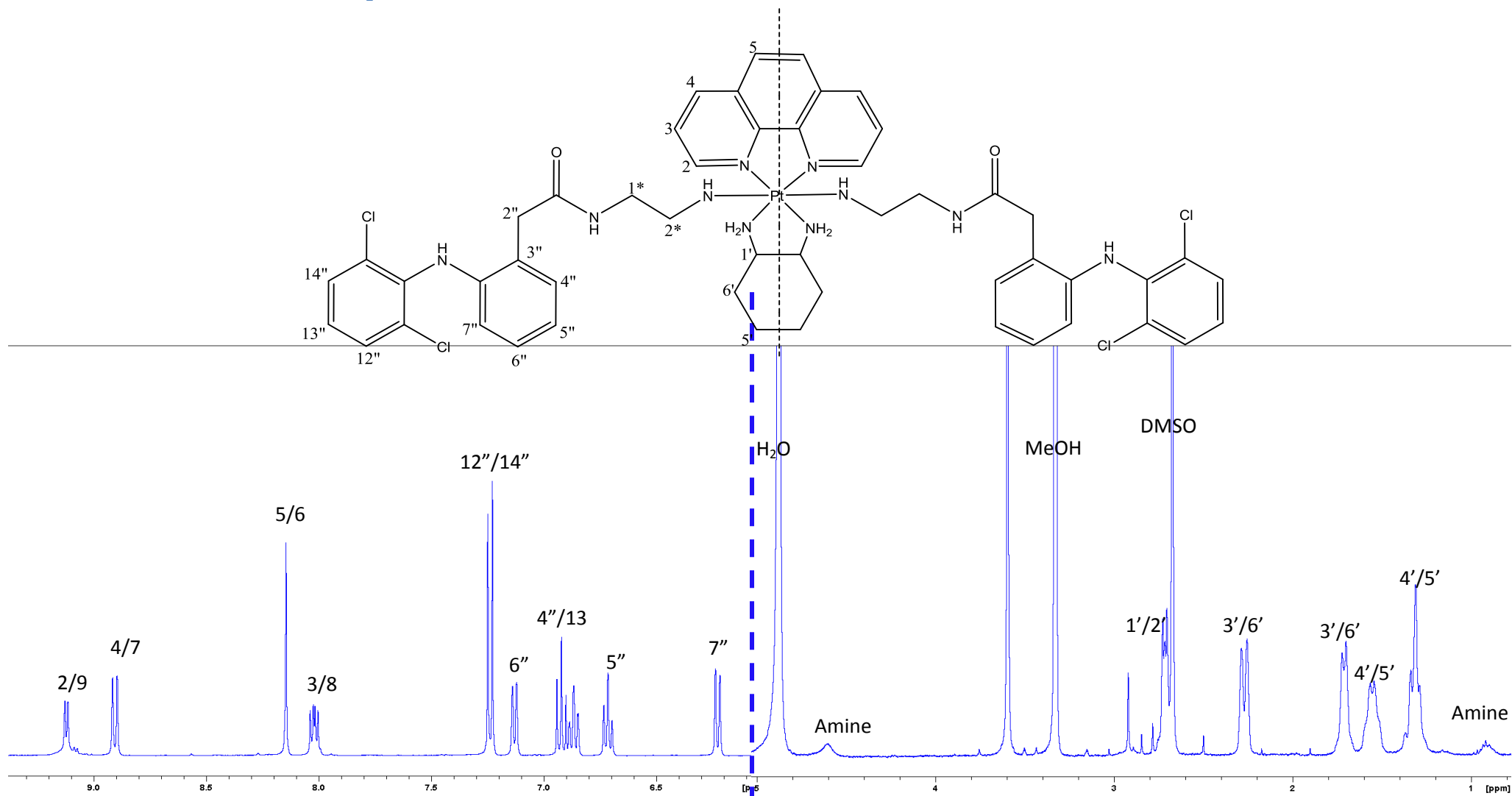


Figure A20: The ¹H spectrum of PHENSS(enDCF) in D₂O, performed on a Bruker Avance 400 MHz NMR spectrometer.

PHENSSenDCF₂ ¹⁹⁵Pt NMR spectra

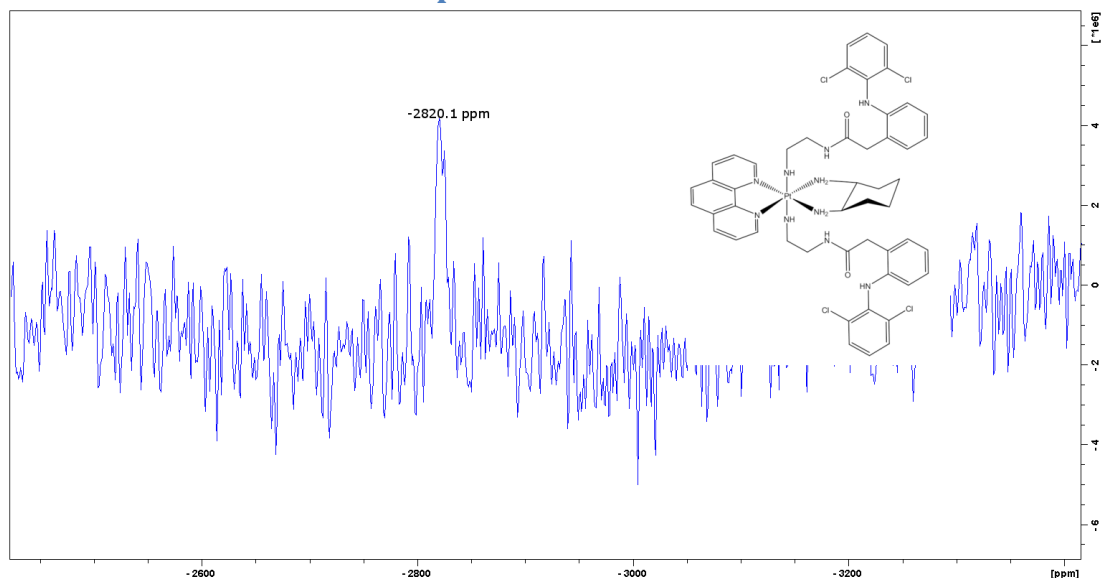


Figure A21: The ¹⁹⁵Pt spectrum of PHENSS(enDCF) in D₂O, performed on a Bruker Avance 400 MHz NMR spectrometer.

PHENSS(DMSO)₂ (in DMSO) ¹H NMR spectra

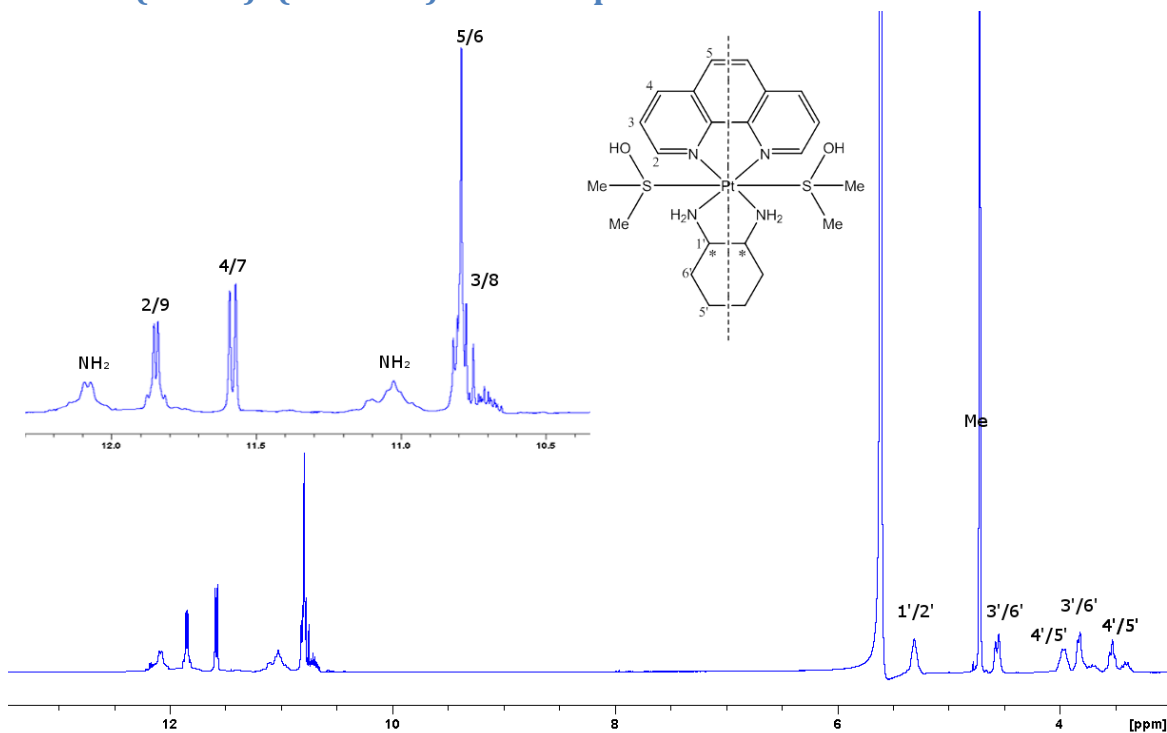


Figure A22: The ¹H spectrum of PHENSS(DMSO)₂ in d-DMSO, performed on a Bruker Avance 400 MHz NMR spectrometer.

PHENSS(DMSO)₂ (in DMSO) ¹⁹⁵Pt NMR spectra

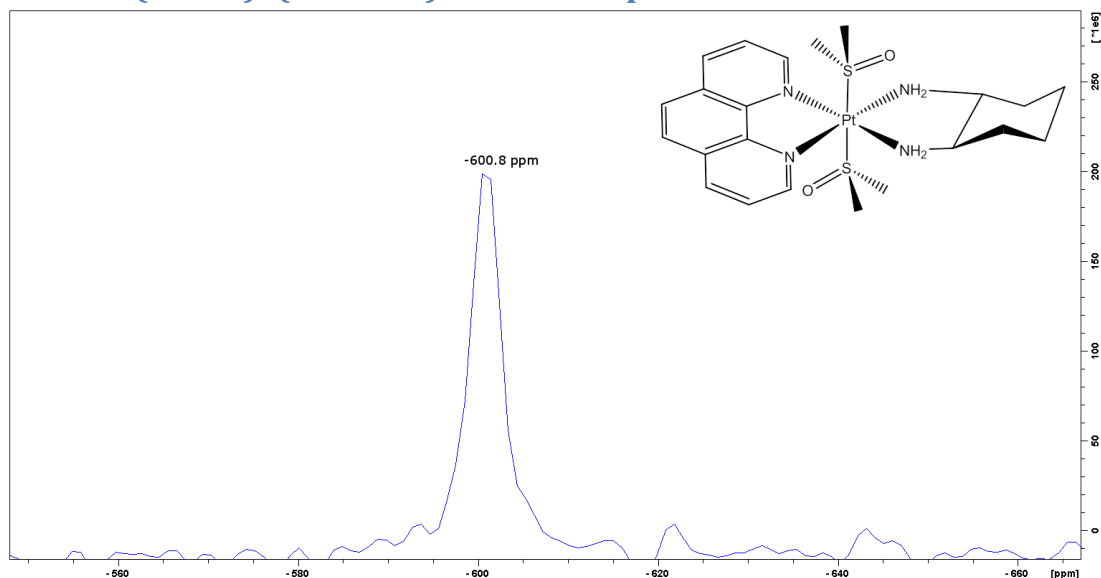


Figure A23: The ¹⁹⁵Pt spectrum of PHENSS(DMSO)₂ in d-DMSO, performed on a Bruker Avance 400 MHz NMR spectrometer.

en-DCF ¹H NMR spectra

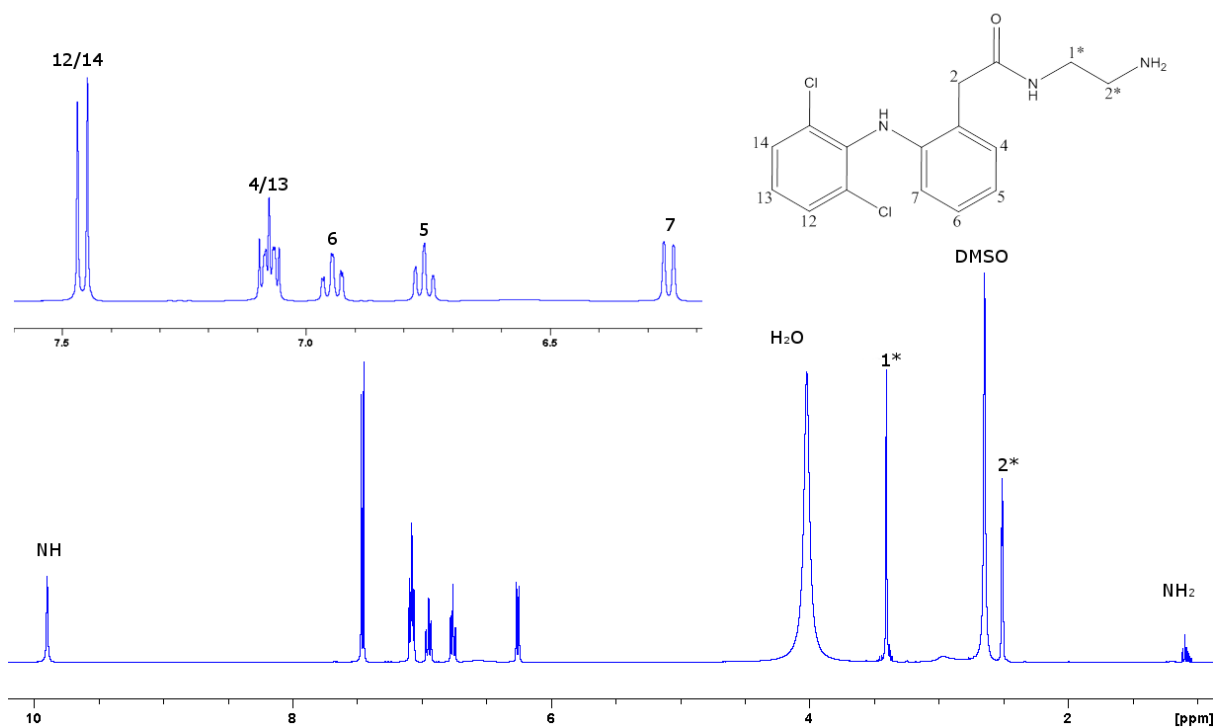


Figure A24: The ¹H spectrum of en-DCF in D₂O, performed on a Bruker Avance 400 MHz NMR spectrometer.

PHENSS ^1H NMR spectra

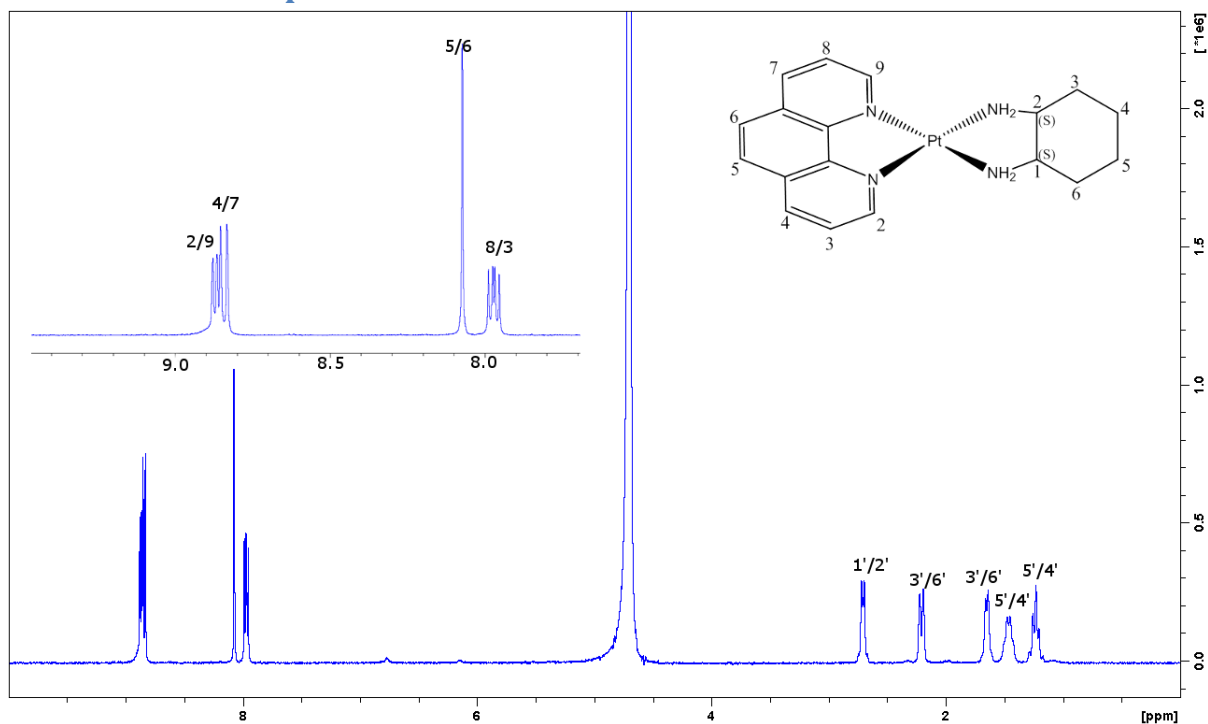


Figure A25: The ^1H spectrum of PHENSS in D_2O , performed on a Bruker Avance 400 MHz NMR spectrometer.

PHENSS ^{195}Pt NMR spectra

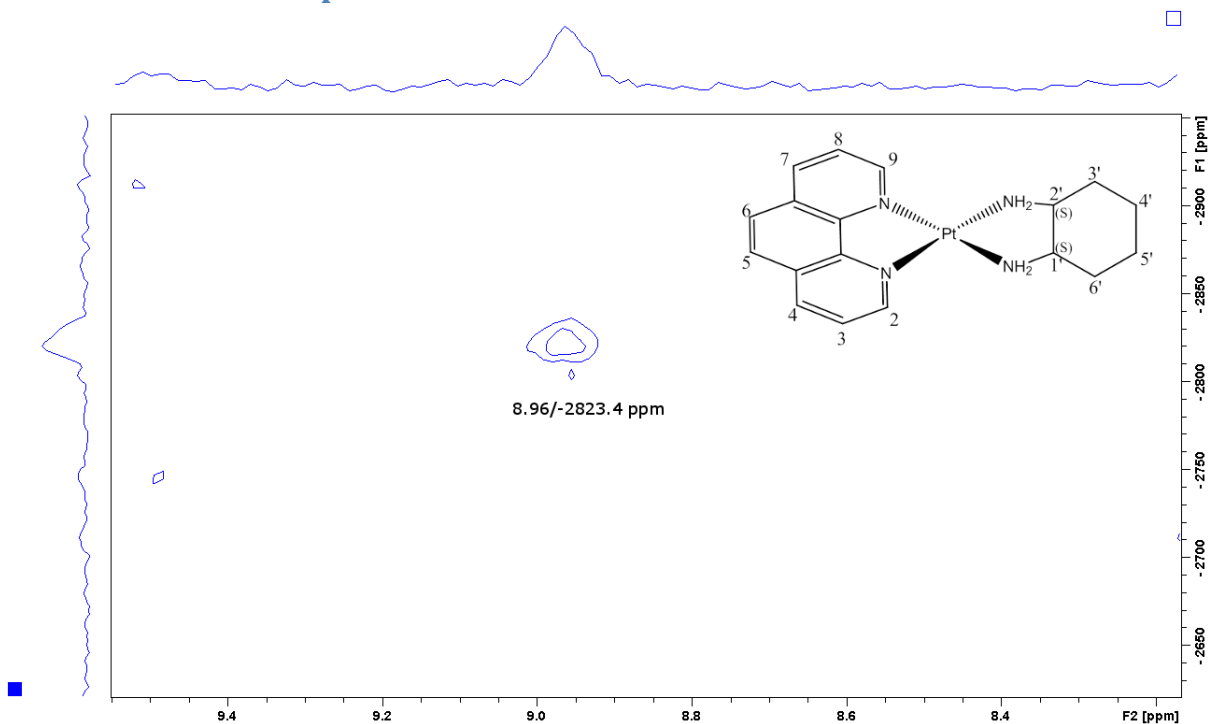


Figure A26: The ^1H - ^{195}Pt HMQC spectrum of PHENSS in D_2O , performed on a Bruker Avance 400 MHz NMR spectrometer.

PHENRR ^1H NMR spectra

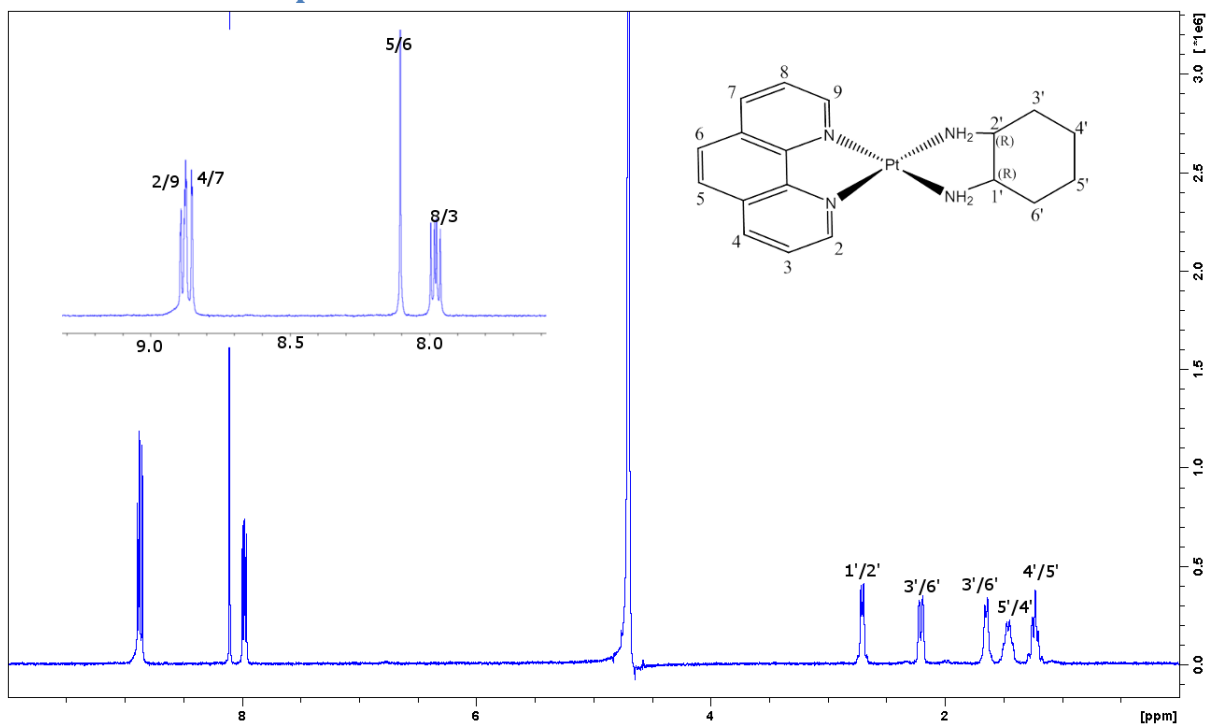


Figure A27: The ^1H spectrum of PHENRR in D_2O , performed on a Bruker Avance 400 MHz NMR spectrometer.

PHENRR ^{195}Pt NMR spectra

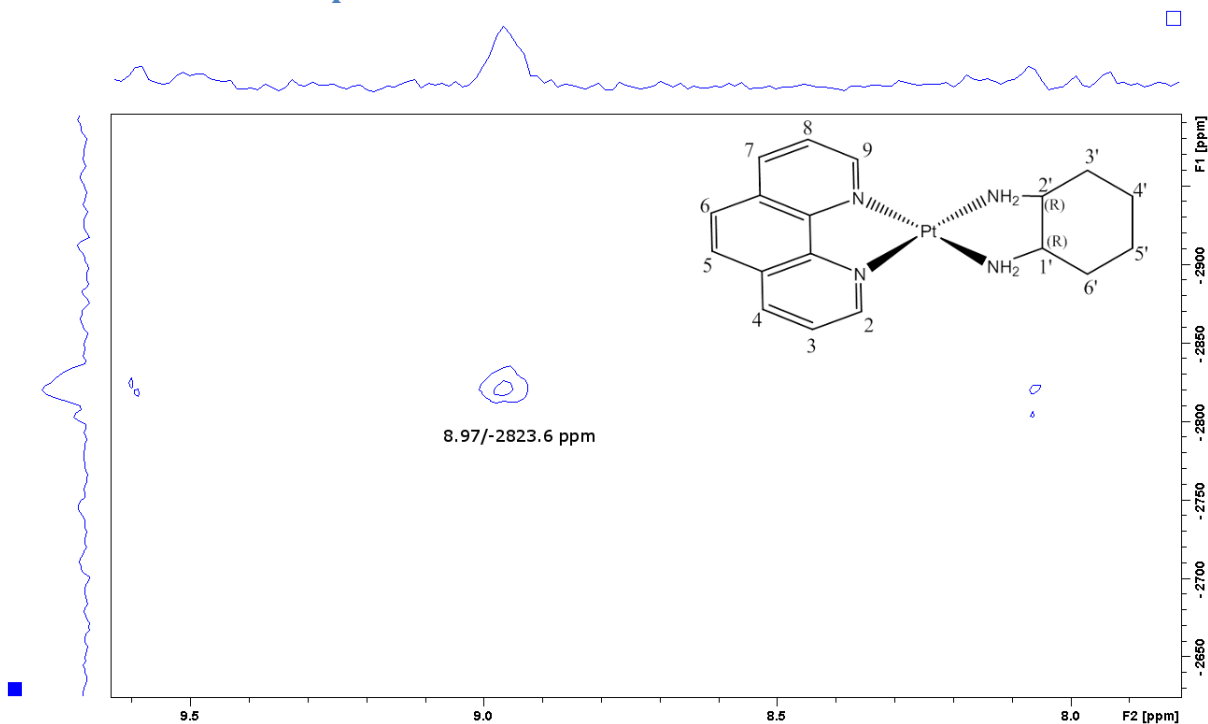


Figure A28: The ^1H - ^{195}Pt HMQC spectrum of PHENRR in D_2O , performed on a Bruker Avance 400 MHz NMR spectrometer.

5MESS ^1H NMR spectra

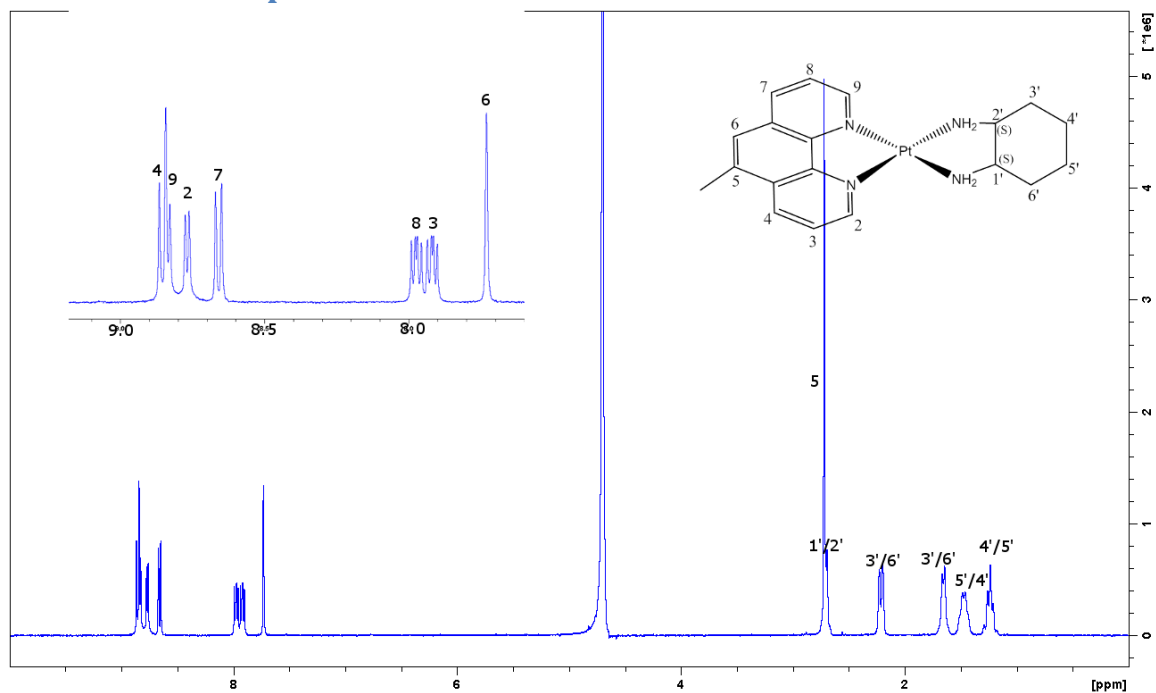


Figure A29: The ^1H spectrum of 5MESS in D_2O , performed on a Bruker Avance 400 MHz NMR spectrometer.

5MESS ^{195}Pt NMR spectra

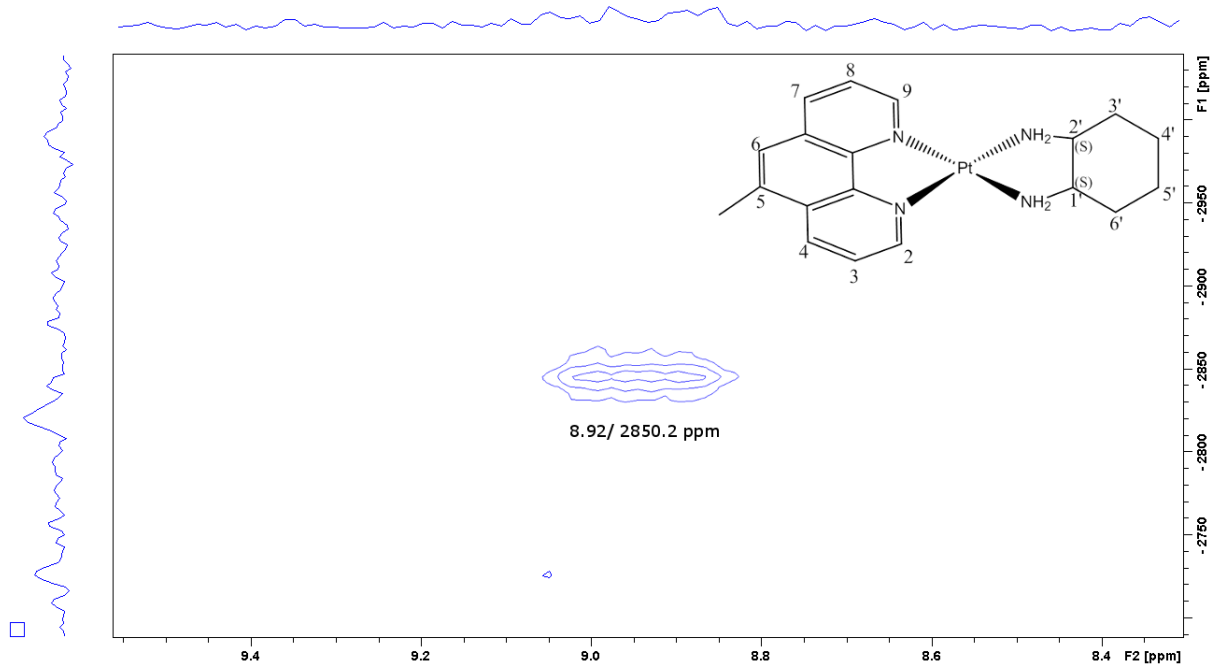


Figure A30: The ^1H - ^{195}Pt HMQC spectrum of 5MESS in D_2O , performed on a Bruker Avance 400 MHz NMR spectrometer.

5MERR ^1H NMR spectra

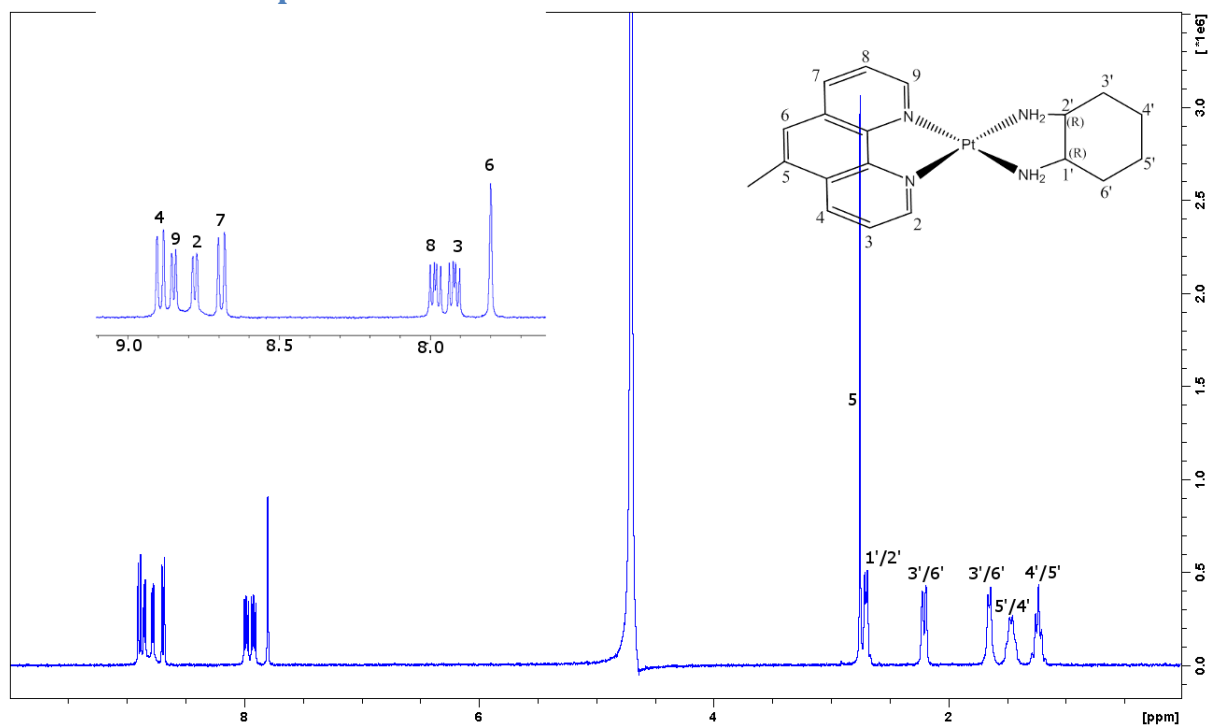


Figure A31: The ^1H spectrum of 5MERR in D_2O , performed on a Bruker Avance 400 MHz NMR spectrometer.

5MERR ^{195}Pt NMR spectra

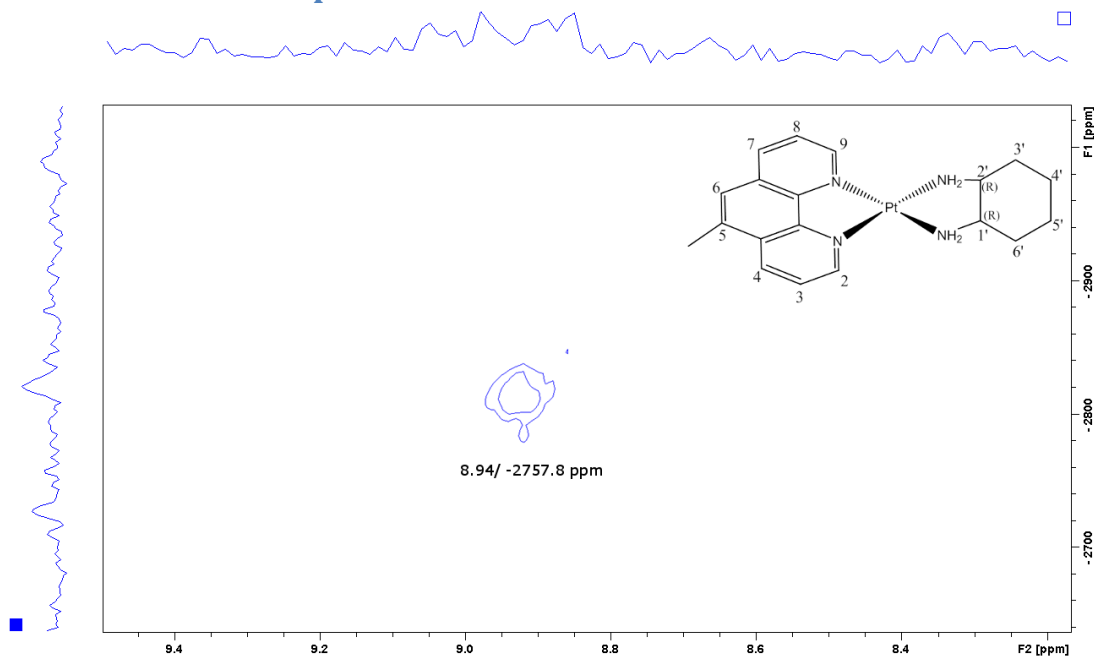


Figure A32: The ^1H - ^{195}Pt HMQC spectrum of 5MERR in D_2O , performed on a Bruker Avance 400 MHz NMR spectrometer.

56MESS ^1H NMR spectra

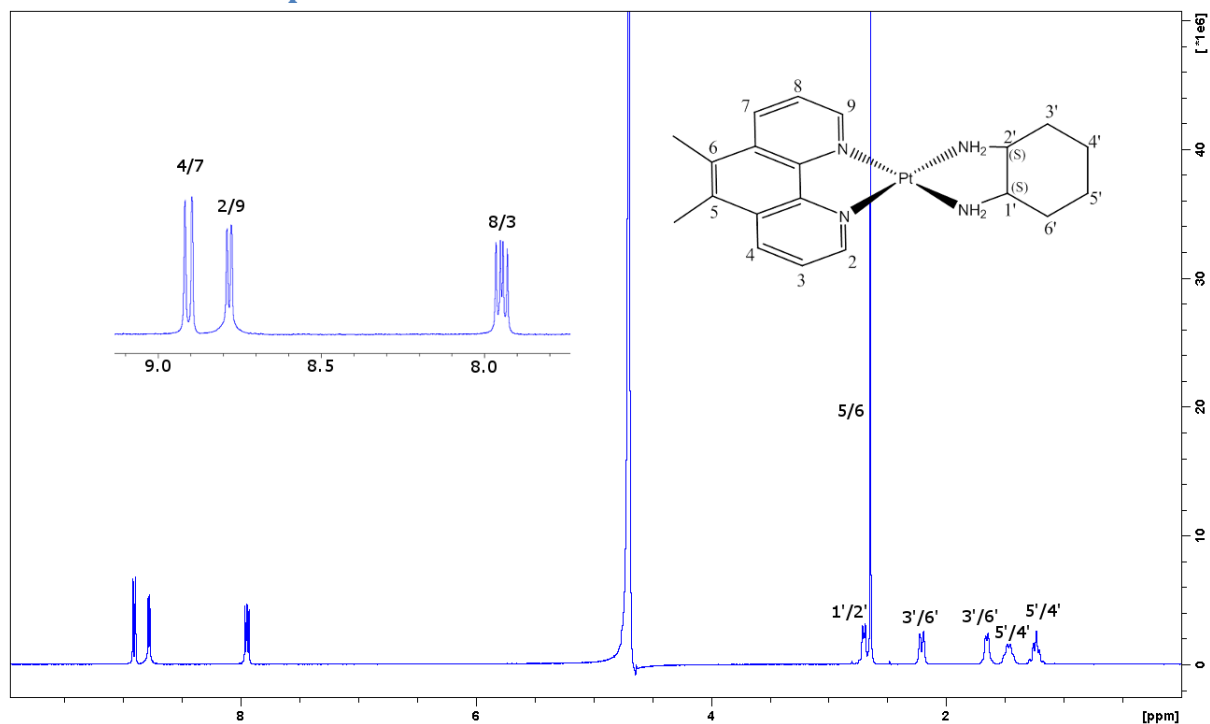


Figure A33: The ^1H spectrum of 56MESS in D_2O , performed on a Bruker Avance 400 MHz NMR spectrometer.

56MESS ^{195}Pt NMR spectra

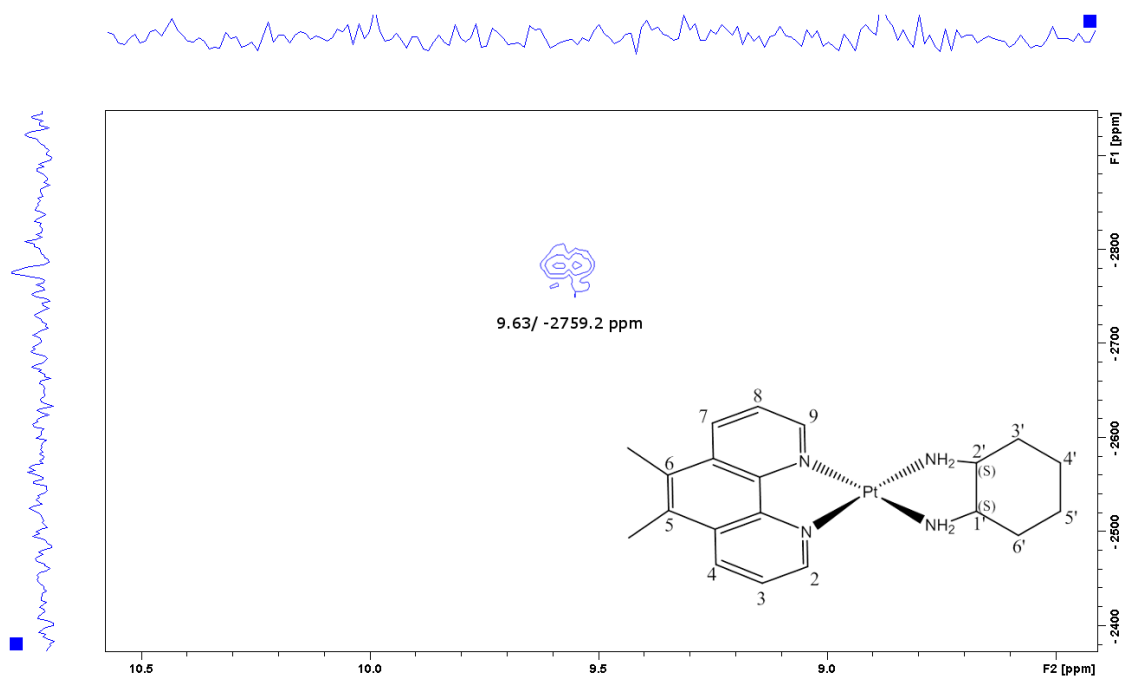


Figure A34: The ^1H - ^{195}Pt HMQC spectrum of 56MESS in D_2O , performed on a Bruker Avance 400 MHz NMR spectrometer.

56MERR ^1H NMR spectra

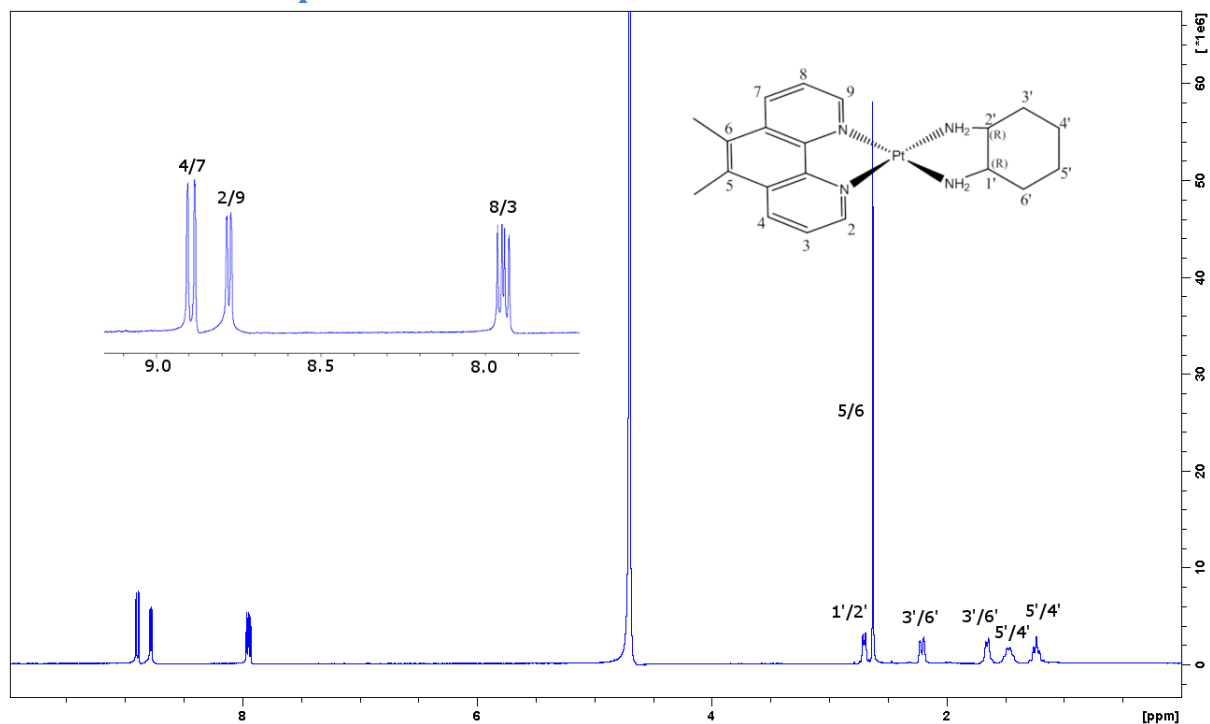


Figure A35: The ^1H spectrum of 56MERR in D_2O , performed on a Bruker Avance 400 MHz NMR spectrometer.

56MERR ^{195}Pt NMR spectra

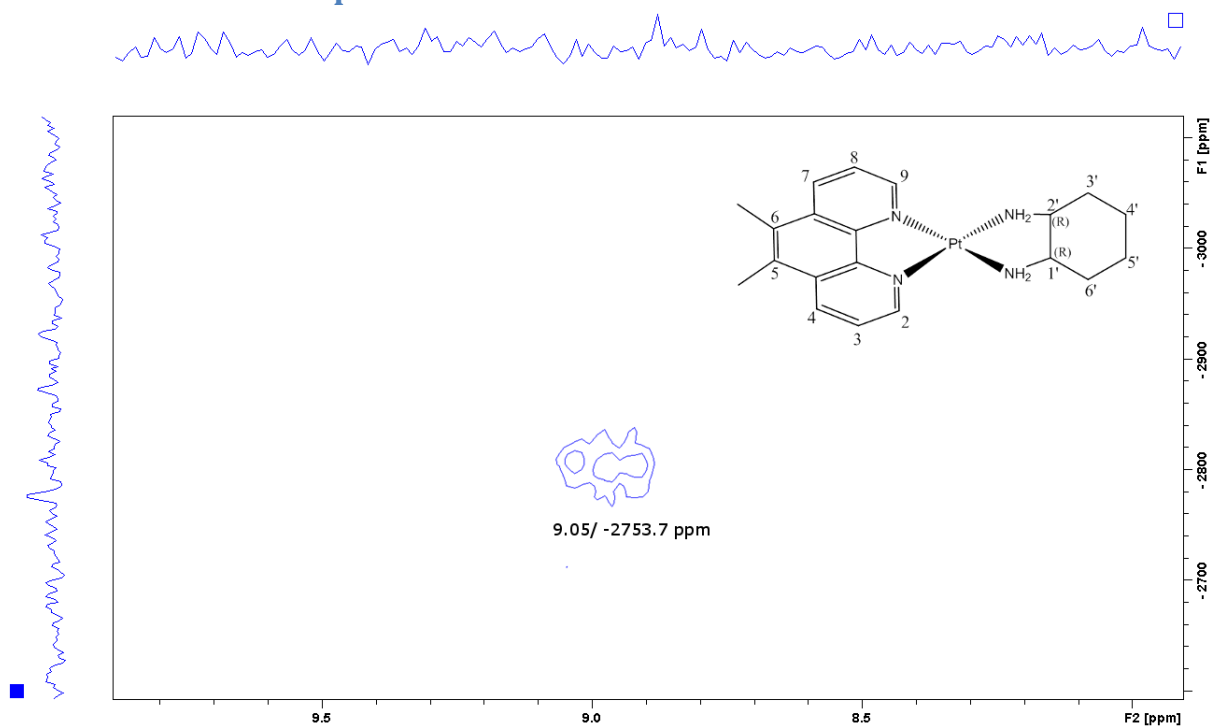


Figure A36: The ^1H - ^{195}Pt HMQC spectrum of 56MERR in D_2O , performed on a Bruker Avance 400 MHz NMR spectrometer.

4MESS ^1H NMR spectra

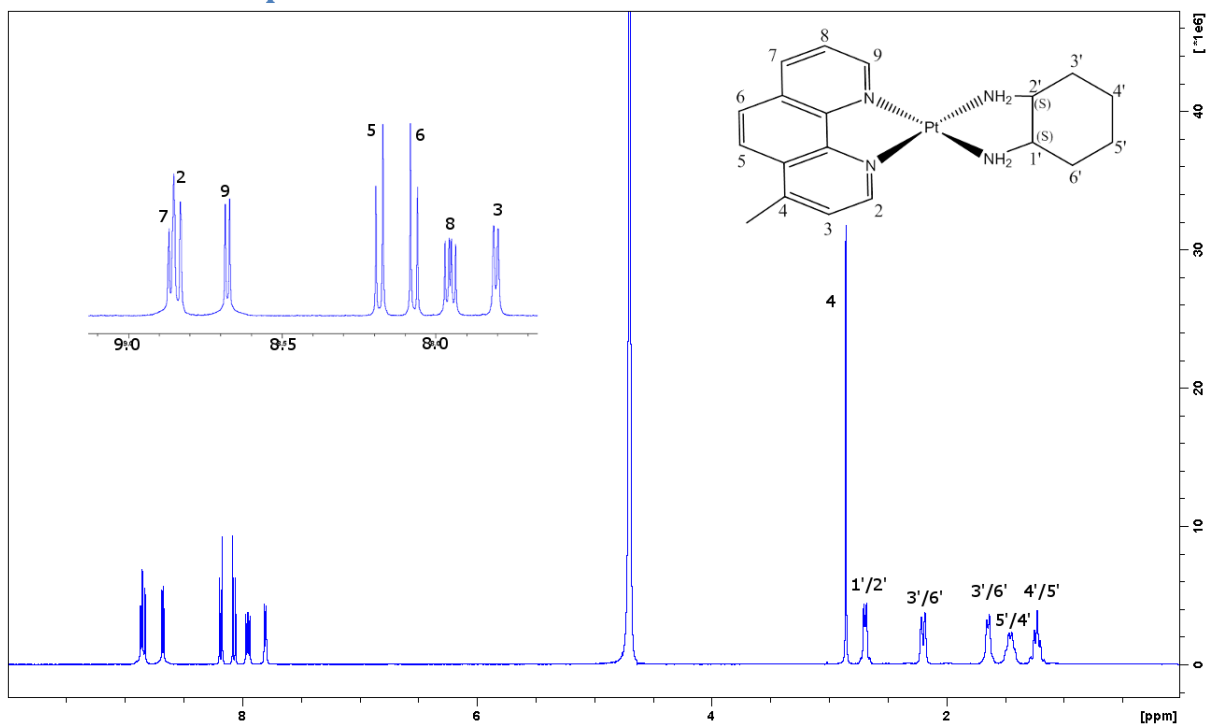


Figure A37: The ^1H spectrum of 4MESS in D_2O , performed on a Bruker Avance 400 MHz NMR spectrometer.

4MESS ^{195}Pt NMR spectra

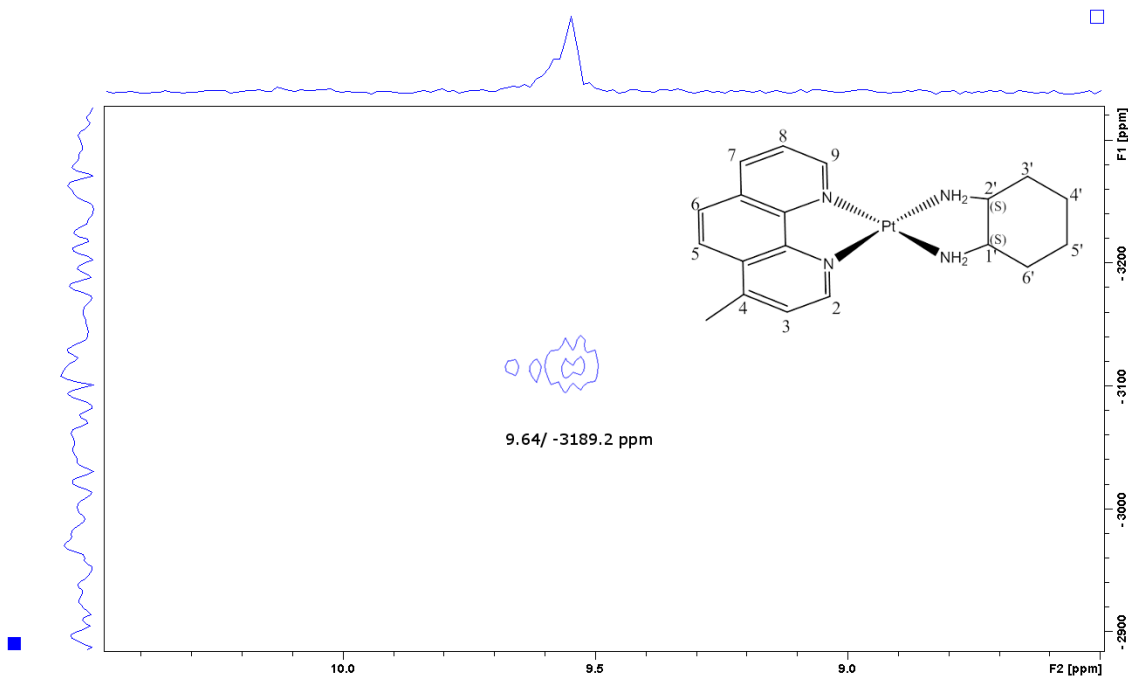


Figure A38: The ^1H - ^{195}Pt HMQC spectrum of 4MESS in D_2O , performed on a Bruker Avance 400 MHz NMR spectrometer.

4MERR ^1H NMR spectra

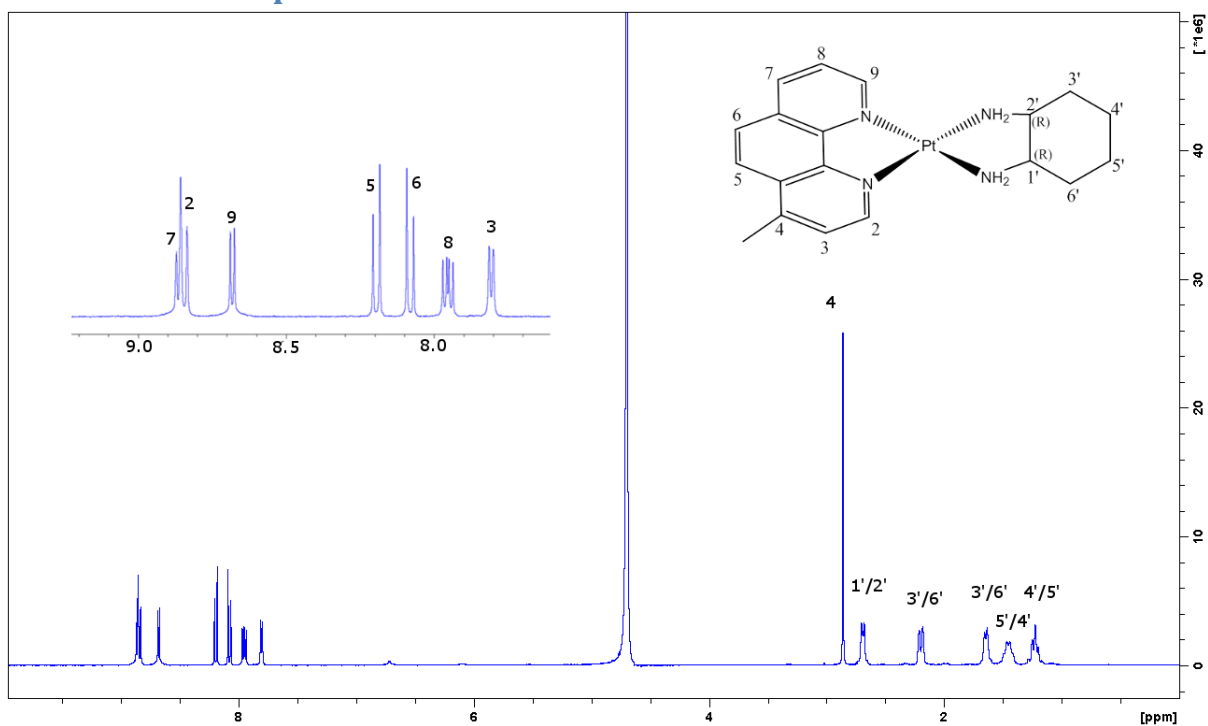


Figure A39: The ^1H spectrum of 4MERR in D_2O , performed on a Bruker Avance 400 MHz NMR spectrometer.

4MERR ^{195}Pt NMR spectra

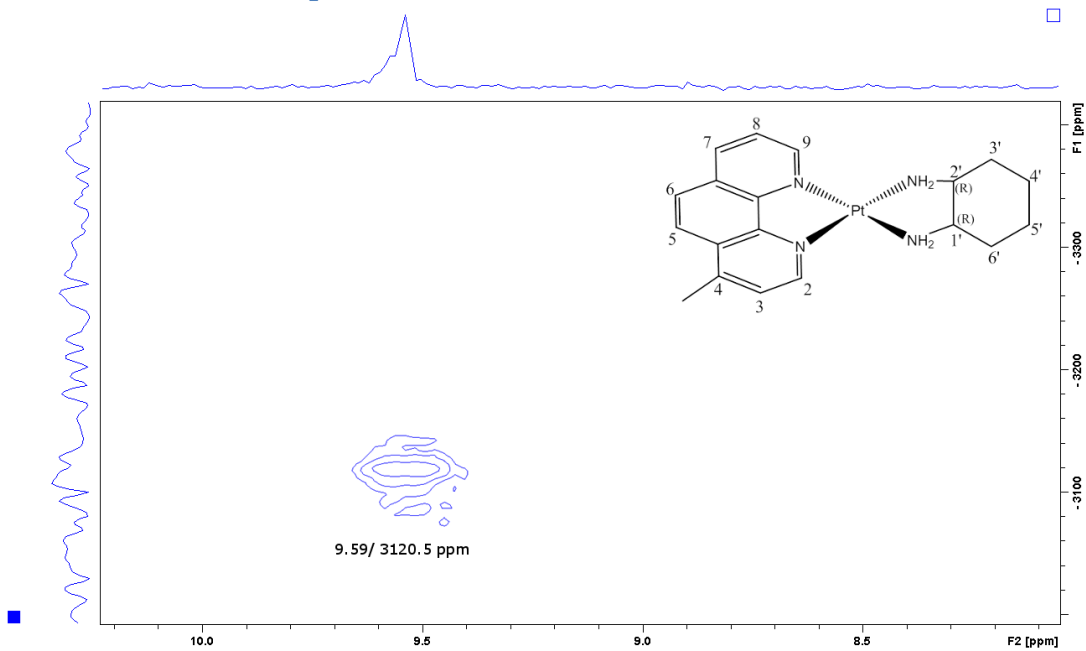


Figure A40: The ^1H - ^{195}Pt HMQC spectrum of 4MERR in D_2O , performed on a Bruker Avance 400 MHz NMR spectrometer.

44BPYSS ^1H NMR spectra

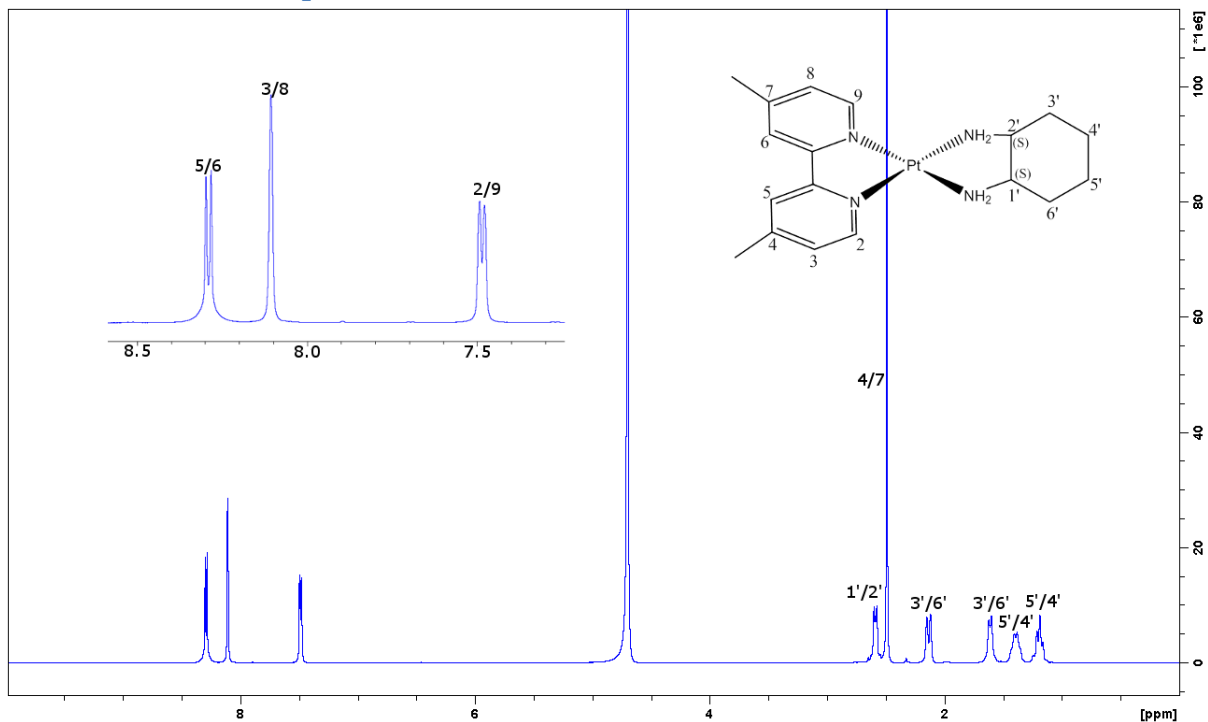


Figure A41: The ^1H spectrum of 44BPYSS in D_2O , performed on a Bruker Avance 400 MHz NMR spectrometer.

44BPYSS ^{195}Pt NMR spectra

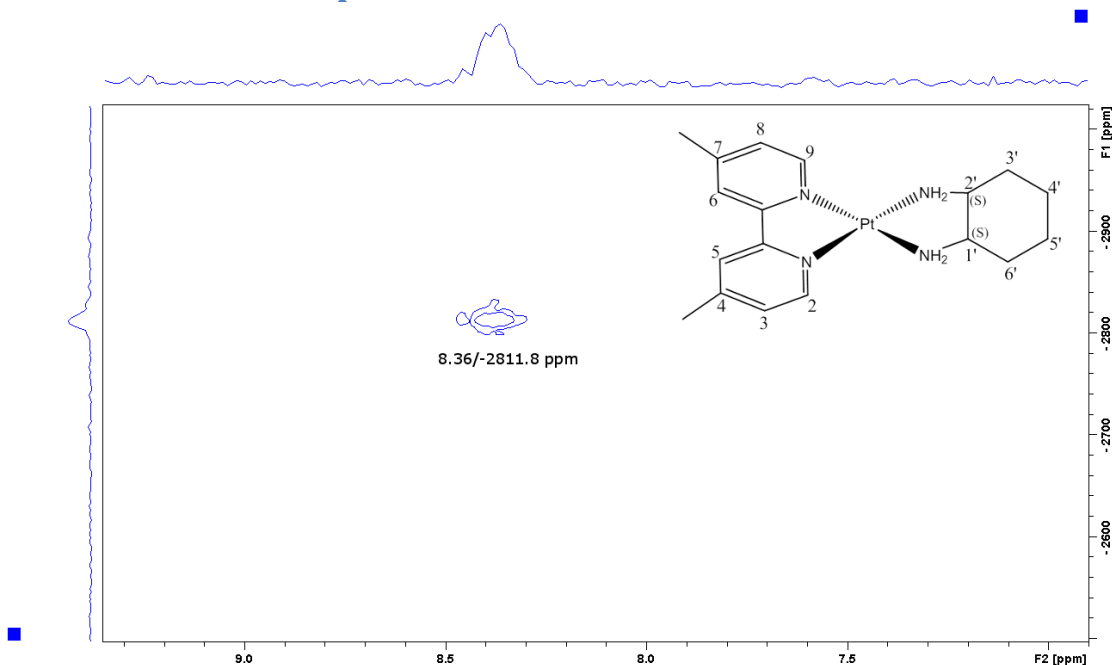


Figure A42: The ^1H - ^{195}Pt HMQC spectrum of 44BPYSS in D_2O , performed on a Bruker Avance 400 MHz NMR spectrometer.

44BPYRR ^1H NMR spectra

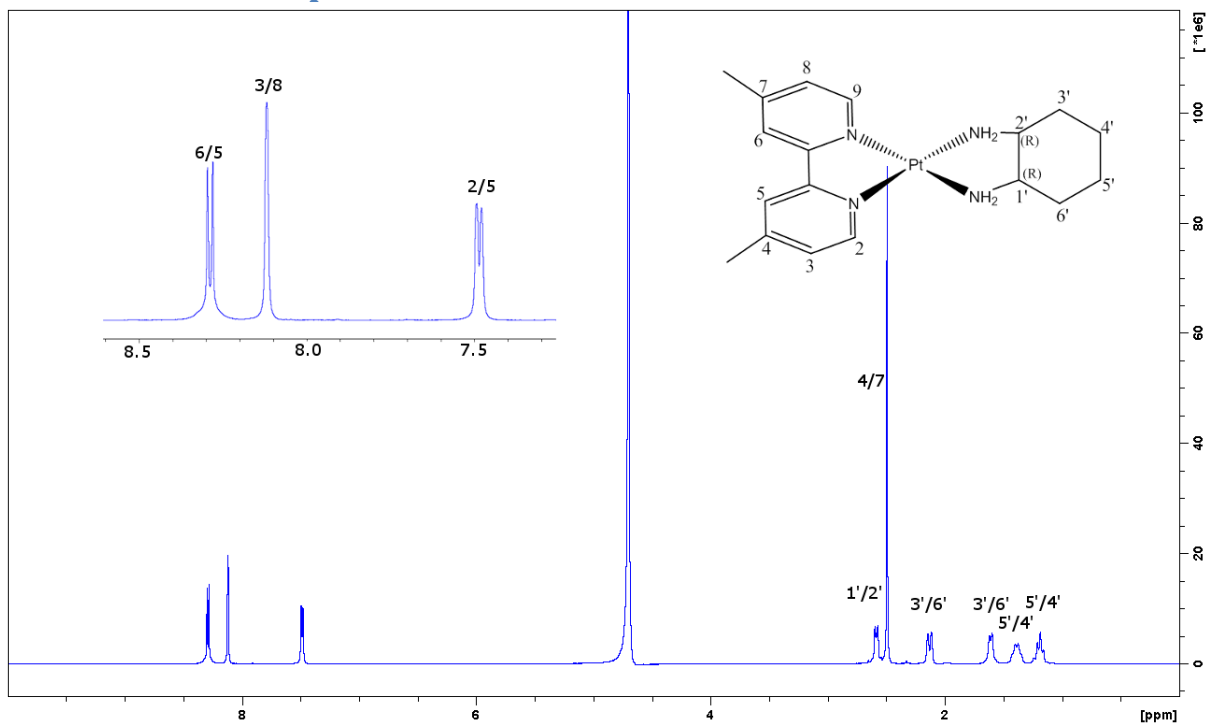


Figure A43: The ^1H spectrum of 44BPYRR in D_2O , performed on a Bruker Avance 400 MHz NMR spectrometer.

BPYRR ^{195}Pt NMR spectra

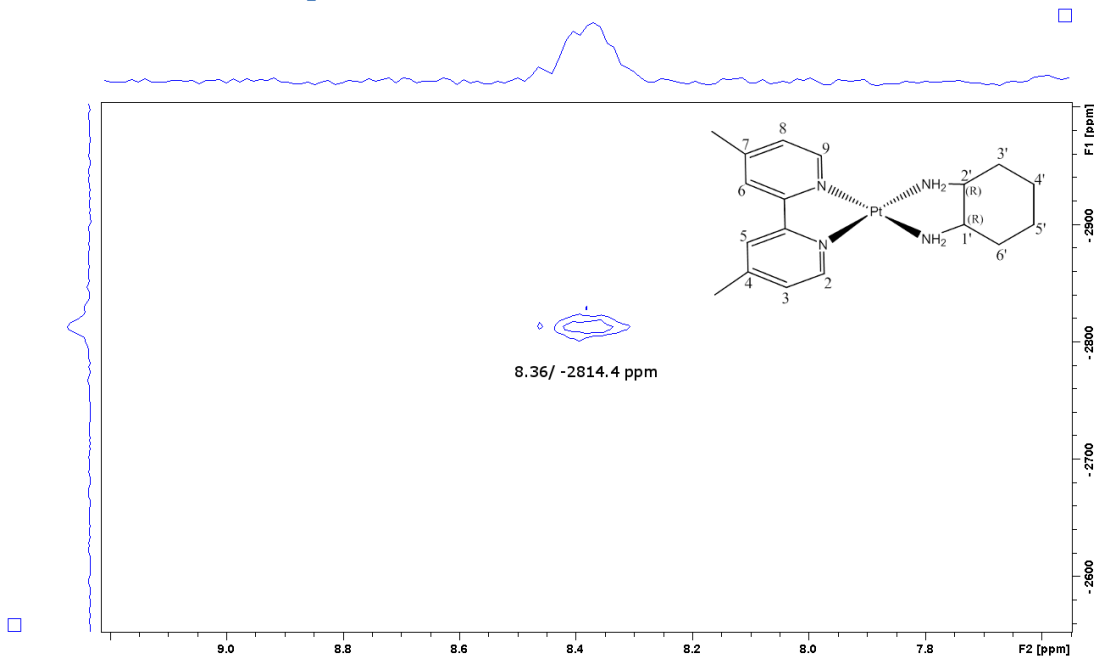


Figure A44: The ^1H - ^{195}Pt HMQC spectrum of 44BPYRR in D_2O , performed on a Bruker Avance 400 MHz NMR spectrometer.

PHENSS(OH)(OAc) ^1H NMR spectra

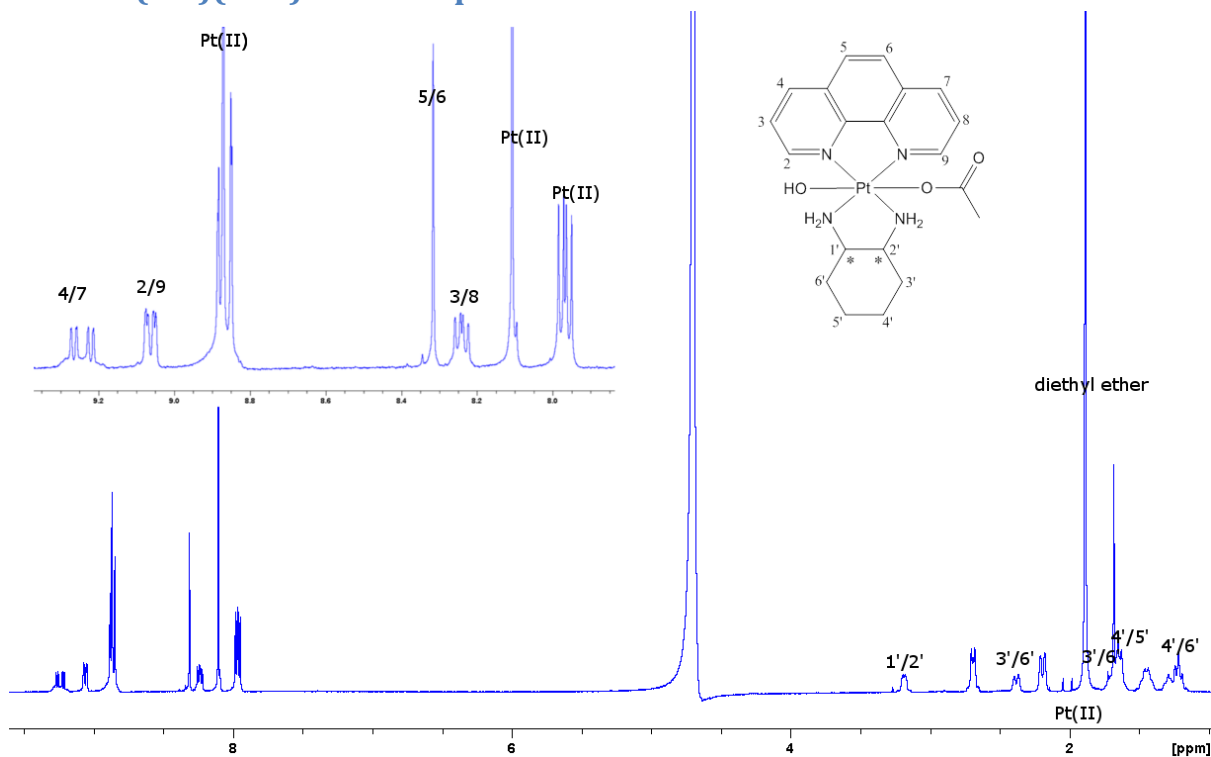


Figure A45: The ^1H spectrum of PHENSS(OH)(OAc) in D_2O , performed on a Bruker Avance 400 MHz NMR spectrometer.

PHENSS(OH)(OAc) ^{195}Pt NMR spectra

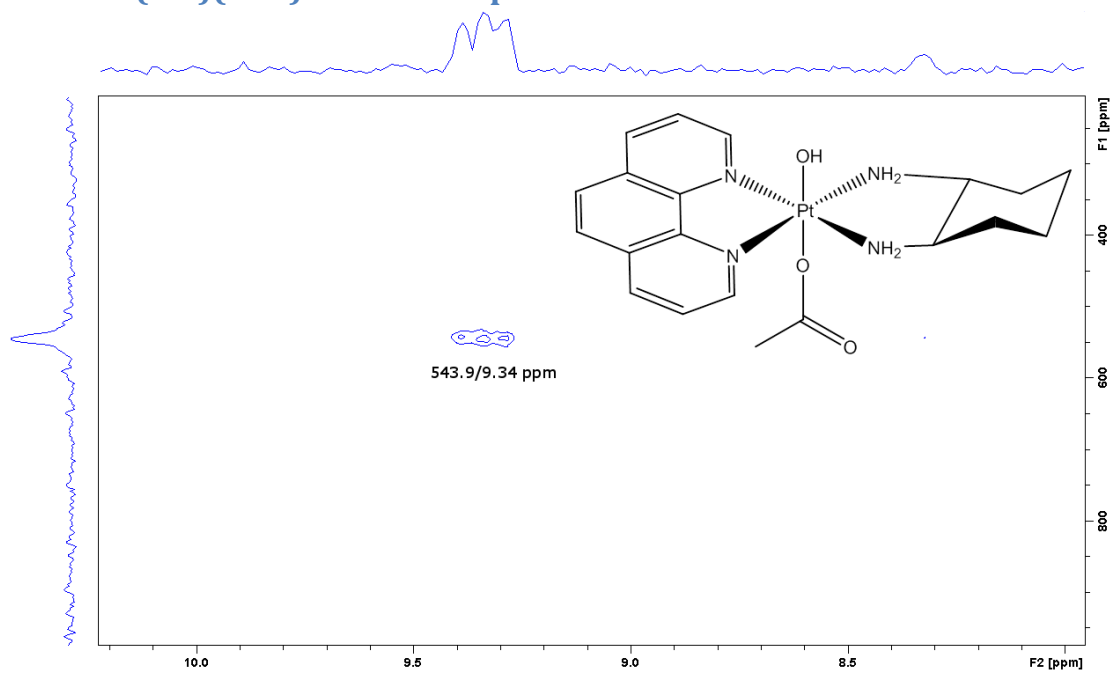


Figure A46: The ^1H - ^{195}Pt HMQC spectrum of PHENSS(OH)(OAc) in D_2O , performed on a Bruker Avance 400 MHz NMR spectrometer.

PHENRR(OH)(OAc) ^1H NMR spectra

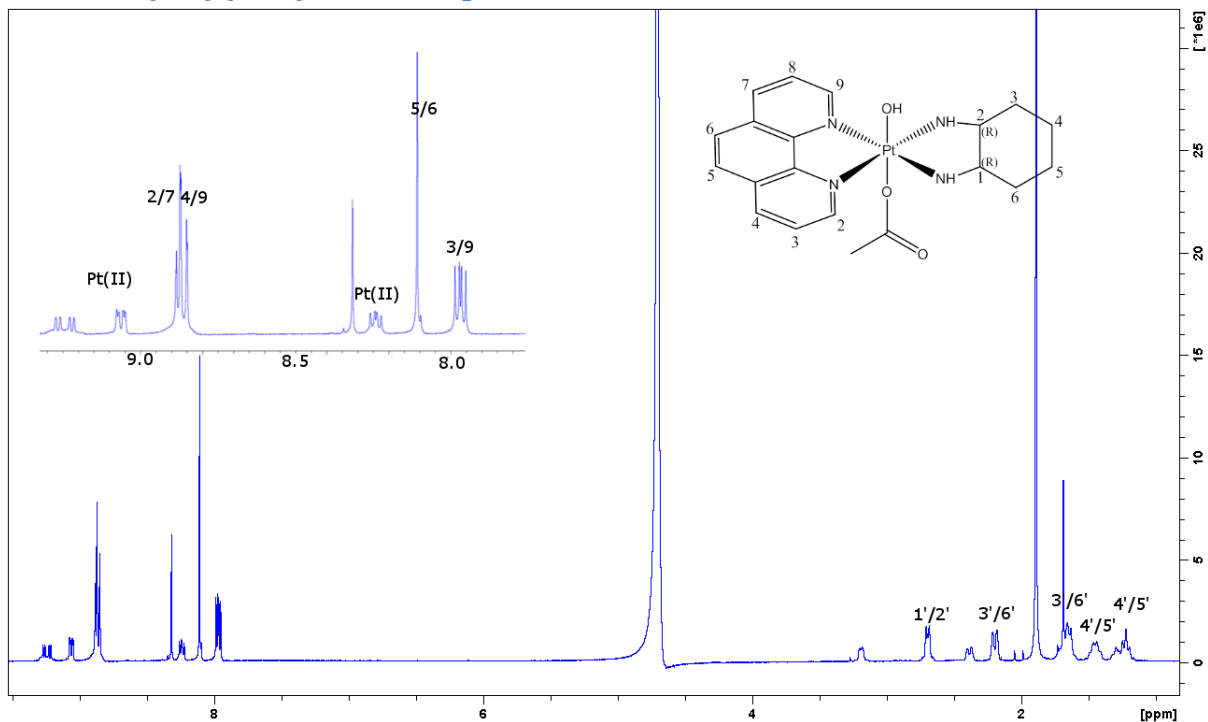


Figure A47: The ^1H spectrum of PHENRR(OH)(OAc) in D_2O , performed on a Bruker Avance 400 MHz NMR spectrometer.

PHENRR(OH)(OAc) ^{195}Pt NMR spectra

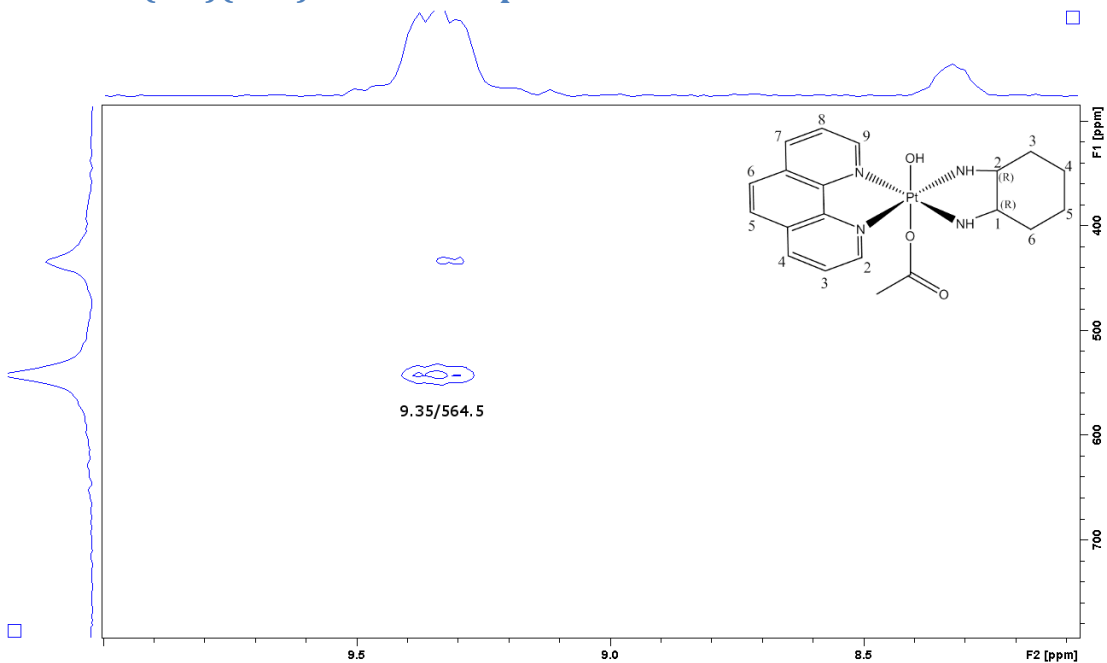


Figure A48: The ^1H - ^{195}Pt HMQC spectrum of PHENRR(OH)(OAc) in D_2O , performed on a Bruker Avance 400 MHz NMR spectrometer.

5MESS(OH)(OAc) ^1H NMR spectra

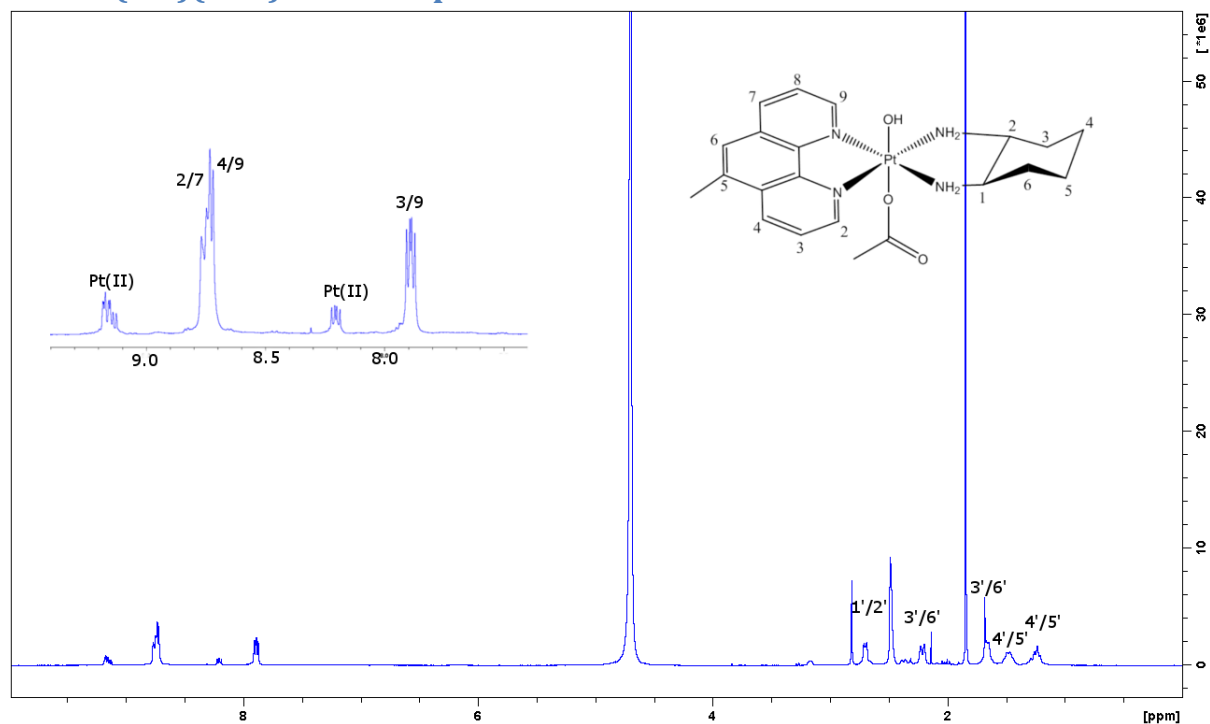


Figure A49: The ^1H spectrum of 5MESS(OH)(OAc) in D_2O , performed on a Bruker Avance 400 MHz NMR spectrometer.

5MESS(OH)(OAc) ^{195}Pt NMR spectra

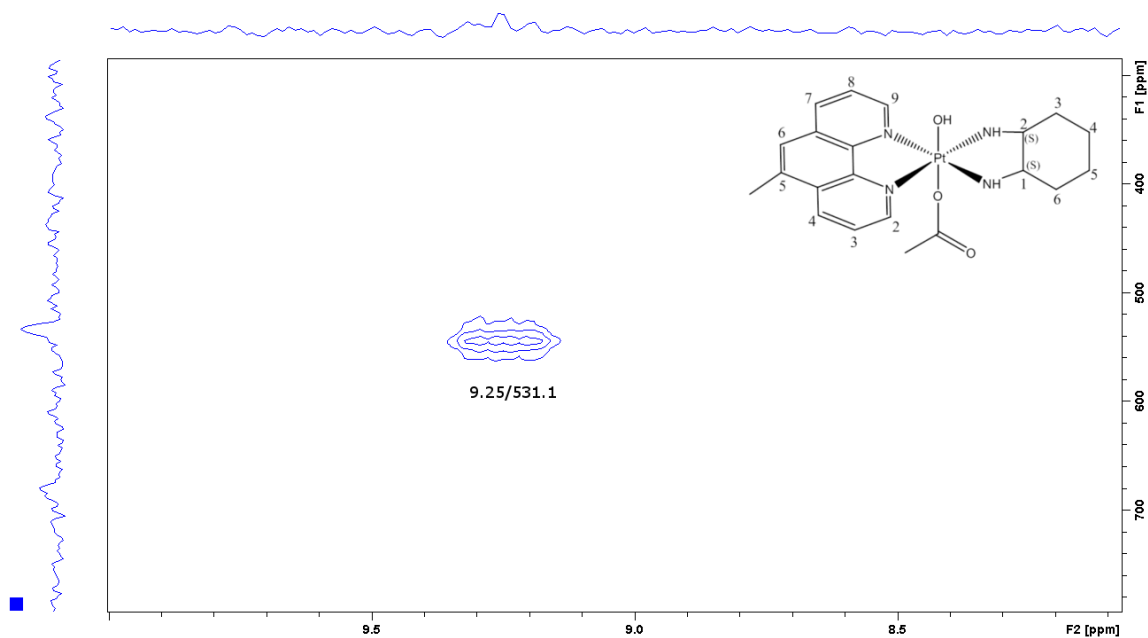


Figure A50: The ^1H - ^{195}Pt HMQC spectrum of 5MESS(OH)(OAc) in D_2O , performed on a Bruker Avance 400 MHz NMR spectrometer.

5MERR(OH)(OAc) ^1H NMR spectra

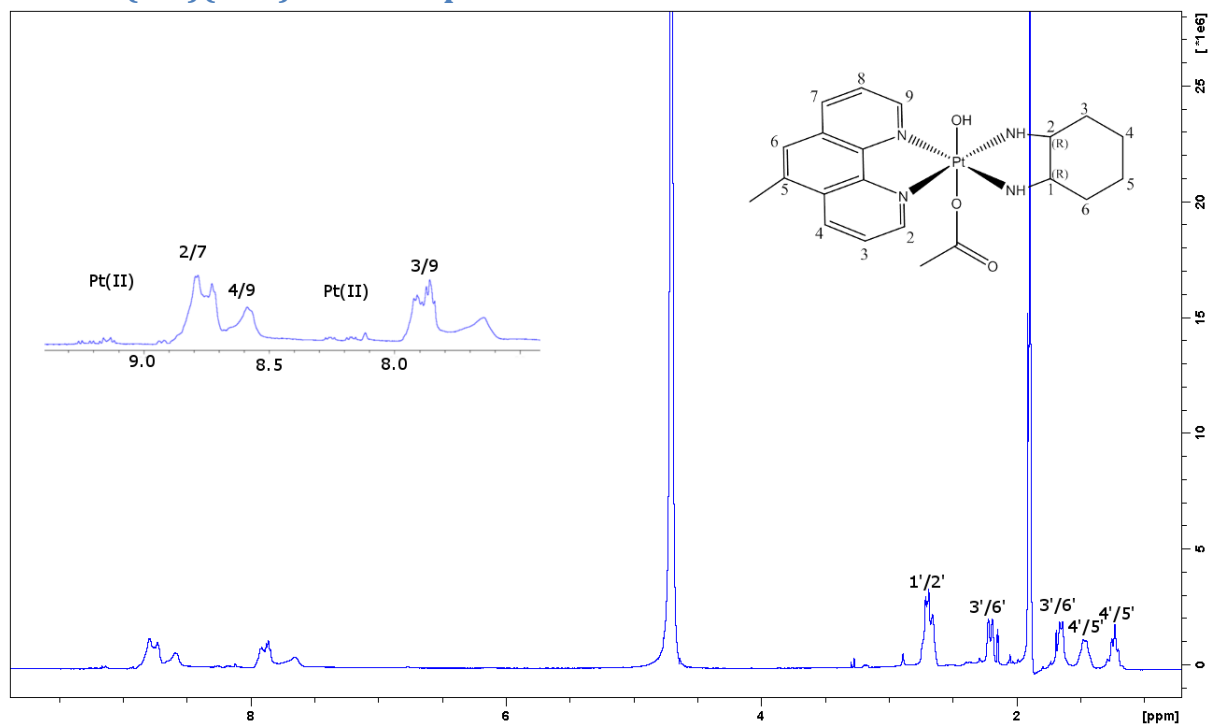


Figure A51: The ^1H spectrum of 5MERR(OH)(OAc) in D_2O , performed on a Bruker Avance 400 MHz NMR spectrometer.

5MERR(OH)(OAc) ^{195}Pt NMR spectra

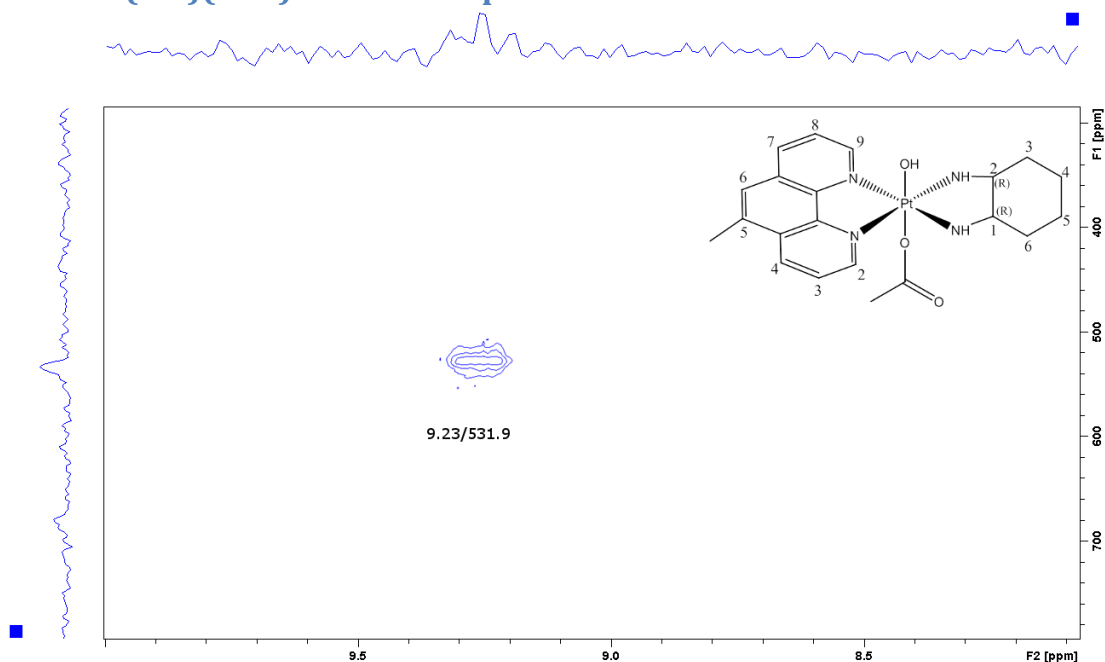


Figure A52: The ^1H - ^{195}Pt HMQC spectrum of 5MERR(OH)(OAc) in D_2O , performed on a Bruker Avance 400 MHz NMR spectrometer.

56MESS(OH)(OAc) ^1H NMR spectra

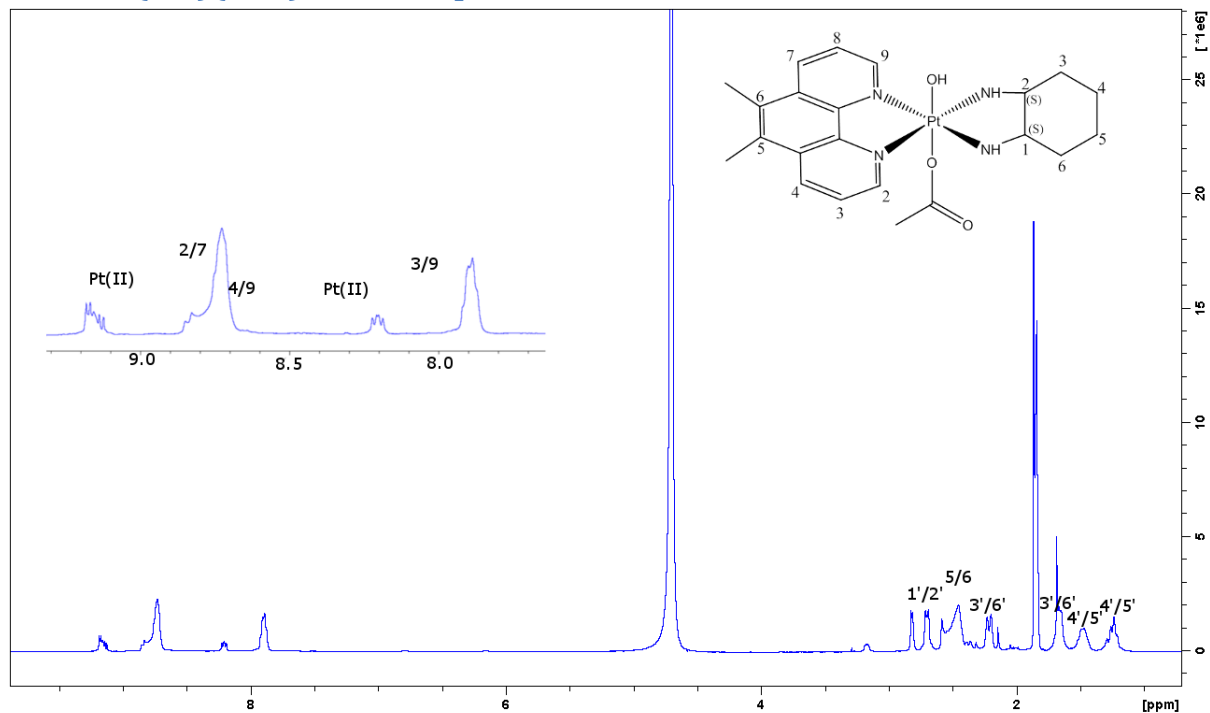


Figure A53: The ^1H spectrum of 56MESS(OH)(OAc) in D_2O , performed on a Bruker Avance 400 MHz NMR spectrometer.

56MESS(OH)(OAc) ^{195}Pt NMR spectra

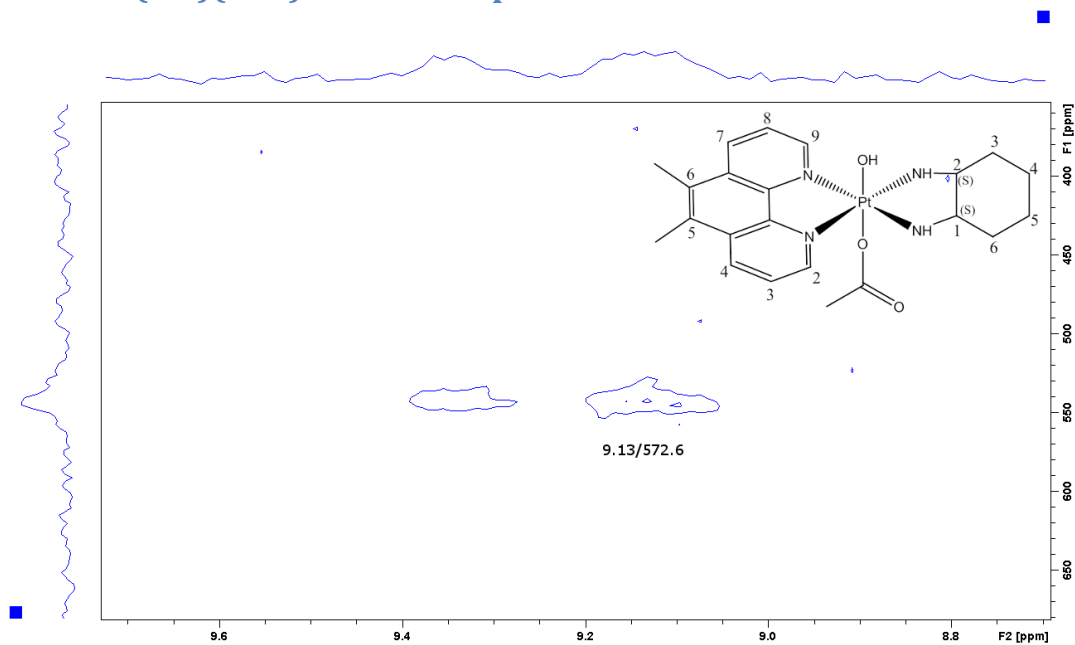


Figure A54: The ^1H - ^{195}Pt HMQC spectrum of 56MESS(OH)(OAc) in D_2O , performed on a Bruker Avance 400 MHz NMR spectrometer.

56MERR(OH)(OAc) ^1H NMR spectra

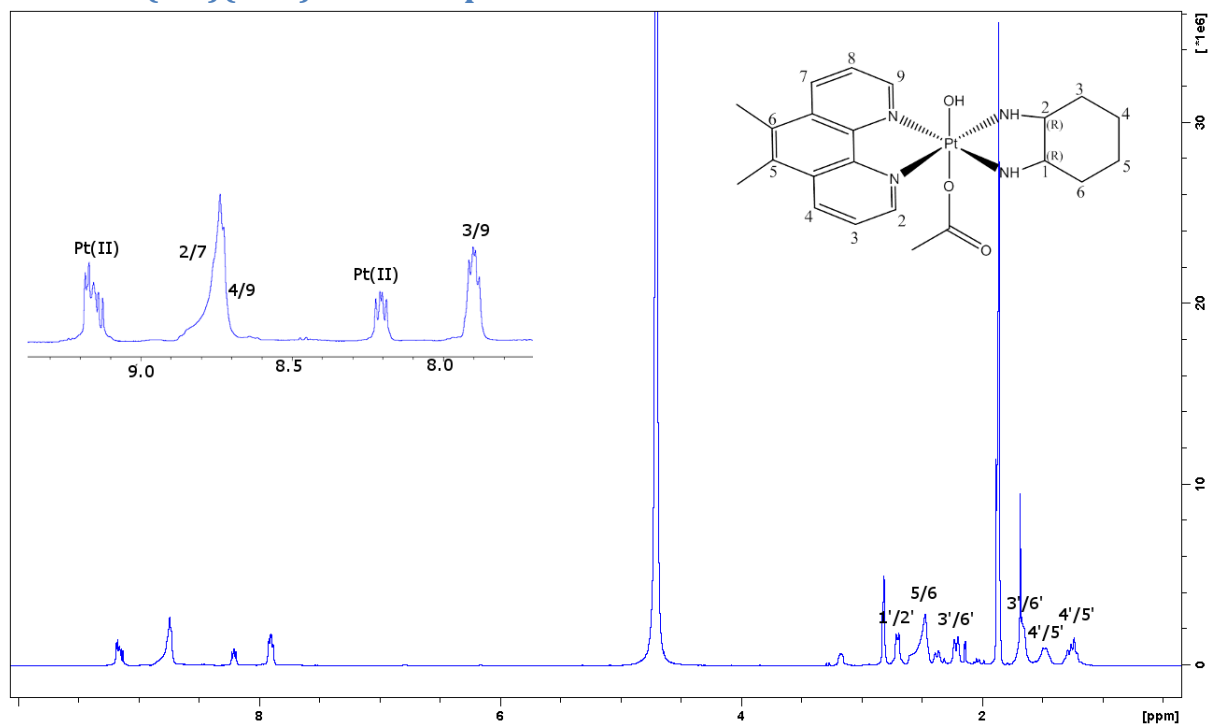


Figure A55: The ^1H spectrum of 56MERR(OH)(OAc) in D_2O , performed on a Bruker Avance 400 MHz NMR spectrometer.

56MERR(OH)(OAc) ^{195}Pt NMR spectra

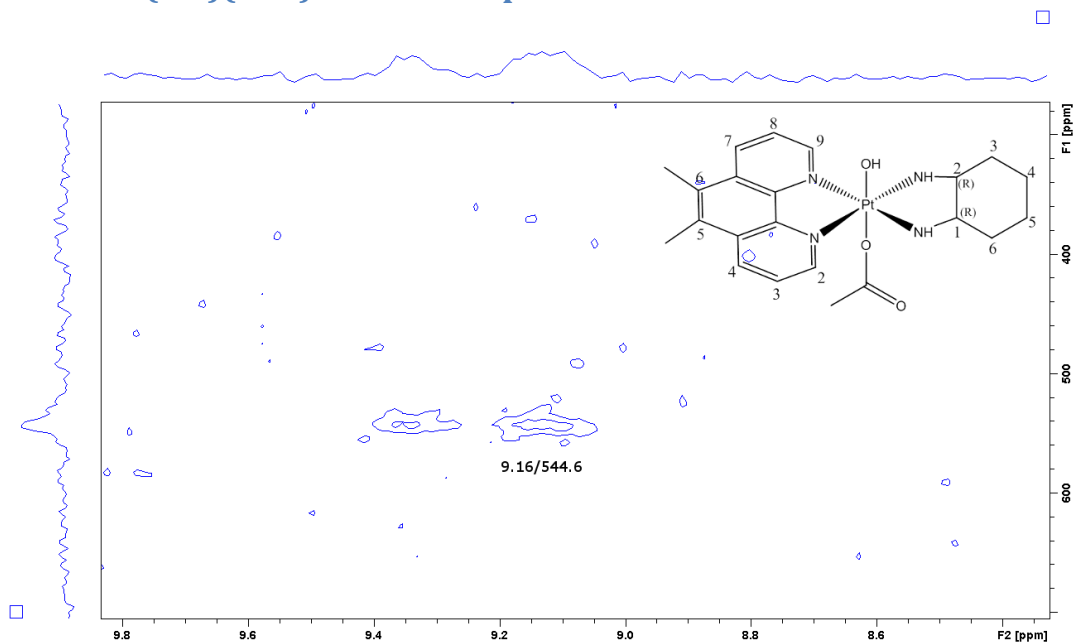


Figure A56: The ^1H - ^{195}Pt HMQC spectrum of 56MERR(OH)(OAc) in D_2O , performed on a Bruker Avance 400 MHz NMR spectrometer.

4MESS(OH)(OAc) ^1H NMR spectra

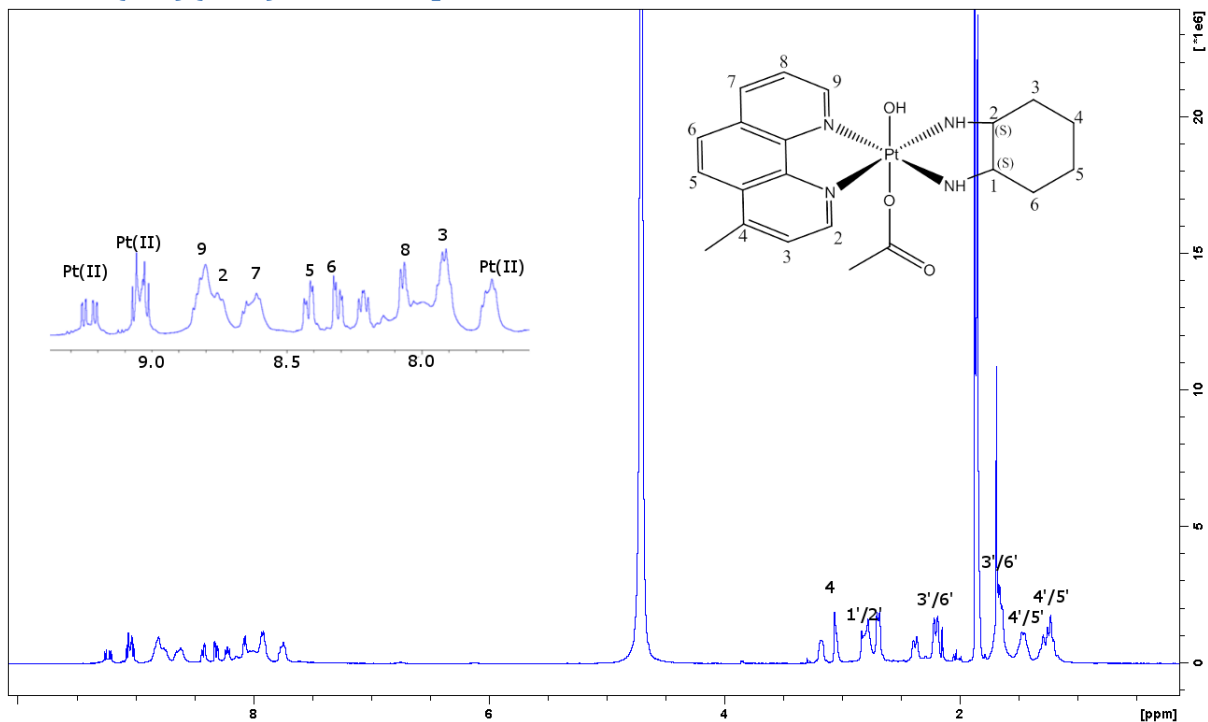


Figure A57: The ^1H spectrum of 4MESS(OH)(OAc) in D_2O , performed on a Bruker Avance 400 MHz NMR spectrometer.

4MESS(OH)(OAc) ^{195}Pt NMR spectra

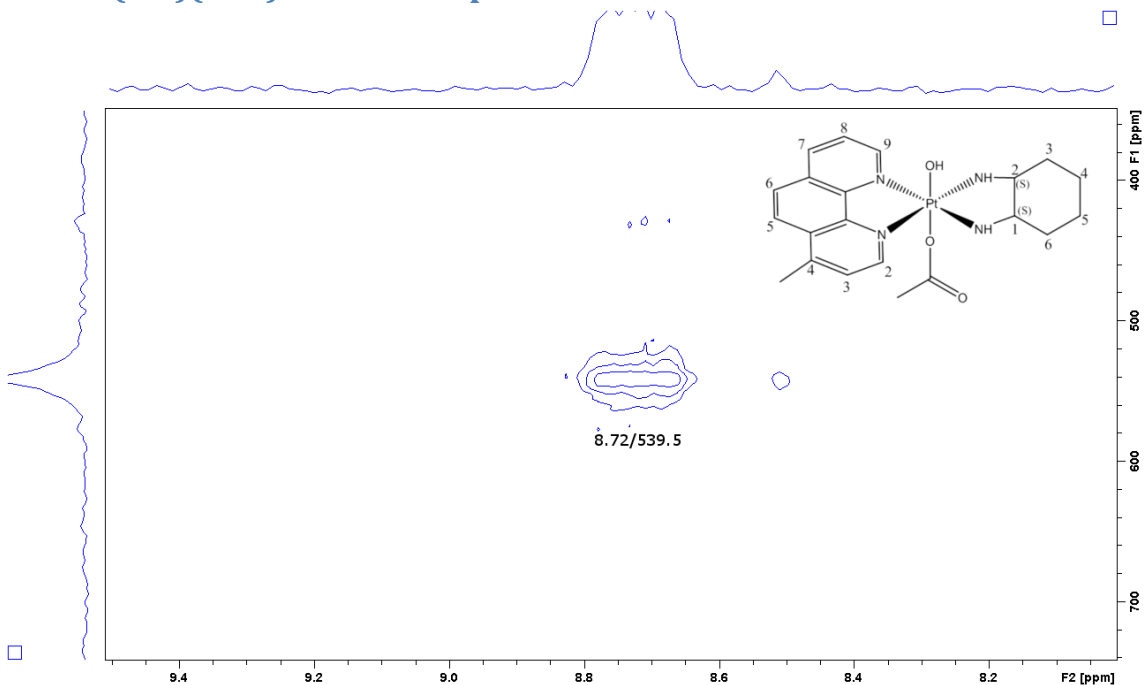


Figure A58: The ^1H - ^{195}Pt HMQC spectrum of 4MESS(OH)(OAc) in D_2O , performed on a Bruker Avance 400 MHz NMR spectrometer.

4MERR(OH)(OAc) ^1H NMR spectra

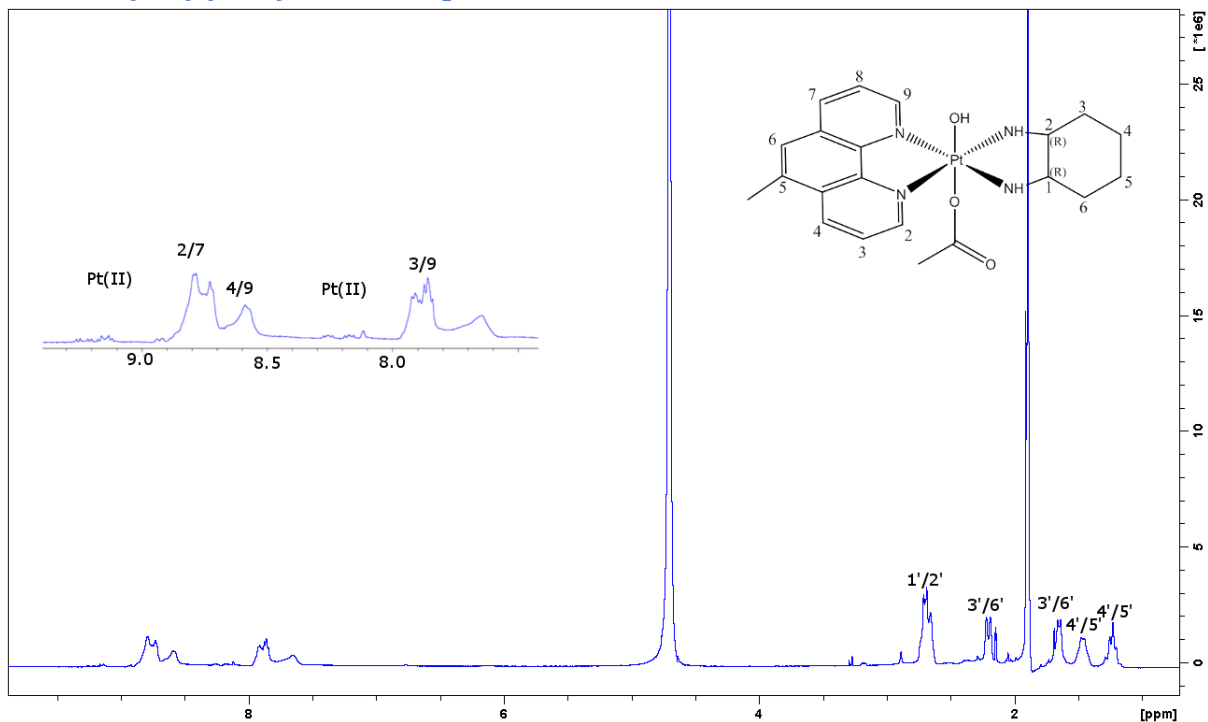


Figure A59: The ^1H spectrum of 4MERR(OH)(OAc) in D_2O , performed on a Bruker Avance 400 MHz NMR spectrometer.

4MERR(OH)(OAc) ^{195}Pt NMR spectra

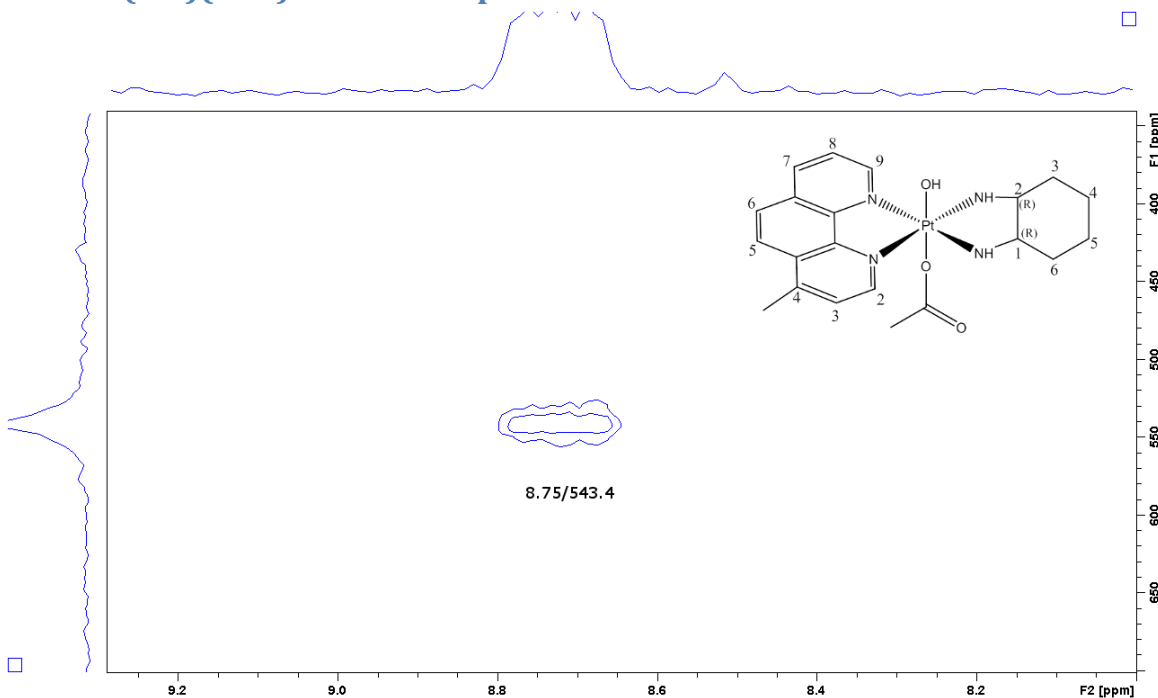


Figure A60: The ^1H - ^{195}Pt HMQC spectrum of 4MERR(OH)(OAc) in D_2O , performed on a Bruker Avance 400 MHz NMR spectrometer.

44BPYSS(OH)(OAc) ^1H NMR spectra

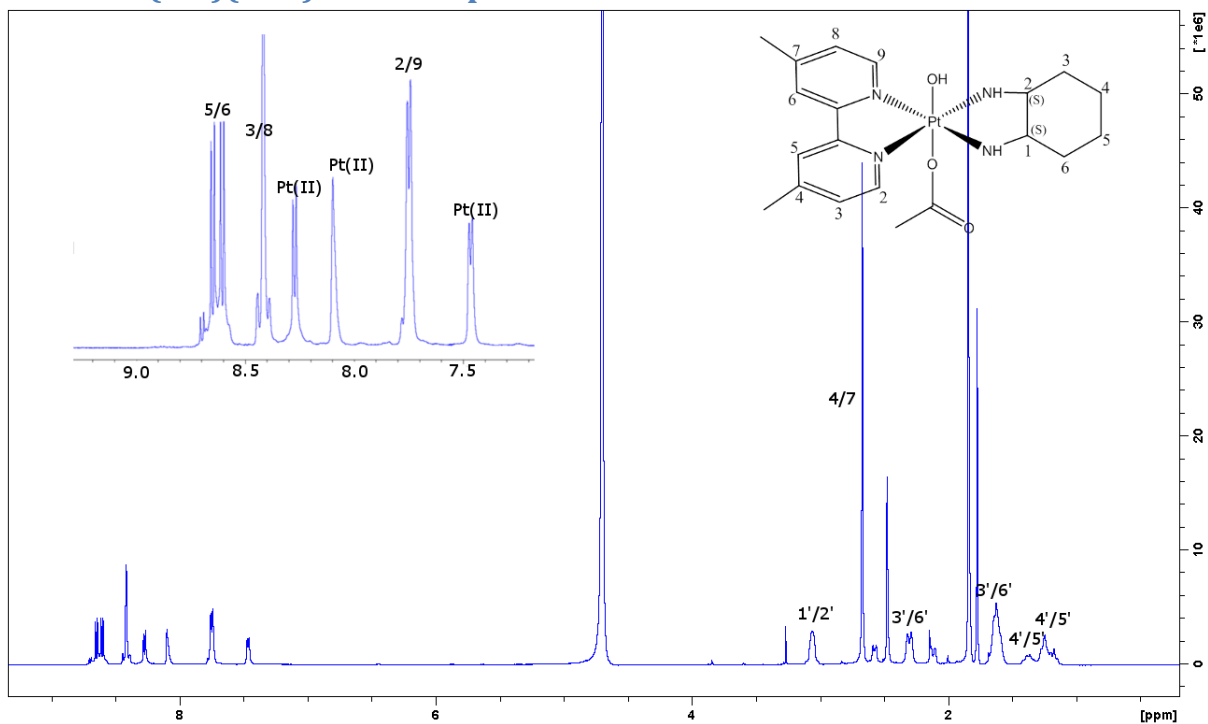


Figure A61: The spectrum of 44BPYSS(OH)(OAc) in D_2O , performed on a Bruker Avance 400 MHz NMR spectrometer.

BPYSS(OH)(OAc) ^{195}Pt NMR spectra

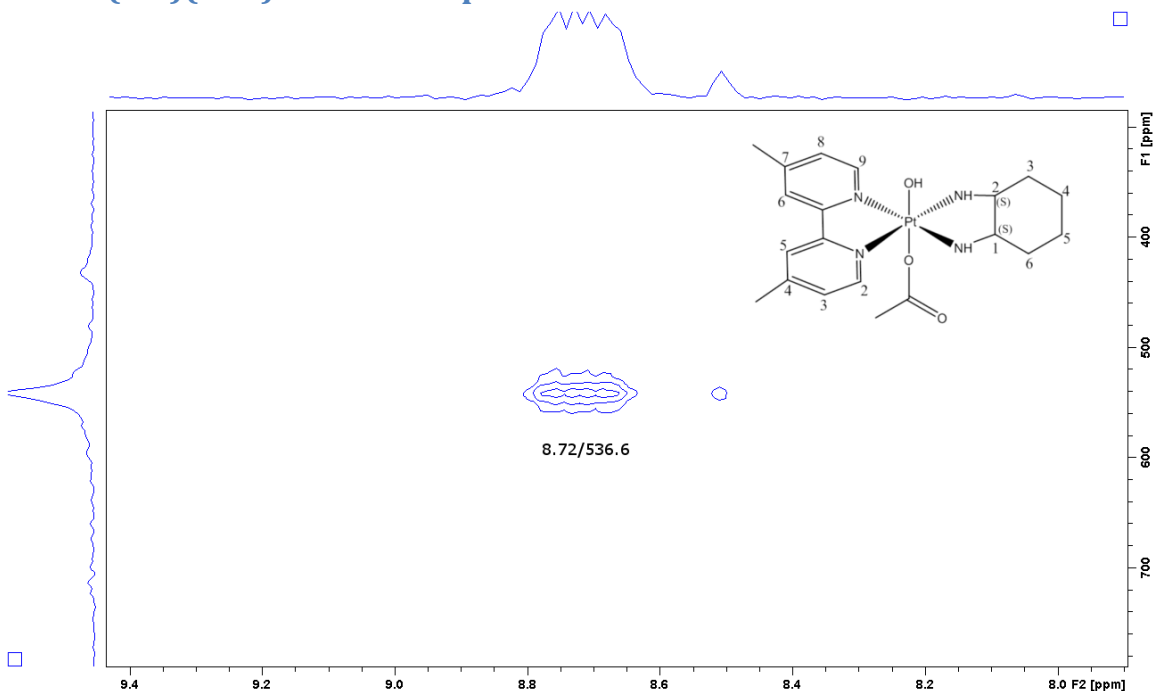


Figure A62: The ^1H - ^{195}Pt HMQC spectrum of 44BPYSS(OH)(OAc) in D_2O , performed on a Bruker Avance 400 MHz NMR spectrometer.

44BPYRR(OH)(OAc) ^1H NMR spectra

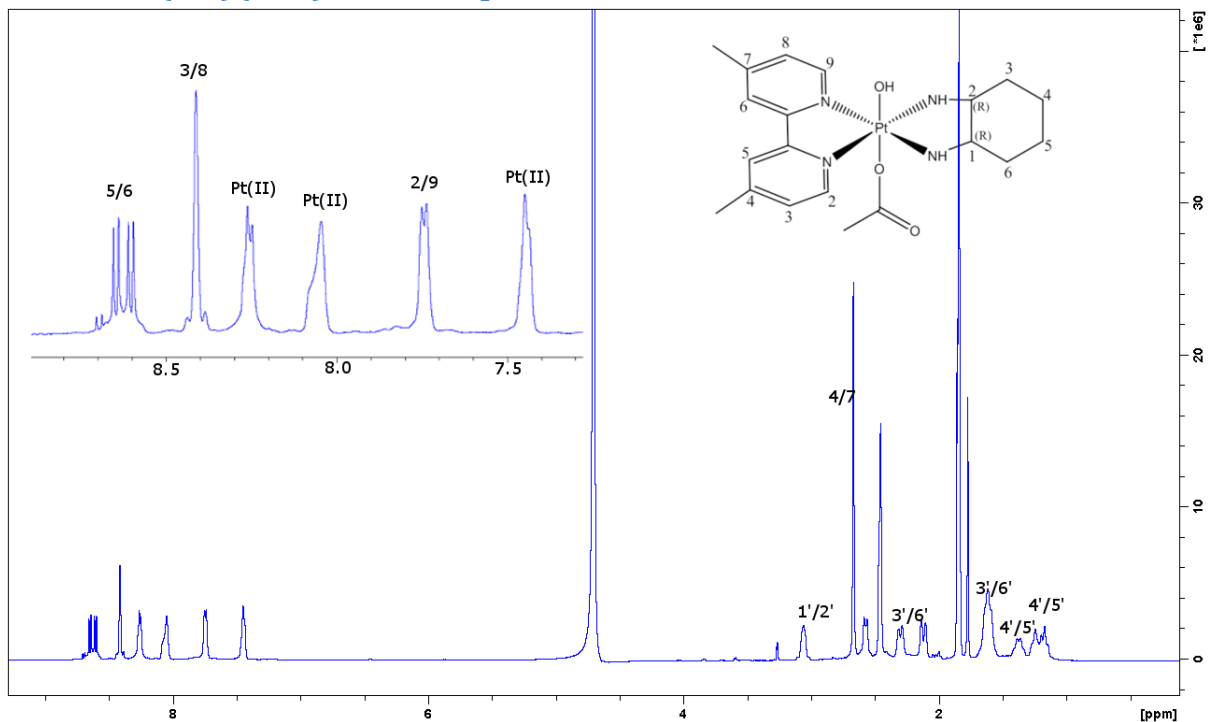


Figure A63: The ^1H spectrum of 44BPYRR(OH)(OAc) in D_2O , performed on a Bruker Avance 400 MHz NMR spectrometer.

44BPYRR(OH)(OAc) ^{195}Pt NMR spectra

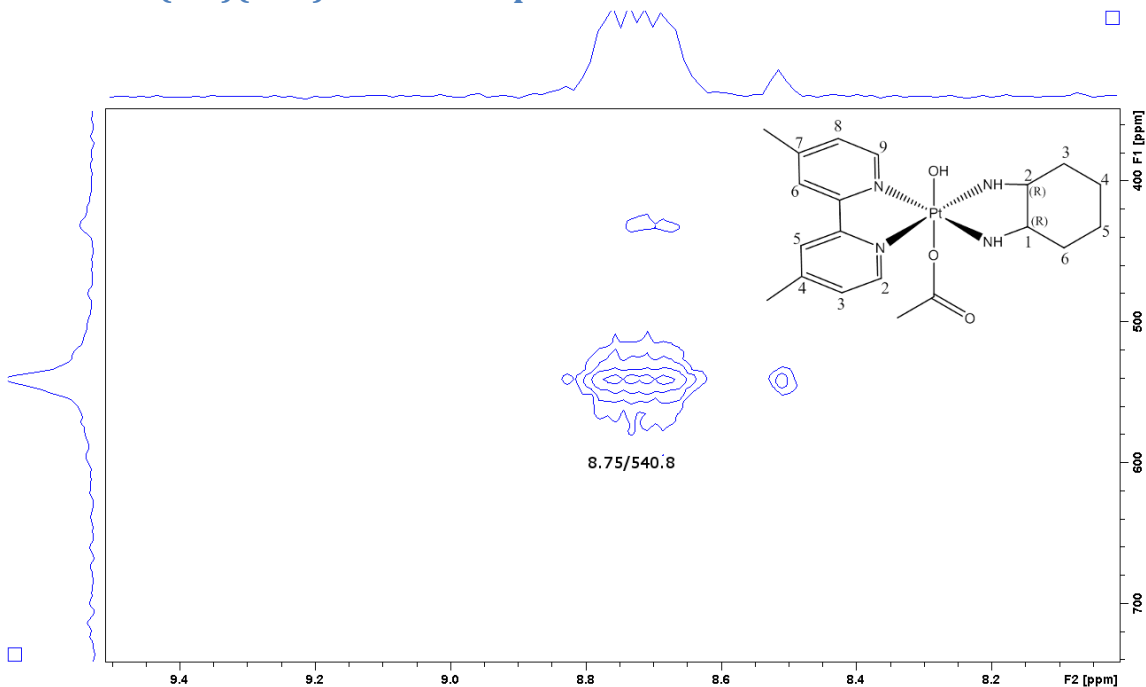


Figure A64: The ^1H - ^{195}Pt HMQC spectrum of 44BPYRR(OH)(OAc) in D_2O , performed on a Bruker Avance 400 MHz NMR spectrometer.

PHENSS(OH)₂ ¹H NMR spectra

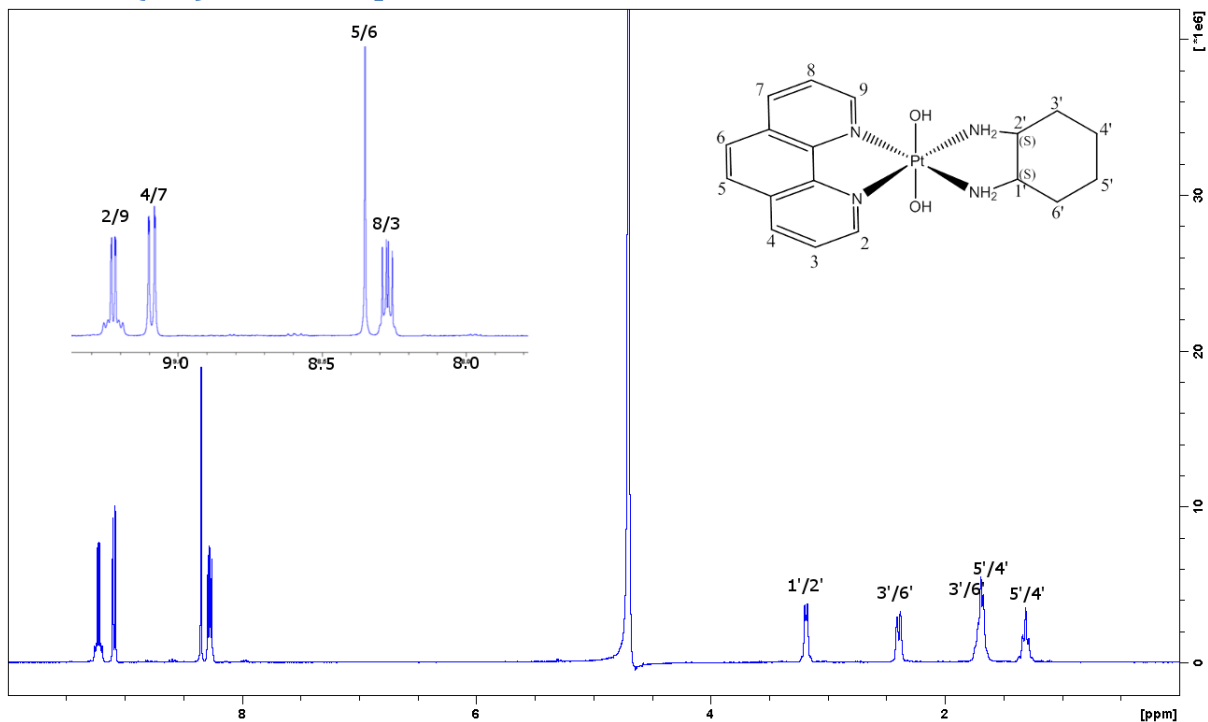


Figure A65: The ¹H spectrum of PHENSS(OH)₂ in D₂O, performed on a Bruker Avance 400 MHz NMR spectrometer.

PHENSS(OH)₂ ¹⁹⁵Pt NMR spectra

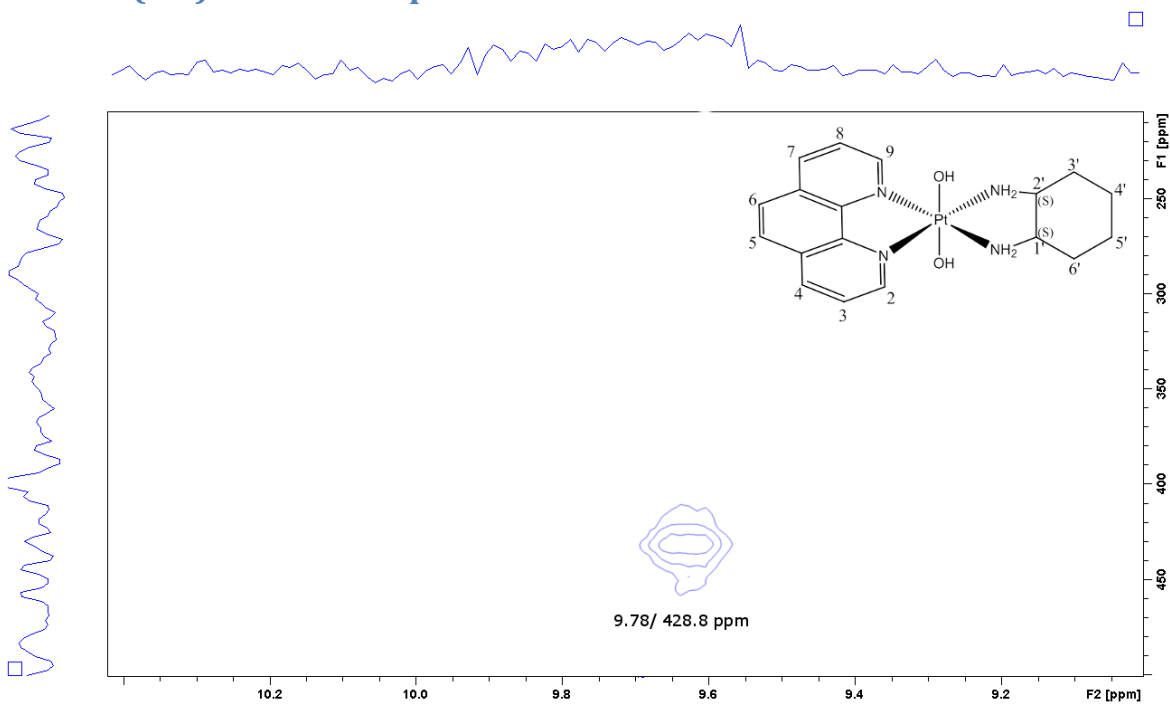


Figure A66: The ¹H-¹⁹⁵Pt HMQC spectrum of PHENSS(OH)₂ in D₂O, performed on a Bruker Avance 400 MHz NMR spectrometer.

PHENRR(OH)₂ ¹H NMR spectra

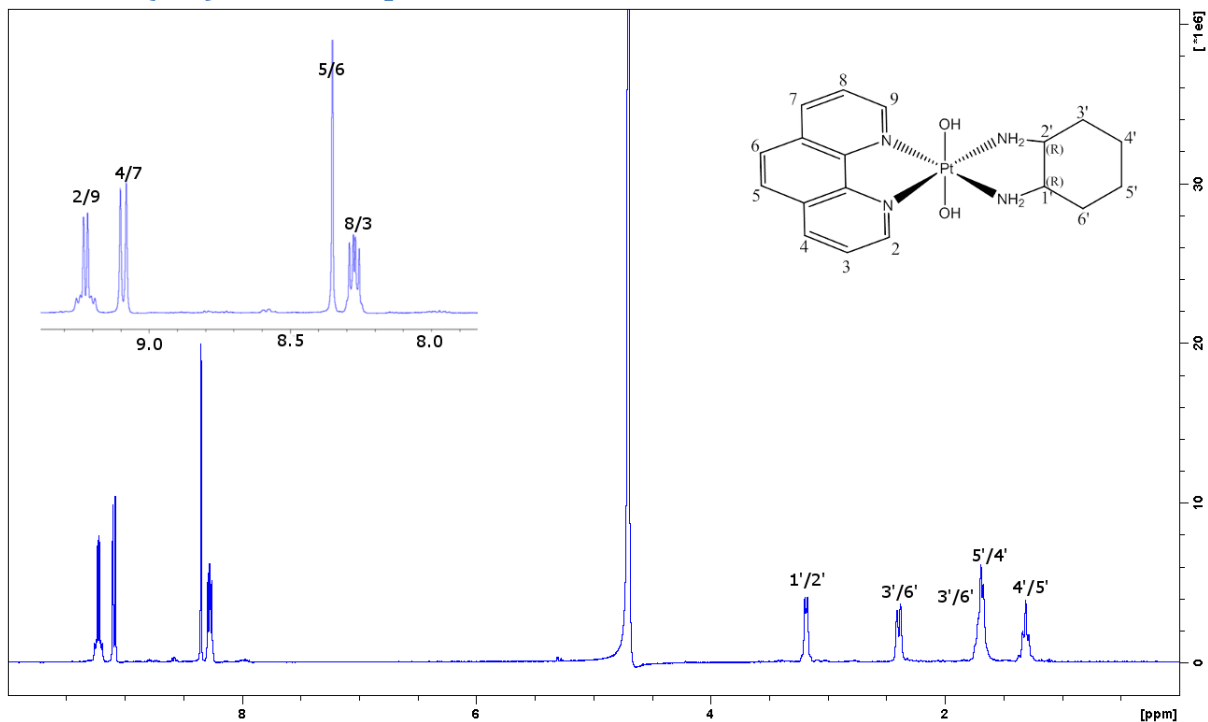


Figure A67: The ¹H spectrum of PHENRR(OH)₂ in D₂O, performed on a Bruker Avance 400 MHz NMR spectrometer.

PHENRR(OH)₂ ¹⁹⁵Pt NMR spectra

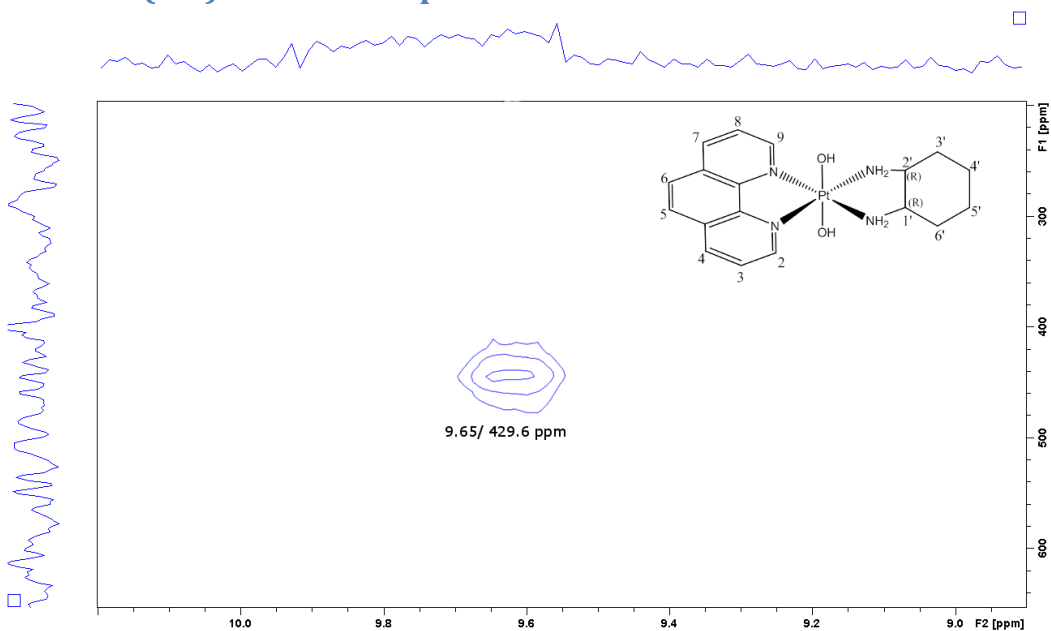


Figure A68: The ¹H-¹⁹⁵Pt HMQC spectrum of PHENRR(OH)₂ in D₂O, performed on a Bruker Avance 400 MHz NMR spectrometer.

5MESS(OH)₂ ¹H NMR spectra

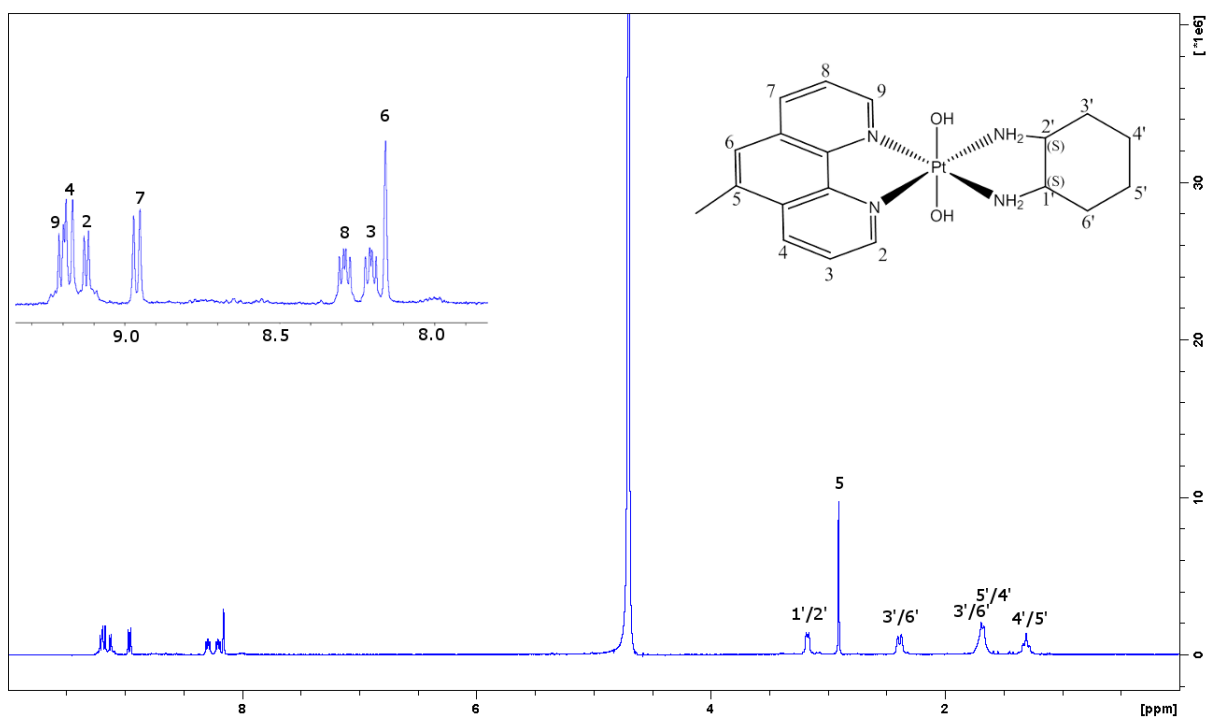


Figure A69: The ¹H spectrum of 5MESS(OH)₂ in D₂O, performed on a Bruker Avance 400 MHz NMR spectrometer.

5MESS(OH)₂ ¹⁹⁵Pt NMR spectra

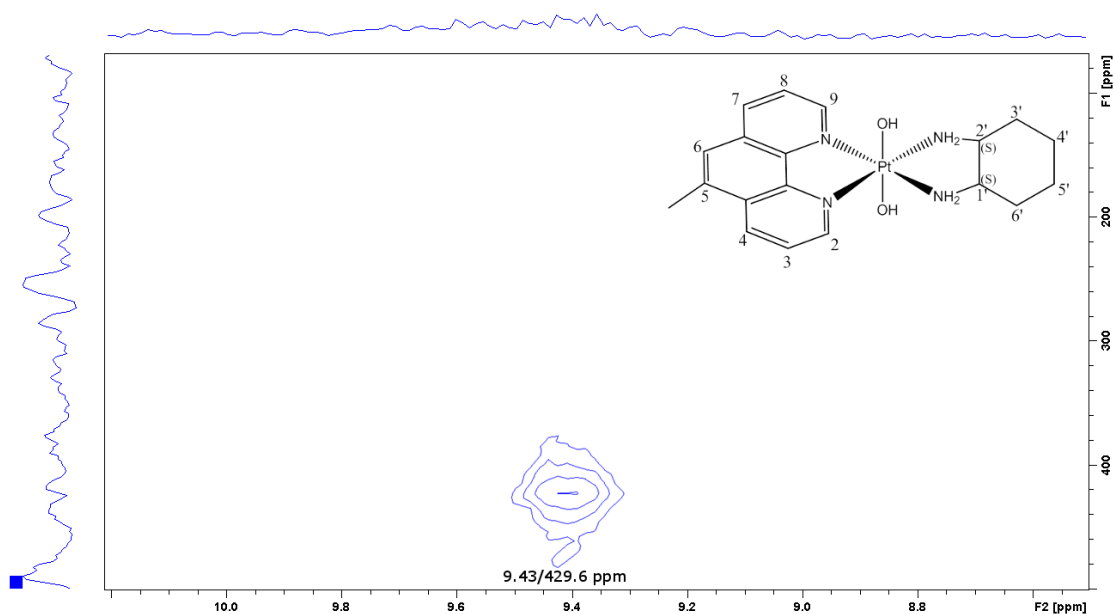


Figure A70: The ¹H-¹⁹⁵Pt HMQC spectrum of 5MESS(OH)₂ in D₂O, performed on a Bruker Avance 400 MHz NMR spectrometer.

5MERR(OH)₂ ¹H NMR spectra

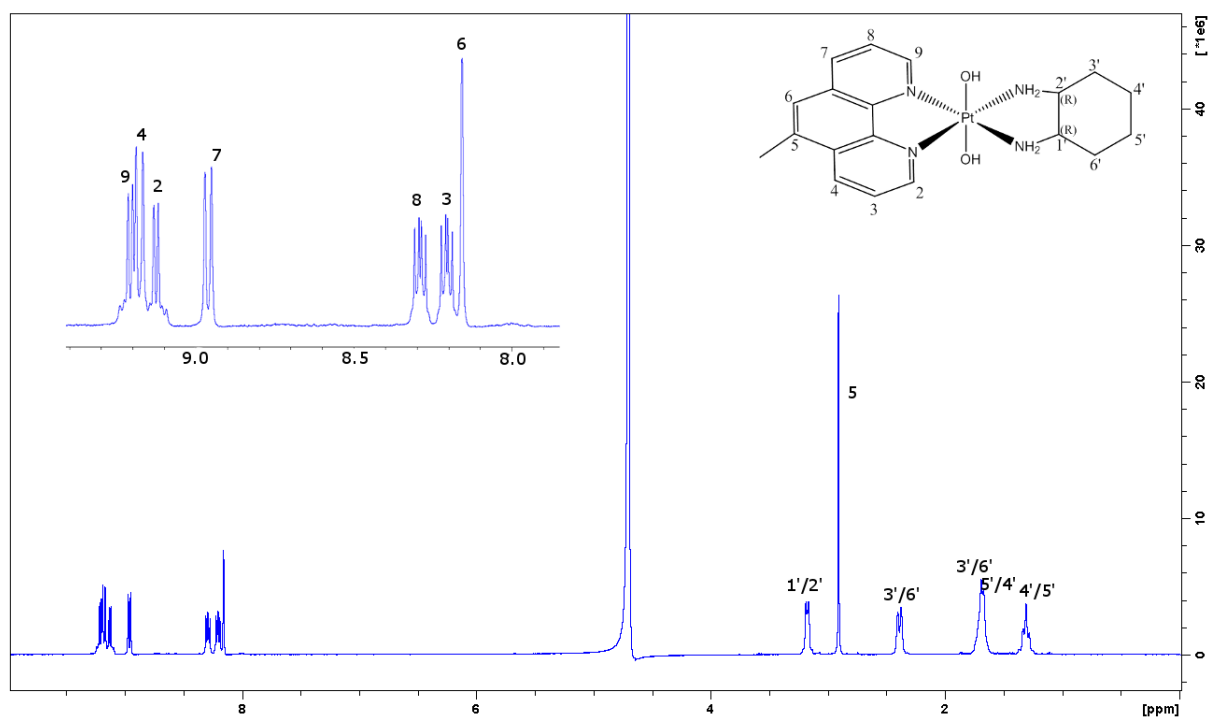


Figure A71: The ¹H spectrum of 5MERR(OH)₂ in D₂O, performed on a Bruker Avance 400 MHz NMR spectrometer.

5MERR(OH)₂ ¹H-¹⁹⁵Pt NMR spectra

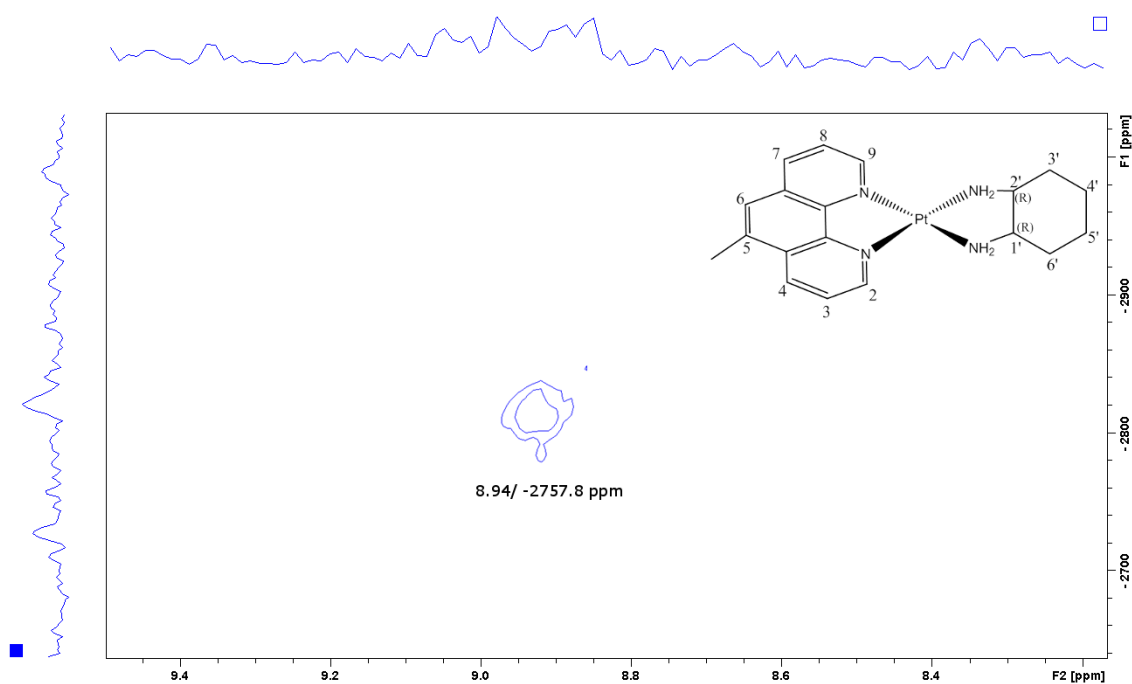


Figure A72: The ¹H-¹⁹⁵Pt HMQC spectrum of 5MERR(OH)₂ in D₂O, performed on a Bruker Avance 400 MHz NMR spectrometer.

56MESS(OH)₂ ¹H NMR spectra

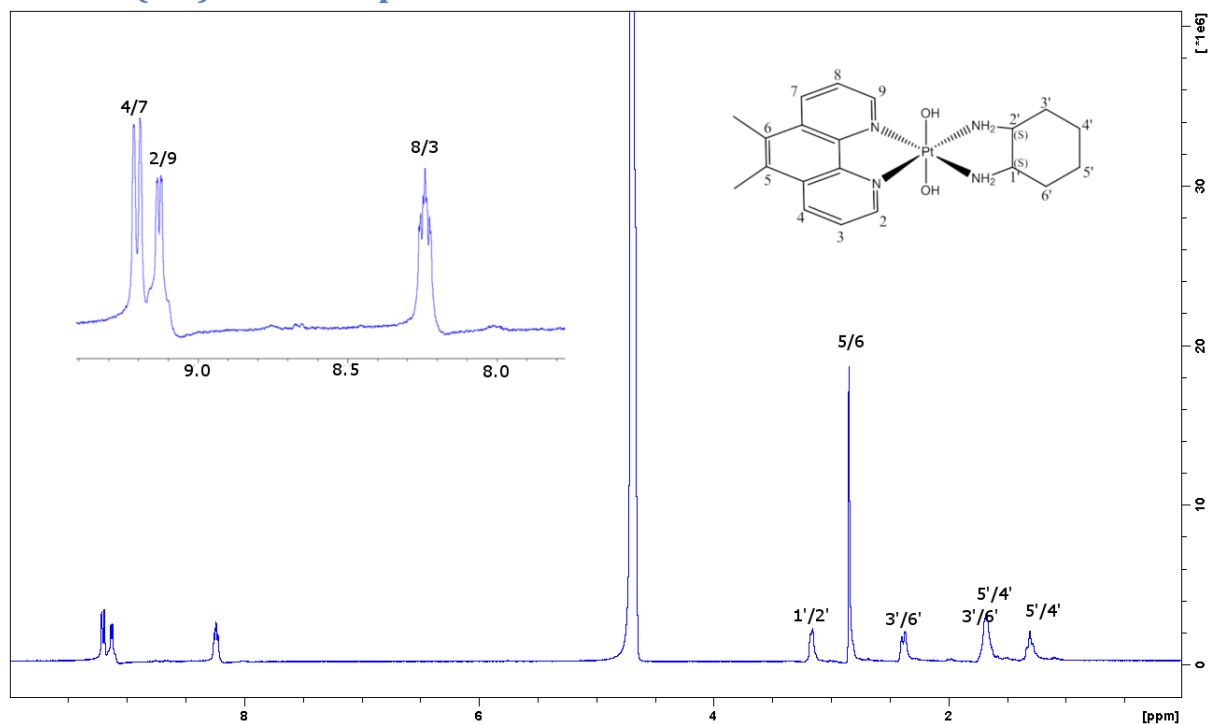


Figure A73: The ¹H spectrum of 56MESS(OH)₂ in D₂O, performed on a Bruker Avance 400 MHz NMR spectrometer.

56MESS(OH)₂ ¹⁹⁵Pt NMR spectra

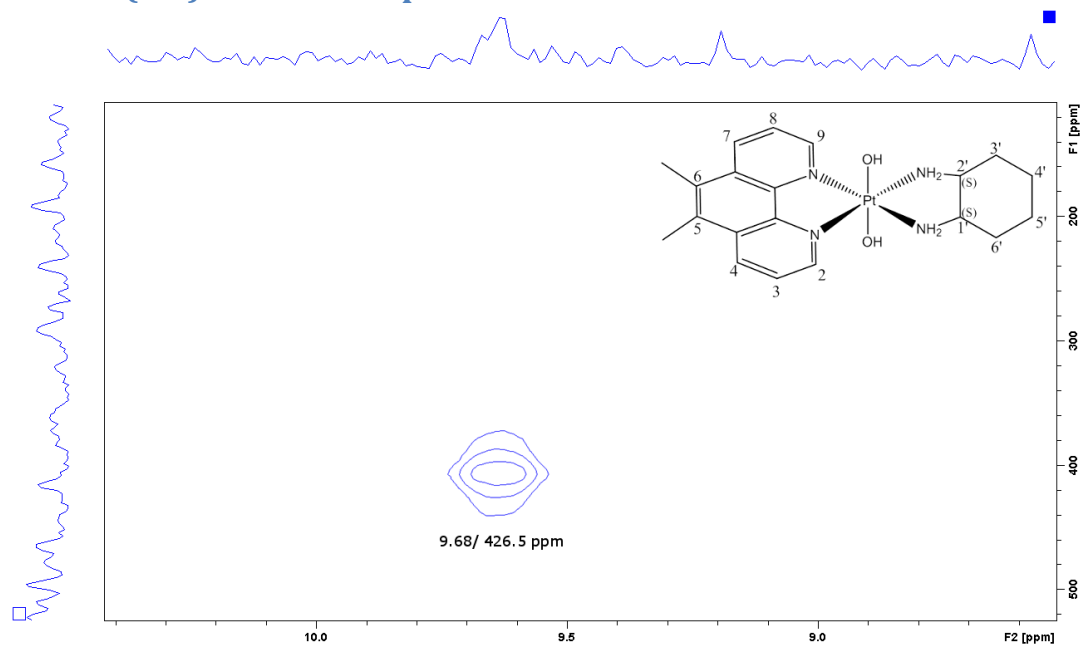


Figure A74: The ¹H-¹⁹⁵Pt HMQC spectrum of 56MESS(OH)₂ in D₂O, performed on a Bruker Avance 400 MHz NMR spectrometer.

56MERR(OH)₂ ¹H NMR spectra

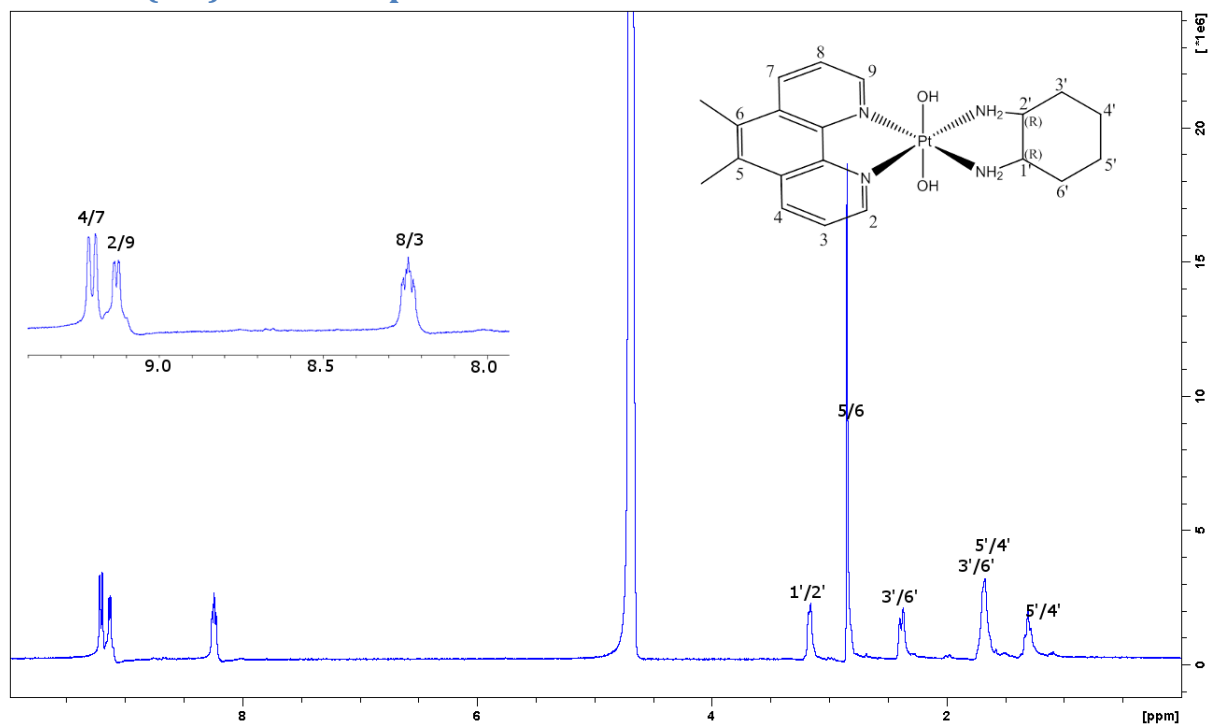


Figure A75: The ¹H spectrum of 56MERR(OH)₂ in D₂O, performed on a Bruker Avance 400 MHz NMR spectrometer.

56MERR(OH)₂ ¹⁹⁵Pt NMR spectra

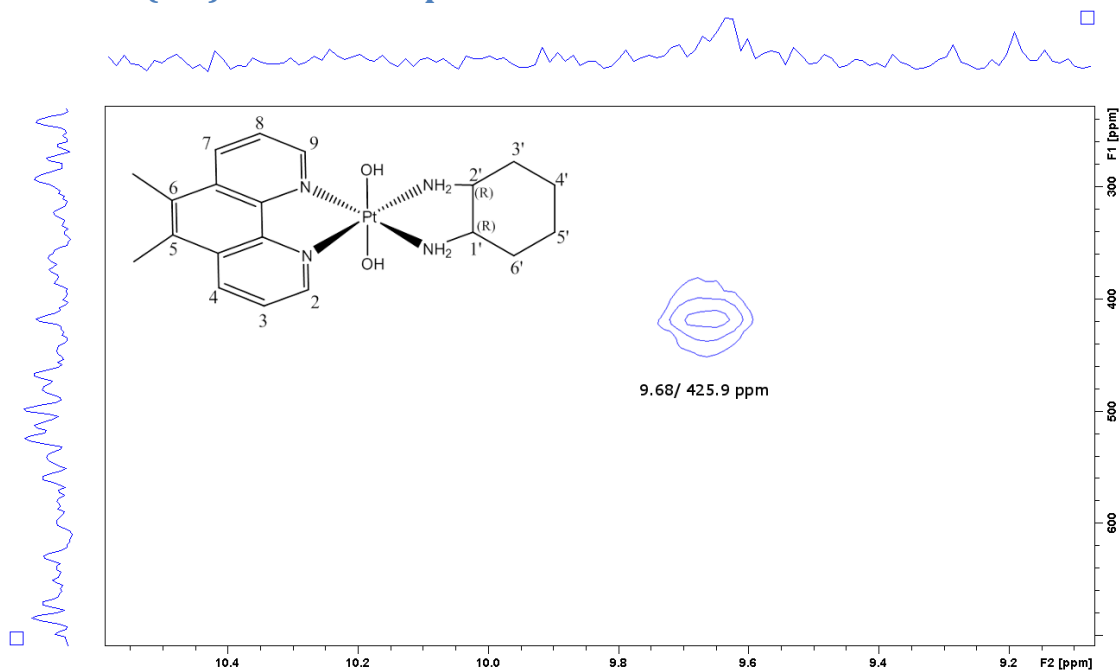


Figure A76: The ¹H-¹⁹⁵Pt HMQC spectrum of 56MERR(OH)₂ in D₂O, performed on a Bruker Avance 400 MHz NMR spectrometer.

4MESS(OH)₂ ¹H NMR spectra

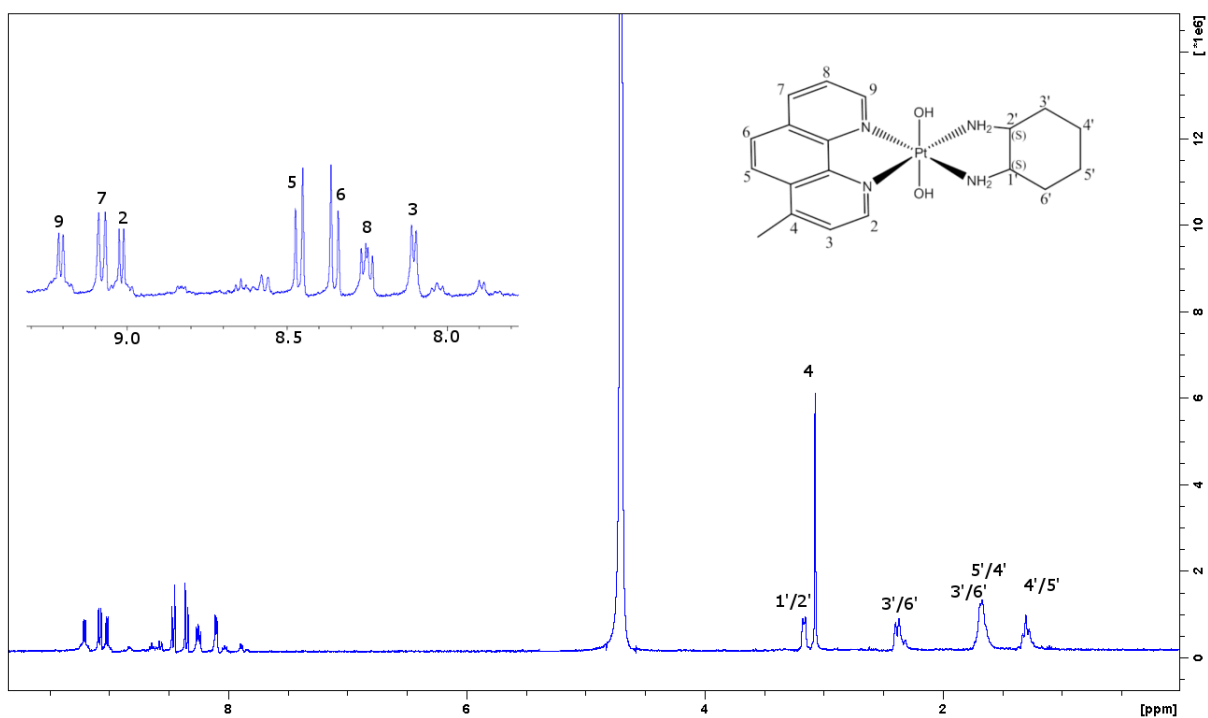


Figure A77: The ¹H spectrum of 4MESS(OH)₂ in D₂O, performed on a Bruker Avance 400 MHz NMR spectrometer.

4MESS(OH)₂ ¹⁹⁵Pt NMR spectra

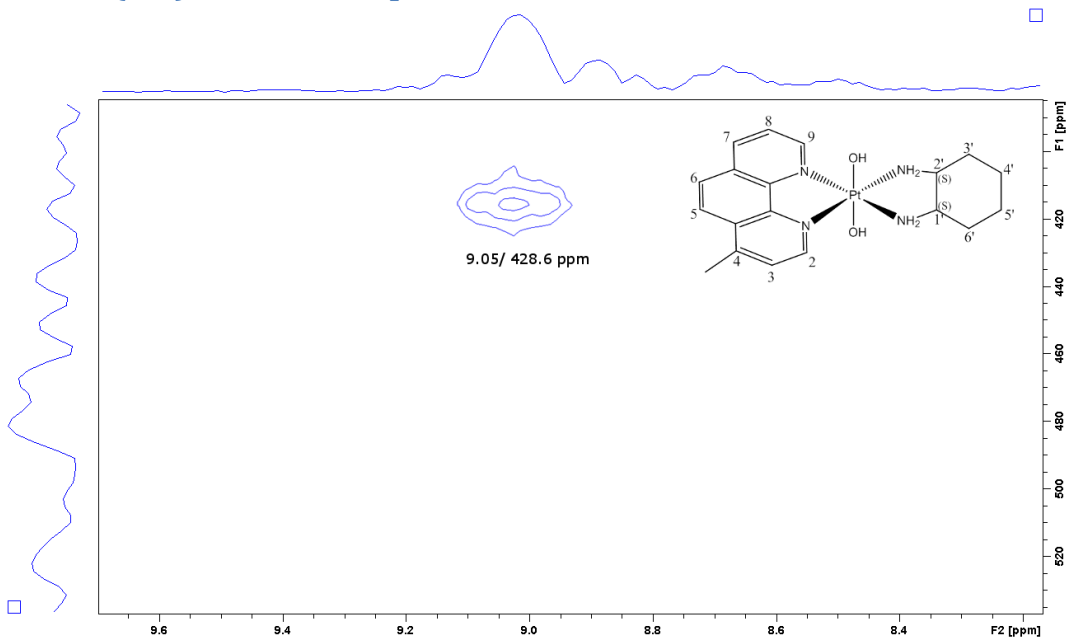


Figure A78: The ¹H-¹⁹⁵Pt HMQC spectrum of 4MESS(OH)₂ in D₂O, performed on a Bruker Avance 400 MHz NMR spectrometer.

4MERR(OH)₂ ¹H NMR spectra

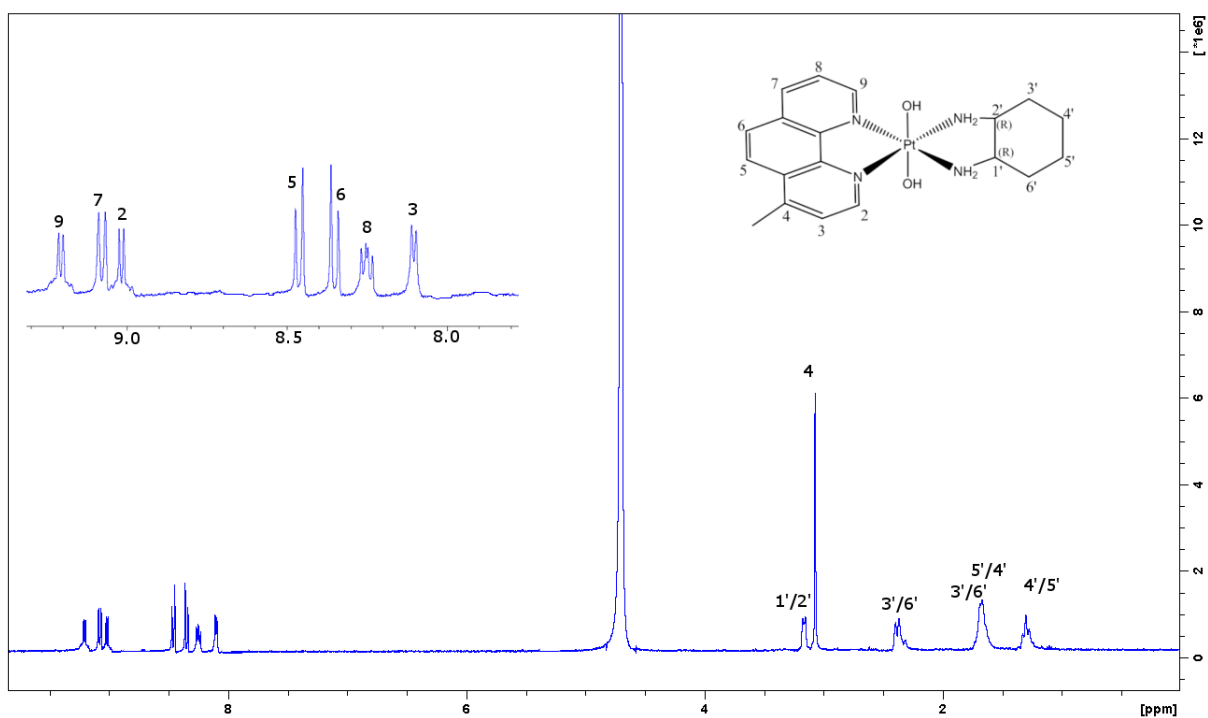


Figure A79: The ¹H spectrum of 4MERR(OH)₂ in D₂O, performed on a Bruker Avance 400 MHz NMR spectrometer.

4MERR(OH)₂ ¹⁹⁵Pt NMR spectra

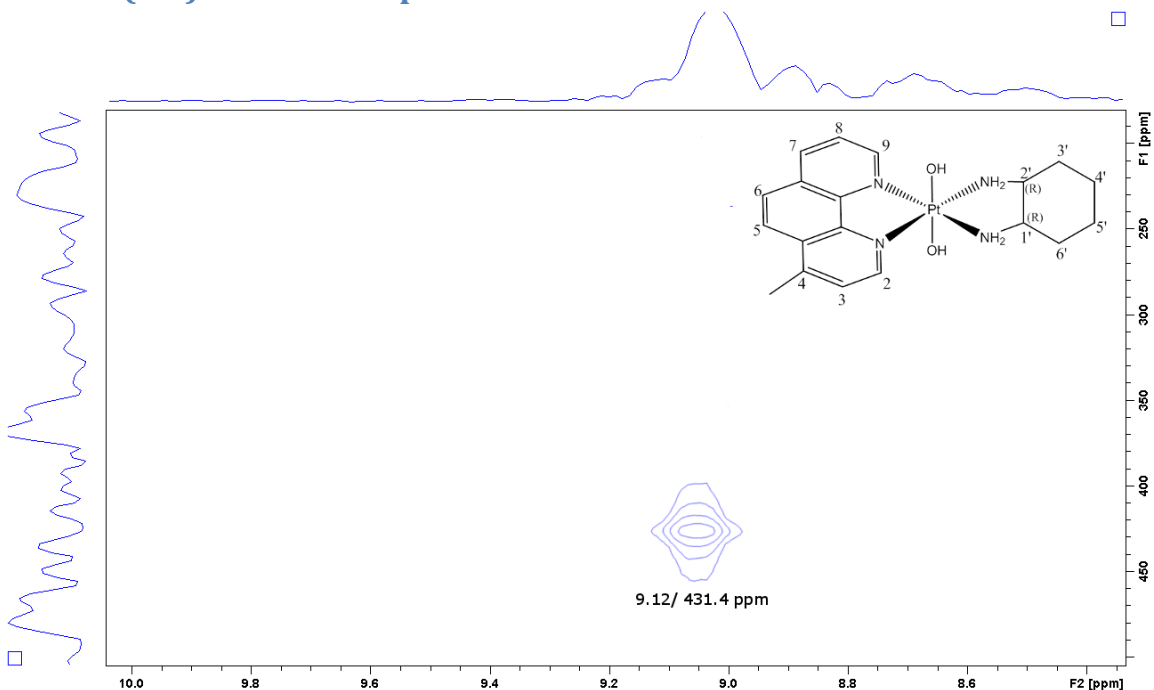


Figure A80: The ¹H-¹⁹⁵Pt HMQC spectrum of 4MERR(OH)₂ in D₂O, performed on a Bruker Avance 400 MHz NMR spectrometer.

44BPYSS(OH)₂ ¹H NMR spectra

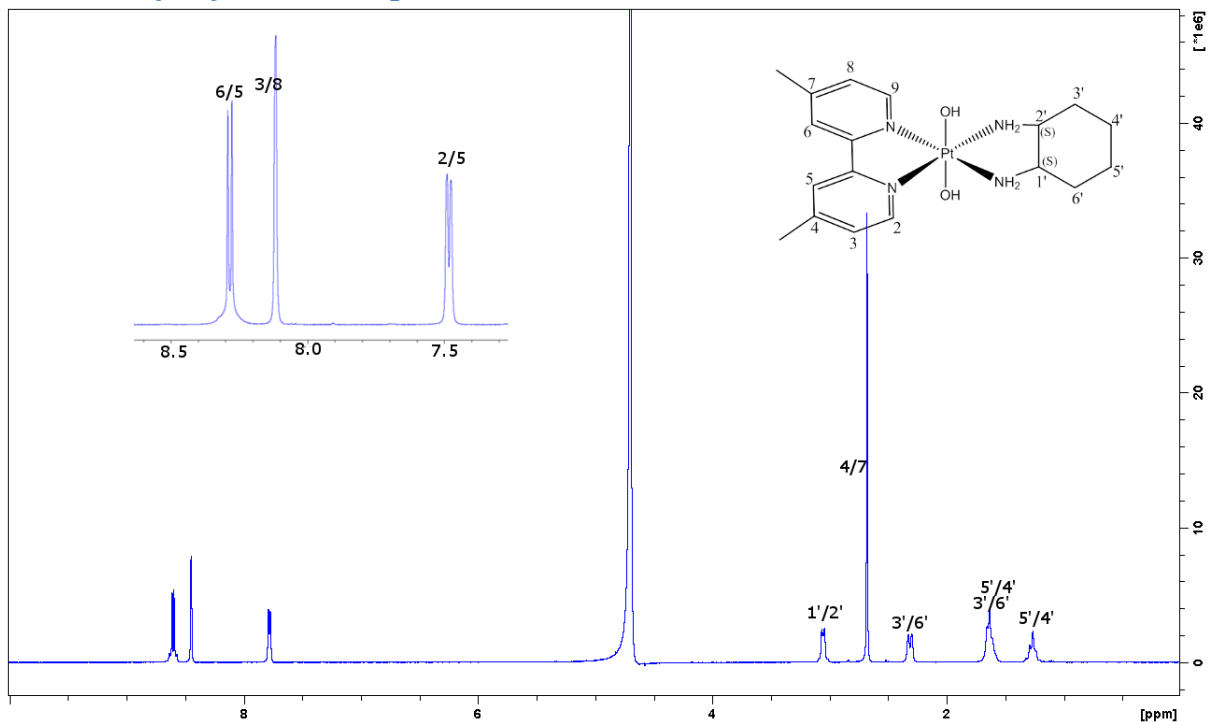


Figure A81: The ¹H spectrum of 44BPYSS(OH)₂ in D₂O, performed on a Bruker Avance 400 MHz NMR spectrometer.

44BPYSS(OH)₂ ¹⁹⁵Pt NMR spectra

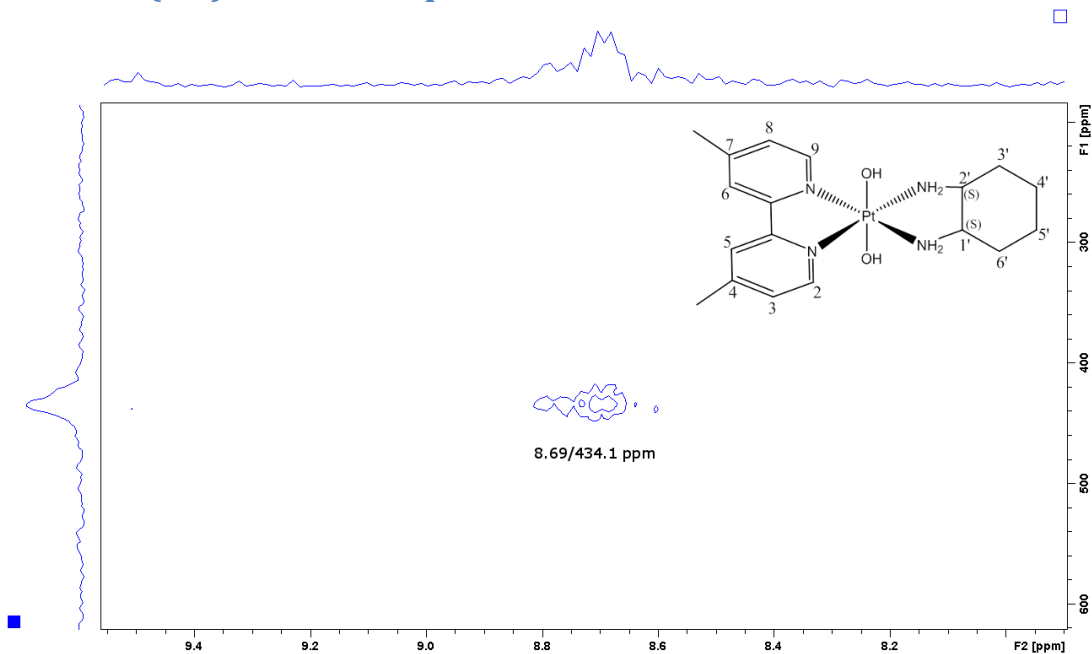


Figure A82: The ¹H-¹⁹⁵Pt HMQC spectrum of 44BPYSS(OH)₂ in D₂O, performed on a Bruker Avance 400 MHz NMR spectrometer.

44BPYRR(OH)₂ ¹H NMR spectra

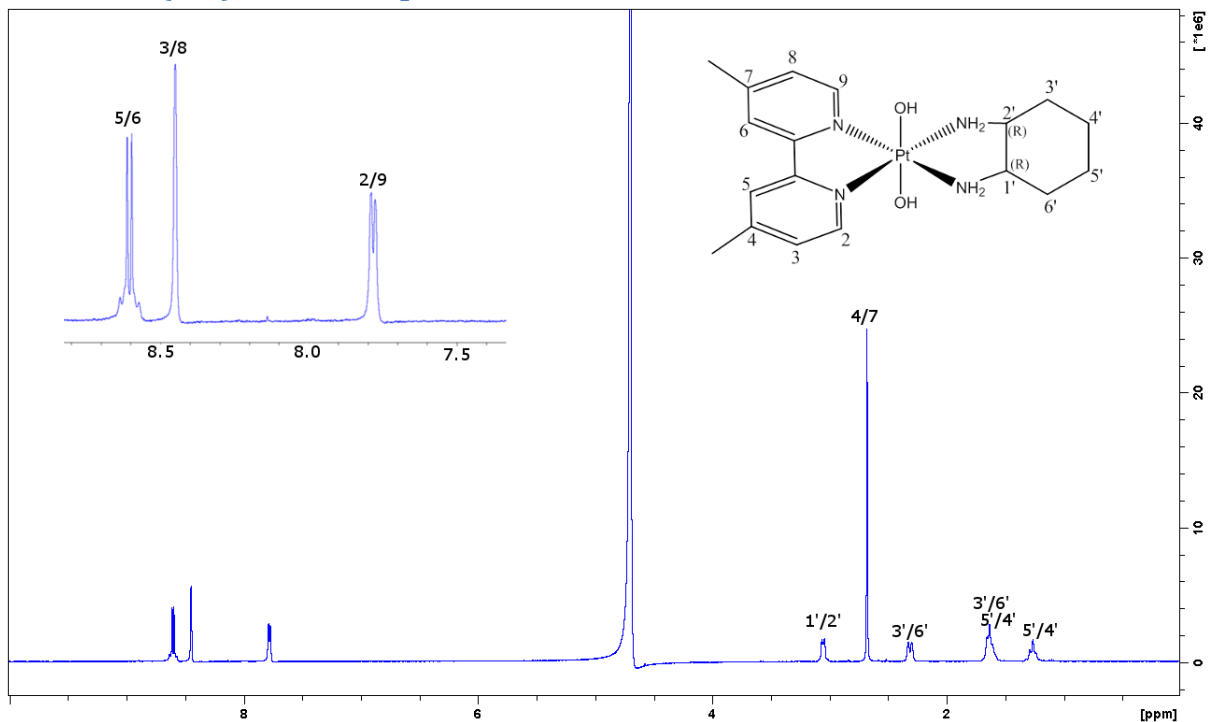


Figure A83: The ¹H spectrum of 44BPYRR(OH)₂ in D₂O, performed on a Bruker Avance 400 MHz NMR spectrometer.

44BPYRR(OH)₂ ¹⁹⁵Pt NMR spectra

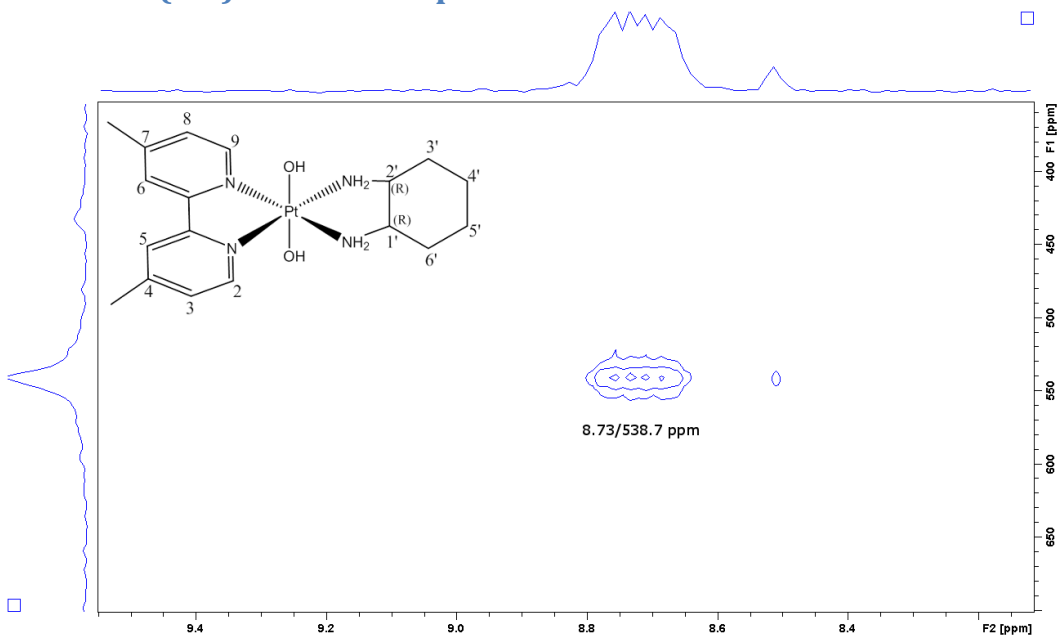


Figure A84: The ¹H-¹⁹⁵Pt HMQC spectrum of 44BPYRR(OH)₂ in D₂O, performed on a Bruker Avance 400 MHz NMR spectrometer.

PHENSS(OH)(Succ) ^1H NMR spectra

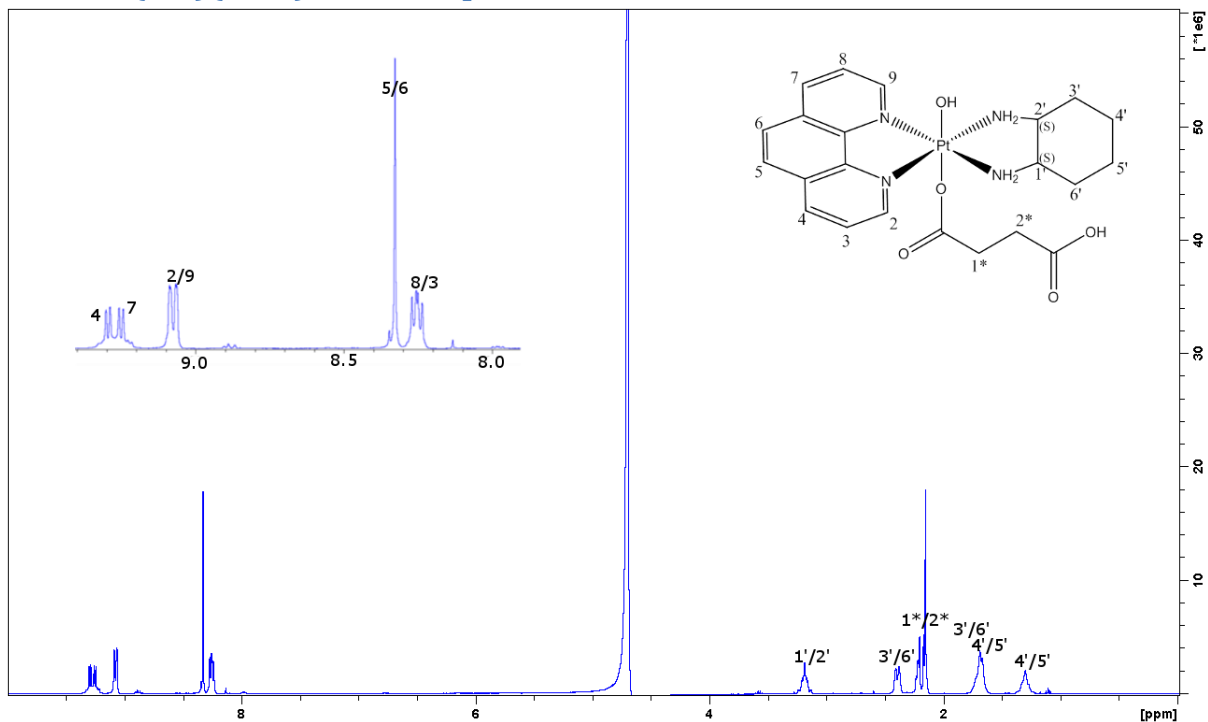


Figure A85: The ^1H spectrum of PHENSS(OH)(Succ) in D_2O , performed on a Bruker Avance 400 MHz NMR spectrometer.

PHENSS(OH)(Succ) ^{195}Pt NMR spectra

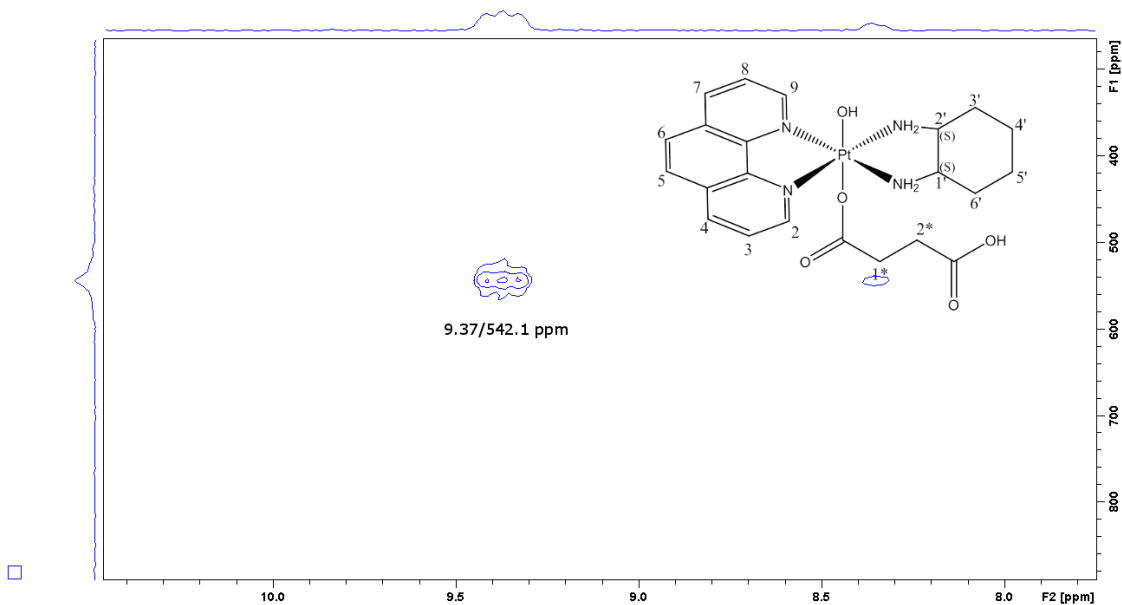


Figure A86: The ^1H - ^{195}Pt HMQC spectrum of PHENSS(OH)(Succ) in D_2O , performed on a Bruker Avance 400 MHz NMR spectrometer.

5MESS(OH)(Succ) ^1H NMR spectra

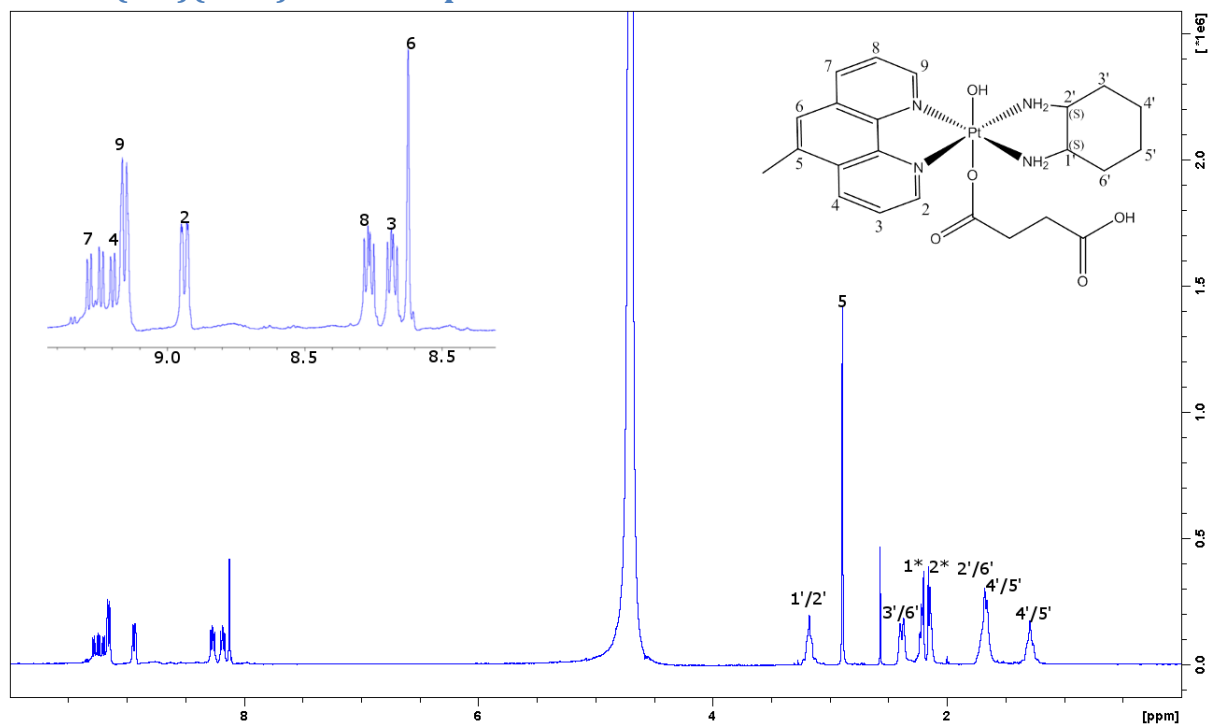


Figure A87: The ^1H spectrum of 5MESS(OH)(Succ) in D_2O , performed on a Bruker Avance 400 MHz NMR spectrometer.

5MESS(OH)(Succ) ^{195}Pt NMR spectra

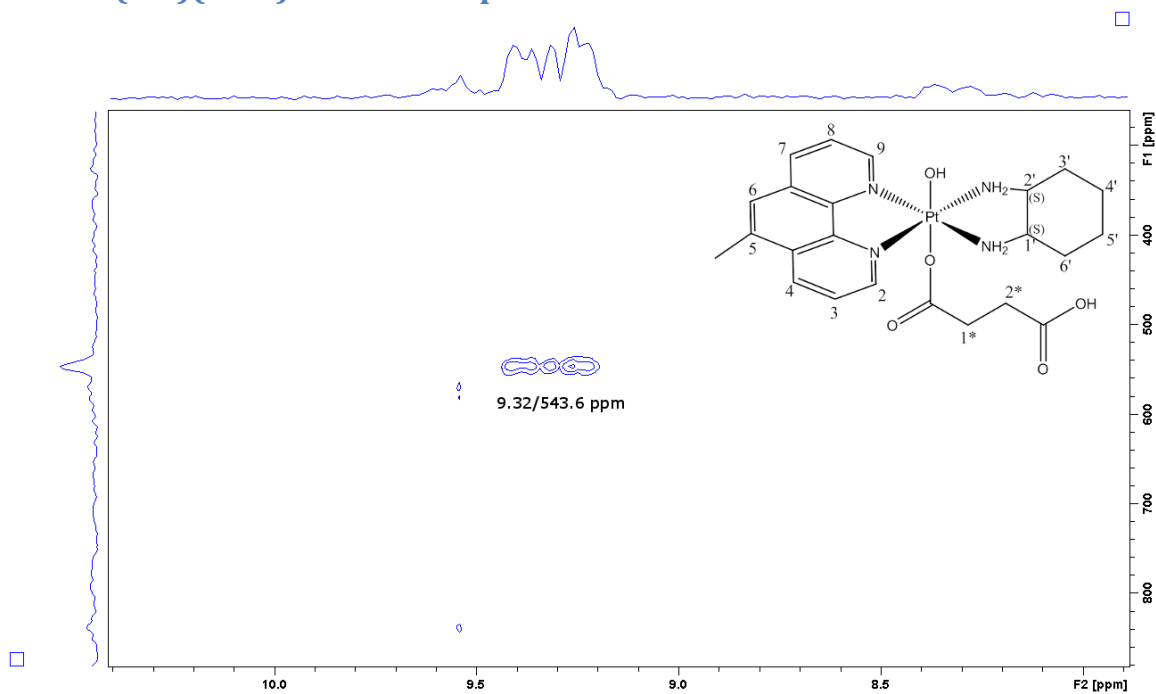


Figure A88: The ^1H - ^{195}Pt HMQC spectrum of 5MESS(OH)(Succ) in D_2O , performed on a Bruker Avance 400 MHz NMR spectrometer.

56MESS(OH)(Succ) ^1H NMR spectra

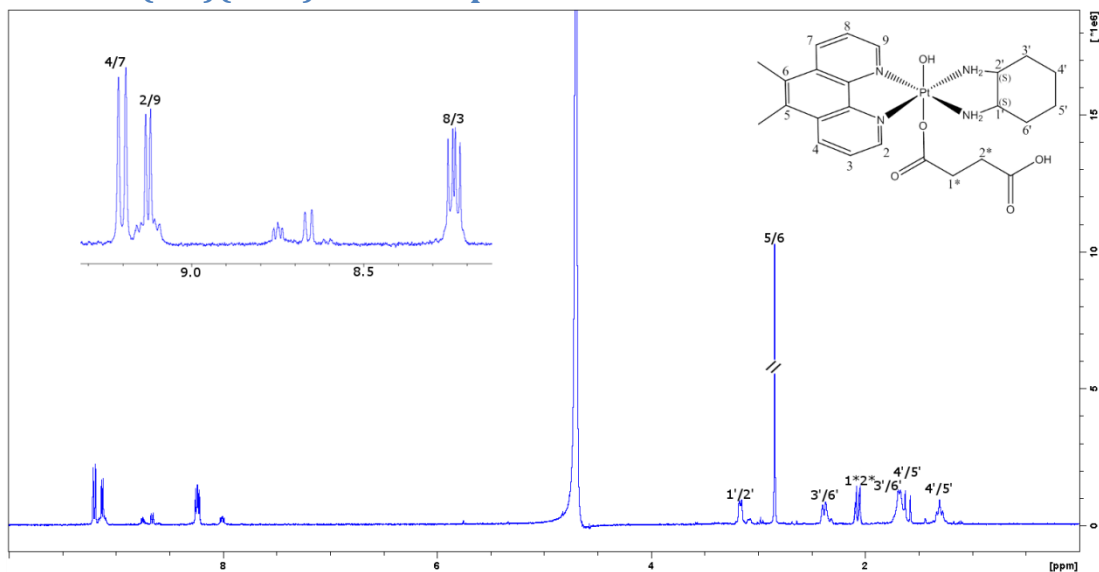


Figure A89: The ^1H spectrum of 56MESS(OH)(Succ) in D_2O , performed on a Bruker Avance 400 MHz NMR spectrometer.

56MESS(OH)(Succ) ^{195}Pt NMR spectra

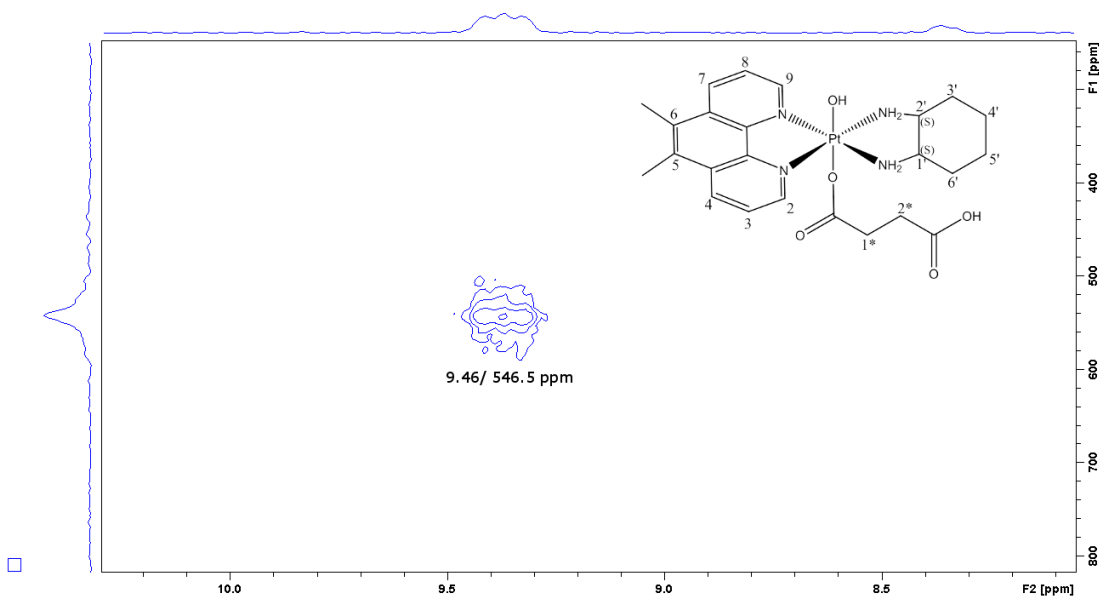


Figure A90: The ^1H - ^{195}Pt HMQC spectrum of 56MESS(OH)(Succ) in D_2O , performed on a Bruker Avance 400 MHz NMR spectrometer.

PHENSS(OH)(SuccPFP) ^1H NMR spectra

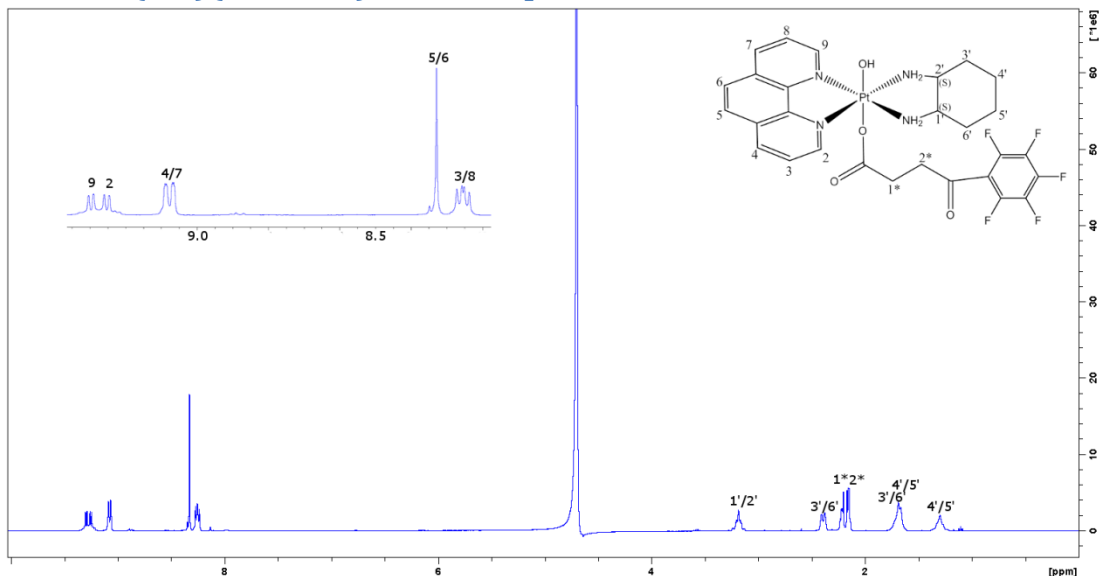


Figure A91: The ^1H spectrum of PHENSS(OH)(SuccPFP) in D_2O , performed on a Bruker Avance 400 MHz NMR spectrometer.

PHENSS(OH)(SuccPFP) ^{195}Pt NMR spectra

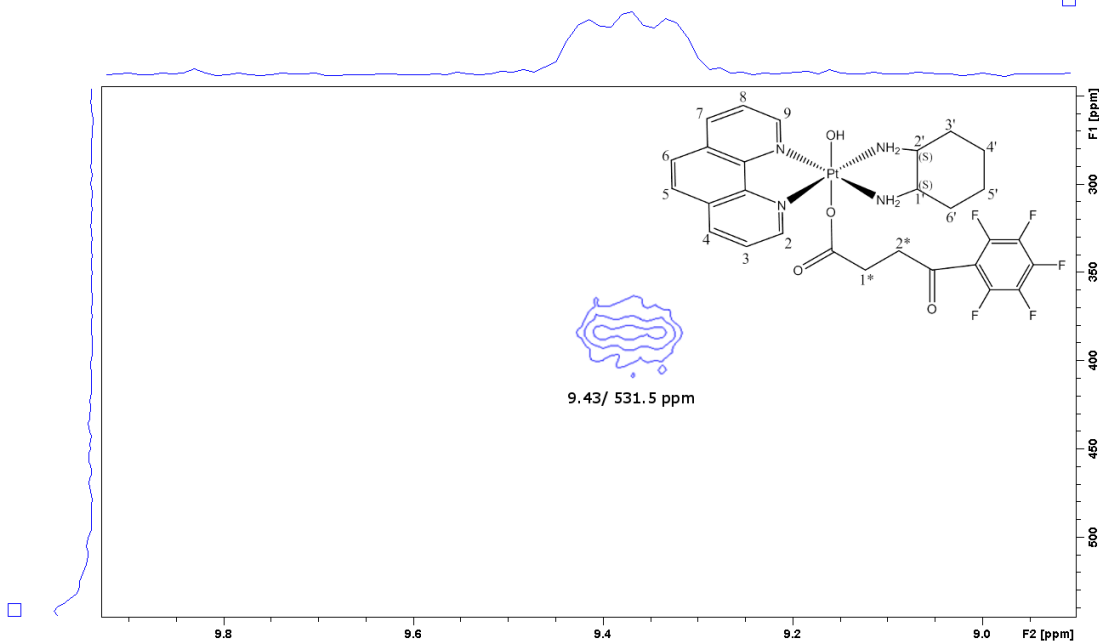


Figure A92: The ^1H - ^{195}Pt HMQC spectrum of PHENSS(OH)(SuccPFP) in D_2O , performed on a Bruker Avance 400 MHz NMR spectrometer.

UV Data

Spectra by Polypyridyl Ligand

UV Spectra of PHENSS(X)₂ complexes

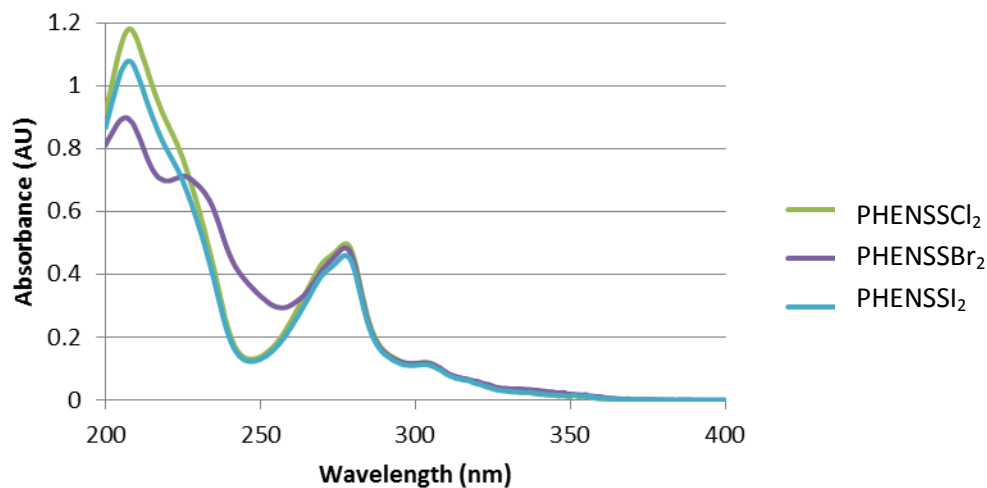


Figure B1: UV spectra of PHENSSCl₂ (green), PHENSSBr₂ (purple) and, PHENSSI₂ (blue); at room temperature in the 200–350 nm range, using a 10 mm quartz cell, corrected for solvent baseline, measured in H₂O at 28.7 μM.

UV Spectra of 5MESS(X)₂ complexes

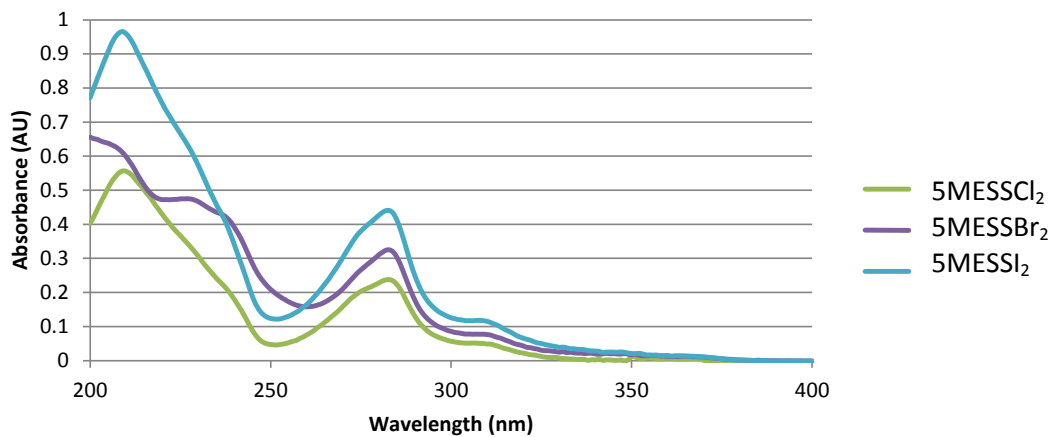


Figure B2: UV spectra of 5MESSCl₂ (green), 5MESSBr₂ (purple) and, 5MESSI₂ (blue); at room temperature in the 200–350 nm range, using a 10 mm quartz cell, corrected for solvent baseline, measured in H₂O at 28.7 μM.

UV Spectra of 56MESS(X)₂ complexes

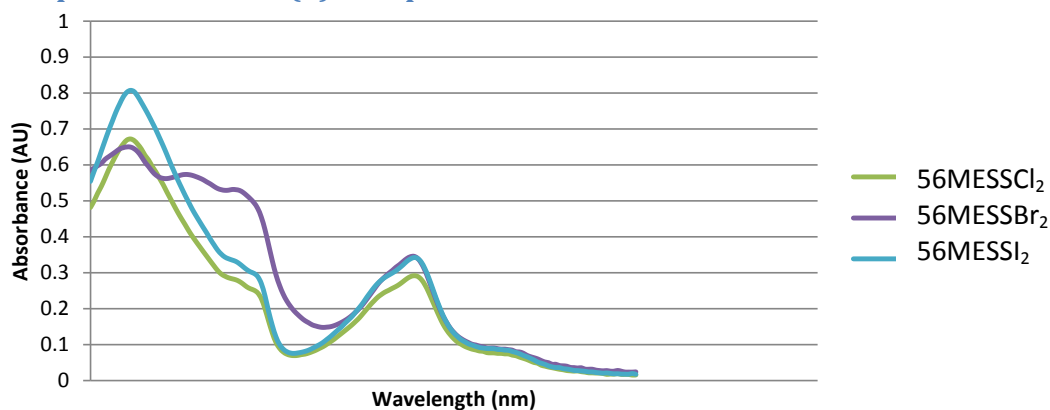


Figure B3: UV spectra of 56MESSCl₂ (green), 56MESSBr₂ (purple) and, 56MESSI₂ (blue); at room temperature in the 200–350 nm range, using a 10 mm quartz cell, corrected for solvent baseline, measured in H₂O at 28.7 μM.

Spectra by Axial Ligand

UV Spectra of Chloro complexes

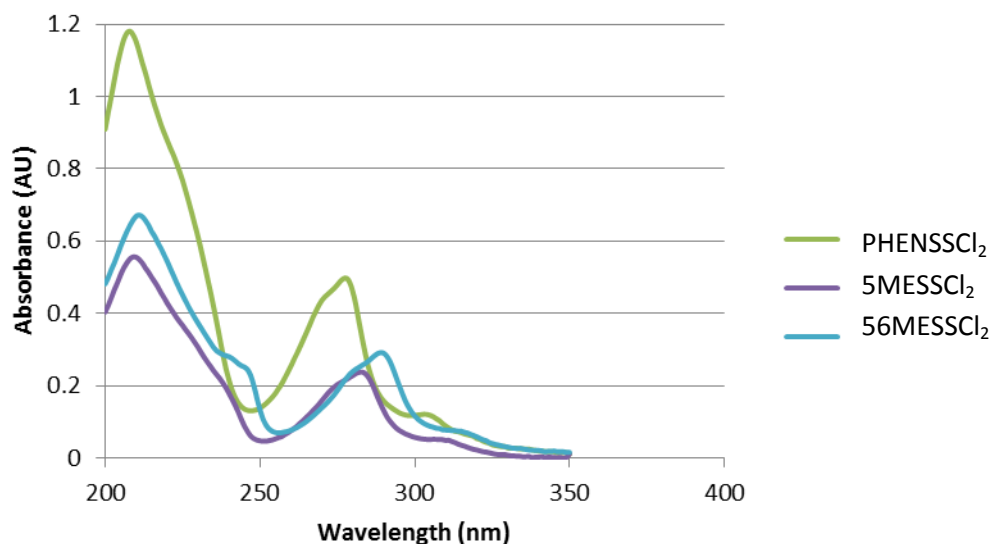


Figure B4: UV spectra of PHENSSCl₂ (green), 5MESSCl₂ (purple) and, 56MESSCl₂ (blue); at room temperature in the 200–350 nm range, using a 10 mm quartz cell, corrected for solvent baseline, measured in H₂O at 28.7 μM.

UV Spectra of Bromo complexes

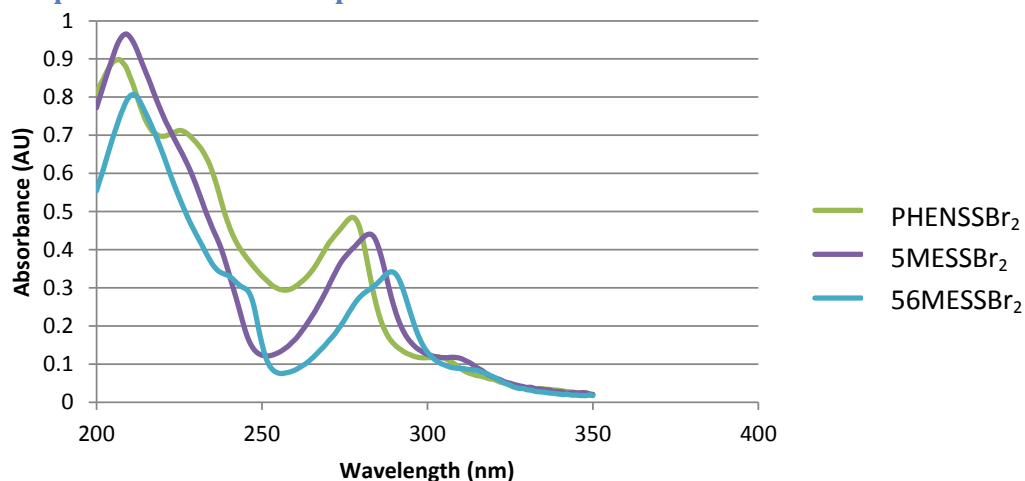


Figure B5: UV spectra of PHENSSBr₂ (green), 5MESSBr₂ (purple) and, 56MESSBr₂ (blue); at room temperature in the 200–350 nm range, using a 10 mm quartz cell, corrected for solvent baseline, measured in H₂O at 28.7 μM.

UV Spectra of Iodo complexes

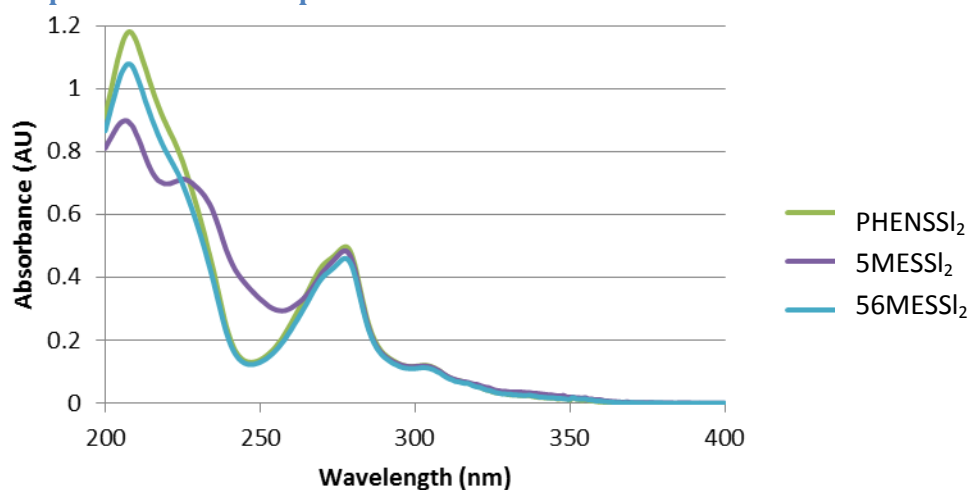


Figure B6: UV spectra of PHENSSI₂ (green), 5MESSI₂ (purple) and, 56MESSI₂ (blue); at room temperature in the 200–350 nm range, using a 10 mm quartz cell, corrected for solvent baseline, measured in H₂O at 28.7 μM.

UV Spectra PhenSS(Cl)₂

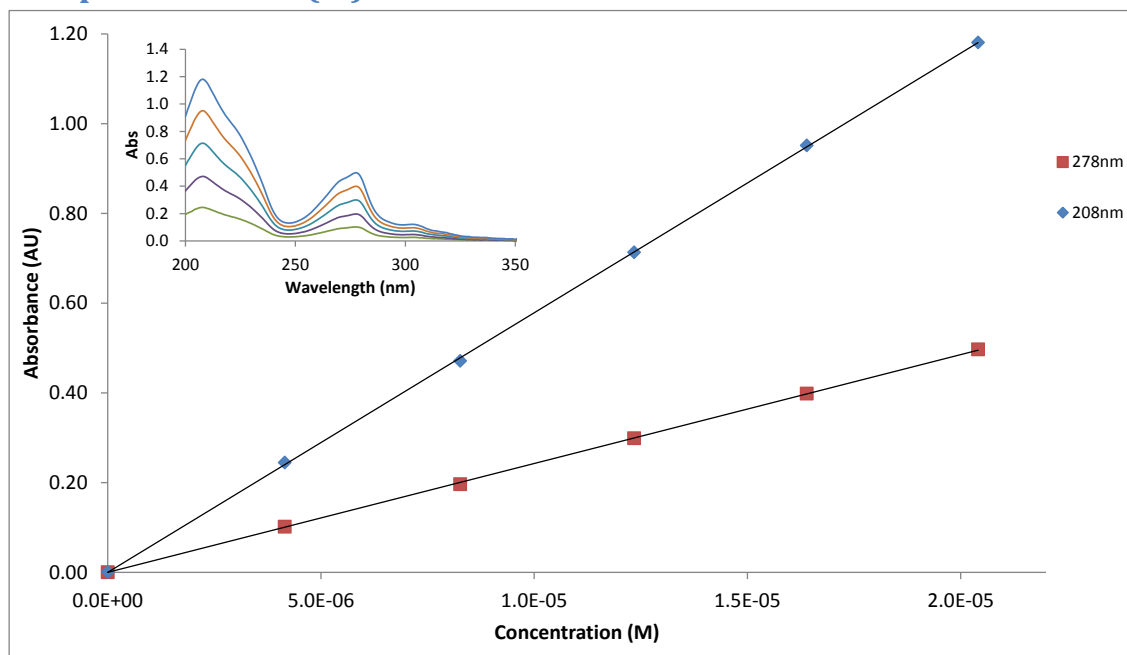


Figure B7: Titration of a stock solution of PHENSSCl₂ into a known concentration in H₂O and the resulting extinction coefficient calculated based on the two main peaks at 278 (red) and 208 nm (blue).

UV Spectra PhenSS(Br)₂

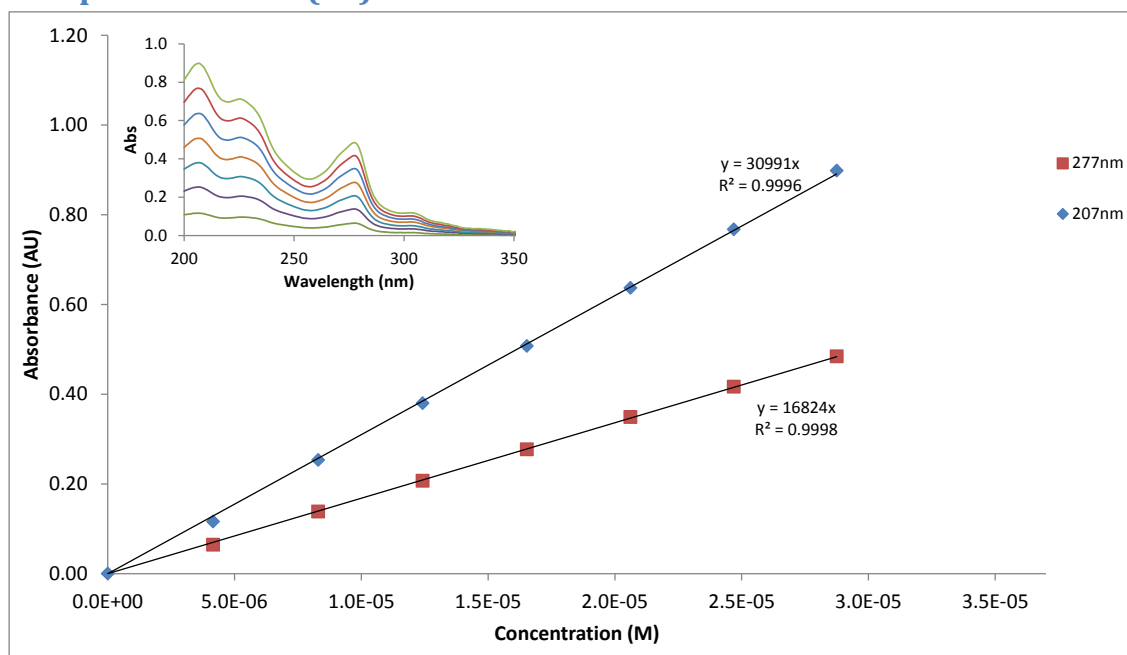


Figure B8: Titration of a stock solution of PHENSSBr₂ into a known concentration in H₂O and the resulting extinction coefficient calculated based on the two main peaks at 277 (red) and 207 nm (blue).

UV Spectra PhenSS(I)₂

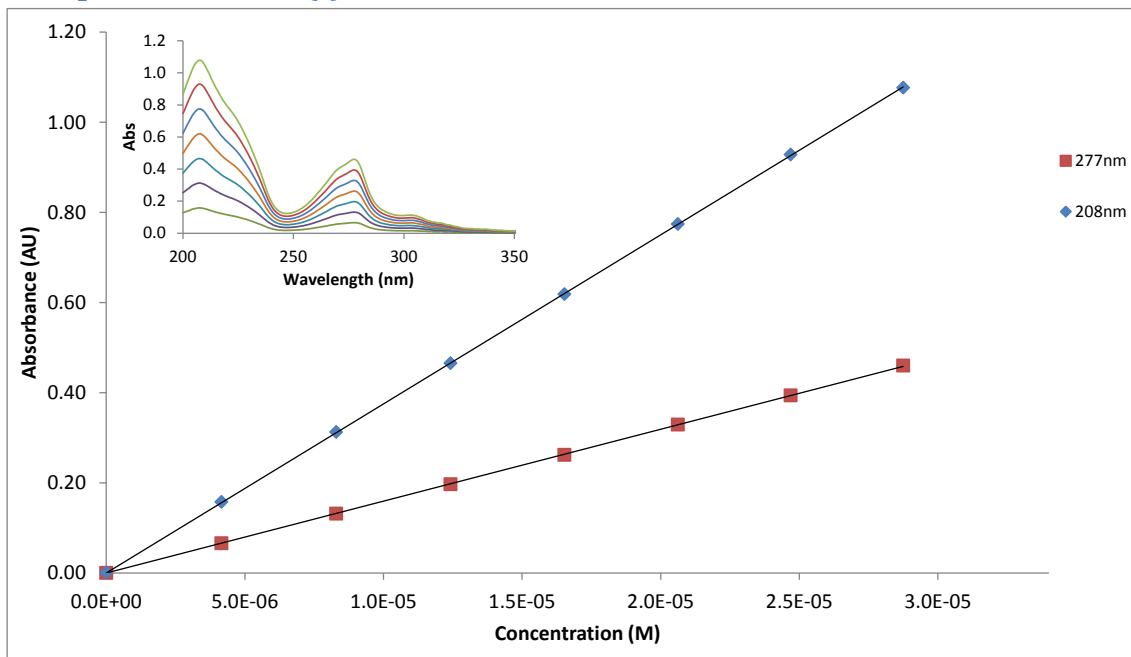


Figure B9: Titration of a stock solution of PHENSSI₂ into a known concentration in H₂O and the resulting extinction coefficient calculated based on the two main peaks at 277 (red) and 208 nm (blue).

UV Spectra 5MeSS(Cl)₂

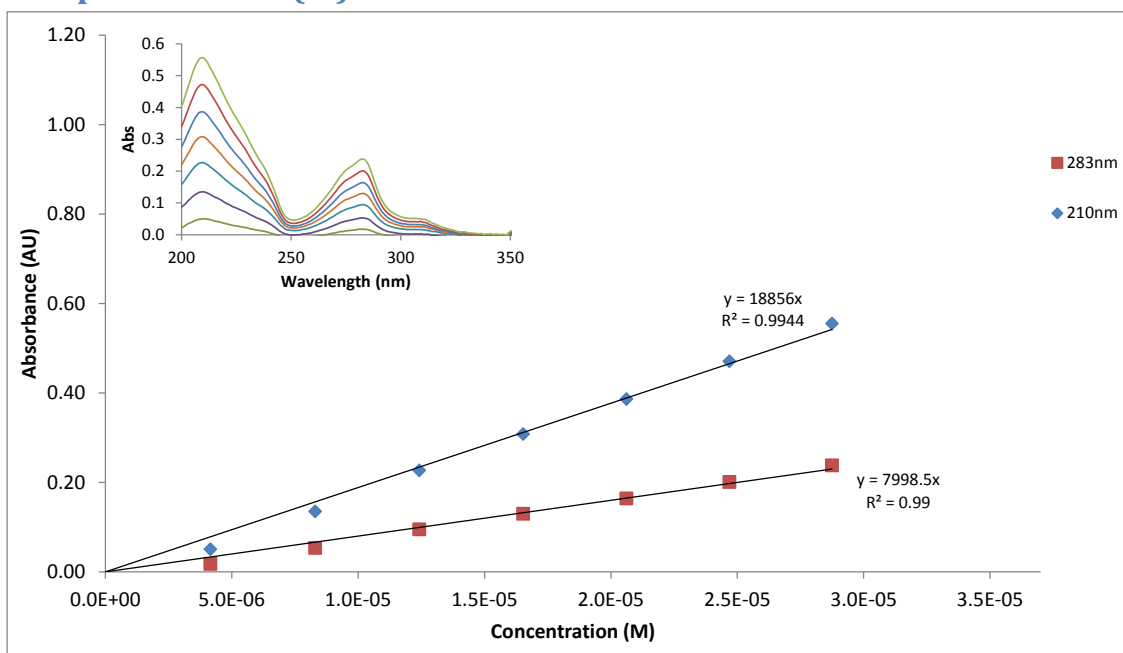


Figure B10: Titration of a stock solution of 5MESSCl₂ into a known concentration in H₂O and the resulting extinction coefficient calculated based on the two main peaks at 283 (red) and 210 nm (blue).

UV Spectra 5MeSS(Br)₂

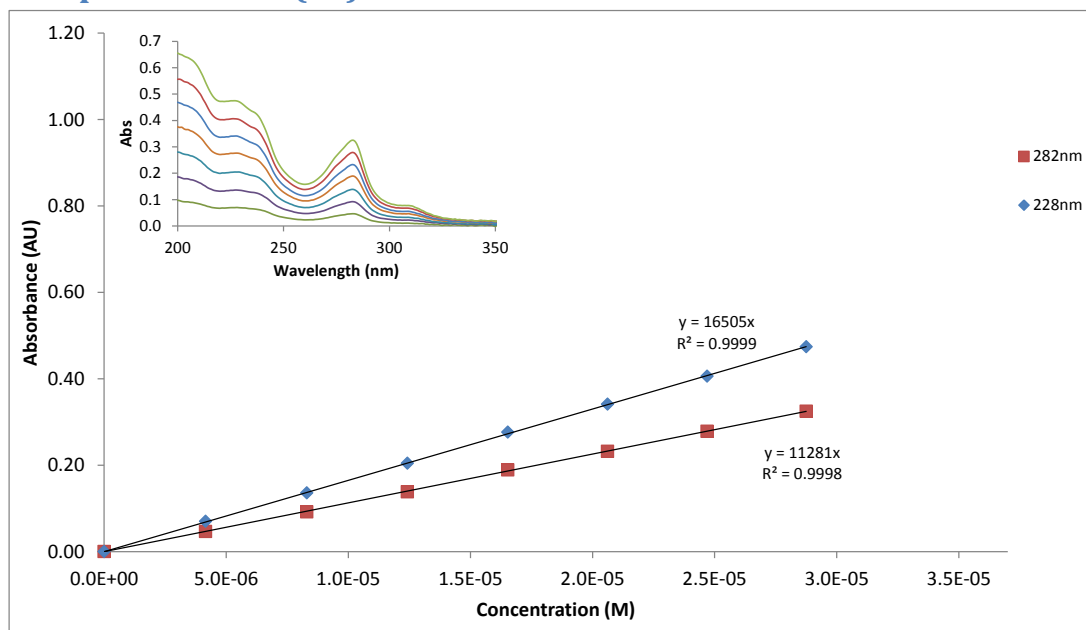


Figure B11: Titration of a stock solution of 5MESSBr₂ into a known concentration in H₂O and the resulting extinction coefficient calculated based on the two main peaks at 282 (red) and 228nm (blue).

UV Spectra 5MeSS(I)₂

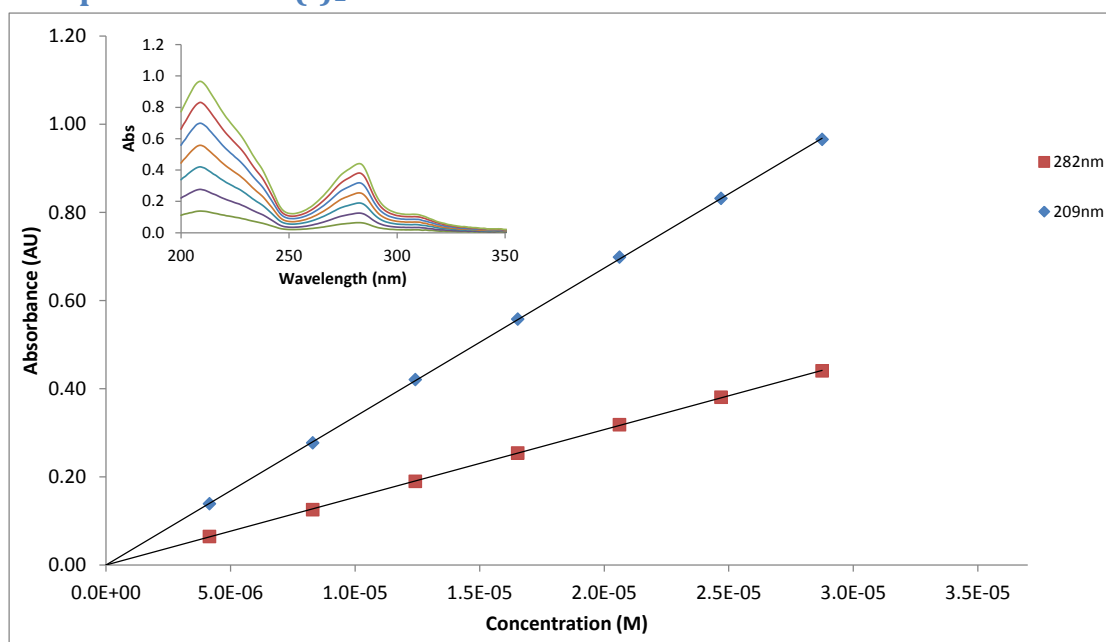


Figure B12: Titration of a stock solution of 5MESSI₂ into a known concentration in H₂O and the resulting extinction coefficient calculated based on the two main peaks at 282 (red) and 209 nm (blue).

UV Spectra 56MeSS(Cl)₂

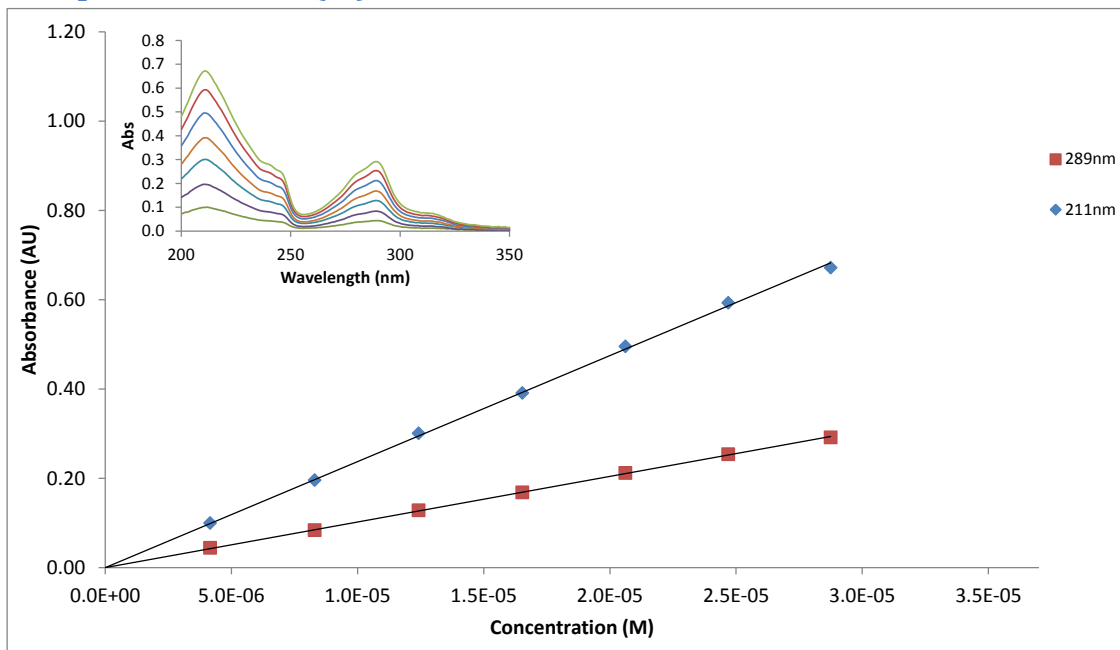


Figure B13: Titration of a stock solution of 56MESSCl₂ into a known concentration in H₂O and the resulting extinction coefficient calculated based on the two main peaks at 289 (red) and 211 nm (blue).

UV Spectra 56MeSS(Br)₂

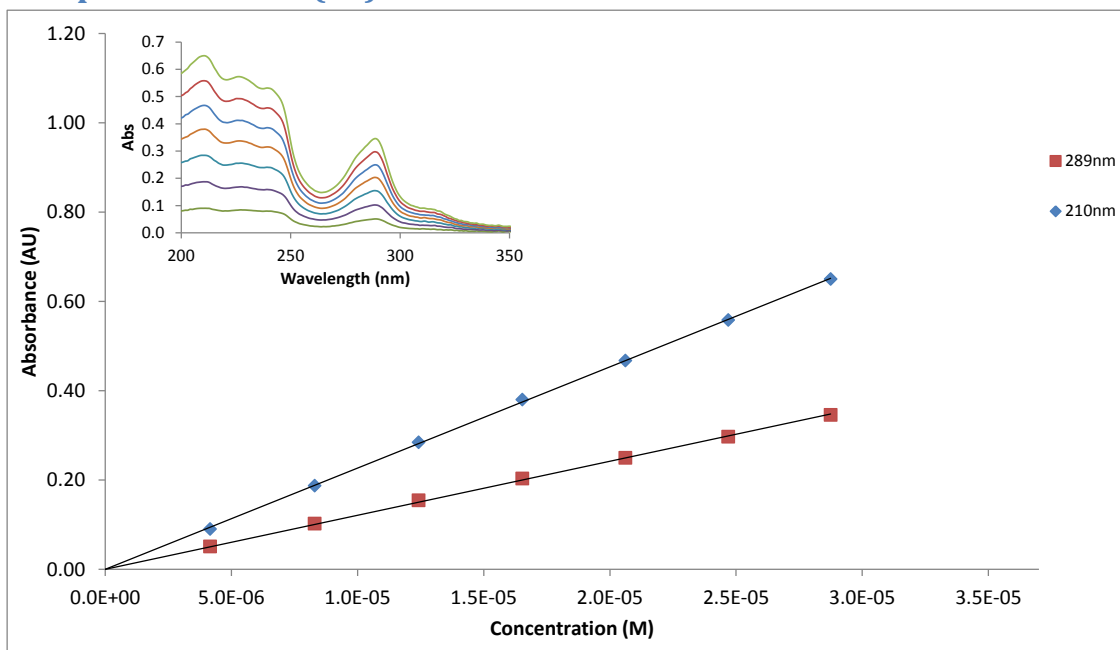


Figure B14: Titration of a stock solution of 56MESSBr₂ into a known concentration in H₂O and the resulting extinction coefficient calculated based on the two main peaks at 289 (red) and 211 nm (blue).

UV Spectra 56MeSS(I)₂

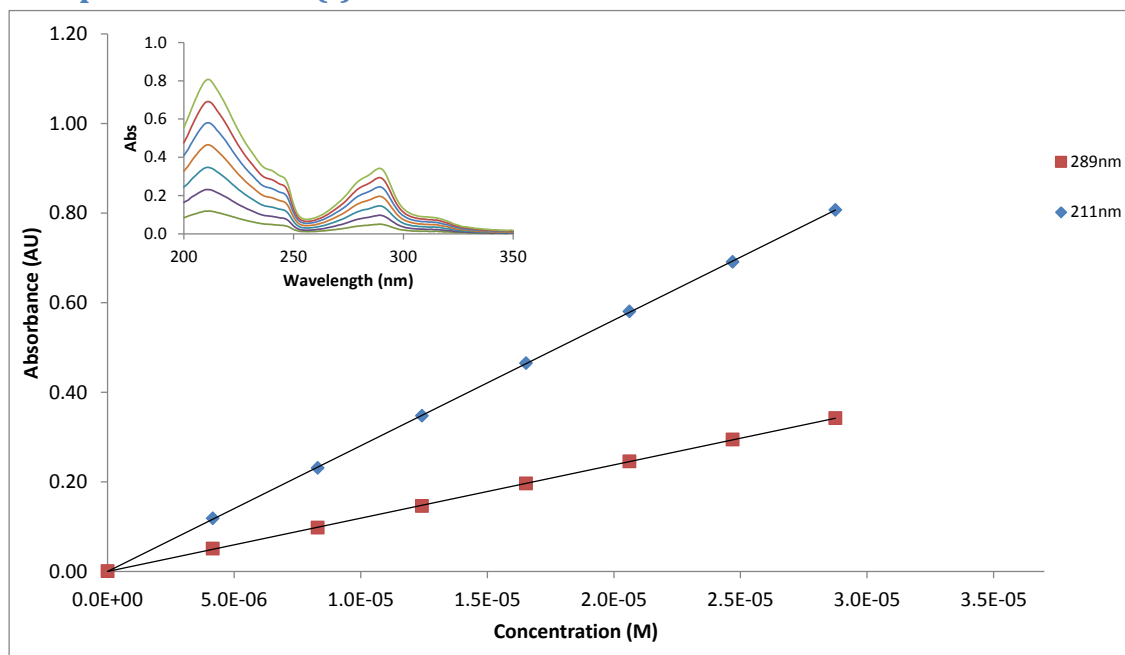


Figure B15: Titration of a stock solution of 56MESSCL₂ into a known concentration in H₂O and the resulting extinction coefficient calculated based on the two main peaks at 289 (red) and 211 nm (blue).

CD Data

Spectra by Polypyridyl Ligand

CD Spectra of PHENSS(X)₂

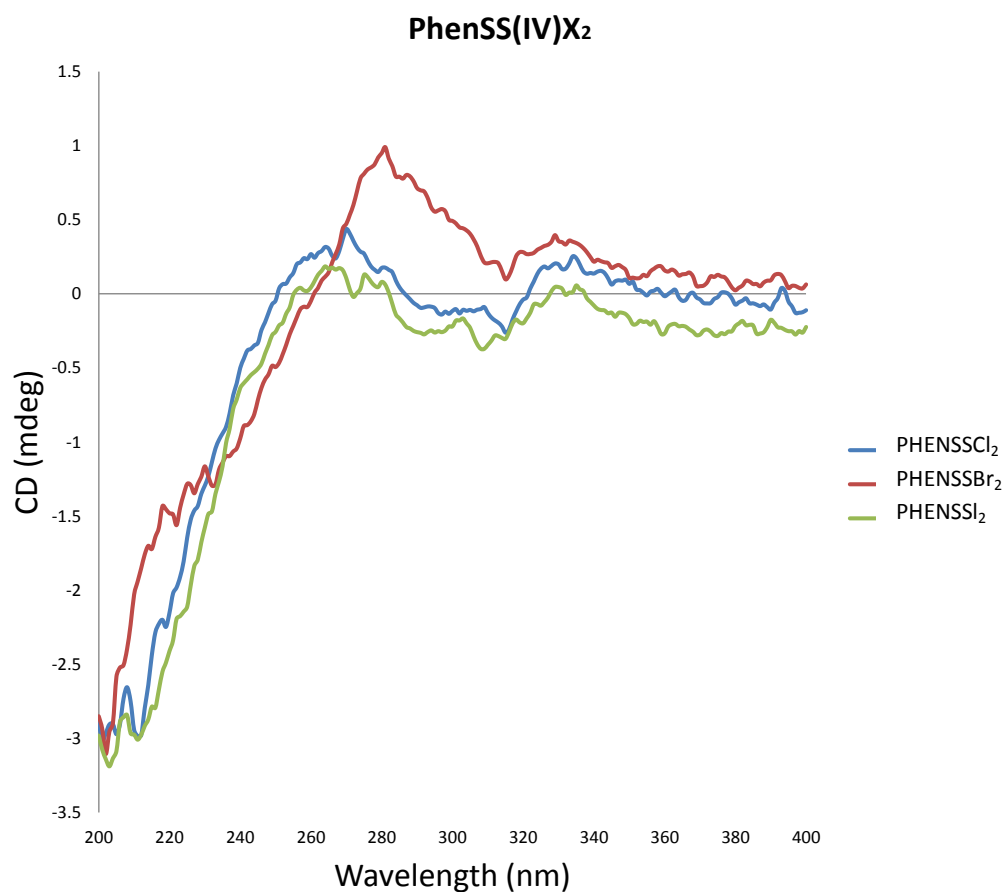


Figure C1: CD spectra of PHENSSCl₂ (blue), PHENSSBr₂ (red) and, PHENSSI₂ (green); at room temperature in the 200–350 nm range, using a 10 mm quartz cell, corrected for solvent baseline, measured in H₂O at 28.7 μM.

CD Spectra of 5MESS(X)₂

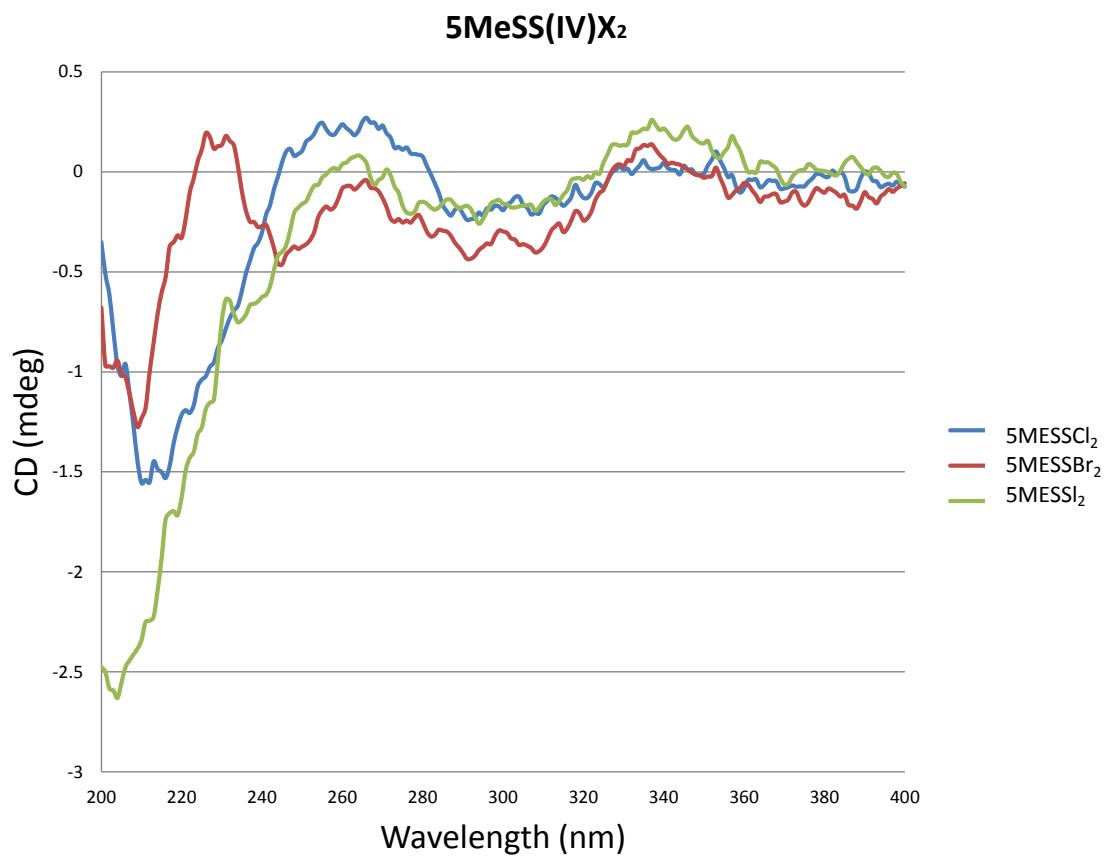


Figure C2: CD spectra of 5MESSCl₂ (blue), 5MESSBr₂ (red) and, 5MESSI₂ (green); at room temperature in the 200–350 nm range, using a 10 mm quartz cell, corrected for solvent baseline, measured in H₂O at 28.7 μM.

CD Spectra of 56MESS(X)₂

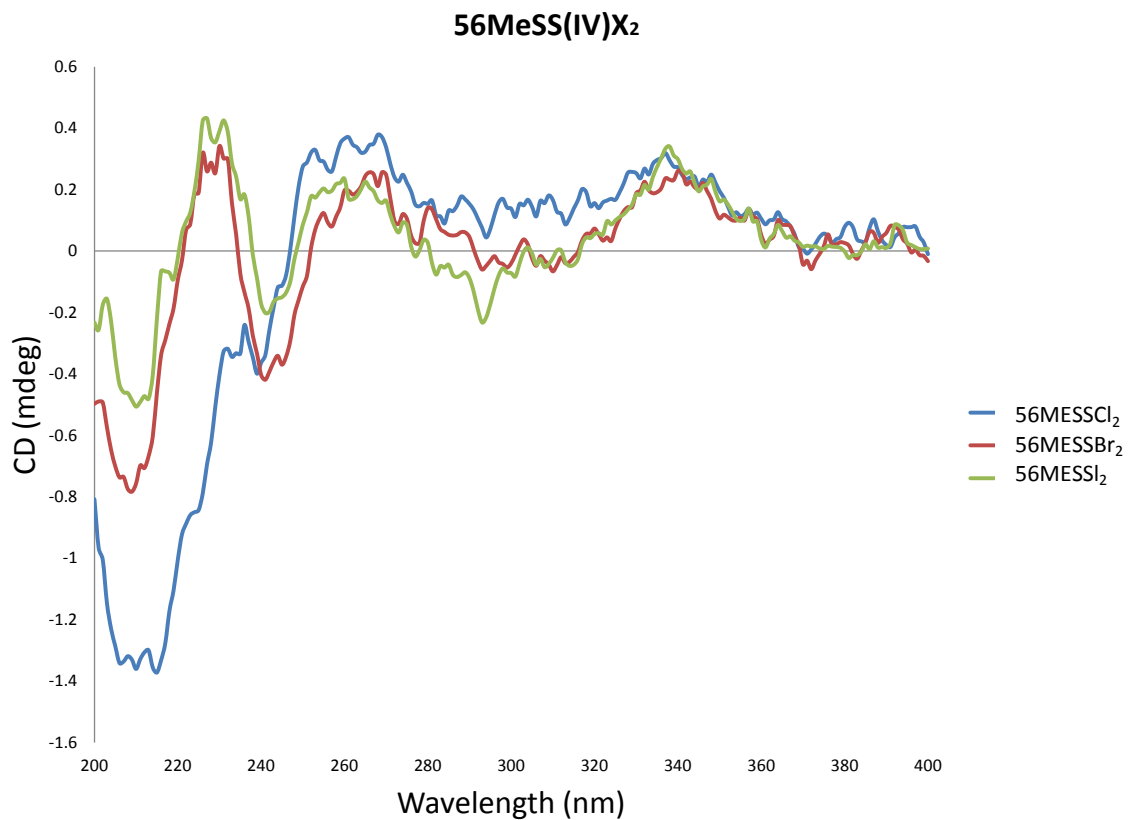


Figure C3: CD spectra of 56MESSCl₂ (blue), 56MESSBr₂ (red) and, 56MESSI₂ (green); at room temperature in the 200–350 nm range, using a 10 mm quartz cell, corrected for solvent baseline, measured in H₂O at 28.7 μM.

Spectra by Axial Ligand

CD Spectra of Chloro complexes

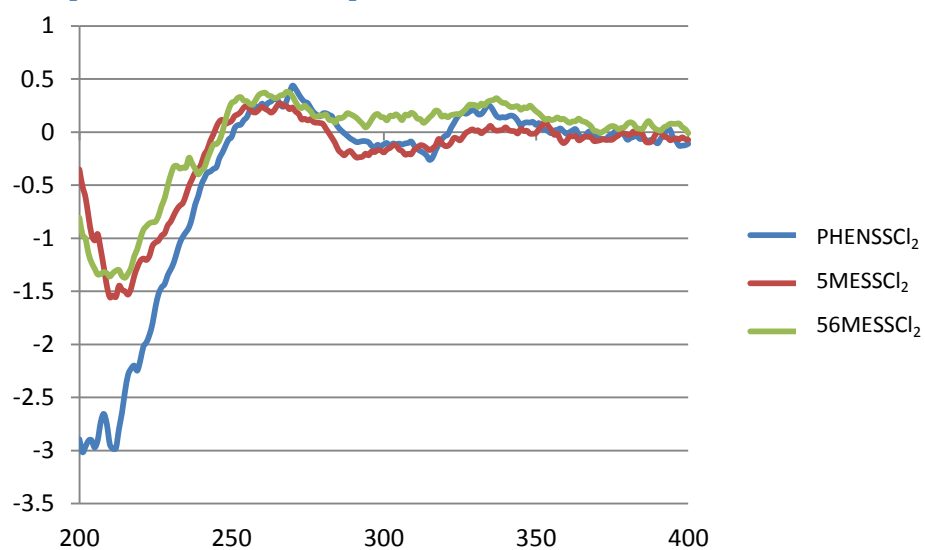


Figure C4: CD spectra of PHENSSCl₂ (blue), 5MESSCl₂ (red) and, 56MESSCl₂ (green); at room temperature in the 200–350 nm range, using a 10 mm quartz cell, corrected for solvent baseline, measured in H₂O at 28.7 μM.

CD Spectra of Bromo complexes

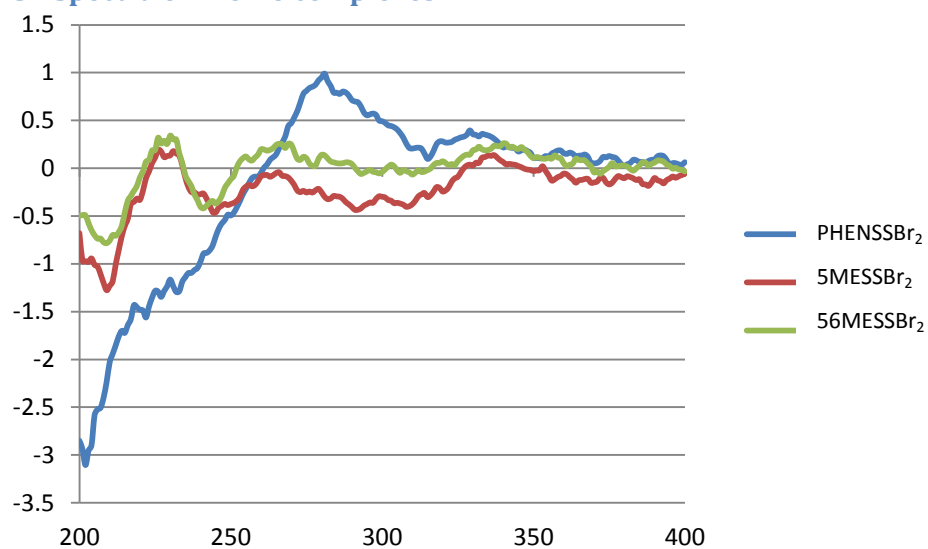


Figure C5: CD spectra of PHENSSBr₂ (blue), 5MESSBr₂ (red) and, 56MESSBr₂ (green); at room temperature in the 200–350 nm range, using a 10 mm quartz cell, corrected for solvent baseline, measured in H₂O at 28.7 μM.

CD Spectra of Iodo complexes

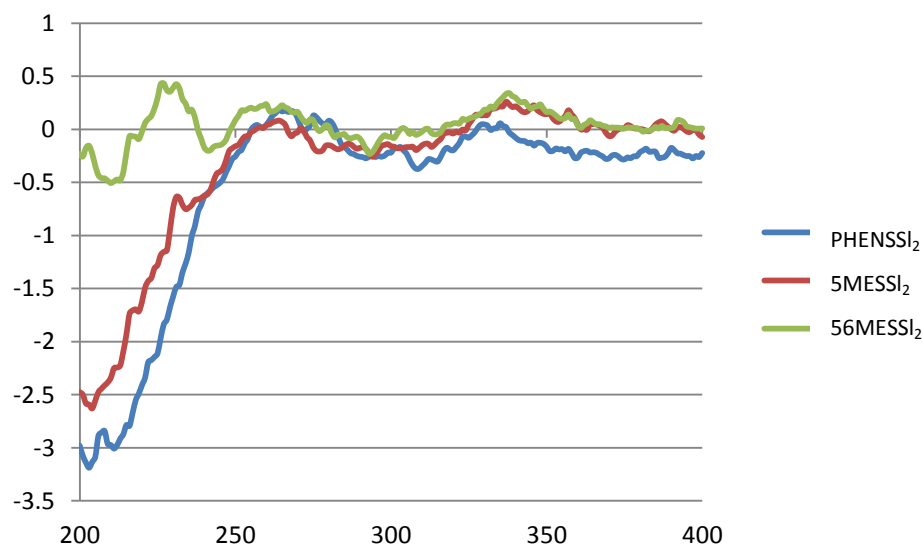


Figure C6: CD spectra of PHENSSI₂ (blue), 5MESSI₂ (red) and, 56MESSI₂ (green); at room temperature in the 200–350 nm range, using a 10 mm quartz cell, corrected for solvent baseline, measured in H₂O at 28.7 μM.

Smoothed individual spectra:

CD Spectra PHENSS(Cl)₂

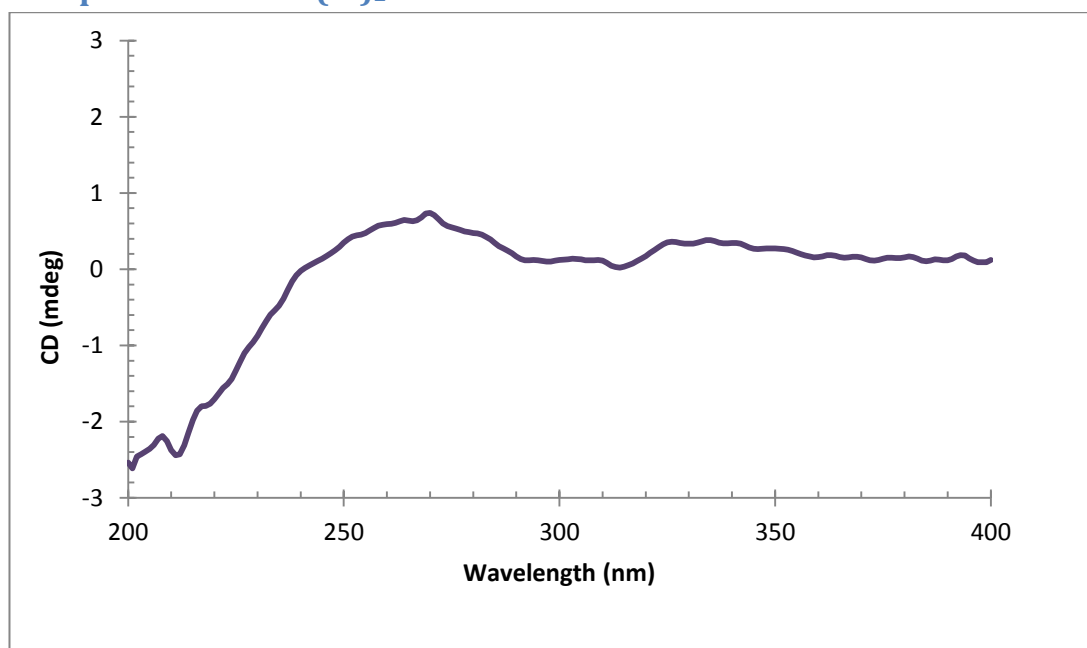


Figure C7: CD spectra of PHENSSCl₂ at room temperature in the 200–350 nm range, using a 10 mm quartz cell, corrected for solvent baseline, measured in H₂O at 28.7 μM.

CD Spectra PHENSS(Br)₂

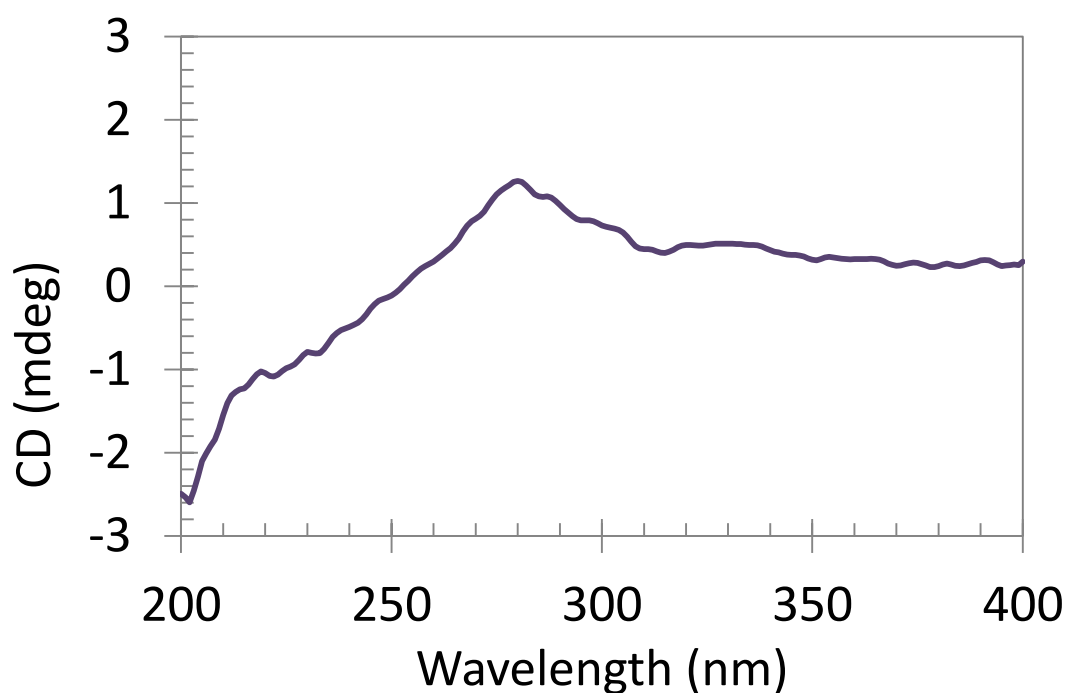


Figure C8: CD spectra of PHENSSBr₂ at room temperature in the 200–350 nm range, using a 10 mm quartz cell, corrected for solvent baseline, measured in H₂O at 28.7 μM.

CD Spectra PHENSS(I)₂

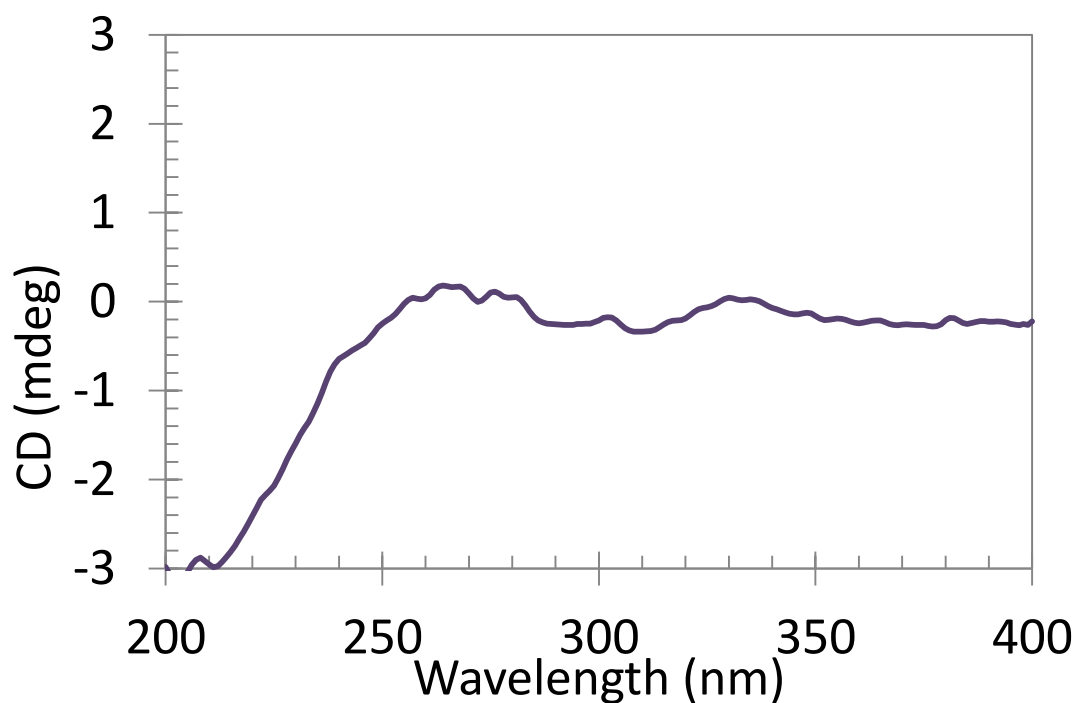


Figure C9: CD spectra of PHENSSI₂ at room temperature in the 200–350 nm range, using a 10 mm quartz cell, corrected for solvent baseline, measured in H₂O at 28.7 μM.

CD Spectra 5MESS(Cl)₂

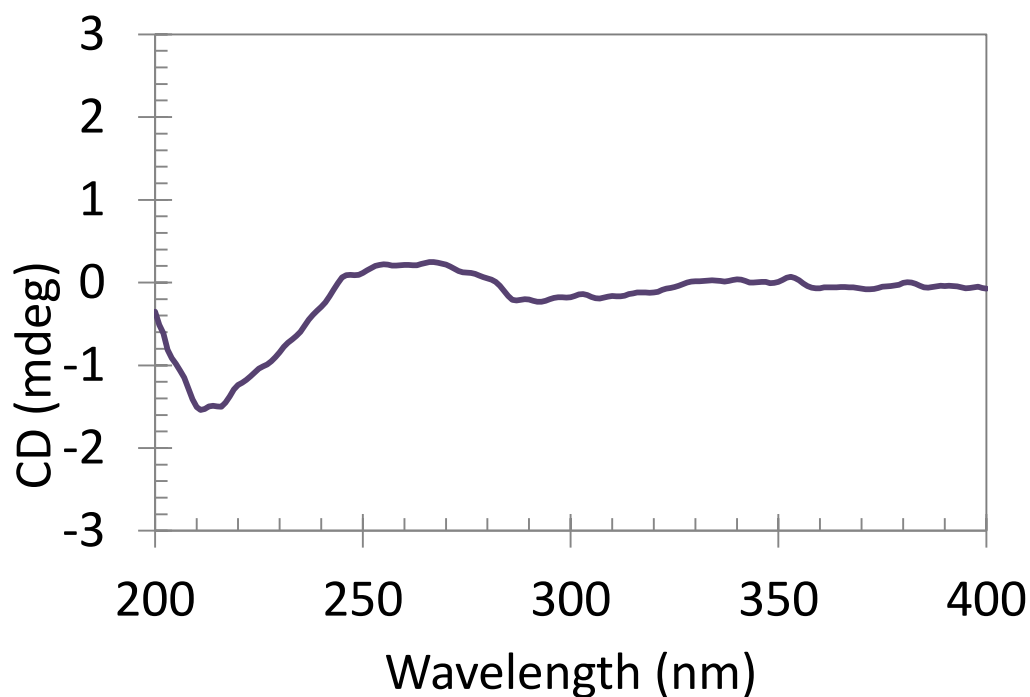


Figure C10: CD spectra of 5MESSCl₂ at room temperature in the 200–350 nm range, using a 10 mm quartz cell, corrected for solvent baseline, measured in H₂O at 28.7 μM.

CD Spectra 5MESS(Br)₂

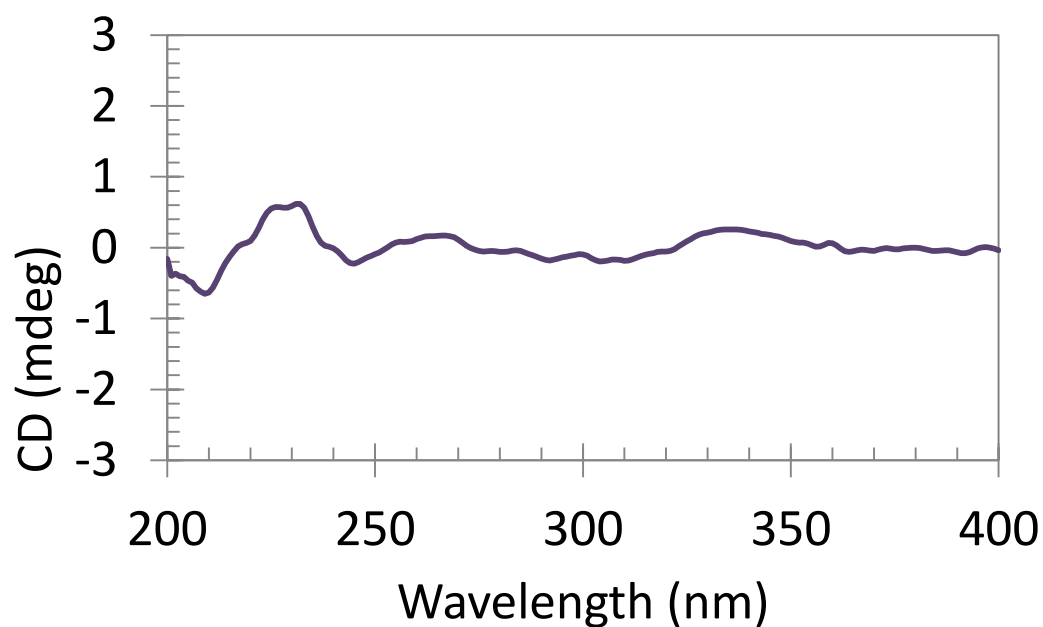


Figure C11: CD spectra of 5MESSBr₂ at room temperature in the 200–350 nm range, using a 10 mm quartz cell, corrected for solvent baseline, measured in H₂O at 28.7 μM.

CD Spectra 5MESS(I)₂

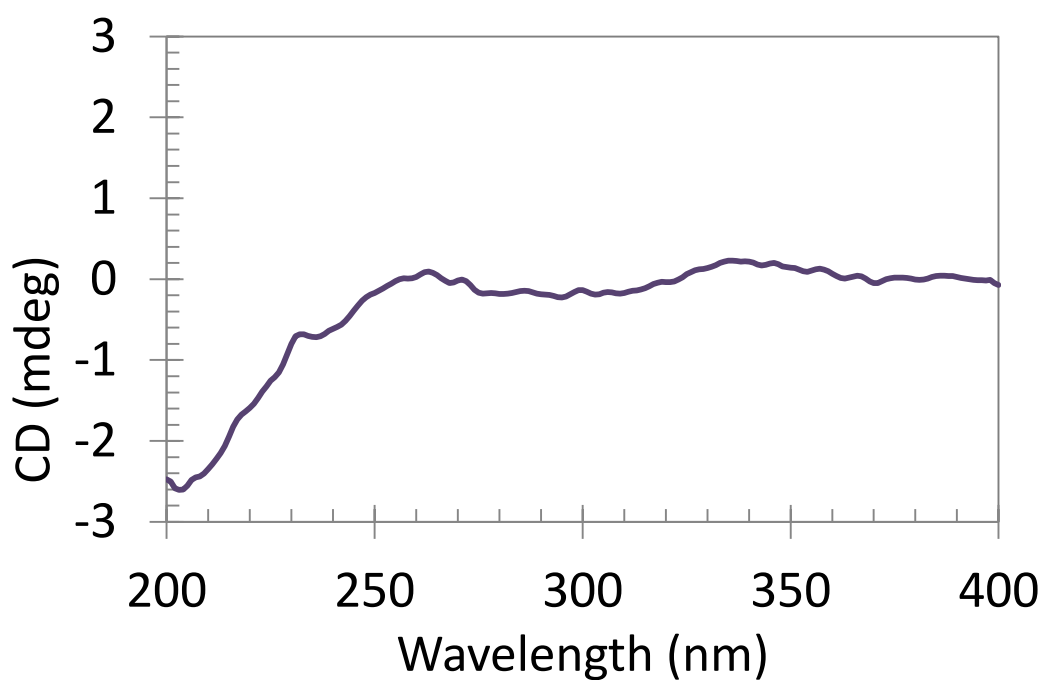


Figure C12: CD spectra of 5MESSI₂ at room temperature in the 200–400 nm range, using a 10 mm quartz cell, corrected for solvent baseline, measured in H₂O at 28.7 μM.

CD Spectra 56MESS(Cl)₂

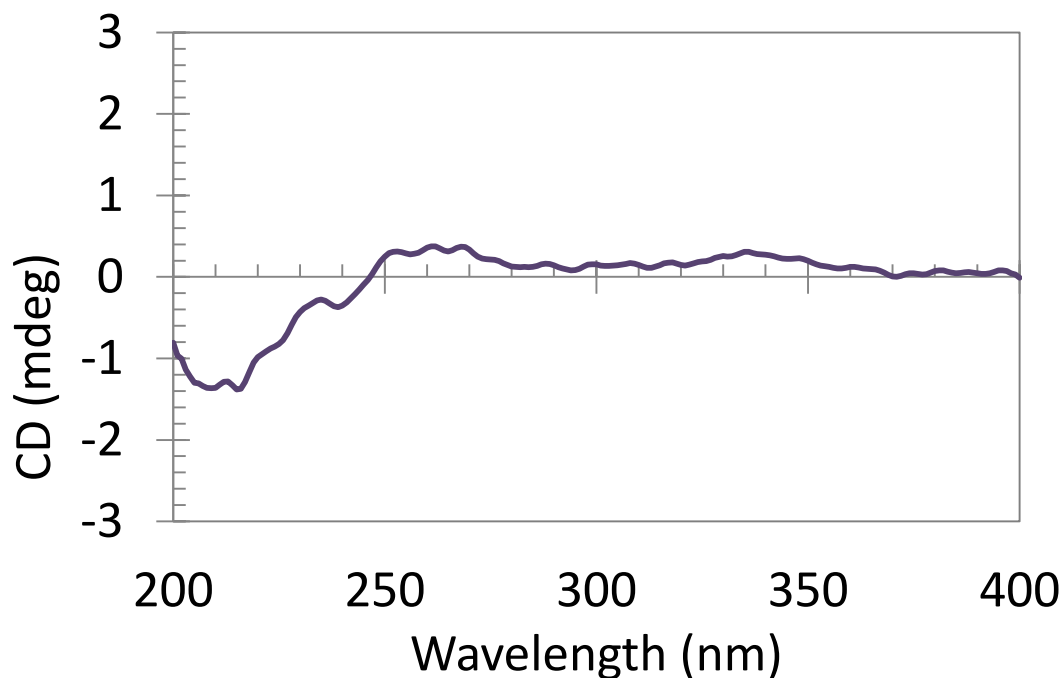


Figure C13: CD spectra of 56MESSCl₂ at room temperature in the 200–400 nm range, using a 10 mm quartz cell, corrected for solvent baseline, measured in H₂O at 28.7 μM.

CD Spectra 56MESS(Br)₂

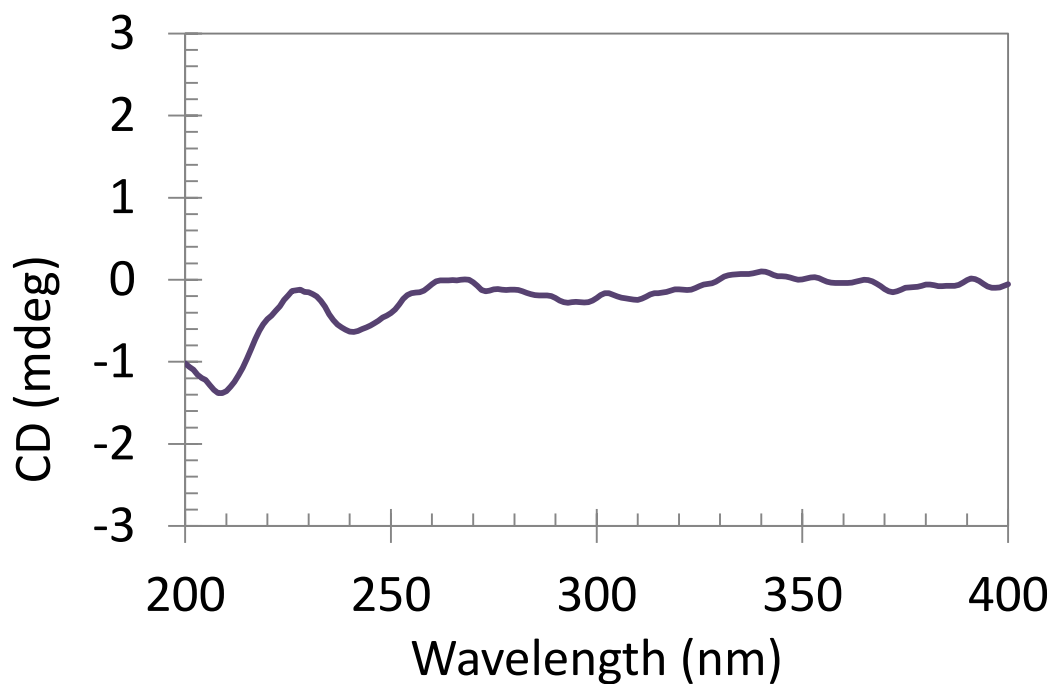


Figure C14: CD spectra of 56MESSBr₂ at room temperature in the 200–350 nm range, using a 10 mm quartz cell, corrected for solvent baseline, measured in H₂O at 28.7 μM.

CD Spectra 56MeSS(I)₂

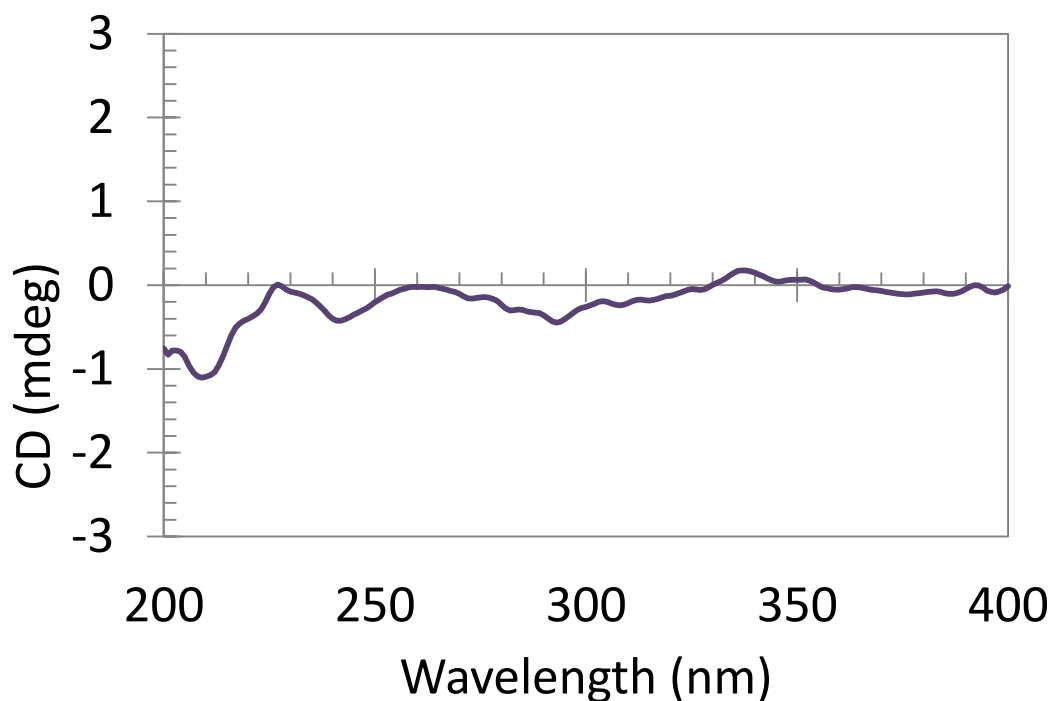


Figure C15: CD spectra of 56MESSI₂ at room temperature in the 200–350 nm range, using a 10 mm quartz cell, corrected for solvent baseline, measured in H₂O at 28.7 μM.

SRCD Data

All SRCD data smoothed using 11 points, spectra for PHENSSBr₂ shown here as an example to show that smoothing does not affect the peak shape or size.

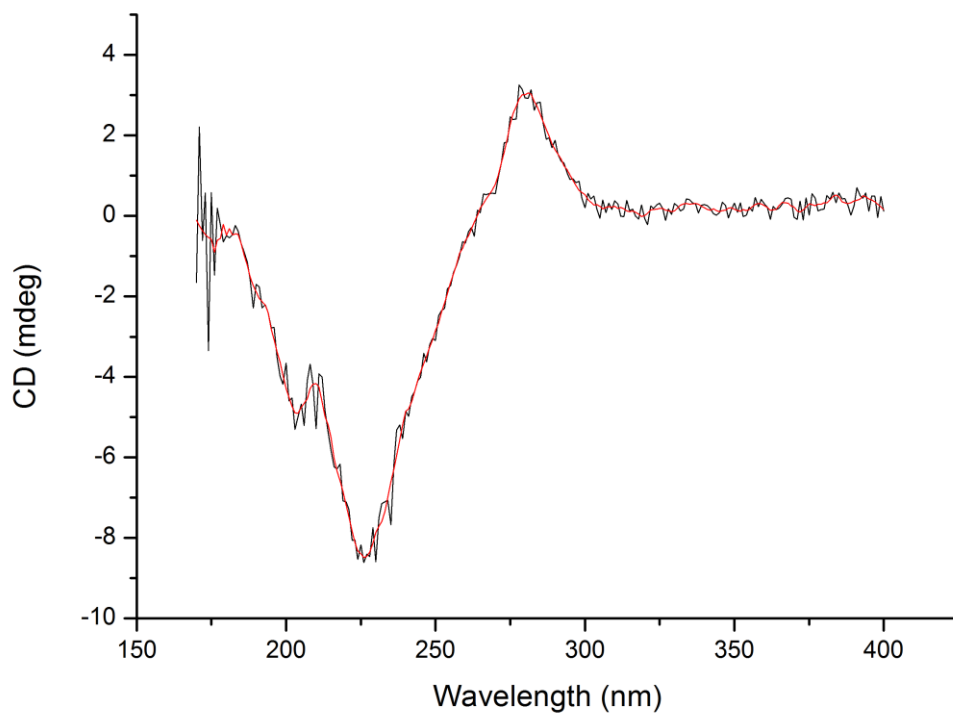


Figure D1: SRCD spectra of PHENSSBr₂ showing the raw data (black) and the 11 point smoothed data (red) , measured in H₂O at 2.74 μ M.

Spectra by Polypyridyl Ligand

SRCD Spectra of PHENSS(X)₂

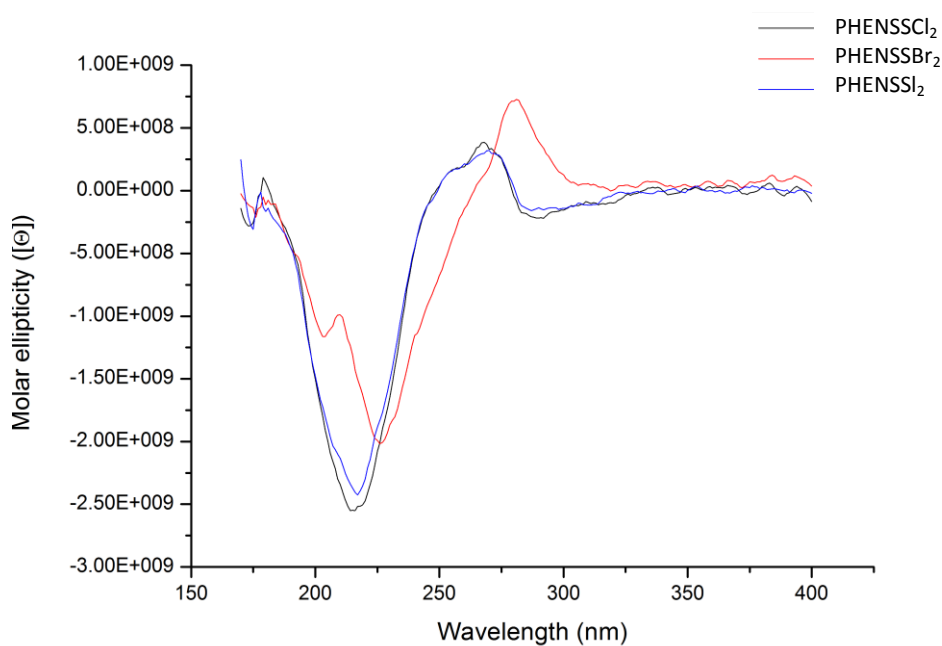


Figure D2: SRCD spectra of PHENSSCl₂ (black), PHENSSBr₂ (red) and, PHENSSI₂ (blue); at room temperature in the 170-400 nm range, using a 0.1 mm cell, corrected for solvent baseline. Samples were measured in H₂O Concentrations were varied due to absorbance: PHENSSCl₂ 1.77 μM, PHENSSBr₂ 28.7 μM and PHENSSI₂ 2.74 μM.

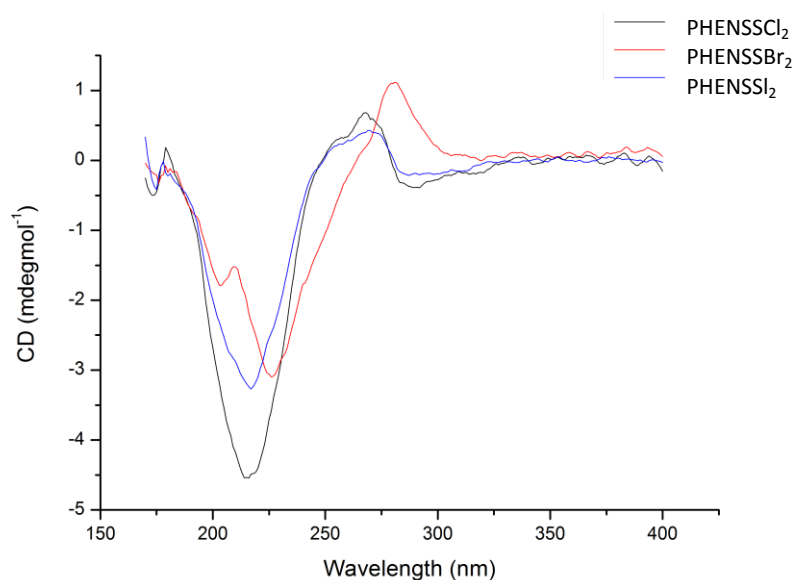


Figure D3: SRCD spectra of PHENSSCl₂ (black), PHENSSBr₂ (red) and, PHENSSI₂ (blue); at room temperature in the 170-400 nm range, using a 0.1 mm cell, corrected for solvent baseline. Samples were measured in H₂O Concentrations were varied due to absorbance: PHENSSCl₂ 1.77 μM, PHENSSBr₂ 28.7 μM and PHENSSI₂ 2.74 μM.

SRCD Spectra of 5MESS(X)₂

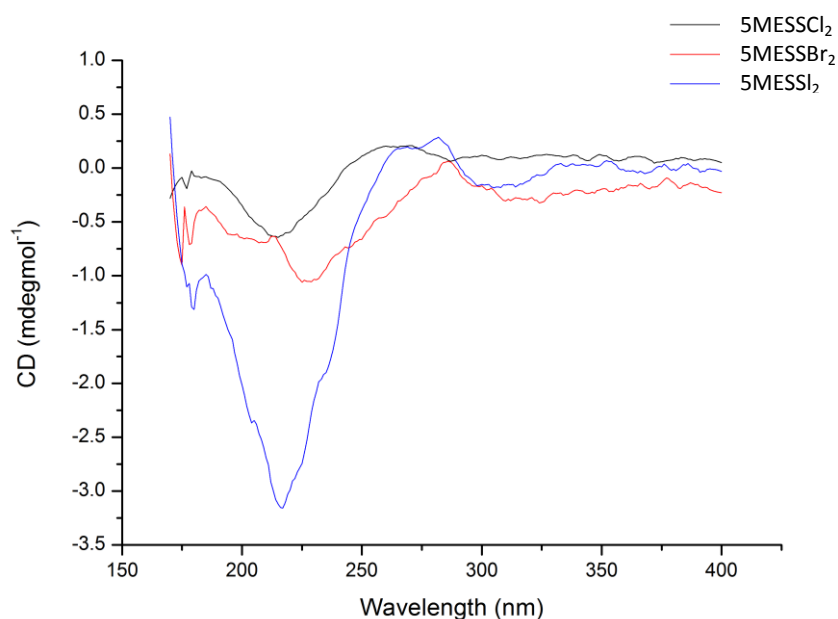


Figure D4: SRCD spectra of 5MESSCl₂ (black), 5MESSBr₂ (red) and, 5MESSI₂ (blue); at room temperature in the 170-400 nm range, using a 0.1 mm cell, corrected for solvent baseline. Samples were measured in H₂O Concentrations were varied due to absorbance: 5MESSCl₂ 4.97 μM, 5MESSBr₂ 2.22 μM and 5MESSI₂ 2.75 μM.

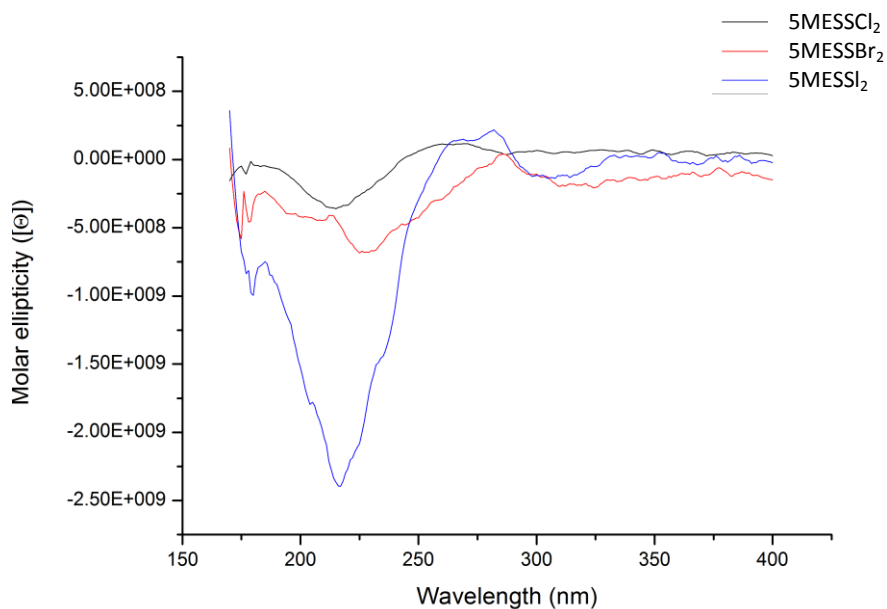


Figure D5: SRCD spectra of 5MESSCl₂ (black), 5MESSBr₂ (red) and, 5MESSI₂ (blue); at room temperature in the 170-400 nm range, using a 0.1 mm cell, corrected for solvent baseline. Samples were measured in H₂O Concentrations were varied due to absorbance: 5MESSCl₂ 4.97 μM, 5MESSBr₂ 2.22 μM and 5MESSI₂ 2.75 μM.

SRCD Spectra of 56MESS(X)₂

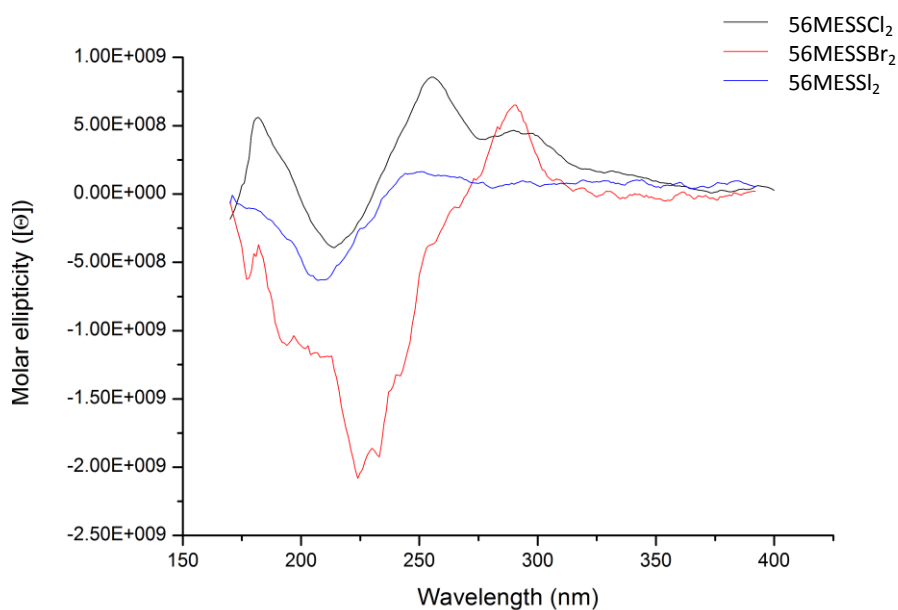


Figure D6: SRCD spectra of 56MESSCl₂ (black), 56MESSBr₂ (red) and, 56MESSI₂ (blue); at room temperature in the 170-400 nm range, using a 0.1 mm cell, corrected for solvent baseline. Samples were measured in H₂O Concentrations were varied due to absorbance: 56MESSCl₂ 4.18 μM, 56MESSBr₂ 3.27 μM and 56MESSI₂ 3.98 μM.

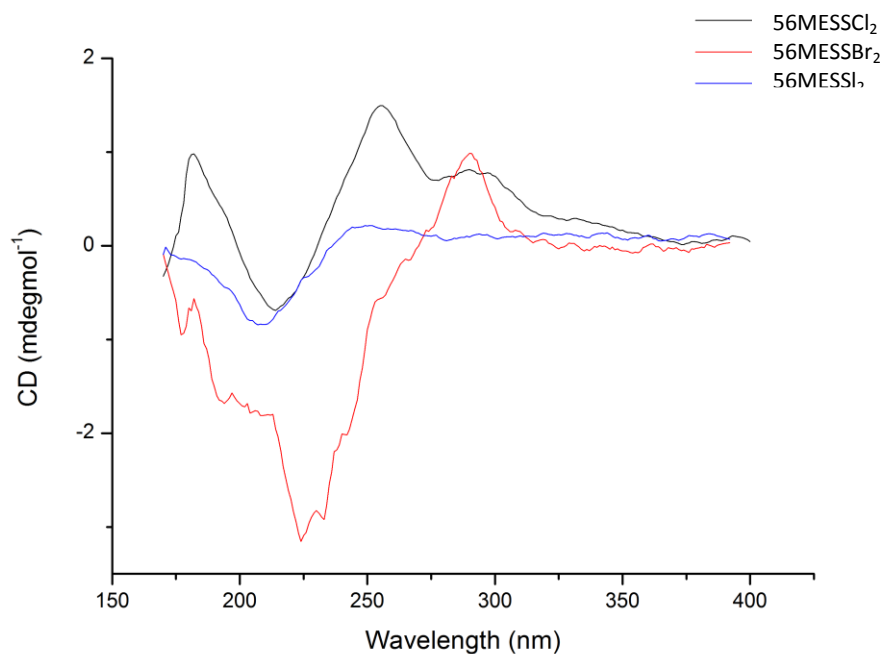


Figure D7: SRCD spectra of 56MESSCl₂ (black), 56MESSBr₂ (red) and, 56MESSI₂ (blue); at room temperature in the 170-400 nm range, using a 0.1 mm cell, corrected for solvent baseline. Samples were measured in H₂O Concentrations were varied due to absorbance: 56MESSCl₂ 4.18 μM, 56MESSBr₂ 3.27 μM and 56MESSI₂ 3.98 μM.

Spectra by Axial Ligand

SRCD Spectra of Chloro compounds

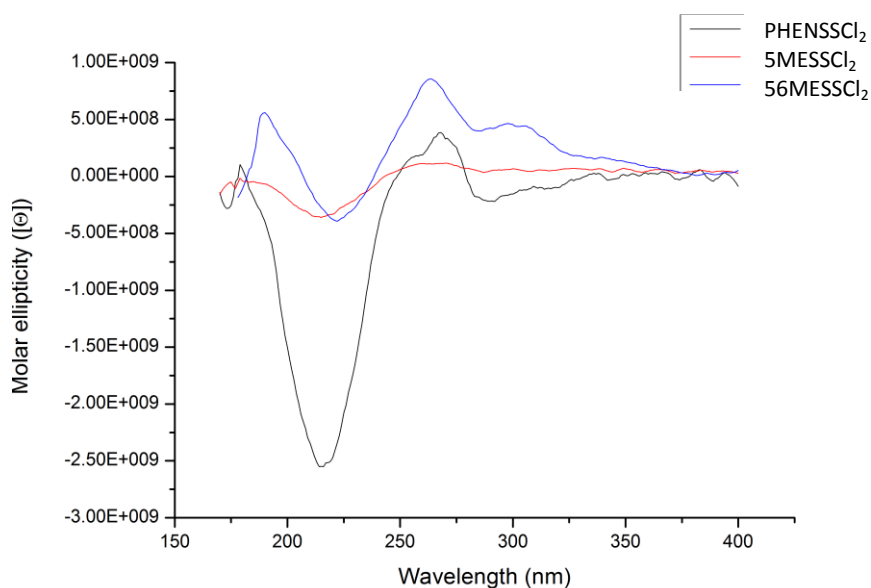


Figure D8: SRCD spectra of PHENSSCL₂ (black), 5MESSCL₂ (red) and, 56MESSCL₂ (blue); at room temperature in the 170-400 nm range, using a 0.1 mm cell, corrected for solvent baseline. Samples were measured in H₂O Concentrations were varied due to absorbance: PHENSSCL₂ 1.77 μM, 5MESSCL₂ 4.97 μM and 56MESSCL₂ 4.18 μM.

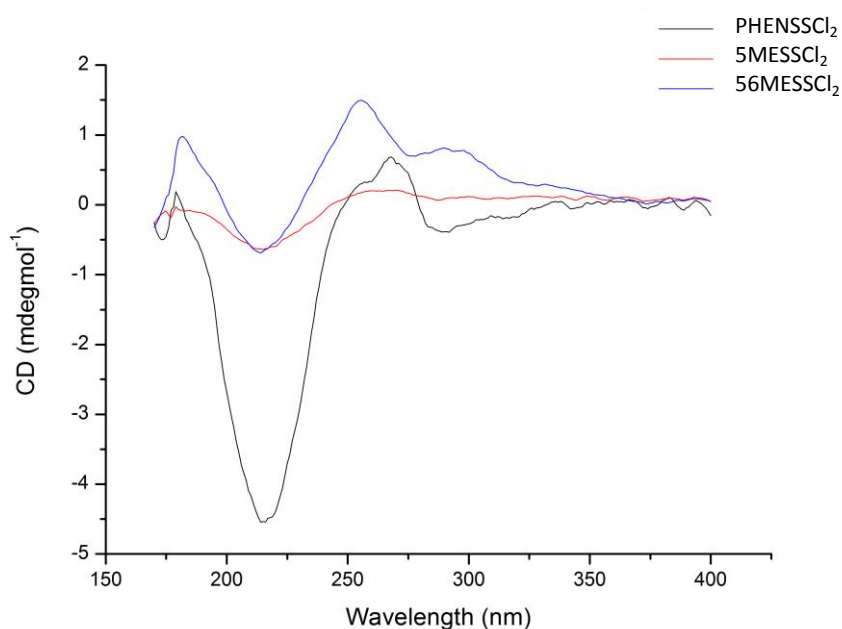


Figure D9: SRCD spectra of PHENSSCL₂ (black), 5MESSCL₂ (red) and, 56MESSCL₂ (blue); at room temperature in the 170-400 nm range, using a 0.1 mm cell, corrected for solvent baseline. Samples were measured in H₂O Concentrations were varied due to absorbance: PHENSSCL₂ 1.77 μM, 5MESSCL₂ 4.97 μM and 56MESSCL₂ 4.18 μM.

SRCD Spectra of Bromo compounds

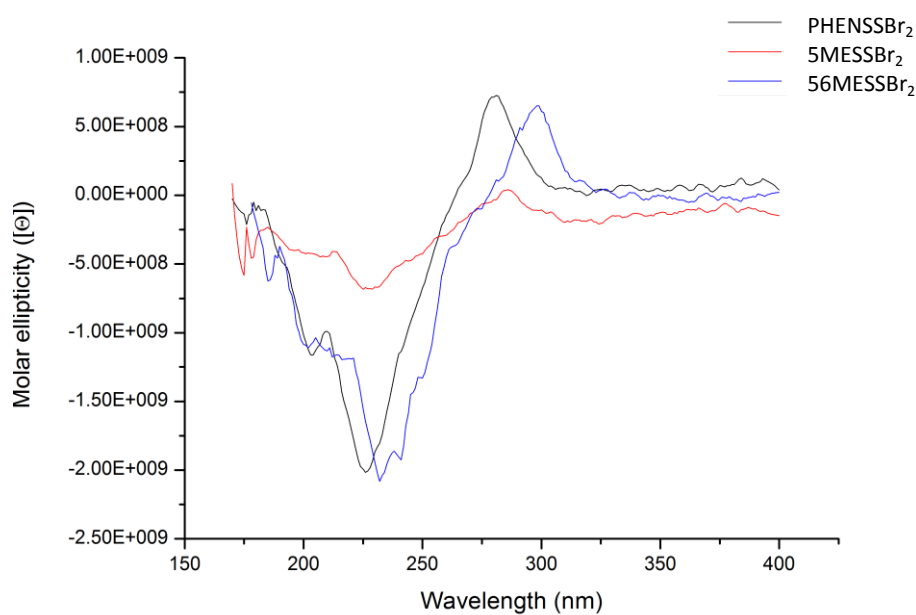


Figure D10: SRCD spectra of PHENSSBr₂ (black), 5MESSBr₂ (red) and, 56MESSBr₂ (blue); at room temperature in the 170-400 nm range, using a 0.1 mm cell, corrected for solvent baseline. Samples were measured in H₂O Concentrations were varied due to absorbance: PHENSSBr₂ 2.74 μM, 5MESSBr₂ 2.22 μM and 56MESSBr₂ 3.27 μM.

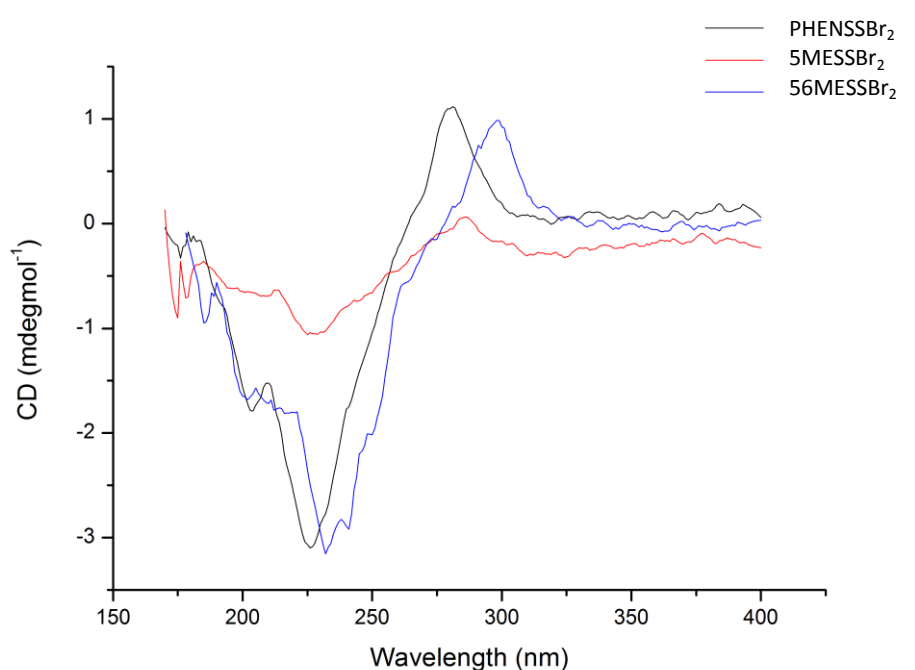


Figure D11: SRCD spectra of PHENSSBr₂ (black), 5MESSBr₂ (red) and, 56MESSBr₂ (blue); at room temperature in the 170-400 nm range, using a 0.1 mm cell, corrected for solvent baseline. Samples were measured in H₂O Concentrations were varied due to absorbance: PHENSSBr₂ 2.74 μM, 5MESSBr₂ 2.22 μM and 56MESSBr₂ 3.27 μM.

SRCD Spectra of Iodo compounds

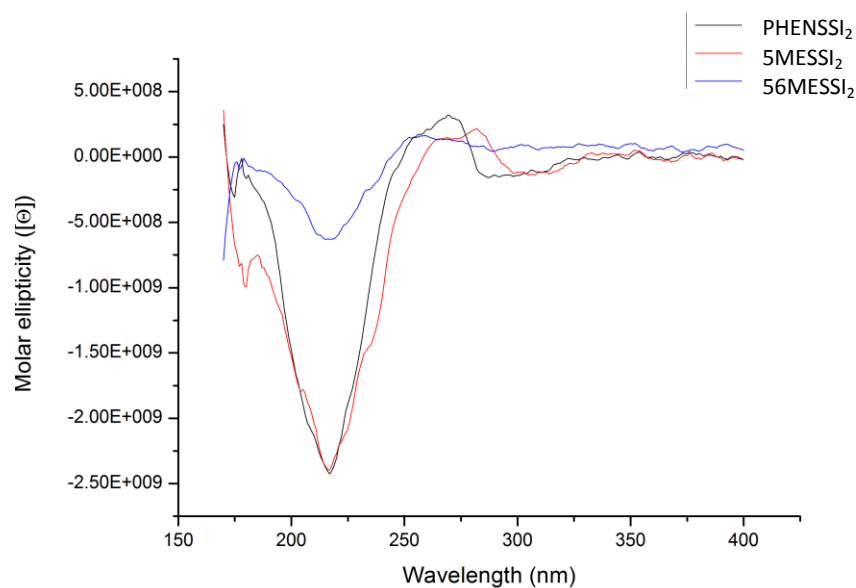


Figure D12: SRCD spectra of PHENSSI₂ (black), 5MESSI₂ (red) and, 56MESSI₂ (blue); at room temperature in the 170-400 nm range, using a 0.1 mm cell, corrected for solvent baseline. Samples were measured in H₂O Concentrations were varied due to absorbance: PHENSSI₂ 2.74 μM, 5MESSI₂ 2.75 μM and 56MESSI₂ 3.98 μM.

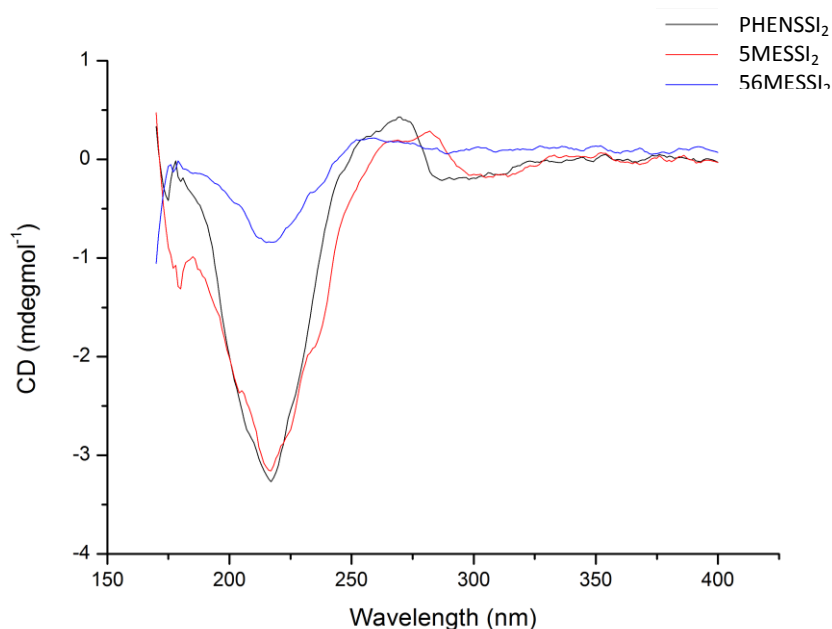


Figure D13: SRCD spectra of PHENSSI₂ (black), 5MESSI₂ (red) and, 56MESSI₂ (blue); at room temperature in the 170-400 nm range, using a 0.1 mm cell, corrected for solvent baseline. Samples were measured in H₂O Concentrations were varied due to absorbance: PHENSSI₂ 2.74 μM, 5MESSI₂ 2.75 μM and 56MESSI₂ 3.98 μM.

SRCD Spectra PHENSS(Cl)₂

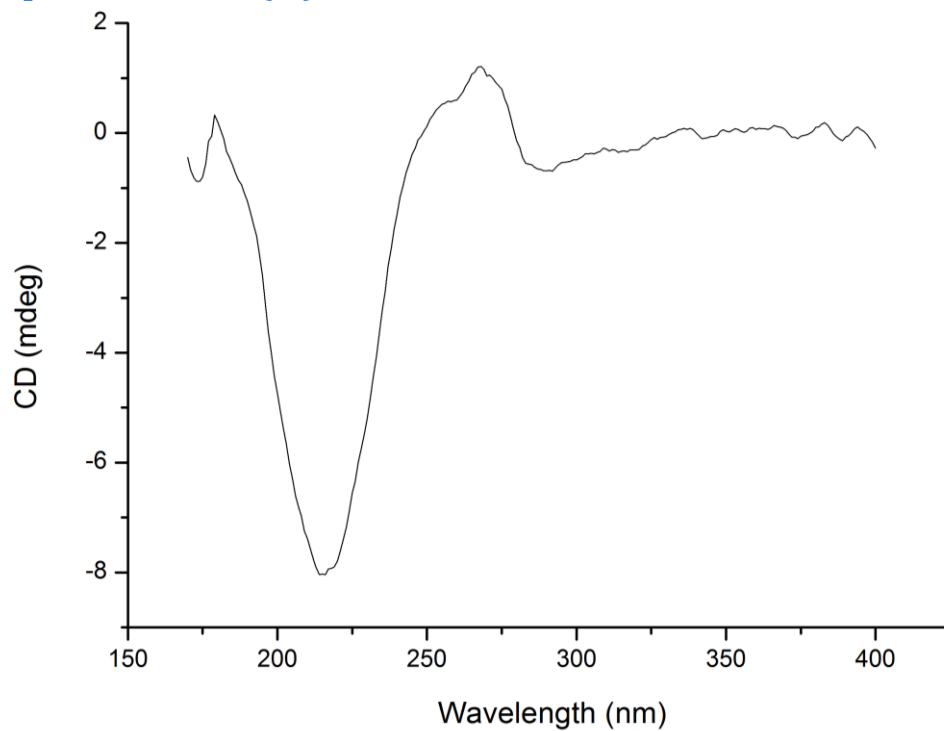


Figure D14: SRCD spectra of PHENSSCl₂ at room temperature in the 170-400 nm range, using a 0.1 mm cell, corrected for solvent baseline, measured in H₂O at 1.77 μM.

SRCD Spectra PHENSS(Br)₂

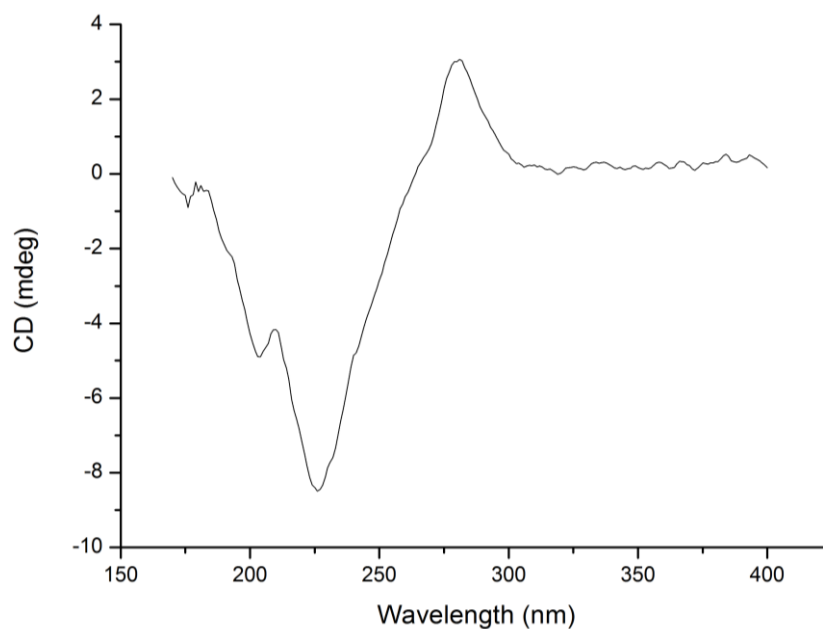


Figure D15: SRCD spectra of PHENSSBr₂ at room temperature in the 170-400 nm range, using a 0.1 mm cell, corrected for solvent baseline, measured in H₂O at 2.74 μM.

SRCD Spectra PHENSS(I)₂

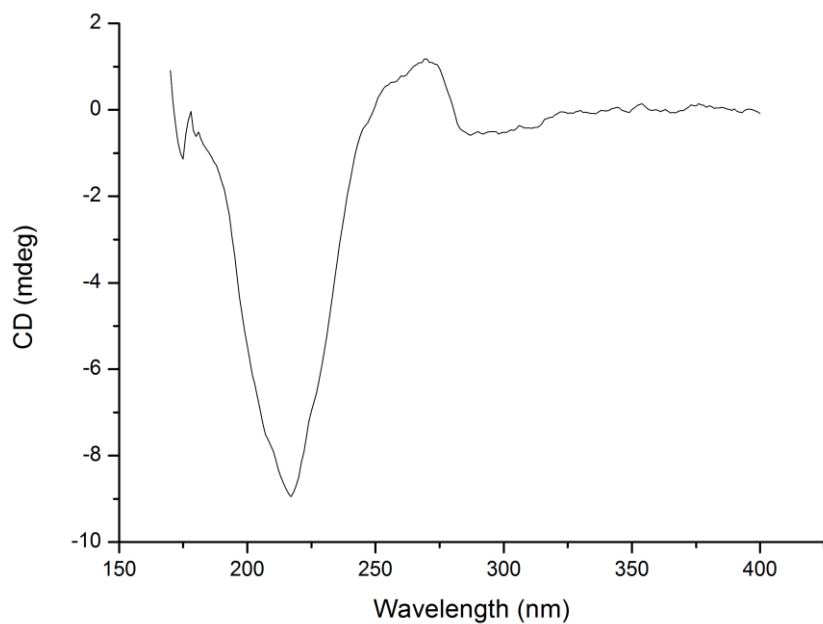


Figure D15: SRCD spectra of PHENSS(I)₂ at room temperature in the 170-400 nm range, using a 0.1 mm cell, corrected for solvent baseline, measured in H₂O at 2.74 μM.

SRCD Spectra 5MESS(Cl)₂

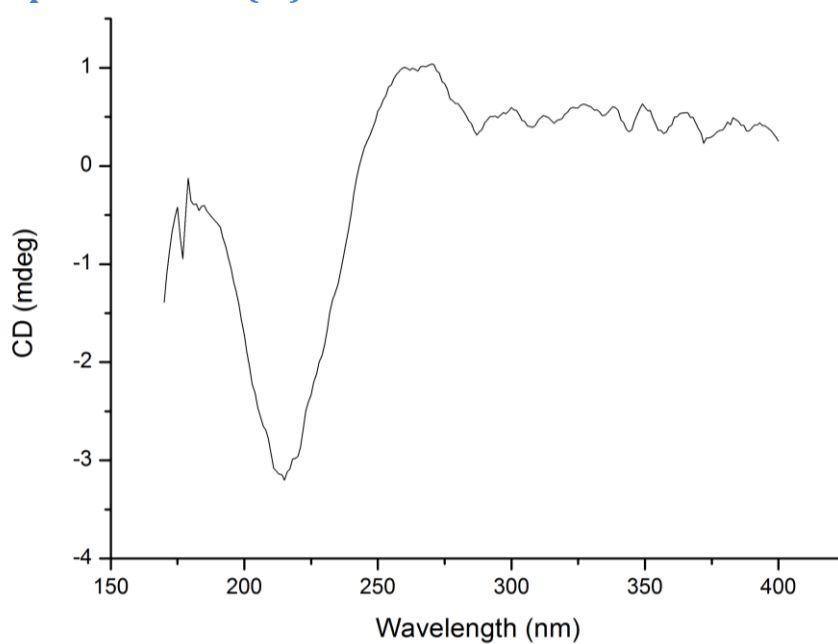


Figure D16: SRCD spectra of 5MESS(Cl)₂ at room temperature in the 170-400 nm range, using a 0.1 mm cell, corrected for solvent baseline, measured in H₂O at 4.97 μM.

SRCD Spectra 5MESS(Br)₂

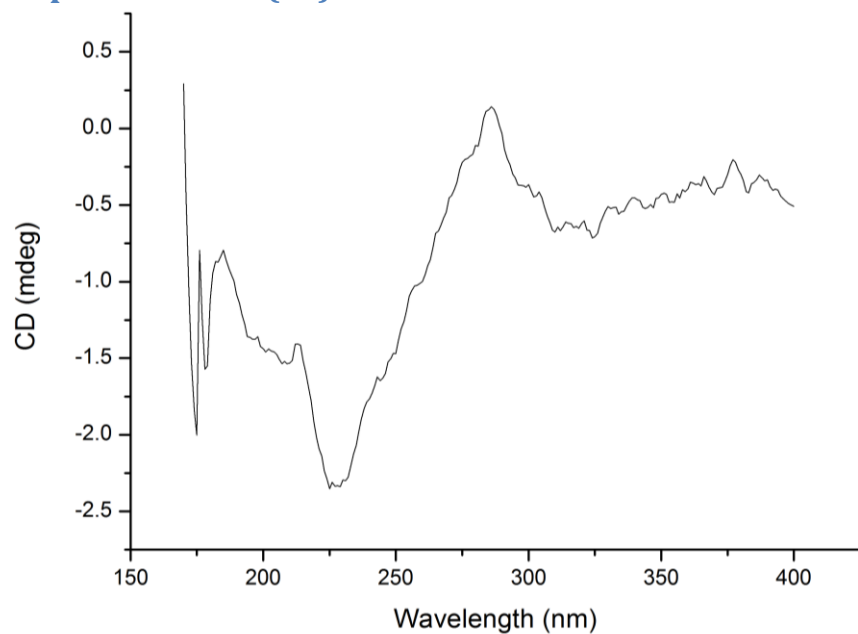


Figure D17: SRCD spectra of 5MESSBr₂ at room temperature in the 170-400 nm range, using a 0.1 mm cell, corrected for solvent baseline. , measured in H₂O at 2.22 μM.

SRCD Spectra 5MESS(I)₂

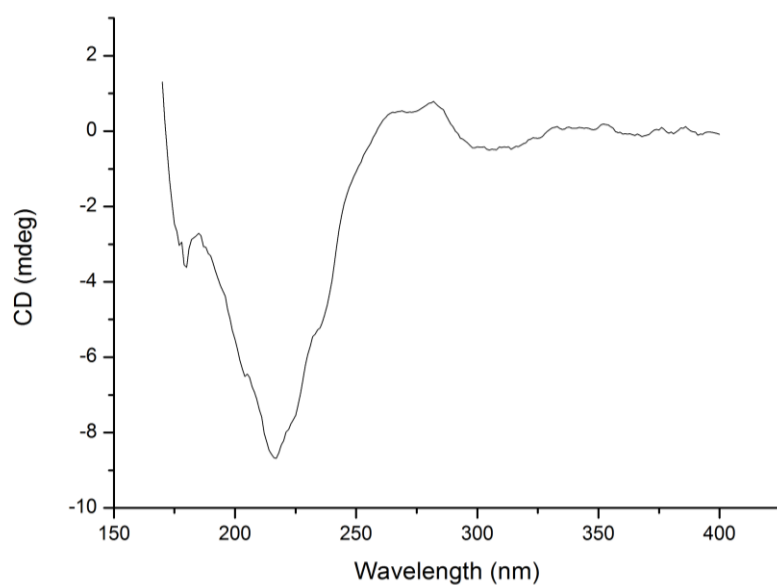


Figure D18: SRCD spectra of 5MESSI₂ at room temperature in the 170-400 nm range, using a 0.1 mm cell, corrected for solvent baseline, measured in H₂O at 2.75 μM.

SRCD Spectra 56MESS(Cl)₂

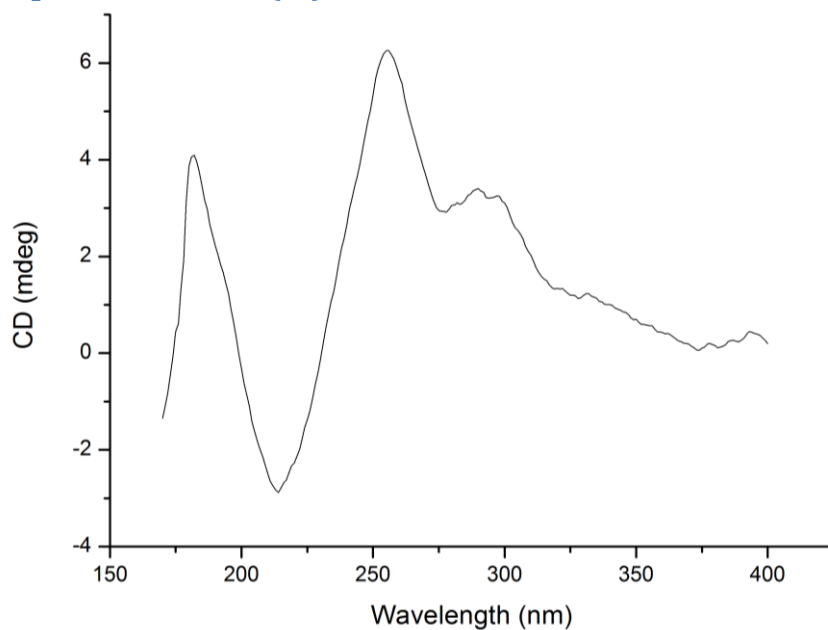


Figure D19: SRCD spectra of 56MESSCl₂ at room temperature in the 170-400 nm range, using a 0.1 mm cell, corrected for solvent baseline, measured in H₂O at 4.18 μM.

SRCD Spectra 56MESS(Br)₂

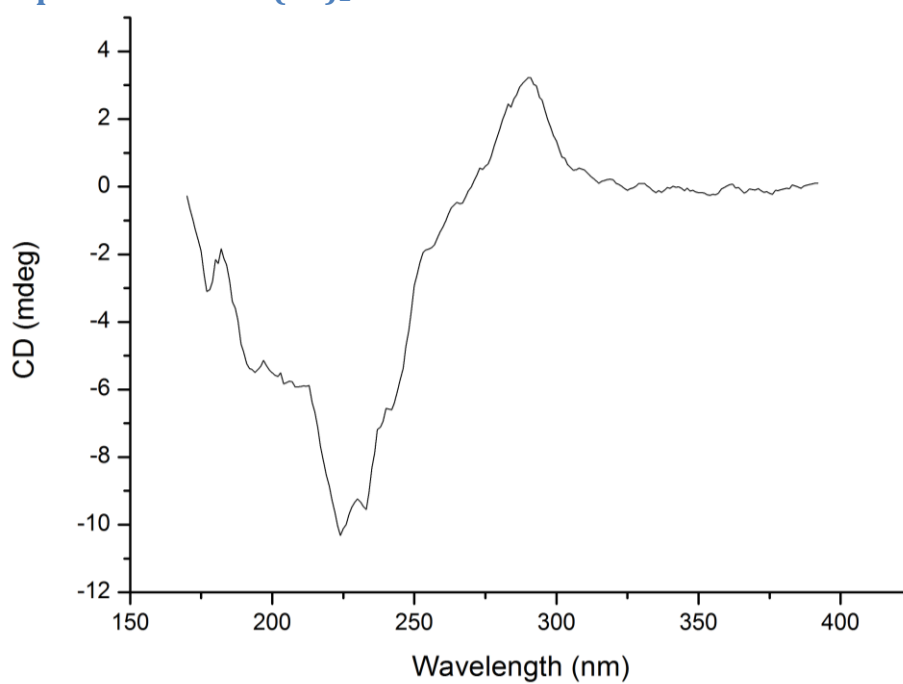


Figure D20: SRCD spectra of 56MESSBr₂ at room temperature in the 170-400 nm range, using a 0.1 mm cell, corrected for solvent baseline, measured in H₂O at 3.27 μM.

SRCD Spectra 56MeSS(I)₂

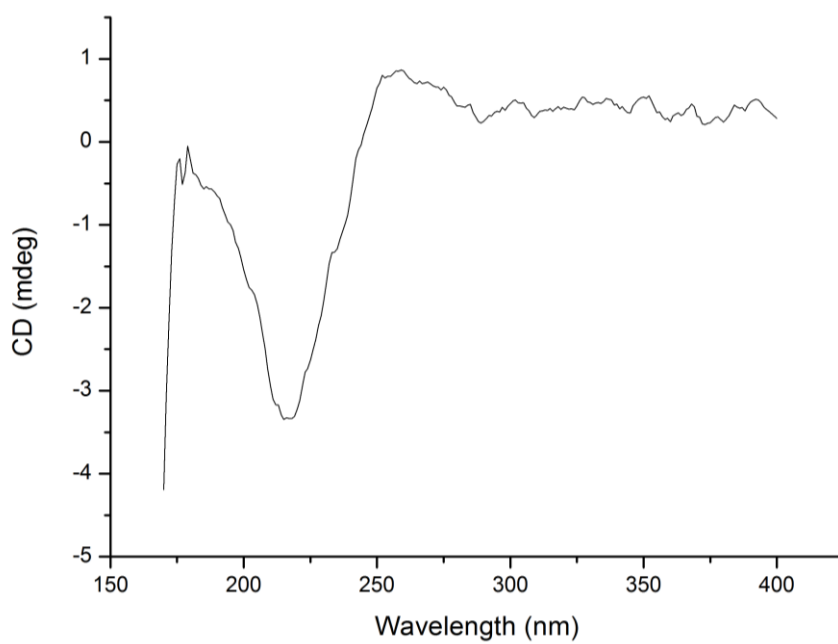


Figure D21: SRCD spectra of 56MESSI₂ at room temperature in the 170-400 nm range, using a 0.1 mm cell, corrected for solvent baseline, measured in H₂O at 3.98 μM.

Cytotoxicity

Tables

DOSE SCREEN:

Table E1: Percentage (%) Cell Growth Inhibition in response to 25 μ M of Drug (*The higher the value the greater the growth inhibition*)

COMPOUND NAME AND TUBE NUMBER:			HT29	U87	MCF-7	A2780	H460	A431	Du145	BE2-C	SJ-G2	MIA	MCF10 A	ADDP
			<i>Colon</i>	<i>Glioblas toma</i>	<i>Breast</i>	<i>Ovarian</i>	<i>Lung</i>	<i>Skin</i>	<i>Prostate</i>	<i>Neurobl astoma</i>	<i>Glioblas toma</i>	<i>Pancrea s</i>	<i>Breast (Normal)</i>	<i>Ovarian</i>
			<i>n=3-6</i>	<i>n=3-6</i>	<i>n=3-6</i>	<i>n=3-6</i>	<i>n=3-6</i>	<i>n=3-6</i>	<i>n=3-6</i>	<i>n=3-6</i>	<i>n=3-6</i>	<i>n=3-6</i>	<i>n=3-6</i>	<i>n=3-6</i>
B16	1	BM01 - PhenSS(IV)Cl₂	>100	>100	>100	>100	>100	>100	>100	>100	>100	>100	>100	>100
B16	2	BM02 - PhenSS(IV)Br₂	>100	>100	>100	>100	>100	>100	>100	>100	>100	>100	>100	>100
B16	3	BM03 - PhenSS(IV)I₂	>100	>100	>100	>100	>100	>100	>100	>100	>100	>100	>100	>100
B16	4	BM04 - 5MeSS(IV)Cl₂	>100	>100	>100	>100	>100	>100	>100	>100	>100	>100	>100	>100
B16	5	BM05 - 5MeSS(IV)Br₂	>100	>100	>100	>100	>100	>100	>100	>100	>100	>100	>100	>100
B16	6	BM06 - 5MeSS(IV)I₂	>100	>100	>100	>100	>100	>100	>100	>100	>100	>100	>100	>100
B16	7	BM07 - 56MeSS(IV)Cl₂	>100	>100	>100	>100	>100	>100	>100	>100	>100	>100	>100	>100
B16	8	BM08 - 56MeSS(IV)Br₂	>100	>100	>100	>100	>100	>100	>100	>100	>100	>100	>100	>100
B16	9	BM09 - 56MeSS(IV)I₂	>100	>100	>100	>100	>100	>100	>100	>100	>100	>100	>100	>100

DOSE RESPONSE:

Table E1: GI₅₀ = Concentration (μM) that inhibits cell growth by 50% (*The higher the value the greater the growth inhibition*)

COMPOUND NAME AND TUBE NUMBER:		HT29	U87	MCF-7	A2780	H460	A431	Du145	BE2-C	SJ-G2	MIA	MCF10 A	ADDP	
		<i>Colon</i>	<i>Glioblast oma</i>	<i>Breast</i>	<i>Ovarian</i>	<i>Lung</i>	<i>Skin</i>	<i>Prostate</i>	<i>Neurobl astoma</i>	<i>Glioblast oma</i>	<i>Pancrea s</i>	<i>Breast (Normal)</i>	<i>Ovarian</i>	
		<i>n=3-4</i>	<i>n=3-4</i>	<i>n=3-4</i>	<i>n=3-4</i>	<i>n=3-4</i>	<i>n=3-4</i>	<i>n=3-4</i>	<i>n=3-4</i>	<i>n=3-4</i>	<i>n=3-4</i>	<i>n=3-4</i>	<i>n=3-4</i>	
B1	1	BM01 -	0.11	0.81	0.46	0.23	0.33 ±	0.44 ±	0.11	0.44	0.34 ±	0.21 ±	0.30 ±	0.23
61		PhenSS(IV)Cl₂	±0.028	±0.15	±0.069	±0.0058	0.0088	0.045	±0.033	±0.050	0.063	0.029	.0033	±0.026
B1	2	BM02 -	0.16	0.82	0.53	0.27	0.36	0.68	0.18	0.52	0.42	0.25	0.36	0.28
61		PhenSS(IV)Br₂	±0.015	±0.090	±0.10	±0.023	±0.029	±0.023	±0.010	±0.025	±0.071	±0.010	±0.032	±0.017
B1	3	BM03 -	0.10	0.70	0.46	0.24	0.32	0.44	0.11	0.37	0.31	0.20	0.29	0.25
61		PhenSS(IV)I₂	±0.0033	±0.055	±0.10	±0.059	±0.031	±0.021	±0.0033	±0.0000 0	±0.031	±0.013	±0.032	±0.020
B1	4	BM04 -	0.032	0.23	0.22	0.25	0.089	0.13	0.023	0.25	0.18	0.044	0.094	0.056
61		5MeSS(IV)Cl₂	±0.0036	±0.033	±0.13	±0.18	±0.018	±0.028	±0.0030	±0.060	±0.034	±0.0045	±0.024	±0.0032
B1	5	BM05 -	0.035	0.20	0.087	0.044	0.070	0.11	0.025	0.20	0.16	0.037	0.062	0.048
61		5MeSS(IV)Br₂	±0.0058	±0.029	±0.032	±0.012	±0.0091	±0.015	±0.0053	±0.010	±0.044	±0.0046	±0.0083	±0.0046
B1	6	BM06 -	0.032	0.22	0.091	0.046	0.065	0.10	0.027	0.20	0.16 ±	0.032	0.061	0.044
61		5MeSS(IV)I₂	±0.0035	±0.030	±0.026	±0.010	±0.0061	±0.0123	±0.0027	±0.0000 0	.040	±0.0022	±0.0082	±0.0058
B1	7	BM07 -	0.025	0.12	0.060	0.037	0.048	0.062	0.012	0.12	0.092	0.028	0.044	0.036
61		56MeSS(IV)Cl₂	±0.0020	±0.018	±0.010	±0.0067	±0.012	±0.013	±0.0017	±0.0000 0	±0.039	±0.0021	±0.0062	±0.0041
B1	8	BM08 -	0.021	0.090	0.11	0.035	0.032	0.061	0.011	0.34	0.074	0.024	0.034	0.033
61		56MeSS(IV)Br₂	±0.0023	±0.012	±0.056	±0.013	±0.0020	±0.011	±0.0031	±0.18	±0.033	±0.0026	±0.0038	±0.0023
B1	9	BM09 -	0.019	0.074	0.033	0.032	0.027	0.037	0.025	0.087	0.067	0.022	0.030	0.027
61		56MeSS(IV)I₂	±0.0032	±0.014	±0.0068	±0.017	±0.0032	±0.0054	±0.017	±0.063	±0.028	±0.0022	±0.0039	±0.0007

Figures

Spectra by axial ligand

IC₅₀ values of [Pt(P_L)(A_L)(Cl)₂]²⁺ type complexes

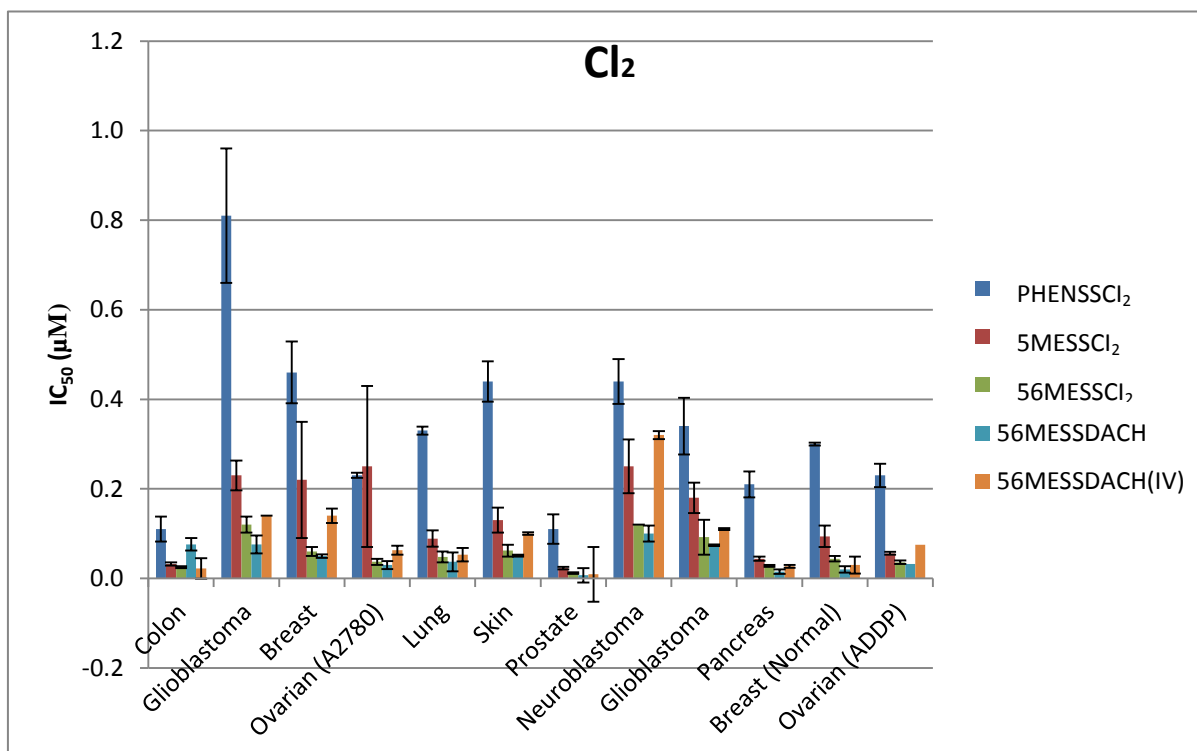


Figure E1: IC₅₀ values of PHENSSCl₂, 5MESSCl₂, 56MESSCl₂, 56MESS, and 56MESSOH₂ in multiple cell lines: HT29 colon, U87 glioblastoma, MCF-7 breast, A2780 ovarian, H460 lung, A431 skin, Du145 prostate, BE2-C neuroblastoma, SJ-G2 glioblastoma, MIA pancreas, MCF10A breast (normal), and SMA glioblastoma (murine).

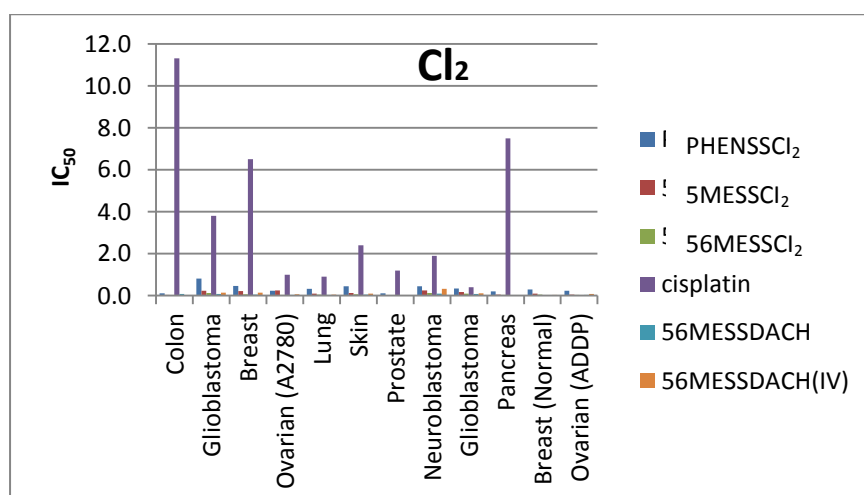


Figure E2: IC₅₀ values of PHENSSCl₂, 5MESSCl₂, 56MESSCl₂, 56MESS, 56MESSOH₂, and cisplatin in multiple cell lines: HT29 colon, U87 glioblastoma, MCF-7 breast, A2780 ovarian, H460 lung, A431 skin, Du145 prostate, BE2-C neuroblastoma, SJ-G2 glioblastoma, MIA pancreas, MCF10A breast (normal), and SMA glioblastoma (murine).

IC₅₀ values of [Pt(P_L)(A_L)(Br)₂]²⁺ type complexes

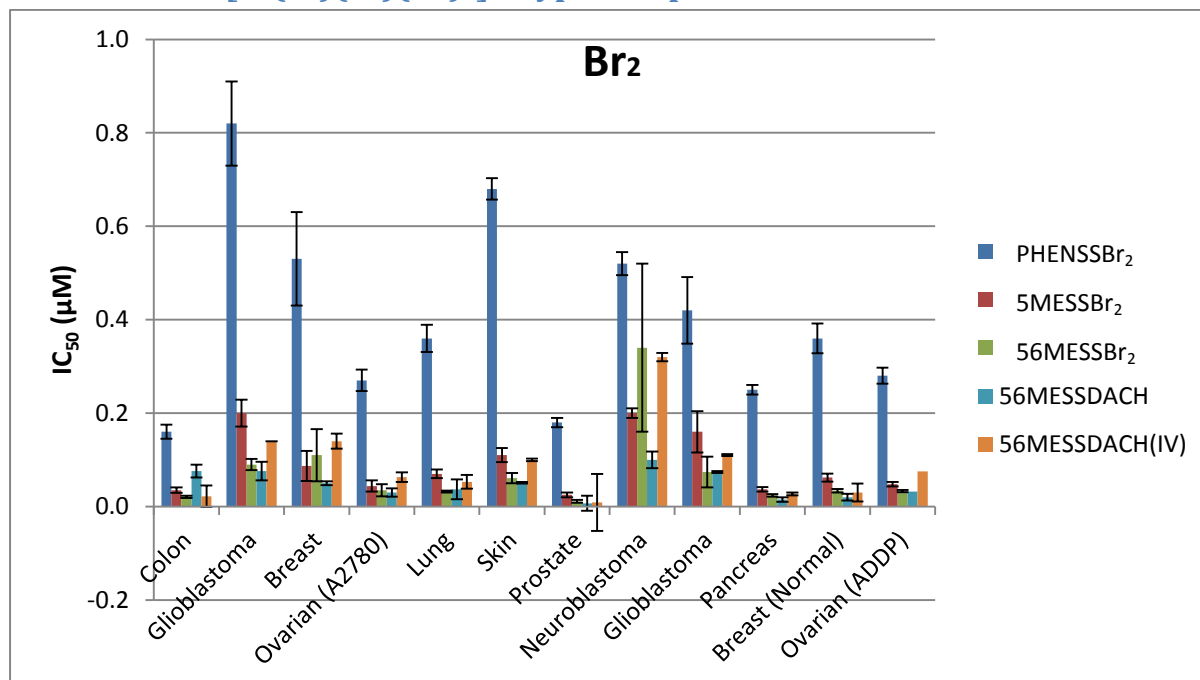


Figure E3: IC₅₀ values of PHENSSBr₂, 5MESSBr₂, 56MESSBr₂, 56MESS, and 56MESSOH₂ in multiple cell lines: HT29 colon, U87 glioblastoma, MCF-7 breast, A2780 ovarian, H460 lung, A431 skin, Du145 prostate, BE2-C neuroblastoma, SJ-G2 glioblastoma, MIA pancreas, MCF10A breast (normal), and SMA glioblastoma (murine).

Compared to cisplatin:

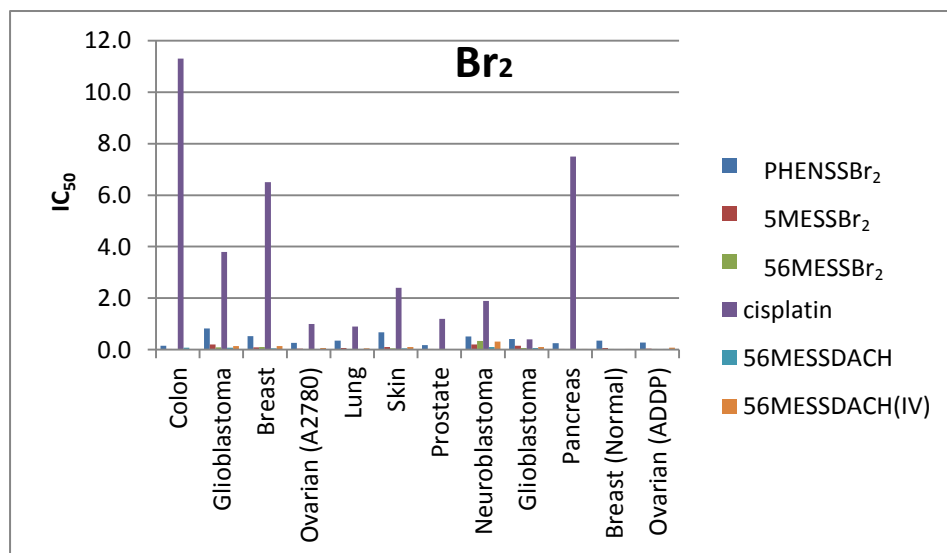


Figure E3: IC₅₀ values of PHENSSBr₂, 5MESSBr₂, 56MESSBr₂, 56MESS, 56MESSOH₂, and cisplatin in multiple cell lines: HT29 colon, U87 glioblastoma, MCF-7 breast, A2780 ovarian, H460 lung, A431 skin, Du145 prostate, BE2-C neuroblastoma, SJ-G2 glioblastoma, MIA pancreas, MCF10A breast (normal), and SMA glioblastoma (murine).

IC₅₀ values of [Pt(P_L)(A_L)(I)₂]²⁺ type complexes

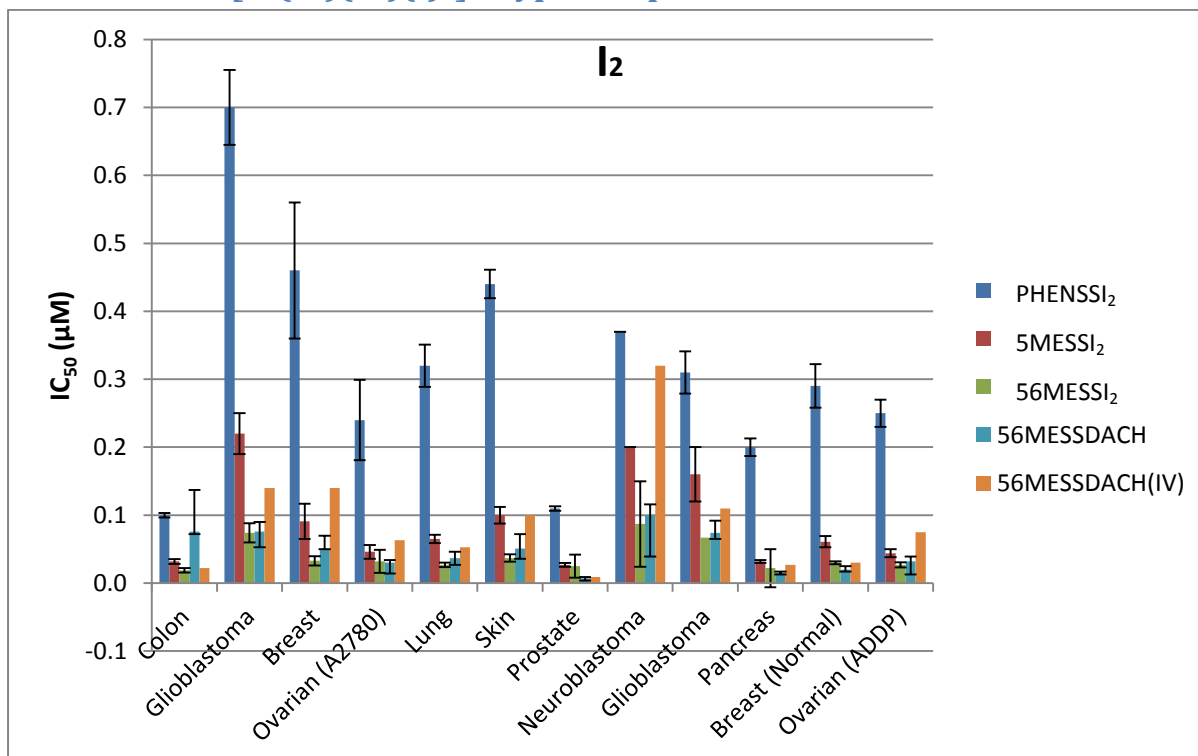


Figure E5: IC₅₀ values of PHENSSI₂, 5MESSI₂, 56MESSI₂, 56MESS, and 56MESSOH₂ in multiple cell lines: HT29 colon, U87 glioblastoma, MCF-7 breast, A2780 ovarian, H460 lung, A431 skin, Du145 prostate, BE2-C neuroblastoma, SJ-G2 glioblastoma, MIA pancreas, MCF10A breast (normal), and SMA glioblastoma (murine).

Compared to cisplatin:

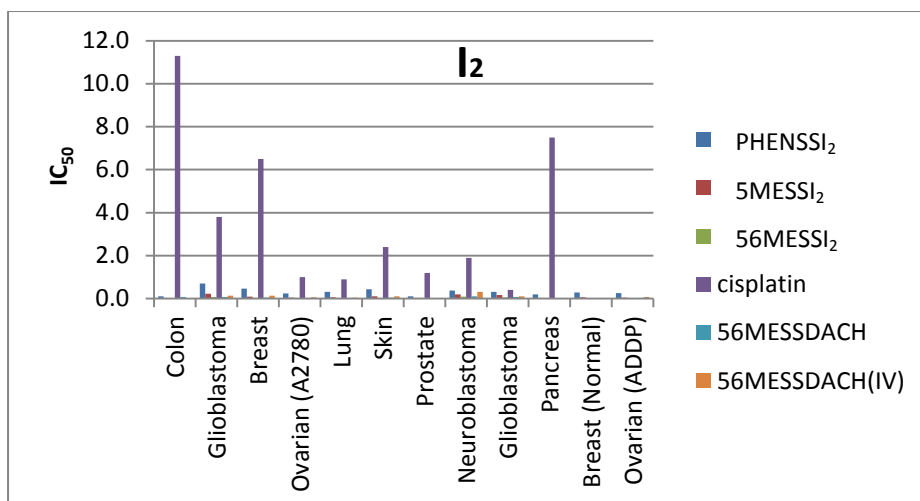


Figure E8: IC₅₀ values of PHENSSI₂, 5MESSI₂, 56MESSI₂, 56MESS, 56MESSOH₂, and cisplatin in multiple cell lines: HT29 colon, U87 glioblastoma, MCF-7 breast, A2780 ovarian, H460 lung, A431 skin, Du145 prostate, BE2-C neuroblastoma, SJ-G2 glioblastoma, MIA pancreas, MCF10A breast (normal), and SMA glioblastoma (murine).

Spectra by polyaromatic ligand

IC₅₀ values of PHENSSX₂ type complexes

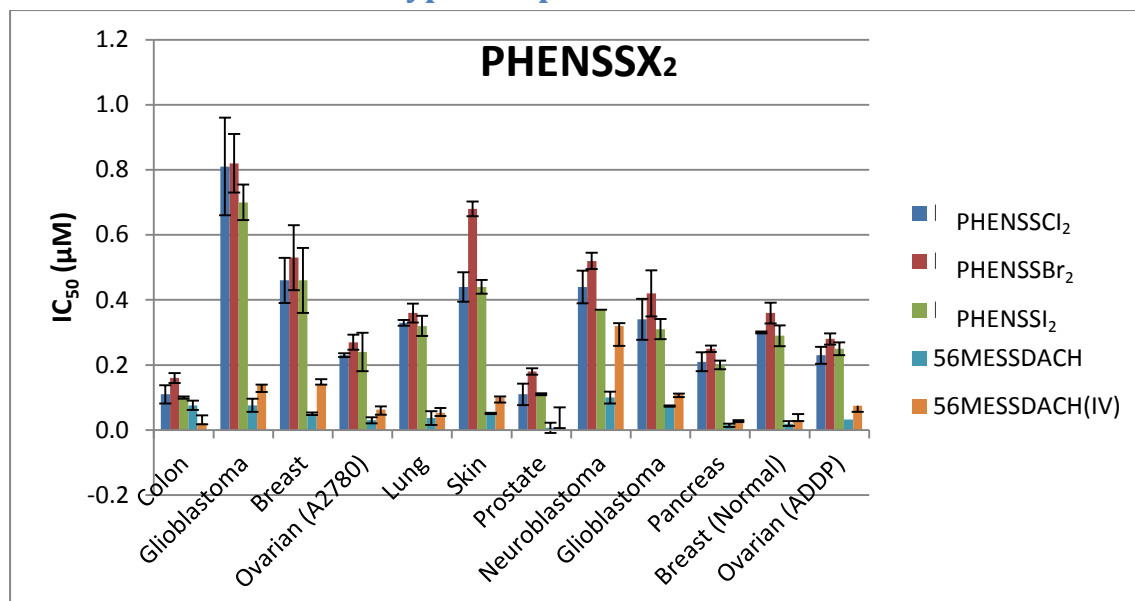


Figure E7: IC₅₀ values of PHENSSCl₂, PHENSSBr₂, PHENSSI₂, 56MESS, and 56MESSOH₂ in multiple cell lines: HT29 colon, U87 glioblastoma, MCF-7 breast, A2780 ovarian, H460 lung, A431 skin, Du145 prostate, BE2-C neuroblastoma, SJ-G2 glioblastoma, MIA pancreas, MCF10A breast (normal), and SMA glioblastoma (murine).

Compared to cisplatin:

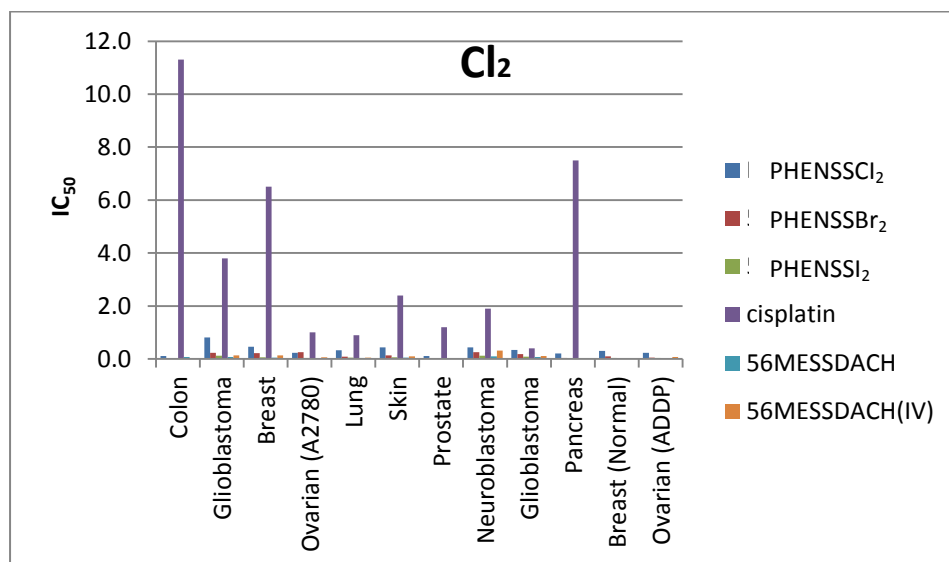


Figure E8: IC₅₀ values of PHENSSCl₂, PHENSSBr₂, PHENSSI₂, 56MESS, 56MESSOH₂, and cisplatin in multiple cell lines: HT29 colon, U87 glioblastoma, MCF-7 breast, A2780 ovarian, H460 lung, A431 skin, Du145 prostate, BE2-C neuroblastoma, SJ-G2 glioblastoma, MIA pancreas, MCF10A breast (normal), and SMA glioblastoma (murine).

IC₅₀ values of 5MESSX₂ type complexes

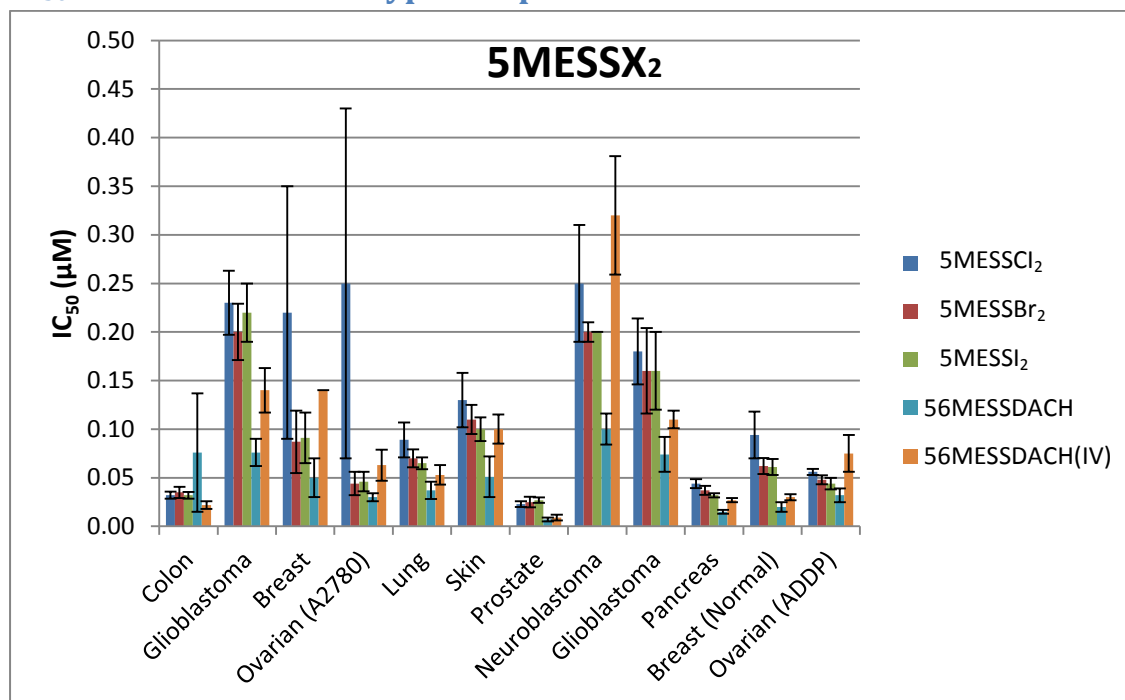


Figure E9: IC₅₀ values of 5MESSCl₂, 5MESSBr₂, 5MESSI₂, 56MESS, and 56MESSOH₂ in multiple cell lines: HT29 colon, U87 glioblastoma, MCF-7 breast, A2780 ovarian, H460 lung, A431 skin, Du145 prostate, BE2-C neuroblastoma, SJ-G2 glioblastoma, MIA pancreas, MCF10A breast (normal), and SMA glioblastoma (murine).

Compared to cisplatin

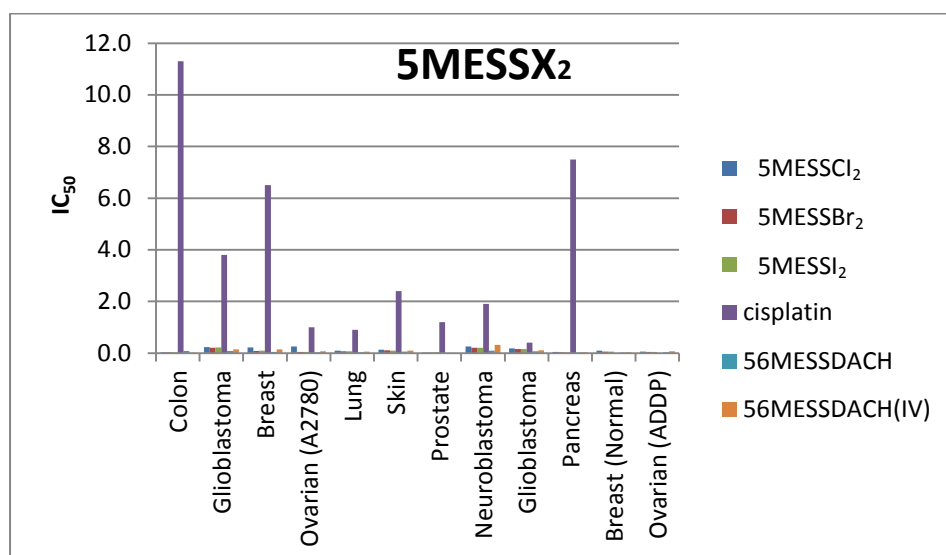


Figure E10: IC₅₀ values of 5MESSCl₂, 5MESSBr₂, 5MESSI₂, 56MESS, 56MESSOH₂, and cisplatin in multiple cell lines: HT29 colon, U87 glioblastoma, MCF-7 breast, A2780 ovarian, H460 lung, A431 skin, Du145 prostate, BE2-C neuroblastoma, SJ-G2 glioblastoma, MIA pancreas, MCF10A breast (normal), and SMA glioblastoma (murine).

IC₅₀ values of 56MESSX₂ type complexes

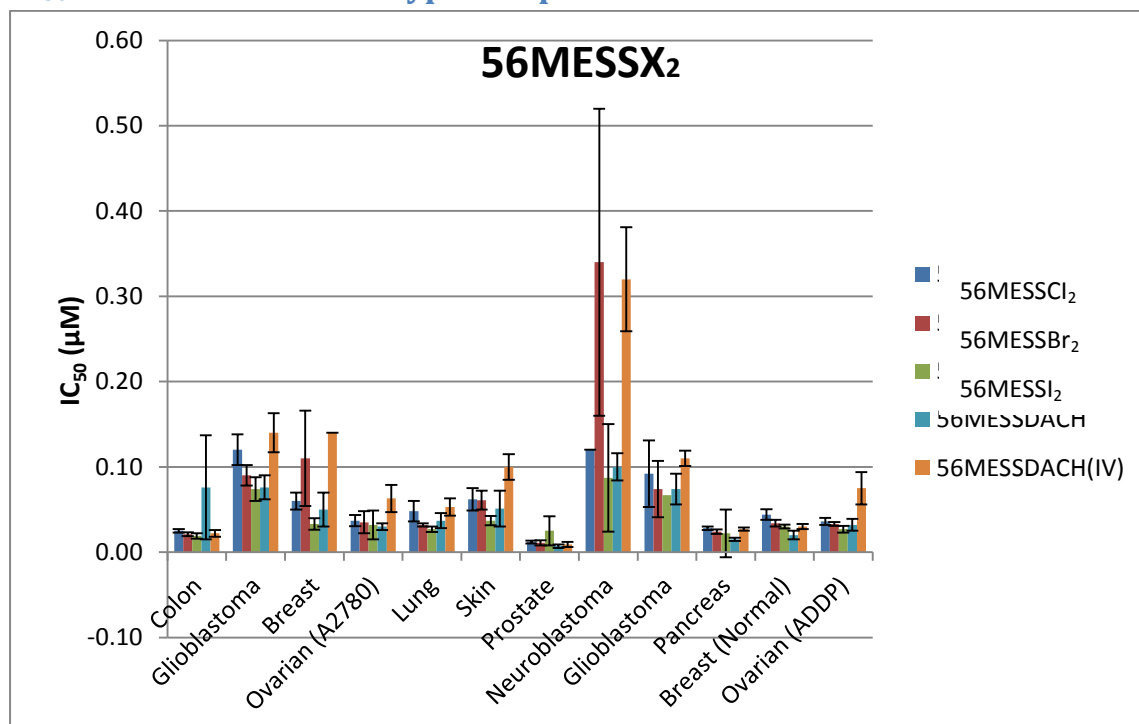


Figure E11: IC₅₀ values of 56MESSCl₂, 56MESSBr₂, 56MESSI₂, 56MESS, and 56MESSOH₂ in multiple cell lines: HT29 colon, U87 glioblastoma, MCF-7 breast, A2780 ovarian, H460 lung, A431 skin, Du145 prostate, BE2-C neuroblastoma, SJ-G2 glioblastoma, MIA pancreas, MCF10A breast (normal), and SMA glioblastoma (murine).

Compared to cisplatin:

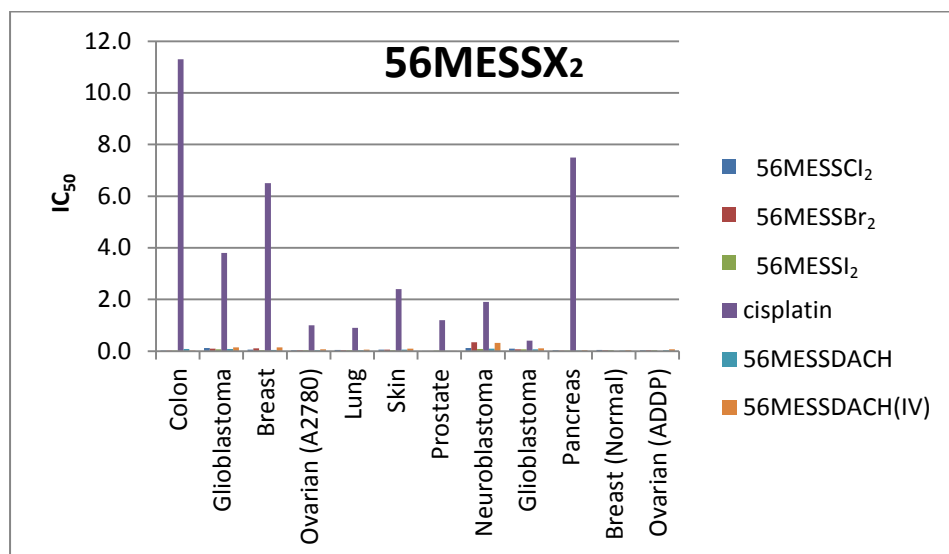


Figure E11: IC₅₀ values of 56MESSCl₂, 56MESSBr₂, 56MESSI₂, 56MESS, 56MESSOH₂, and cisplatin in multiple cell lines: HT29 colon, U87 glioblastoma, MCF-7 breast, A2780 ovarian, H460 lung, A431 skin, Du145 prostate, BE2-C neuroblastoma, SJ-G2 glioblastoma, MIA pancreas, MCF10A breast (normal), and SMA glioblastoma (murine).

ESIMS Data

PHENSSCl₂

180725_Sample01 22 (0.450) Cm (22)

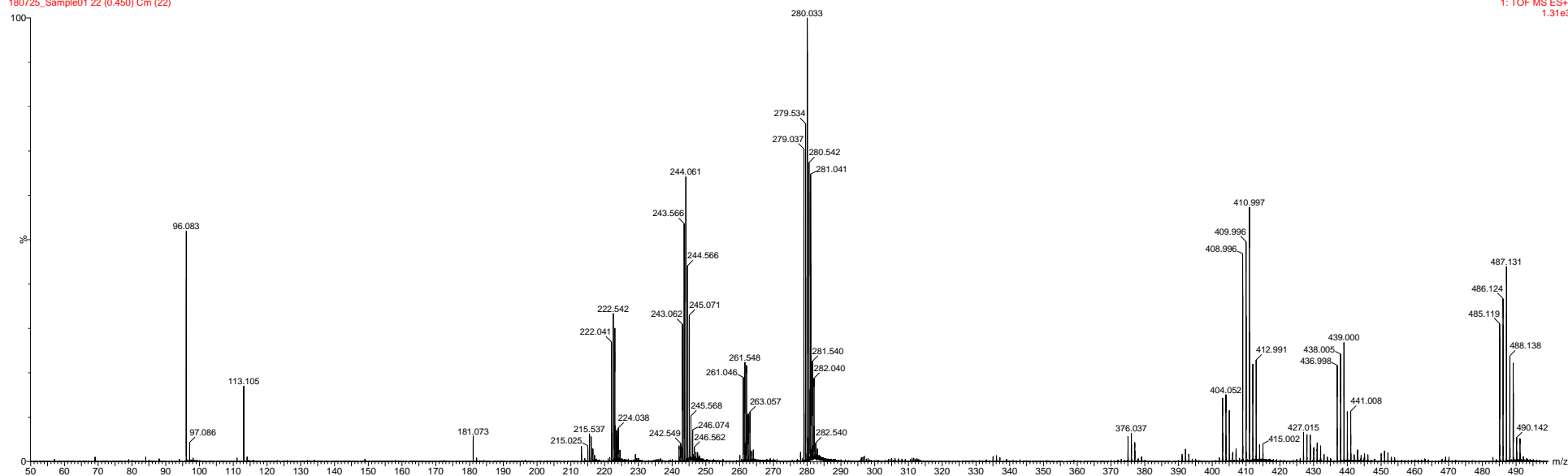


Figure F1: ESIMS spectrum of PHENSSCl₂ measured on a Waters TQ-MS triple quadrupole mass spectrometer. Sample solutions were made up to 0.5 mM in H₂O and flowed at 0.1 mL/min.

PHENSSBr₂

0.1mM in water
180725_Sample02.1 (0.054)

1: TOF MS ES+
848

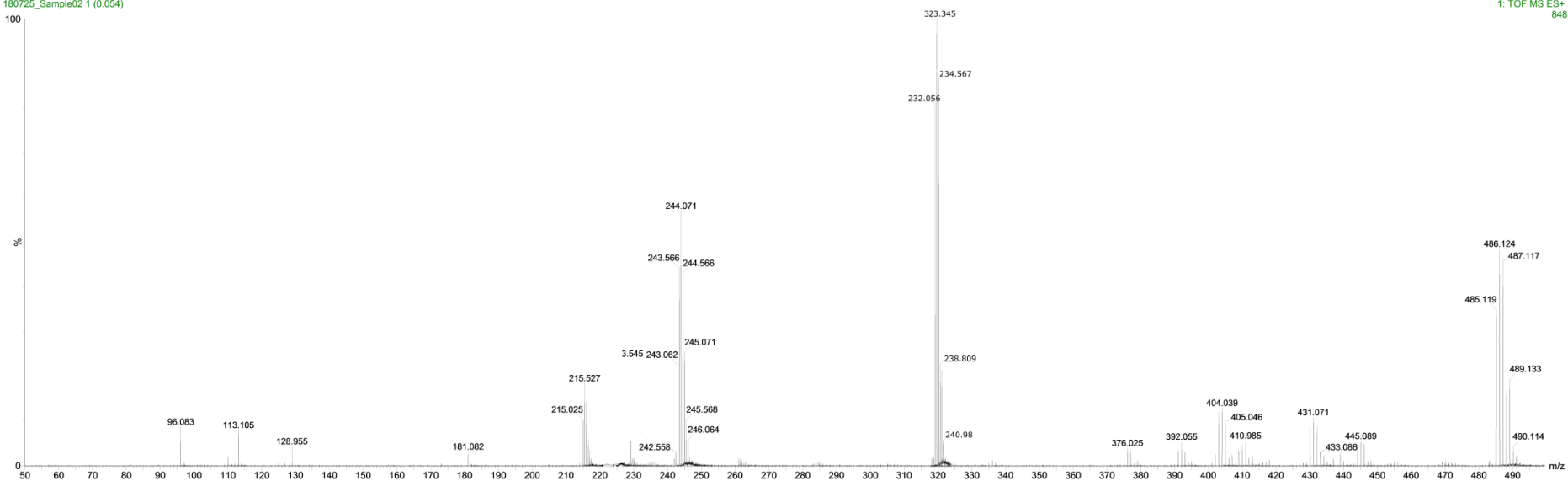


Figure F2: ESIMS spectrum of PHENSSBr₂ measured on a Waters TQ-MS triple quadrupole mass spectrometer. Sample solutions were made up to 0.5 mM in H₂O and flowed at 0.1 mL/min.

PHENSSI₂

0.01mM in water
180725_Sample03 1 (0.054)

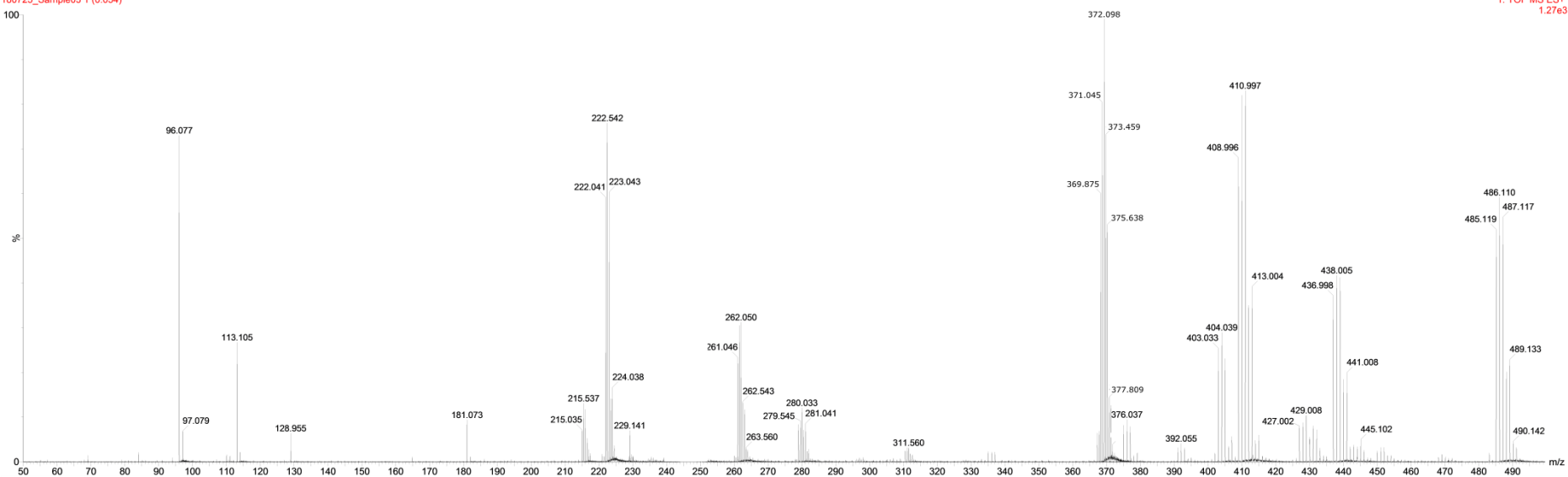


Figure F3: ESIMS spectrum of PHENSSI₂ measured on a Waters TQ-MS triple quadrupole mass spectrometer. Sample solutions were made up to 0.5 mM in H₂O and flowed at 0.1 mL/min.

5MESSCl₂

0.1mM in water
180725_Sample04 1 (0.054)

1: TOF MS ES+
3.67e3

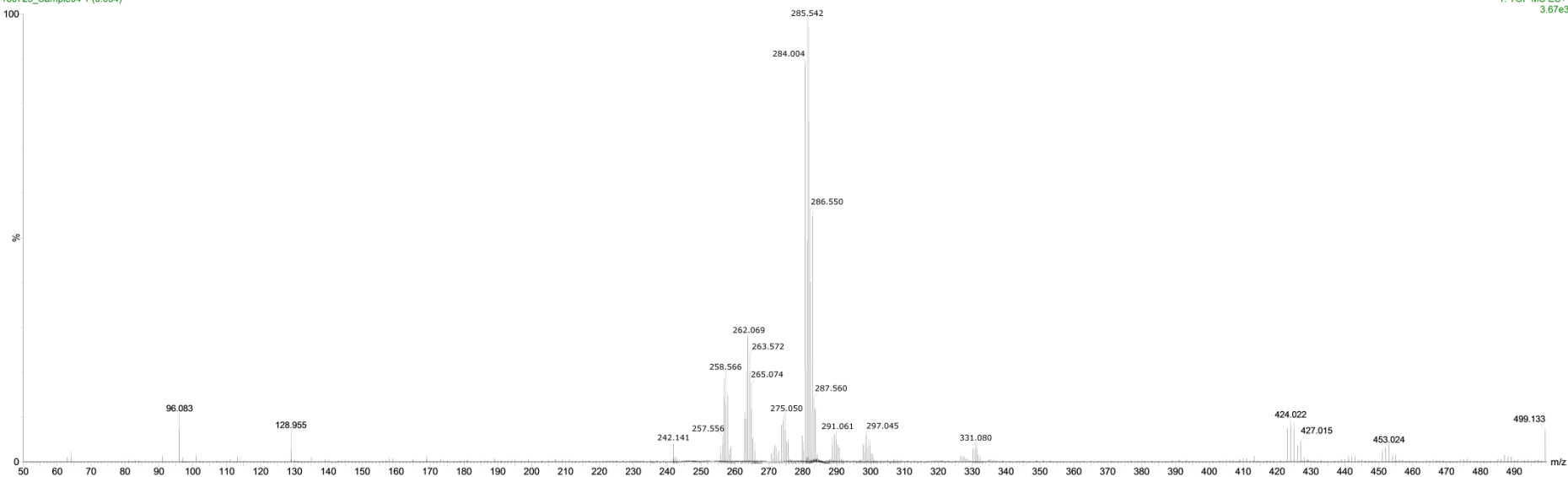


Figure F4: ESIMS spectrum of 5MESSCl₂ measured on a Waters TQ-MS triple quadrupole mass spectrometer. Sample solutions were made up to 0.5 mM in H₂O and flowed at 0.1 mL/min.

5MESSBr₂

0.1mM in water
180725_Sample05 1 (0.054)

1: TOF MS ES+
2.69e3

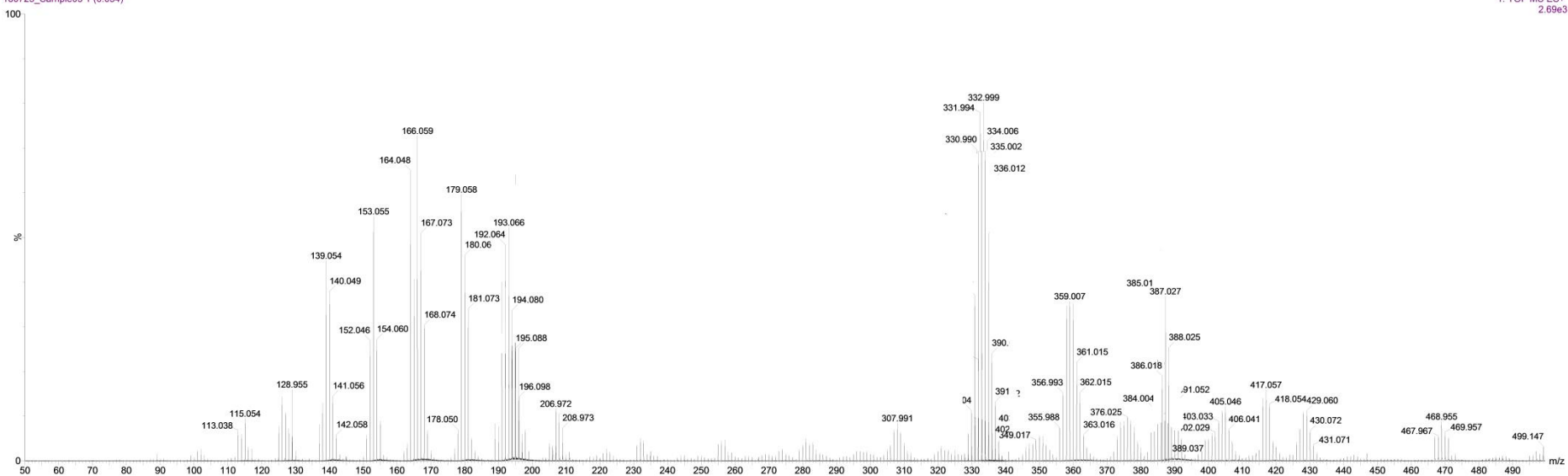


Figure F5: ESIMS spectrum of 5MESSBr₂ measured on a Waters TQ-MS triple quadrupole mass spectrometer. Sample solutions were made up to 0.5 mM in H₂O and flowed at 0.1 mL/min.

5MESSI₂

0.1mM in water
180725_Sample06 1 (0.054)

1: TOF MS ES+
901

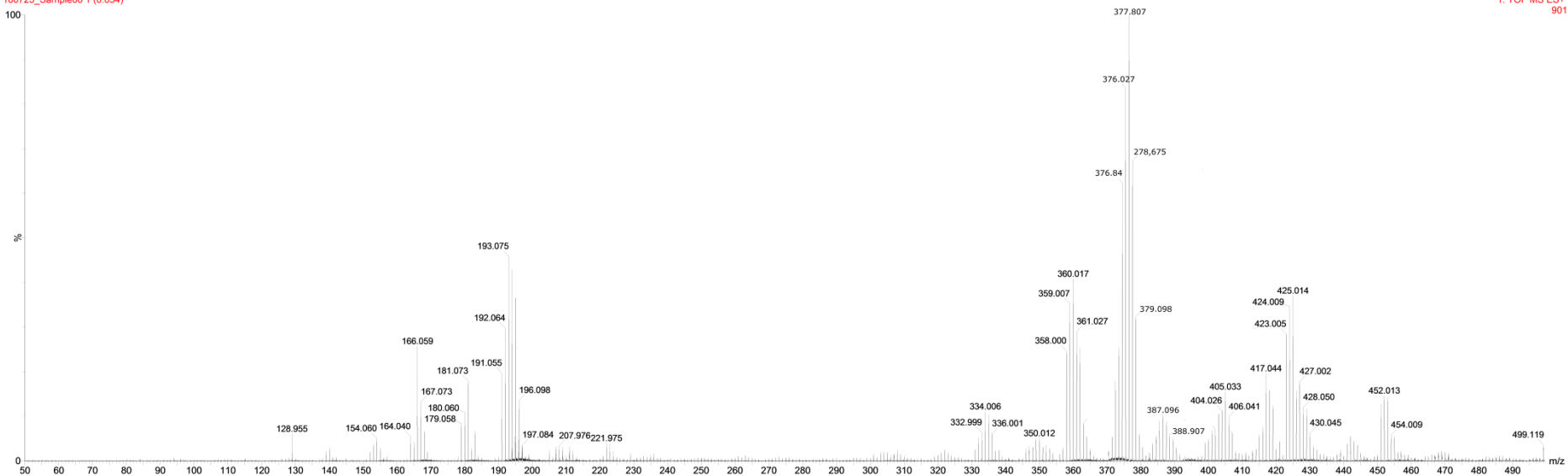


Figure F6: ESIMS spectrum of 5MESSI₂ measured on a Waters TQ-MS triple quadrupole mass spectrometer. Sample solutions were made up to 0.5 mM in H₂O and flowed at 0.1 mL/min.

56MESSCl₂

0.01mM in water
180725_Sample07.1 (0.054)

1: TOF MS ES+
95

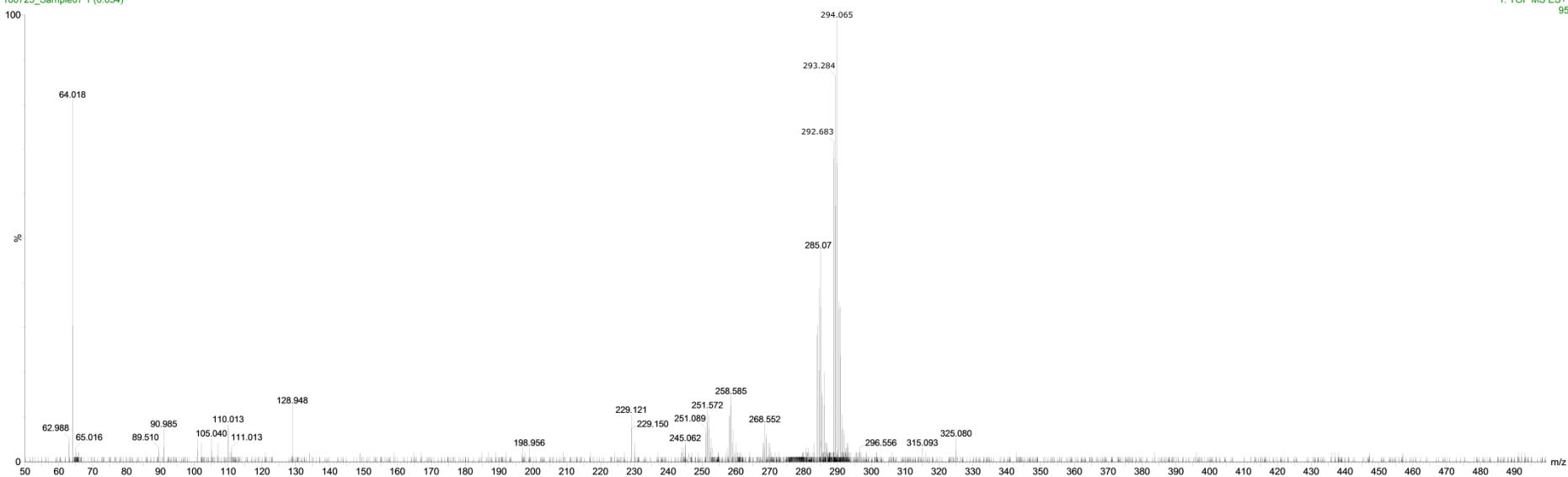


Figure F7: ESIMS spectrum of 56MESSCl₂ measured on a Waters TQ-MS triple quadrupole mass spectrometer. Sample solutions were made up to 0.5 mM in H₂O and flowed at 0.1 mL/min.

56MESSBr₂

0.01mM in water
180725_Sample08 1 (0.054)

1: TOF MS ES+
184

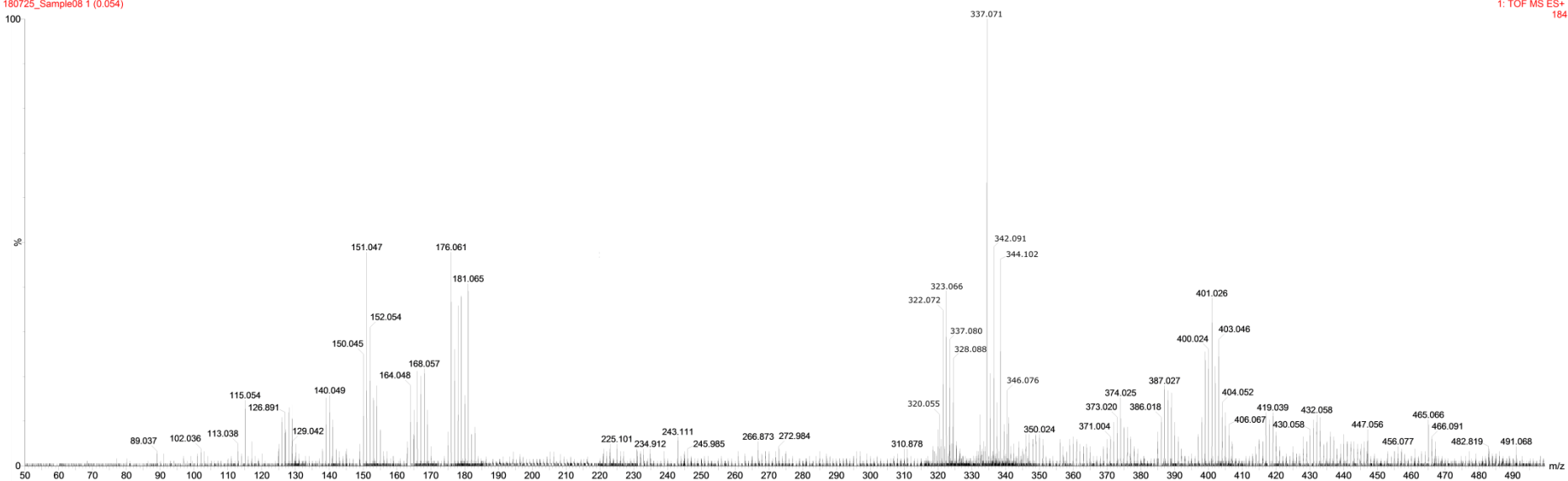


Figure F8: ESIMS spectrum of 56MESSBr₂ measured on a Waters TQ-MS triple quadrupole mass spectrometer. Sample solutions were made up to 0.5 mM in H₂O and flowed at 0.1 mL/min.

56MESSI₂

0.01mM in water
180725_Sample09 1 (0.054)

1: TOF MS ES+
3.89e3

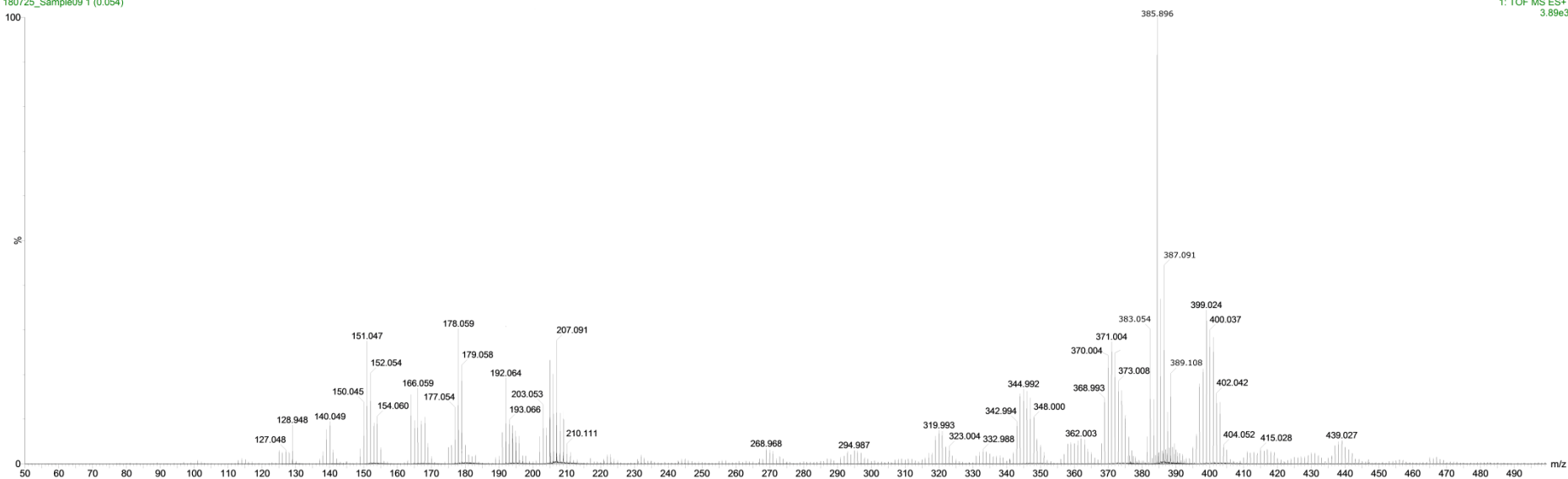


Figure F9: ESIMS spectrum of 56MESSI₂ measured on a Waters TQ-MS triple quadrupole mass spectrometer. Sample solutions were made up to 0.5 mM in H₂O and flowed at 0.1 mL/min.